Investigation into Advanced Coatings for Bandsaw Blades

Fahd Nawaz Khan

Ph. D. 2011

Investigation into Advanced Coatings for Bandsaw Blades

Fahd Nawaz Khan

A thesis submitted in partial fulfilment
of the requirements of the
University of Northumbria at Newcastle
for the degree of
Doctor of Philosophy

Research undertaken in the
School of Computing, Engineering and Information Sciences

July 2011

Abstract

Bandsawing is an important metal cutting operation carried out in a variety of industries in order to remove raw material for secondary operations. Due to its continuous cutting action, bandsawing has over taken other cutting processes such as power hack sawing and circular sawing. Bandsawing operation offers numerous advantages such as high cutting rate, low kerf loss, longer tool life and high automation possibilities, due to its efficient and continuous cutting action.

It is costly and time-consuming to test the wear of the full bandsaw products on a full-scale bandsaw machine. In order to overcome this, a single tooth test rig has been developed at Northumbria University, which utilizes a single bandsaw tooth instead of the complete bandsaw loop. Previous research has utilized this test rig for evaluating bi-metal saws while machining steels.

Development of new, wear resistant and difficult-to-cut materials such as titanium alloys (*e.g.* Ti-17) imposes greater demands on bandsawing operations. Traditionally, high speed steels and cemented carbides have been employed to cut/machine these materials. The main disadvantage of high speed steel cutting tools is that it undergoes severe plastic deformation when cutting at temperatures above 600ºC. Tungsten carbide cutting tools have proven their supremacy in almost all the machining processes and interrupted cutting of these difficult-to-cut titanium alloys.

One of the challenges in design of cemented tungsten carbide tools is the optimization of toughness and wear resistance. This has led to the development of coated carbide tools, which accounts for the major portion of all commercial metal cutting inserts sold worldwide.

This current research has furthered the use of single tooth test rig, by using un-coated and coated tungsten carbide tipped bandsaw blades while machining high performance titanium alloys (Ti-17). The purpose is to evaluate and assess the performance of un-coated and coated carbide bandsaw teeth and ascertain wear mechanisms and modes of single bandsaw tooth, in a way that is representative of full product testing.

Two different coatings (AlTiN and TiAlSiN) were chosen to be deposited using arc evaporation PVD technique. These coatings were selected due to their properties in terms of wear resistance and structure: TiAlSiN is nano-structured, while AlTiN is conventional in terms of its grain size. These coatings were characterized using various techniques, such as electron microscopy and nano-indentation.

Cutting tests were carried out using un-coated and coated carbide bandsaw teeth. Adhesive wear and diffusion wear were identified as the wear mechanisms, while flank wear and chipping were confirmed as the principal wear modes for the un-coated carbide bandsaw teeth. Cutting forces were found to be less while machining Ti-17 alloy using coated teeth as compared to the forces obtained while machining with un-coated teeth. Less material was found to be adhering to the coated teeth as compared to un-coated teeth.

Finite element analyses (FEA) were carried out on interaction of the cutting tool and the workpiece to determine the stress concentration during the cutting process. It was found that the increase in the honing lengths on the carbide teeth reduced the stresses and moved the maximum stress from the edge of the rake face to the honed edge.

Acknowledgements

The research was carried out within the School of Computing, Engineering and Information Sciences, Northumbria University in collaboration with SNA Europe (AB) Industries, Sweden. I would like to express my sincere gratitude to Northumbria University and SNA Europe, for providing me with a studentship and funding to carry out the research.

My special thanks goes to my supervisory team –Prof. Hellbergh, Dr. Daadbin, Dr. Persson and Per Holm – for providing continuous support, guidance and encouragement. I would like to thank them for giving me the opportunity to undertake the study under their supervision. Without their constructive advice and swift feedback, including on this thesis, it would not have been possible to carry out my research. I must specially thank Dr. Daadbin and Dr. Persson for their understanding, patience, and most importantly, guidance. There were many moments during my stay here that I lost faith and confidence in myself, but Dr. Daadbin and Dr. Persson never lost their faith in me. For this, thank you so much.

Special thanks to Mr. Classon at SNA Europe for helping me to carry out the experimentation and to Dr. Haider for his help, guidance and discussions. I am grateful for the technical support at CEIS from Phil Donnelly and Bob Best, for helping me in the experimental work and electron microscopy. I would also like to thank Dr. Noel Pererra for the countless chats and for the laughers.

I must thank my fellow PhD students in E - 411 for making this room such a lively place to work, some of whom were part of the "squash" club. Thanks Pietro, Remi, Balaji, Arash, Sujan, Rupak, Caroline, Qing Lu (Larry), Matthew and Andrew for all the nice discussions that we had. Special thanks to Dr. Gillian Brooks, Research Administrator, one of the nicest persons I have ever met, for helping and guiding me and the other research students. I owe special thanks to Jamie Thompson for making my life so comfortable here in Newcastle and treating me like a family member. You put up with me, in spite of myself.

I would like to thank my friends back in Pakistan, namely Sajjad, Haroon and Waqas for their numerous phone calls and keeping me updated.

Lastly, I profoundly thank my beloved family for their continuous support, prayers and unwavering love. When I was coming to Newcastle in 2007, my mother said that I should return within three years and instead I stayed for more than 4 years. I hope she will forgive me.

God bless you all.

Declaration

I declare that the work presented in this thesis has not been submitted for any other award and that is it all my own work.

Fahd Nawaz Khan

Table of Contents

CHAPTER 2: SINGLE TOOTH TEST

CHAPTER 3: COATING CHARACTERIZATION

CHAPTER 4: RESULTS AND DISCUSSION

CHAPTER 5: STRESS ANALYSIS DURING CUTTING

List of Figures

List of Tables

List of Abbreviations

γ	Rake angle, orthogonal cutting
β	Clearance angle, orthogonal cutting
ϕ	Angle of primary shear zone, shear plane angle
A_{chip}	Cross-sectional chip area (undeformed layer)/(mm^2)
E_{sp}	Specific cutting energy/(GJ/m^3)
n	Exponent depending on machine and workpiece properties, for Taylor equation
T	Machining time to life criterion in Taylor equation /(s)
V_w	Velocity of workpiece, orthogonal cutting/ (m/s)
V_c	Chip velocity, orthogonal cutting /(m/s)
F_p	Thrust (feed) force/(N)
F_v	Cutting force/(N)
F_s	Side (lateral) force/(N)
h_c	Compressed chip thickness, orthogonal cutting /(mm)
h_o	Layer of metal removed, orthogonal cutting /(mm)

CHAPTER 1: INTRODUCTION AND LITERATURE SURVEY

1.0 Introduction

The project "Advanced Surface Coatings for Tungsten Carbide Tipped Bandsaws" was carried out at Northumbria University, in collaboration with SNA Europe [Industries] AB, one of Europe's largest bandsaw blade manufacturers, based in Lidkoping, Sweden. This research work was undertaken owing to the following reasons:

- Tungsten carbide tipped (TCT) blades are seen to be major players in the bandsawing industry.
- It has been established by the researchers and the industry that there is a clear need for new knowledge associated with tungsten carbide tipped bandsaws with respect to establishing tool material design and manufacturing parameters.

1.1.0 Aims and objective of the research programme

Previous work carried out at Northumbria University has been carried out on the performance and cutting actions of the High Speed Steel (HSS) bi-metal bandsaw products [1, 2], whereas the present work is associated with the performance of un-coated and coated TCT bandsaw blades. The aims of the research programme are:

1. To scientifically evaluate the TCT bandsaws using the existing Single Tooth Test developed at Northumbria University [1].
2. Assess performance and life of TCT bandsaws when cutting titanium alloy (Ti-17) and Inconel 718 (nickel-based superalloy) using advanced coatings, which are selected on a scientific basis (hardness, porosity, wear resistance, adhesion to substrate *etc*). The end of the useful life of these coated blades can be judged by measuring the tooth wear or by measuring the change in Specific Cutting Energy (E_{SP}) over that of the newly coated blade.
3. To establish performance/wear/failure modes and mechanisms of these coated bandsaw teeth when machining high performance alloys (nickel-based superalloys and titanium alloys) and to form a picture library of these teeth and the chips produced.

4. Establish a systems approach to optimise advanced coatings for the TCT bandsaws by making specific measurements. This can be done by establishing scientific data, such as forces, chip formation characteristics, wear and failure characteristics and the specific cutting energy.

The objective of the proposed research programme is to introduce advanced coatings (single and multi-layer) which will enhance the life and performance of the tungsten carbide metal cutting bandsaws.

1.2.0 Cutting-off processes – bandsawing

Sawing is a cutting process that has been the subject of increasing interest in recent years as the need for efficiency and quality for all machining processes has increased. It is a process of cutting the workpiece materials with bandsaws, hacksaws and circular saws. Each of these processes is used for cutting workpiece materials to required length, although bandsawing also provides a method for cutting contours [3]. Bandsawing has become a favourite for cutting-off to size alloy workpieces as a primary operation due to several advantages it has over other sawing operations such as high metal removal rate and low kerf loss [4]. Bandsawing is now a well understood process, due to the work carried out by several researchers, which was stimulated by demands for higher efficiency, better accuracy and improved surface quality [4-10]. Metal cutting tools are classified as single-point or multi-point and they are briefly discussed as follows.

1.2.1 Single-point cutting tools

Single-point tools are cutting tools that have one cutting part (or chip-producing element) and one shaft. They are commonly used in lathes, shapers and similar machines. All the turning operations use single point cutting tools, *i.e.* tools that have only a single cutting edge in contact with the workpiece.

The most important features of the single-point cutting tool are the cutting edges and the adjacent surfaces. These features are shown in Figure 1.1 and defined as follows:

- The rake face is the surface over which the chip flows, whereas the clearance (or flank) surface is the one which moves on the newly formed workpiece surface.
- The cutting edge is that edge of the face which is intended to perform the cutting.
- The corners are the relatively small portion of the cutting edge and which may be straight or curved [11].

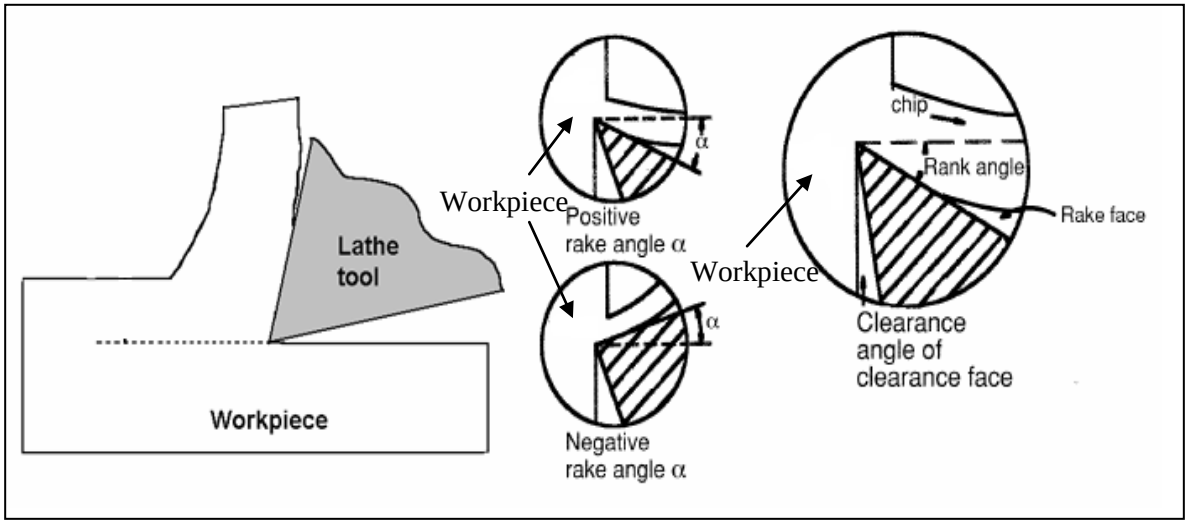

Figure 1.1. An example (lathe tool) and main features of a single point cutting tool [11].

1.2.2 Multi-point cutting tools

A multi-point cutting tool can be regarded as a series of two or more cutting (chip-producing) parts attached to a common body. The majority of the multi-point cutting tools (such as milling cutters, drills) are intended to be rotated and have either a conical (taper) or parallel (cylindrical) shaft for holding purposes. Terms such as 'rake', 'flank' and 'cutting edges' which have been defined for single point cutting tools previously in the literature, are applicable and the cutting action at a selected point on one of the cutting edges is the same.

In contrast to the circular saw and hacksaw blades, the bandsaw blade is flexible and thin. The stability required for sawing is due to the tension in the band, therefore a heavy duty design is required for a production bandsaw machine. The feed force is transferred across the two band guides onto the cutting edges of the bandsaw blade. There is a limit to the amount of feeding force that can be transferred as the band is thin. Therefore high cutting rates can only be achieved by increasing the band speed. The bandsaw consists of a slender continuous band with cutting teeth over its entire length, driven between two wheels. These wheels also apply some tension to the blade, making the blade rigid. This rigidity in the band ensures that the bandsaw blade is guided to a position which is perpendicular to the surface of the workpiece throughout the cutting operation. The cutting motion of the bandsaw loop is supplied by the wheel, which is rotated by an electric motor.

Bandsawing also differs from other sawing methods – its blade and cutting action allow the cutting edge to follow a contoured path while cutting. When compared to other cutting operations (*e.g.* milling), contour cutting has the following advantages:

- Unwanted material is removed in sections instead of the chips.
- The fixture is simplified as the downward cutting force (vertical bandsaws only) holds the workpiece to the table.
- Narrow tooth kerf minimizes power requirements for cutting [3].

The characteristic feature of the material removal in bandsawing operations is the function of the cutting edge with limited sharpness (5 μm to 15 μm) with the layer of material being removed also being very small (5 μm to 50 μm). The cutting action in bandsawing operations is intermittent, with several cutting edges in contact with the workpiece material. This is one of the major differences between the sawing operation and the other single-point cutting operations, *e.g.* turning, where only one sharp edge is in contact with the workpiece material. Moreover, the chip needs to be accommodated in the gullet and ejected at the end of the cut [2, 12].

1.3.0 Bandsaw blades

Doraisingam reviewed the historical development of metal-cutting bandsaw blades [1]. The blades used in 1935 were made from carbon steels and could not be used for high production volumes, due to the wear of the blades and loss of mechanical properties (especially hardness). High Speed Steel blades were produced in 1953, resulting in increased blade life and productivity as high cutting speeds could be achieved. This revolutionized bandsawing, enabling machine operators to cut conventional materials up to 10 times faster, with blade life 30 times longer than plain carbon steels under normal cutting conditions [13]. These HSS steels have higher hardness, hot hardness and abrasion resistance compared with carbon alloy steels, but are not as ductile as carbon steels as explained previously.

The bi-metal bandsaw blades, which combined the flexibility of carbon steel with the wear resistance of high speed steel, were introduced in 1953 and still comprise the vast majority of the blades in use today. In this bi-metal bandsaw blade, a HSS wire is welded onto a flexible spring steel backing material, resulting in HSS tooth tips. The teeth are then milled into high speed steel strip through to the backing material so that the finished blade

has a high speed steel cutting edge. High speed bi-metal blades can cut up to 13 m^2 of metal at improved cutting speeds [14].

Further improvement in the cutting performance has been made by the introduction of tungsten carbide bandsaw blades, which consist of tungsten carbide materials being welded or brazed onto the flexible spring steel backing material. Carbide-tipped blades are well suited to run at higher cutting speeds (90-180 m/min) and last 5 times longer than HSS bi-metal blades [14]. This allows cutting of difficult-to-cut materials such as hardened steels, superalloys and titanium alloys and such blades show superior performance compared to the blades made from carbon steel or bi-metal. The carbide tipped bandsaw blades are more expensive than bi-metal bandsaw blades. However, the higher blade cost can be balanced by the savings in cutting costs [15, 16].

In order to enhance the performance of these TCT blades, advanced surface coatings are now being applied, mainly to increase their life and cutting speeds, in order to increase productivity [17]. Materials used for single layer coatings include titanium nitride (TiN), titanium carbide (TiC), aluminium titanium nitride (AlTiN), aluminium oxide (Al_2O_3), chromium nitride (CrN) *etc*. These will be discussed later in this report.

The main features of a modern bandsaw blade are shown in Figure 1.2.

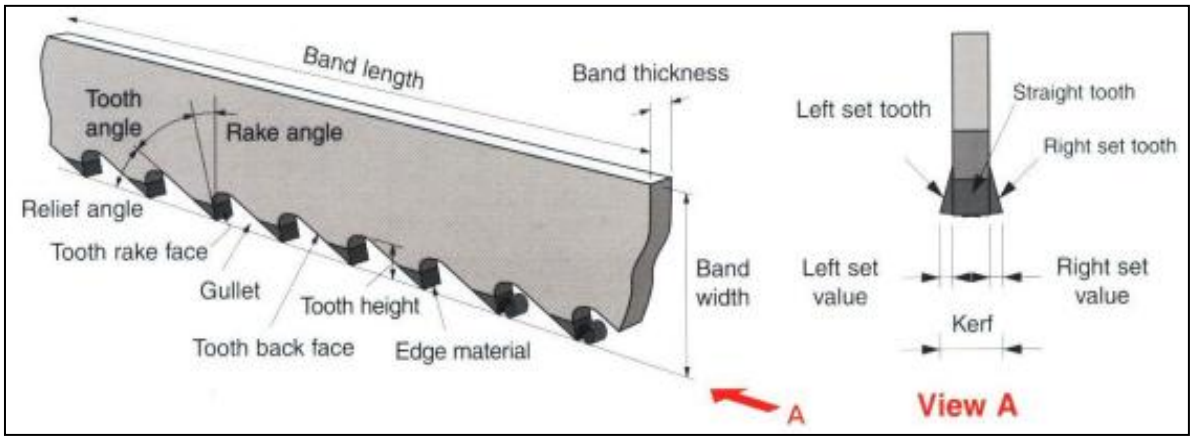

Figure 1.2. The main features of a bandsaw blade.

1.3.1 Blade design

Pitch, width and thickness of the blade, and the type of set and set dimensions are important factors in selection of a blade for a particular application.

The pitch of a blade is the number of teeth per 25 mm (approx. 1 inch) of the blade. The pitch of a blade is primarily selected on the basis of thickness and the shape of the cross-section to be cut, whereas the type of material to be cut is of minor importance. The noise

from band sawing can be reduced considerably by using blades with different pitch combinations. This variable spacing of teeth causes interference in sound patterns, thus reducing the amplitude of the resulting noise. Variable pitch reduces the amplitude of the vibrations, which is important when sawing thin workpieces [3].

The blade thickness plays an important role in the blade's performance. Beam strength of a blade increases in proportion to the cube of blade thickness, thus permitting the use of higher feed force. Moreover, the accuracy of cutting along a straight line is superior for wider blades. In general, a blade of standard thickness is adequate for all applications, except those involving large workpieces and requiring extreme accuracy. For such applications, a heavier gauge is recommended due to the fact that it will offer increased resistance to side displacement [3].

The teeth of a saw band are intentionally offset (called the set tooth) to provide clearance for the back of the band and to permit cutting of contours. This is required to avoid the jamming of the blade in the kerf. The set dimension is the distance between the extreme corner of one tooth to the extreme corner of the tooth set to the opposite direction. There is a wide range of setting patterns available, as shown in Figure 1.3. The most widely used is known as Raker set, which has 0-R-L configuration (one straight tooth followed by one right-set tooth followed by left-set). There are also other patterns, such as Combo set (O-R-L-R-L-R-L) and Alternate set (L-R-L-R-L-R). The magnitude of the set to right and left is called the "set magnitude" and if combined with the defined setting tool will result in a setting angle or those teeth. A "set twist angle" is the clearance angle in the direction of cutting as shown in Figure 1.3.

1.3.2 High/low teeth configuration

Most bandsaw blade manufacturers produce blades with "high/low" teeth configuration". This means that some of the cutting edges are placed higher than the others, and the "high" teeth will perform the cutting action. The high/low tooth configuration is a modification from the 1970s, when it was observed that bandsaw users normally put too small a depth of cut into the bandsaw machines. By making every second tooth too low, the bandsaw effectively became twice as coarse and each tooth would take twice the set depth of cut. It is, indeed better to cut deeper and with fewer teeth, since the total vertical force becomes less. Since the 1970s, it has been a popular way to make some of the bands this way (but not all bands). Nowadays, there are similar concepts, using different levels of set

magnitude, so that each tooth is cutting narrow, but thick chips. The schematic diagram for the high/low teeth configuration is shown in Figure 1.4.

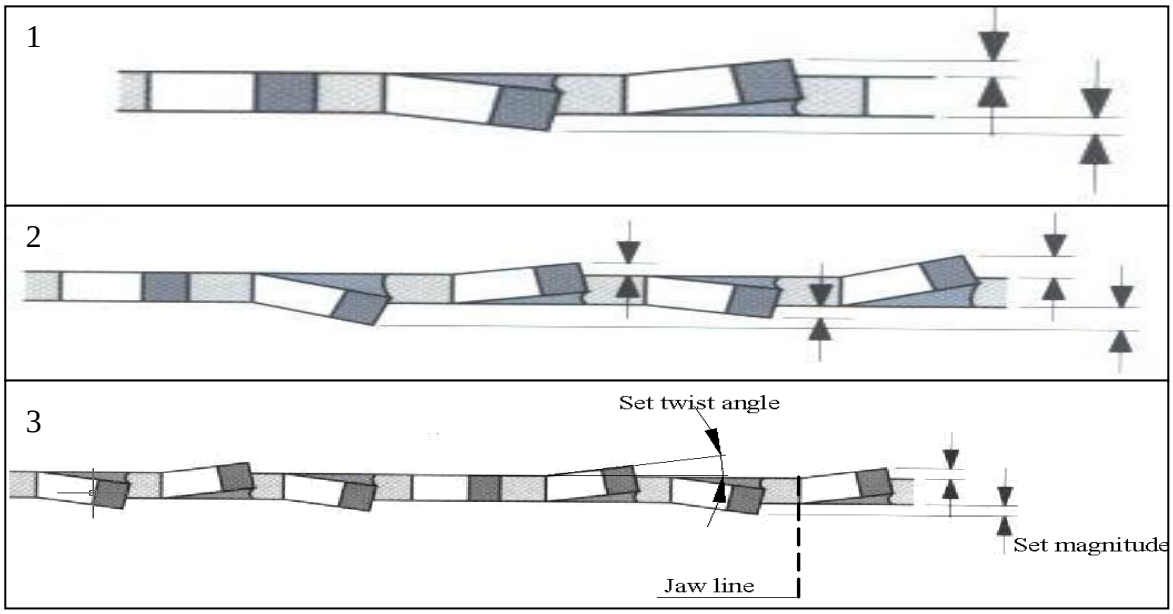

Figure 1.3. Different tooth set patterns: 1- Raker tooth set pattern, 2- Combo tooth set pattern, 3- Alternate tooth set pattern [3].

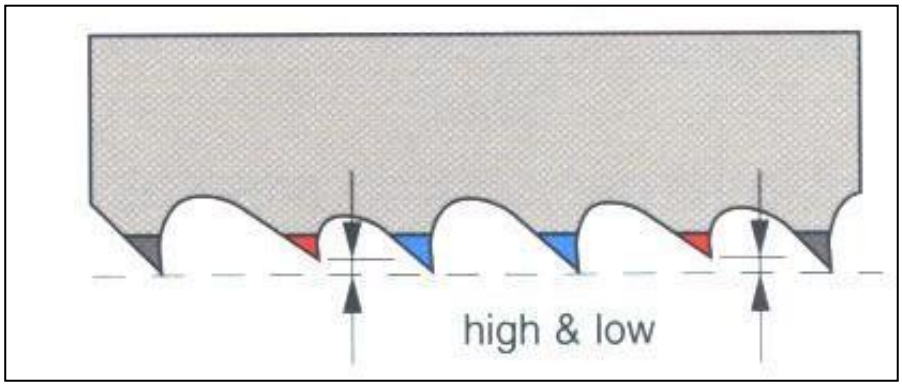

Figure 1.4. High/low tooth configuration.

1.4.0 Fundamental mechanism of metal cutting

It has been stated by Trent and Wright [18] that in metal cutting "the tool has to take the form of a large angled wedge, which is driven asymmetrically into the work material, to remove a thin layer from a thicker work material body. The layer must be sufficiently thin to enable the tool and work to withstand the imposed stress. A clearance angle must be formed on the tool to ensure that the clearance face does not make contact with the new work surface." This statement holds true for all metal cutting operations [18].

In 1906, Taylor presented his ground-breaking work [19] on the effect of tool material and cutting conditions on tool life and his empirical law, relating tool life to cutting speed. Taylor's work is still used today for calculation of machining economics as shown in Equation 1.1:

$$VT^{n} = C \qquad \text{(Equation 1.1)}$$

where V = cutting speed, T = machining time to life criterion, n = exponent depending on machine and material properties, and C = empirical constant depending on specific machine and work material of particular operation.

The primary aim of Taylor's research was to establish a model which could answer questions related to cutting speeds, feeds and cutting tools to be used.

Merchant [20] states that the modelling of metal cutting processes has gone through three well defined historical stages:

1. Empirical modelling, starting in the early 1900s.
2. Science-based modelling, beginning in the 1940s.
3. Computer-based modelling, starting in the 1970s.

With the development of computer-based modelling and software (*e.g.* Solidworks, Pro E) associated with modelling and simulation, it became possible to combine both empirical and science-based modelling into the simulation of metal cutting.

1.4.1 Cutting models

A brief discussion of the fundamental nature of the deformation processes is helpful in understanding the assumptions that accompany the mechanics before the mechanics of machining are presented. Material removal in metal cutting is a plastic deformation process. At slow speeds, it occurs along the shear zone and at higher speeds, along the shear plane and will be explained later in Section 1.4.3.

The machining geometry can be simplified from the three-dimensional (oblique) geometry, which is the case in most industrial processes, to a two-dimensional (orthogonal) geometry. Oblique cutting is obtained when the cutting edge and the cutting motion are not perpendicular to each other.

Since the orthogonal case is easy to model, it will be used to describe the deformation process.

1.4.2 Orthogonal machining fundamentals

Orthogonal machining setups are used to model oblique machining processes. Processes such as turning, drilling, milling and shaping are all three-force, or oblique, cutting methods. However, the orthogonal model shown in Figure 1.5 is an excellent illustration of the behaviour of oblique processes without the complications due to the third dimension. The workpiece is moving towards the tool with a cutting speed, V_w and the cutting edge is perpendicular to the cutting speed vector and the feed motion, shearing off a chip along surface of the tool. The simple cutting tool is a wedge shape and consists of two intersecting planes to form a cutting edge as shown in Figure 1.6. The surface of the tool on which the chip forms and flows is called the 'rake face' and the surface that is facing the newly machined workpiece is called the 'clearance face'. Figure 1.6 also shows the rake angle (γ) and clearance angle (β).

Many metal cutting operations are dissimilar to orthogonal cutting, due to their different cutting geometry and different modes of operations (such as circular motion *etc*). However, the bandsawing operation represents a linear operation with the proportion of cutting edges that are positioned in a straight line, hence the orthogonal case can be used to represent the cutting action. Furthermore, it is assumed that the state of stress for the chip formation in the bandsawing operation is plane strain.

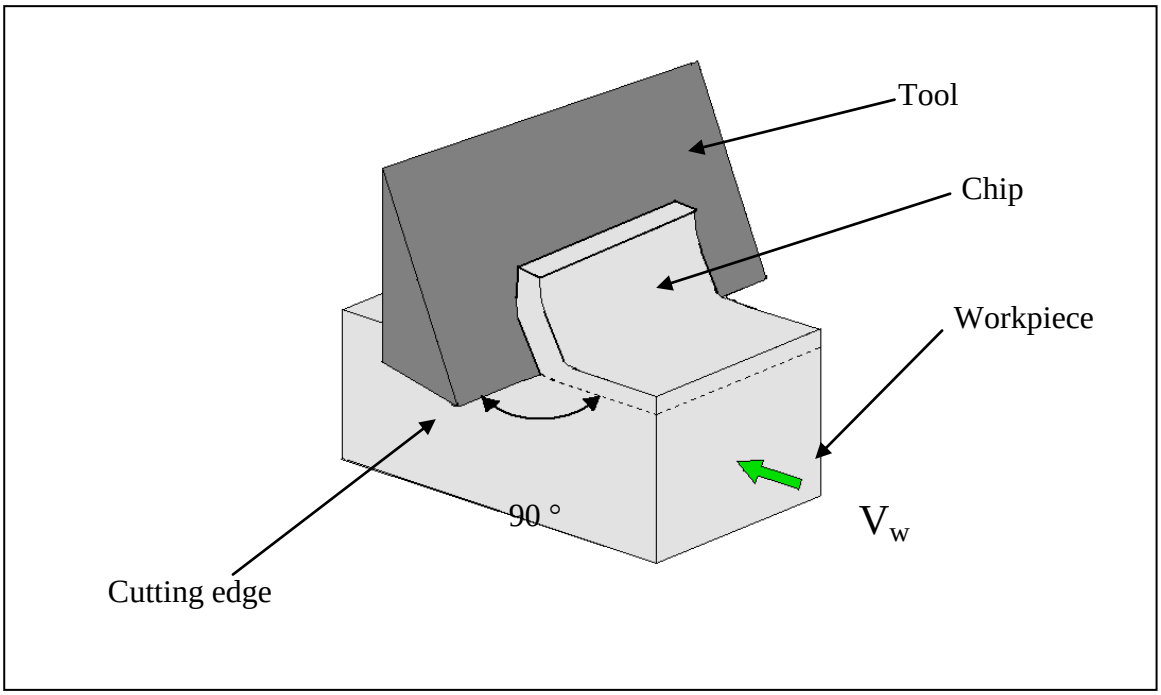

Figure 1.5. Orthogonal cutting according to Sarwar [21].

1.4.3 Chip ratio

Orthogonal machining can be accomplished by machining a workpiece plate or can be approximated by cutting the end of a tube wall in a turning setup. For the purposes of modelling, the following are assumed:

The tool cuts the workpiece by removing the chip by plastic deformation, with the workpiece moving at the velocity of V_w. Material that is situated in front of the cutting tool is first compressed and then plastically deformed along the line A-B as shown in Figure 1.7, and this region is known as the 'primary shear zone'. The chip is formed along the rake angle. The chip has a velocity V_c, which is less than the velocity of workpiece V_w. A layer of material of thickness h_o is removed from the workpiece, but it is compressed due to plastic deformation in the primary and secondary zones, and the thickness of this compressed chip is called h_c. The ratio between h_o and h_c is known as 'chip thickness ratio'.

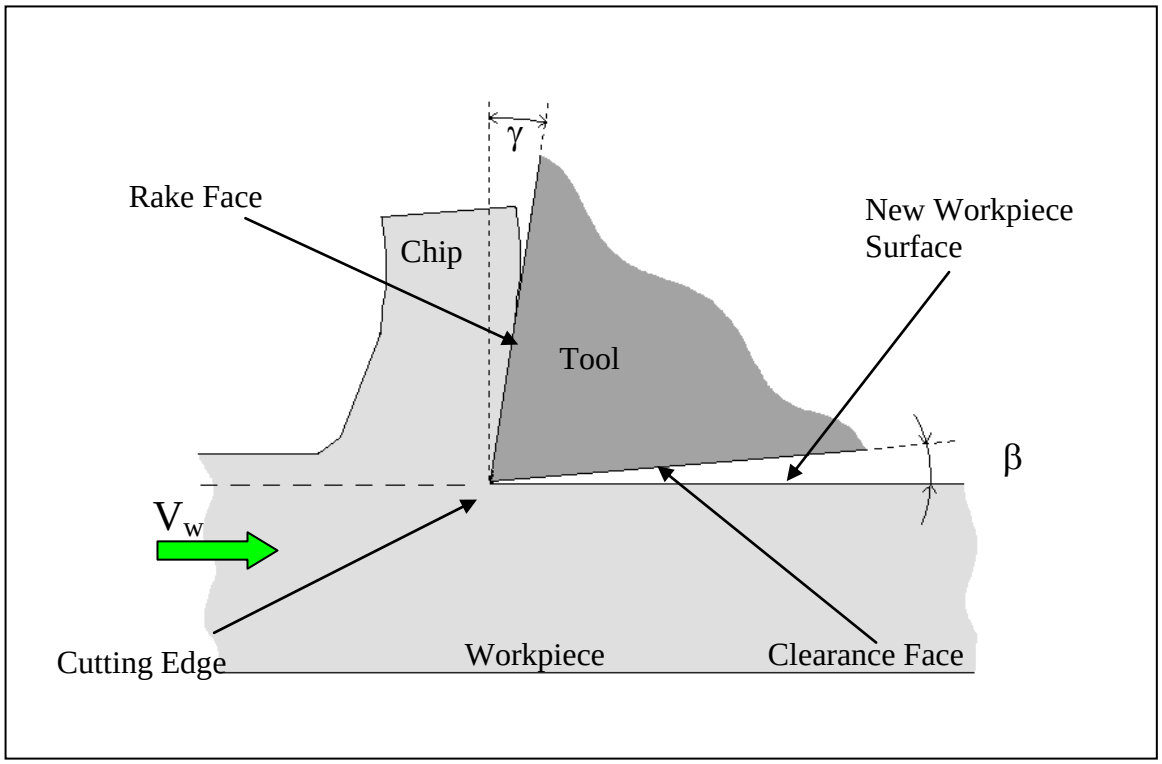

Figure 1.6: Orthogonal cutting, terms used in metal cutting, also shown are the rake face angle (γ) and clearance angle of tool (β) [21].

In practical tests, the average chip thickness can be obtained by carefully measuring the length (L) and the weight (W) of a piece of a chip, as shown in Equation 1.2:

Chip thickness ratio = $W/\rho tL$ (Equation 1.2)

where ρ is the density of the work material and "t" is the feed or uncut chip thickness. Chip thickness is usually greater than the depth of cut and is constrained by the rake face of the cutting tool. The higher is the chip thickness ratio, the less is the cutting force and heat generated and higher is the efficiency of the machining operation.

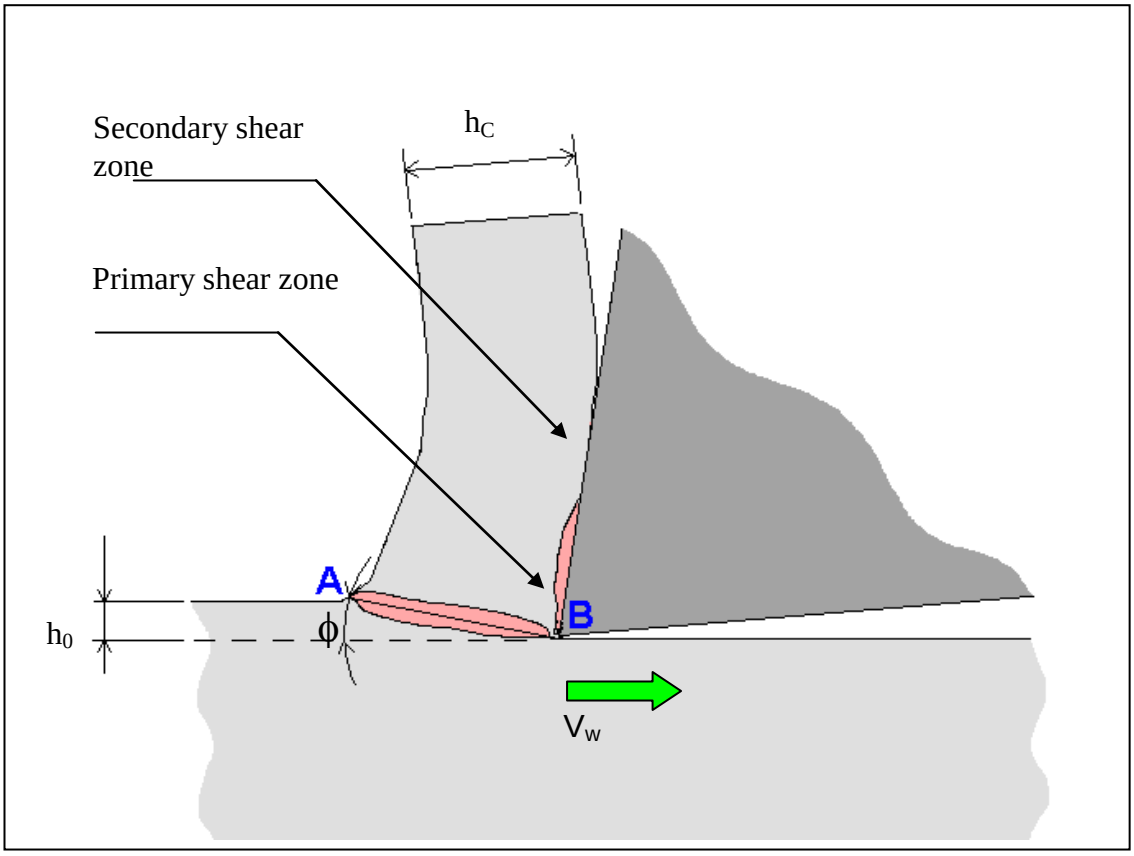

Figure 1.7: Deformation zones and cutting geometry. ϕ is the shear plane angle of the primary deformation zone, h_0 is the depth of cut, h_C is the (compressed) chip thickness. V_W is the cutting speed. [11, 18].

1.4.4 Principal chip types

The properties of the work material control chip formation. Work material properties include:

- yield strength,
- shear strength under compressive loading,
- strain-hardening characteristics,
- friction behaviour,
- hardness,

- thermal properties and
- ductility.

Highly ductile materials not only permit extensive plastic deformation of the chip during cutting (which increases work, heat generation and temperature) but also result in longer, continuous chips that remain in contact longer with the tool face, thus causing more frictional heat. Chips of this type are severely deformed and curl in a characteristic way. On the other hand, some materials, such as grey cast iron, lack the ductility necessary for appreciable plastic chip formation.

The compressed material ahead of the tool can fail in a brittle manner anywhere ahead of the tool, producing small fragments. Such types are termed 'discontinuous' chips. The cutting parameters also influence chip formation. Cutting parameters include tool materials, tool angles, edge geometries (which change due to wear, cutting speed, feed and depth of cut), and the cutting environment (machine tool deflections, cutting fluids *etc*).

A Built-Up Edge (BUE) is workpiece material that is deposited on the rake face near the cutting edge. It is the product of the localized high temperature and extreme pressure at the tool/chip interface. When machining alloys with multi-phase microstructure, the strain hardened material accumulates, adhering around the cutting edge (similar to a dead-metal zone in extrusion). Although this material protects the cutting edge, it also modifies the geometry of the tool. Built-up edges are not stable and will be removed periodically by either adhering to the chip or passing under the tool and adhering to the machined surface. Built-up edge formation can often be eliminated or minimized by reducing the depth of the cut, increasing the cutting speed, using positive rake tools, or applying a coolant, but these techniques greatly increase the complexity of the chip formation process analysis. The built-up edge is not observed when cutting pure metals, but is observed frequently when machining commercial alloys because they usually have more than one phase in their structure, which strain hardens leading to the formation of the built-up edge [18].

The three main types of chips that are formed during machining are shown in Figure 1.8.

1.5.0 Cutting tool materials

Any machining operation which involves the removal of metal by a cutting action requires that the materials used for the machining operation will stand up to the severity of that

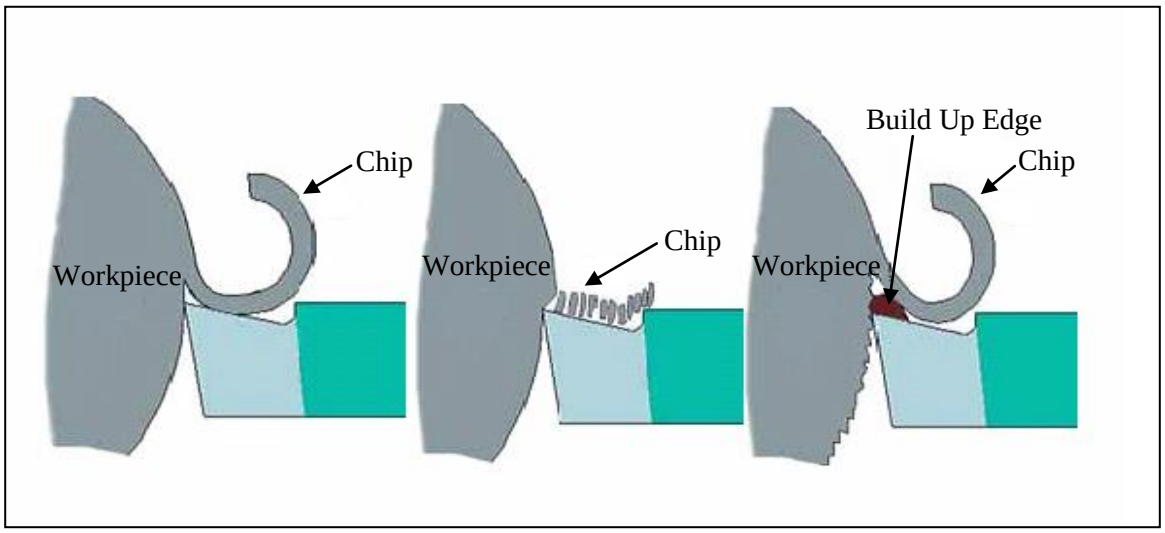

Figure 1.8. Three characteristic types of chips (a) continuous, with no built-up edge, (b) discontinuous (c) continuous with built-up edge.

cutting action. The main properties which any cutting material must possess in order to carry out its function are as follows:

1. Hardness to combat/withstand the wearing action.
2. Hot strength/hardness to overcome the heat evolved during machining.
3. Sufficient toughness to withstand any interruptions or vibration occurring during the machining operation.
4. Chemical inertness (low chemical affinity) with respect to the workpiece material to resist diffusion, chemical and oxidation wear.
5. High thermal conductivity to reduce cutting temperature near the tool edge.
6. High thermal shock resistance to prevent tool breakage in interrupted cutting [26].

The following materials are commonly used for metal cutting:

- High speed steels
- Cermets (cemented carbides)
- Ceramics (silicon nitride, cubic boron nitride)
- Diamond

The major types of cutting tool materials and their properties are shown in Table 1.1 whereas Table 1.2 shows the softening points of the commercially available tool materials.

Table 1.1. Major classes of tool materials along with their trends for mechanical properties [26].

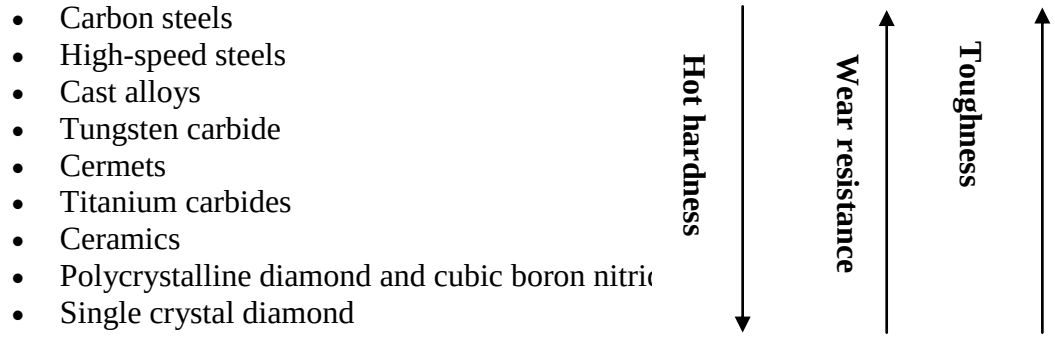

Table 1.2. Softening points of commercially available tool materials [27].

Tool Material	Softening point temperature °C
High speed steel	600
Tungsten carbide	1100
Al_2O_3	1400
Cubic boron nitride (CBN)	1500
Diamond	1500

Since this project involves tungsten carbide-tipped bandsaw blades, therefore tungsten carbide will be discussed briefly.

1.5.1 Sintered tungsten carbide

Sintered tungsten carbide-based hard metals are the most common tool materials for turning, milling, threading and boring operations. There are two carbides of tungsten –WC which melts at 2600°C and W_2C which melts at 2750°C. Both these carbides are very hard and can only be melted and cast with difficulty. They can be ground to shape using diamond grinding wheels, but these castings are coarse in structure and hence have many flaws and therefore fracture easily. The use of the powder manufacturing route solved this problem. Cemented tungsten carbide inserts and blanks are manufactured by mixing, compacting and sintering WC and Co powders, in which Co powder acts as a binder for the hard WC grains. Cobalt was found to be the most effective bonding agent because unlike many powder-metal products, tungsten carbide/cobalt mixtures can be sintered to full density, free from porosity in a single sintering (heat treatment) cycle. This is due to the formation of liquid phase solution in cobalt at approximately 1300°C, which wets and pulls together the remaining WC particles. On cooling to room temperature, the liquid

solidifies and the product is fully dense. Characteristics of WC include high transverse rupture strength, high fatigue and compressive strength, and good hot hardness. The modulus of elasticity is twice that of HSS. The carbides in the tool conduct the heat away, and the tool can also be tailored to meet specific thermal shock requirements. A relative balance of hardness and toughness can be achieved by varying the cobalt content and WC grain size. The major drawback of WC 'hard metals' is that they have average chemical and thermal stability at elevated temperatures. For non-ferrous workpieces, WC tools will exhibit two to three times the productivity and 10 times the life of HSS tools; in steels twice the productivity and five times the life [26]. The typical microstructures of a sintered tungsten carbide are illustrated in Figure 1.9 – also evident is the effect of alloying elements on tungsten carbides.

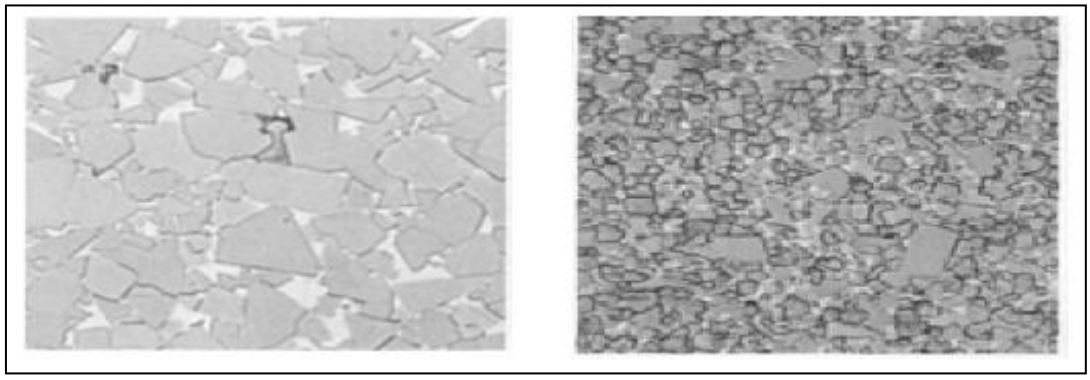

Figure 1.9. Microstructures of straight WC-Co alloys and steel-cutting grades of tungsten carbide (78WC-15(Ta,Ti,Nb)C-7Co), mag. X 1500 [3].

1.6.0 Applications and machinability of high performance alloys

This project deals with the machining of high performance alloys, namely titanium alloy (Ti-17). It is therefore important to discuss the metallurgy, cutting tools and problems associated with the machining of some of the high performance alloys.

Aerospace alloys, such as nickel-base and titanium alloys, are usually employed in the manufacture of components for aerospace, dental, orthopaedic and sea water services because of their unique combination of properties such as high strength at elevated temperatures, resistance to chemical degradation and wear resistance. Ability to maintain these properties at elevated temperatures severely hinders the machinability of these alloys, thus they are generally referred to as 'difficult-to-cut' alloys. Energy consumed in a typical turning operation is largely converted into heat. Most problems encountered during

machining are due to heat generation, mainly during the deformation process and friction at the tool/chip and tool/workpiece interfaces, and the consequent high temperatures [28].

The cutting region usually encounters more intense heat generation when machining difficult-to-cut alloys since the machining process requires more energy than that in cutting a low strength material. The low thermal conductivities of titanium alloy (~8 W/mK), nickel alloy (~11 W/mK) and silicon nitride (~13 W/mK), relative to conventional steels (~50 W/mK for AISI 1045) or cast iron, also lead to a significant increase in temperature at the cutting tool and the workpiece during machining [29].

Other characteristics of aerospace superalloys include their austenitic matrix which makes them work-harden rapidly; their ability to react with almost all the tool materials under atmospheric conditions; their tendency to form built-up edge and to weld to cutting tools; the presence of abrasive carbides in their microstructure. These characteristics cause rapid flank wear, crater wear and notching during machining.

Superalloys are heat-resistant alloys of nickel, nickel-iron, or cobalt that exhibit a combination of mechanical strength and resistance to surface degradation generally unmatched by other metallic alloys. The primary uses of these alloys are in:

- aircraft gas turbines, *e.g.* disks, combustion chambers, bolts, castings, shaft exhaust systems, blades, vanes,
- steam turbine power plants, *e.g.* bolts, blades,
- reciprocating engines, *e.g.* turbocharger, exhaust valves, hot plugs,
- metal processing, *e.g.* hot work tool and dies, casting dies,
- medical applications, *e.g.* dentistry uses, prosthetic devices,
- space vehicles,
- heat-treating equipment,
- nuclear power systems,
- chemical and petrochemical industries,
- pollution control equipment, and
- coal gasification and liquefaction systems [30].

These superalloys (Ni, Fe-Ni, Co-base) are further sub-divided into wrought, cast and powder metallurgy alloys.

Nickel-base alloys contain at least 50% nickel, whereas in nickel-iron-base alloy, nickel is the major solute component. In addition, detrimental elements such as silicon, phosphorus, sulphur, oxygen and nitrogen must be controlled through appropriate melting practices.

Other trace elements such as selenium, bismuth and lead should be held to very small levels (parts per million) for the manufacturing of critical parts.

Many wrought nickel-base superalloys contain 10–20% Cr, up to about 8% Al and Ti combined, 5–15% Co, and small amounts of boron, zirconium, magnesium and carbon. Other additives are molybdenum, niobium and tungsten. Chromium and aluminium are also necessary to improve surface stability [31]. Amongst the commercially available superalloys, 718 stands out as the most prominent alloy in production, accounting for as much as 45% of wrought nickel-based alloy production and 25% of cast nickel-based products.

Nickel-base superalloys have some characteristics that are responsible for their poor machinability. They have an austenitic matrix (face-centred cubic, FCC) and like stainless steels, they work-harden rapidly during machining. Moreover, localization of shear in the chip produces abrasive saw-toothed edges which make swarf (chips) handling difficult. These alloys also have a tendency to weld to the tool material at the high temperature generated during machining.

The tendency to form a built-up edge during machining and the presence of hard abrasive carbides in their microstructure also adversely affects their machinability. For example, in turning operations, depending on the cutting conditions used, these characteristics of superalloys, cause high temperature (>1000°C) and stresses (>3450 MPa) at the tool/workpiece interface, leading to accelerated flank wear, cratering and notching [32].

The nickel-base superalloys harden by the precipitation of a gamma phase of the type $Ni_3(Ti,Al)$, titanium and aluminium being interchangeable. Generally, increasing the amount of gamma phase by increasing the amount of titanium and aluminium increases the rate of tool wear.

As mentioned previously, nickel-base superalloys have a tendency to work harden and retain the major part of their strength during machining. This generates high heat at the interface of the cutting tool and the workpiece giving rise to thermal stresses. Investigations carried out by some researchers regarding the temperature distribution in a tool used to machine nickel-base alloys have shown that the tool temperatures are much higher than with conventional steels, but the temperature gradients are lower [33, 34]. Moreover, the tip of the cutting edge was the hottest spot when machining nickel-base alloys, whilst the maximum temperature when machining steels was always on the rake face, at some distance from the cutting edge.

The properties of Ni-based alloys which contribute to their poor machinability are summarized as follows:

- a major segment of their strength is maintained while machining due to their high temperature properties,
- rapid work hardening occurs during machining, which is a major governing factor contributing to notch wear at the tool nose,
- cutting tools suffer from high abrasive wear owing to the presence of hard abrasive carbides ($M_{23}C_6$, M_6C) in the superalloys,
- chemical reaction occurs at high cutting temperatures when machining with commercially available cutting tool materials, leading to a high diffusion wear rate,
- adhesion (welding) of nickel alloys onto the cutting tool often occurs during machining, causing severe notching as well as spalling on the tool rake face owing to the consequent pull-out of the tool materials,
- production of a tough and continuous chip, which is difficult to control during machining, thereby contributing to the degradation of the cutting tool by seizure;
- poor thermal properties of nickel-based alloys leads to the generation of high temperature at the tool tip as well as high thermal gradients in the cutting tool [29, 30].

1.6.1 Machinability of Austenitic stainless steels

The austenitic steels represent another class of high performance alloys currently used in a variety of applications such as power plants, medical devices, heat exchangers and furnaces. The austenitic stainless steels represent the largest group of stainless steels in use, making up 65–70% of the total for the past several years [35]. The austenitic alloys used most often are those of the AISI 300 series and problems with their poor machinibility are often reported. These problems have been attributed to the work-hardening of the material even at low deformation rates and low thermal conductivity. These characteristics make austenitic stainless steels (γ-SS) more difficult to machine than carbon steels, low alloy carbon steels and non-austenitic stainless steels [3, 18, 35]. The high toughness and high ductility of the austenitic stainless steel lead to the formation of long continuous chips and to the intensive sticking of the workpiece material to the cutting tool surface, which results in an adhesive wear enhancement.

Moreover, high temperatures at the tool/chip interface leads to increase in diffusion and chemical wear [18, 35]. In addition, the built-up edge formation and tearing-off during cutting can also lead to machining force instability, which results in chipping of the cutting edge. A severe condition of attrition wear usually occurring during machining of stainless steels [18]. Some researchers have presented ways to improve machinability of steels by adding oxide-forming elements such as S or Ca [36]. This improvement is associated with the plastic behaviour of the sulphides during machining. Lubricating compounds accumulate on the tool surface, leading to cutting force reduction and lower heat generation.

1.6.2 Machinability and metallurgy of Titanium alloys

Titanium and its alloys are used extensively in aerospace because of their excellent combination of high specific strength (strength-to-weight ratio) which is maintained at elevated temperature, their fracture resistant characteristics, and their exceptional resistance to corrosion. They are also being used increasingly (or being considered for use) in other industrial and commercial applications, such as petroleum refining, chemical processing, surgical implantation, pollution control, nuclear waste storage, food processing and marine applications [37, 38]. In fact, titanium alloys have become established engineering materials available in a range of alloys and in all forms, such as billet, bar, plate, sheet, strip, hollows, extrusions and wire.

Pure titanium undergoes an allotropic transformation at 882°C, changing from the low-temperature hexagonal close-packed (HCP) α-phase to the higher-temperature body-centred cubic (BCC) β-phase [39]. The HCP structure of titanium offers a limited number of slip or shear planes, whereas the BCC structure has more slip systems, therefore enabling more deformation locally wherever the structure has transformed from HCP to BCC. Alloying elements in titanium tend to stabilise either the α-phase, or the allotrope β-phase that amends/alters the transformation temperature and modifies the shape and extent of the α/β field [40]. Elements that raise the transformation temperature are α-stabilisers and these alloying additions include aluminium (Al), oxygen (O), nitrogen (N) and carbon (C), of which Al is an effective α-strengthening element at moderate and elevated temperatures up to 550°C. Elements that decrease the transformation temperature are known as β-stabilisers and they include alloying additions such as molybdenum (Mo), vanadium (V) and niobium (Nb).

Titanium alloys are generally classified into four main groups, according to their basic metallurgical characteristics: α-alloys, near α-alloys, α - β alloys and β-alloys.

- α-alloys: these contain α-stabilisers, usually in combination with neutral elements, and hence have an α-phase microstructure. These α-alloys are used mainly for corrosion resistance and cryogenic applications.

- Near α-alloys: these alloys are highly α -stabilized and contain only small quantities of β-stabilising elements and hence are characterized by a microstructure consisting of α-phase, with only small quantities of β-phase. These alloys behave more like α-alloys and are generally capable of operating at higher temperatures than α-alloys.

- α-β alloys: this group of alloys contains additions of α- and β-stabilizers and therefore possess microstructures consisting of mixtures of α- and β-phases. Ti-6Al-4V and Ti-4Al-2Sn-4Mo-0.5Si are the most common alloys of this category. These alloys can be heat treated to high strength levels and therefore are used mainly for high strength applications at elevated temperatures of between 350 and 400°C.

- β-alloys: these alloys contain significant quantities of β-stabilizers and are characterized by high density, hardenability, improved forgeability and cold formability. Their moderate temperature strength are equivalent to that of α-β alloys, but their elevated temperature properties are inferior to those of the α-β alloys [41].

Despite the increased usage and production of titanium and its alloys, they are expensive when compared to many other metals because of the complexity of the extraction process, difficulty of melting, and problems during fabrication and machining [40, 42]. It was pointed out in 1955 by Siekmann that "machining of titanium and its alloys would always be a problem, no matter what techniques are employed to transform this metal into chips", a statement which is valid even now [43]. Near net-shape methods such as casting, isothermal forging, and powder metallurgy have been introduced to reduce the cost of titanium components. However, most titanium parts are still manufactured by conventional machining methods. Virtually all types of machining operations – such as turning, milling, drilling, reaming, tapping, sawing and grinding – are employed in producing titanium components [44–46].

The machinability of titanium and its alloys is generally considered to be poor owing to several inherent properties of the materials. When ranked in descending order in terms of their machinibility, the materials are: commercially pure titanium, α-alloys, α-β alloys and β-alloys. Titanium is chemically very reactive and, therefore, has a tendency to weld to the cutting tool during machining, thus leading to chipping and premature tool failure.

Possible reasons for making titanium alloys difficult to cut are listed below:

1. The poor thermal properties of titanium alloys make it difficult to machine. Their thermal conductivity is almost ~7 W/m K (for Ti-6Al-4V), while that of stainless steels is ~18 W/m K and that of carbon steels is ~50 W/m K. Therefore the heat generated during the machining operation is concentrated mainly at the tool's cutting edge, causing it to lose its hardness and mechanical resistance leading to rapid degradation of the tool [47].
2. Machining of titanium leads to the formation of very thin chips and therefore an unusually small contact area with the tool and consequently leading to the generation of high stresses at the tip. This combination of small contact chip area and low thermal conductivity leads to the generation of very high cutting temperatures. The maximum temperatures between the tool and the chip can reach 1000°C when turning Ti-6Al-4V alloy at high cutting speeds [48, 49].
3. The ability of titanium alloys to maintain their mechanical properties at elevated temperatures hampers their machinibility as it interferes with plastic deformation needed for chip formation [45].
4. Titanium alloys have high affinity for almost all tool materials, which, along with high temperatures generated in the cutting zone, leads to strong adhesion of workpiece material on the tool edge [50, 51].
5. The low Young's modulus of titanium alloys can lead to chatter and deflection and thereby impairing their machinibility [43, 45].
6. The long stringy swarf along with its tendency to ignite during machining operations makes it difficult to handle.

When machining titanium alloys, a segmented chip is normally produced. This type of chip formation is believed to be due to either the growth of cracks from the outer surface of the chip or adiabatic shear band formation which is caused by the localized shear deformation resulting from the dominance of thermal softening over strain hardening [52–

54]. Recent publications tend to agree that both these methods co-exist when machining titanium alloys [55].

As stated previously, one of the major problems associated with the machining of titanium alloys is their low modulus of elasticity, which can lead to high thrust forces. It is because of the low modulus of elasticity, which causes excessive deflection of the surface being machined, therefore leading to the spring back of the material behind the cutting edge. The work carried out by Fang *et al* on the turning of Inconel 718 and Ti-6Al-4V alloys using un-coated and coated (TiC/TiN/TiCN) carbide tool with an edge radius of 0.06 mm showed thrust force can be higher than the cutting force while machining Ti-6Al-4V alloy [56]. The results indicated that at small feed of 0.075 mm while machining Ti-6Al-4V alloy, the cutting force was less than the thrust force. This was attributed to the magnified effect of the tool edge radius under small feed conditions as well as to the inherent properties of the workpiece material [57, 58].

1.6.3 Cutting tool materials for Superalloys

Nickel-base superalloys are normally machined with WC–Co grades with cutting speeds of around 50 m/min. With the introduction of sialon (Si_3N_4/Al_2O_3) materials, it is possible to increase the cutting speed by a factor of five and recently silicon carbide whisker-reinforced alumina tools have made it possible to machine at cutting speeds of up to ten times those used with cemented carbides [60].

Tungsten carbides can be used in high feed-rate cutting and severe interrupted cutting, but because of their poor thermo-chemical stability, they cannot be used at high speed. Coated carbides on the other hand, have good wear resistance and strength. The introduction of carbide tools has made it possible to machine these alloys at speeds of the order of 50 m/min [60]. However, carbide tools cannot be used for high-speed machining because they cannot withstand the high temperature and stresses in the cutting zone encountered during such machining.

There are two basic ceramic materials that are used as cutting tools: aluminium oxide (Al_2O_3) and silicon nitride (Si_3N_4). The pure alumina ceramic is based on Al_2O_3 but contains a small amount of zirconia (ZrO_2) for added toughness, whilst the mixed ceramic tool is based on Al_2O_3 but contains titanium carbide (TiC) which gives it better thermal properties. Aluminium oxide ceramic has high hardness and high compressive strength. It is chemically stable at very high temperature with respect to nickel and iron [61]. However, it has low fracture toughness and low thermal shock resistance. This white

ceramic is chemically very stable and inert to most aggressive environments, which makes it suitable for high-temperature applications. However, it has worse thermal and mechanical shock resistance properties than the tungsten carbides. The fracture toughness of alumina ceramics can be improved by adding zirconia, whilst its thermal shock resistance properties can be improved by the addition of titanium carbide or titanium nitride. Adding titanium carbide makes the material black, whilst alumina with titanium nitride is dark brown in colour. These mixed aluminas are thermally tougher and retain their hardness at high temperature. These mixed alumina tools have been reported to be successful in machining nickel-base alloys because of their improved thermal shock resistance properties.

Another material that is used as a cutting tool for superalloys is *silicon nitride-based ceramics*. Silicon nitride ceramics are two-phase materials consisting of silicon nitride crystals in an inter-granular bonding phase [60]. This material can be yttria-stabilized silicon aluminium oxynitride. A mixture of alumina (~13%), silicon nitride (~77%), yttria (~10%), and aluminium nitride is used as the sintering material to produce sialon ceramics. The main advantage of this ceramic is its high toughness. It is much tougher than alumina-TiC and is used for the rough machining of nickel-iron-base superalloys. Due to their superior mechanical and thermal properties, these tools can be employed to machine nickel-base alloys at higher cutting speed and feed rate compared to those for mixed alumina tools.

Cubic boron nitride is one of the hardest materials available after diamond, and does not occur in nature. The synthesis of polycrystalline CBN is composed of about 50–90% CBN and ceramic binders such as titanium carbide and titanium nitride. A high CBN content helps whilst cutting superalloys. Higher CBN content generally increases chipping resistance. It has been reported that whilst turning Inconel 718, the performance of tools with high CBN content was better because of their high hardness. Compared to other ceramics, CBN has better hardness and resistance to fracture but poorer chemical resistance. These tools are used to machine nickel- or cobalt-base alloys of hardness equal to or greater than 340 H_V.

1.6.4 Cutting tool materials for Titanium alloys

High cutting temperatures, high mechanical pressure and high dynamic loads in the machining of titanium alloys, result in plastic deformation and/or rapid tool wear. Cutting tools also suffer from the strong chemical reactivity of titanium while machining titanium

alloys. As mentioned previously, titanium and its alloys react chemically with almost all tool materials available at cutting temperatures in excess of 500°C due to their strong chemical reactivity. The tendency for chips to pressure-weld to cutting tools, severe dissolution-diffusion wear, which rises with increasing temperature, and other peculiar characteristics already mentioned, require additional criteria in the choice of the cutting tool materials for titanium alloys.

Two categories of carbide tools are available for commercial machining of titanium alloys, namely: straight and mixed grade carbides. The usual composition of straight grade carbides is 6 wt % Co and 94 wt % WC, with the composition of cobalt varying from 5 to 12 wt %. The mixed grade carbides have titanium carbide (TiC), tantalum carbide (TaC) or niobium carbide (NbC) and may also include the addition of other rare-earth elements to the base composition of the straight grade. Straight tungsten carbide (WC/Co) cutting tools have established their domination in almost all machining processes of titanium alloys and interrupted cutting (end milling, tapping, broaching, *etc*), whereas drilling and reaming being performed best by high-speed steel tools [62, 63]. Many researchers studying the machinibility of titanium alloys, have suggested that straight cemented carbide (WC-Co) with a cobalt content of 6 wt % and WC grain size of between 0.8 to 1.4 µm gives the optimum performance [63, 64]. Milling of titanium alloys is carried out at cutting speeds between 11 to 140 m/min and feed rates of between 0.04 to 0.15mm per tooth whereas the cutting speeds are limited to about 45 m/min in turning operations, when using straight grade cemented carbides [65, 66]. Machining of titanium alloys at higher cutting speeds will cause rapid chipping of the cutting edge, leading to catastrophic failure of the inserts. Rapid cratering and or/plastic deformation of the edge will be the outcome of machining titanium alloys at higher cutting speeds [64, 66, 67]. This is due to the temperature generated which tends to be concentrated at the cutting edge closer to the nose of the carbide inserts. It has been computed by means of finite-difference methods that the maximum temperature between chip and the tool reaches 1400°C when machining Ti-6Al-4V alloy at a cutting speed of 120 m/min [68]. Most often tool failure occurred when machining titanium alloys, failure was due to adhesion, diffusion and attrition wear mechanisms. Chipping is the major failure mode when titanium alloys are milled using un-coated and coated carbide tool. Chipping of the carbide tools while machining titanium alloys takes place due to the combination of high temperatures, high thermal, mechanical and cyclical stresses as well as due to the adhesion of the workpiece material on the tool faces [69]. The performance of the mixed grade tungsten carbide has been found to be

inferior to the straight tungsten carbide tools while machining titanium. This is due to the high diffusion rates of TiC and TaC, which cause the preferential dissolution of these carbides from the tool [64].

Research carried out by Waiter [70] showed that straight cobalt-base tungsten carbide cutting tools ion-implanted with either chlorine or indium was very effective in the machining of titanium and its alloys.

Even though ceramics have improved in quality and found increased application in the machining of difficult-to-cut materials, especially high-temperature alloys (such as nickel-based alloys), they have not replaced cemented carbides and high-speed steels due to the poor thermal conductivity of most ceramics, relatively low fracture toughness and their reactivity with titanium [71].

The super-hard cutting tool materials (cubic boron nitride and polycrystalline diamond) have also shown a good performance in terms of wear rate in the machining of titanium [41]. However, their applications are limited due to their high price.

To attain higher cutting speeds, it is imperative to suppress the cutting temperatures at the tool/workpiece interface, by dissipating heat quickly [63]. It was found by Wang *et al*, that the tool life can be improved by a factor of three if liquid nitrogen was applied as a coolant instead of conventional cutting fluids when performing turning operations on titanium alloys. However, this requires expensive modifications in the machining setup [72].

A novel solution to prevent rapid wear and plastic deformation of the tool edge is to use rotary tools that rotate around the tool axis, thereby providing a fresh cutting surface. By using this technique, the effect of heat on the cutting edge is reduced, therefore reducing softening and diffusion wear. However, this technique requires specialized machine tool equipment and there are limited workpiece geometries that can be machined [73].

1.6.5 Tool coatings

High speed steels, tungsten carbide and ceramic tools are often coated to increase tool life and allowable cutting speeds. Coatings act as a chemical and thermal barrier between tool and the workpiece; they increase the wear resistance of the tool, prevent chemical reactions at the interface, reduce built-up edges, decrease friction between the tool and chip or between tool and the workpiece, and prevent the deformation of the cutting edge due to excessive heating. Coated tools can be used at higher cutting speeds, provide longer tool life than uncoated tools, and broaden the application range of a given grade of tool.

Moreover, coatings may also lead to improvement of the workpiece surface after machining [74, 75].

A number of factors affect coatings performance, including the coating's thickness, hardness, chemical compatibility and interfacial adhesion with the substrate, crystal structure, chemical and thermal stability, elastic modulus, fracture toughness, wear resistance, thermal conductivity, diffusion stability, frictional properties, as well as the tool geometry and the intended application.

1.7.0 Surface engineering

Surface engineering involves changing the properties of the surface and near-surface region in a desirable way. Surface engineering can involve an overlay process or a surface modification process. In overlay processes a material is added to the surface and the underlying material (substrate) is covered and is not detectable on the surface. A surface modification process changes the properties of the surface but the substrate material is still present on the surface.

A useful working definition of the term *surface engineering* is, "**treatment of the surface and near-surface regions of a material to allow the surface to perform functions that are distinct from those functions demanded from the bulk of the material"** [76].

The choice of a particular coating/treatment depends on many factors such as surface preparation, processing/fabrication temperatures, working temperature, applied load, relative velocity, counter face material to be in contact, lubrication and the cost [77].

Although the surface normally cannot be modified independent from the bulk, the demands on surface and bulk properties are usually very different. For example, in the case of a turbine blade for a high-performance jet engine, the bulk of the material must have sufficient creep resistance and fatigue strength at the service temperature in order to provide an acceptable safe service life. The surface of the component, on the other hand, must have sufficient resistance to oxidation and hot corrosion under the conditions of service to achieve the same performance as that of the bulk material.

Surface engineering will remain a growth industry in the future, because surface-engineered products increase performance, reduce costs, and control surface properties independently of the substrate, thus offering enormous potential due to the following:

- creation of entirely new products;
- solution of previously unsolved challenging (engineering) problems;

- improved functionality of existing products – engineering or decorative;
- conservation of scarce materials.

In general, coatings are desirable/necessary, for a variety of reasons including economics, materials conservation, unique properties, or design flexibility which can be obtained by separating the surface properties from the bulk properties. Numerous coatings and surface treatments have been developed and applied to improve wear and reduce corrosion of engineering components and metal machining tools. The choice of a particular treatment/coating depends on numerous factors: processing / fabrication temperature, temperature of the working environment, applied load, relative velocity, counter-face material to be in contact, lubrication and the environment itself. Coatings can be hard or soft, thin or thick, porous or dense, single or multi-layer depending on the application [76, 77].

1.7.1 Introduction to wear

When two surfaces move relative to each other under load, one or both of the surfaces will experience wear, *i.e.* loss or displacement of material. Wear is a complex phenomenon as it occurs by many mechanisms and hence there is no universally-accepted classification of the process. However one popular wear mode classification, which is quoted by many researchers, is based on Burwell and Strang and contains four categories – *adhesive, abrasive, fatigue* and *corrosive* [22]. However various sub-mechanisms of wear can be found within each category [23, 24]. These mechanisms are principally concerned with wear debris-creation, modification and eventual ejection out of the system.

Adhesive wear, also known as sliding wear, can occur when two similar or dissimilar materials slide against each other. Under mild wear situations, some oxidation can also take place. The presence of hard debris particles may lead to further self-initiated abrasive wear. Adhesive wear is further categorized into mild wear, severe wear and scuffing. Galling and seizure represent severe forms of adhesive metal transfer. *Abrasive wear* is due to the presence of hard asperities of the counter face material or loose particles at the sliding interface. Depending on the size and shape of the abrasives, load and other conditions, various recognized mechanisms of abrasive wear can occur – machining wear, low stress sliding abrasion, three-body abrasion and gouging abrasion.

Fatigue wear occurs due to repeated loading either the result of asperity movement at the micro level or to gross movement of the counterface. Contact fatigue, cavitation erosion

and delamination are some of the types of damage related to fatigue wear. When the environment contains reactive constituents the engaging surfaces may form reaction products such as oxides, hydroxides, *etc*. These surface films may consequently be removed by rubbing actions, thus exposing naked, new surface to the environment. The combination of tribological and corrosive actions leads to enhanced material removal and thus a synergism is established. For example, *fretting wear*, one of the types of *corrosive wear***,** is due to small amplitude oscillation or vibrational movement [25]. A schematic diagram for all the major types of wear is presented in Figure 1.10.

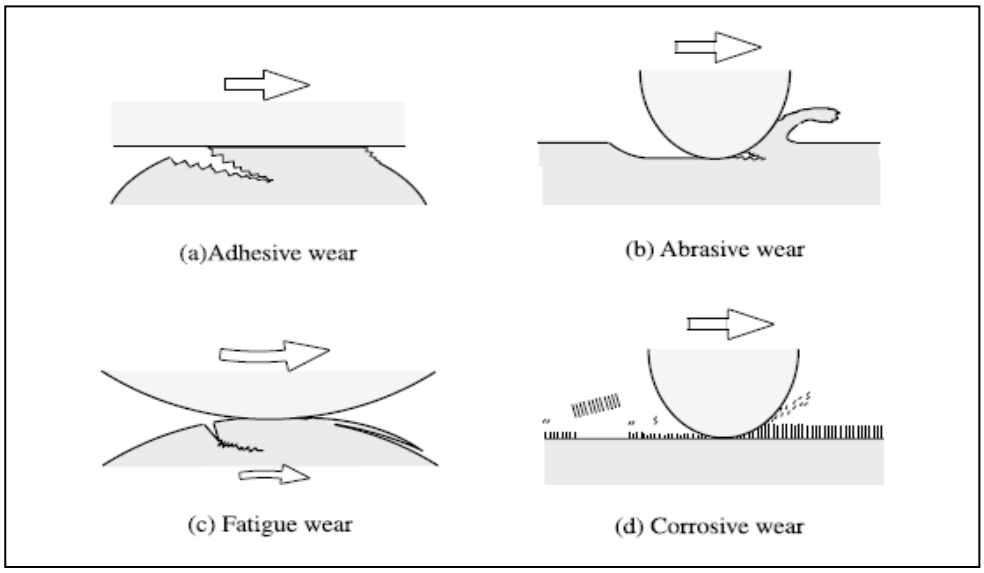

Figure 1.10. Schematic images of four representatives wear modes [25].

1.7.2 Wear of metal cutting tools

Wear of cutting tools occurs by many modes – abrasion, adhesion, diffusion, thermal softening, oxidation, micro chipping, fatigue, *etc*. These various modes of wear, however, can be grouped into the four types already discussed previously. Depending on cutting speed, feed rate, geometry of contact, lubricant/coolant, tool material and work material, one or more modes of wear dominate the machining process. Generally, under mild conditions (low speed and feed rate) abrasive wear dominates, whereas under more severe machining conditions thermal properties are important – here diffusive wear and oxidation may occur simultaneously with plastic deformation or softening of the tool. Kramer and Judd have developed a model of cutting tool wear based on Rabinowicz's abrasion theory [78] and the free energy of chemical dissolution. Although these models have limited scope because of simplification, it is possible to at least rank various materials which can

show potential as coatings for cutting tool applications. The major issue, however is that wear of cutting tools is not as simple as that predicted or assumed in various models. For example, the presence of small hard inclusions in a workpiece material will wear the tool at a higher rate than expected and the resultant change in the geometry due to this wear will influence the cutting conditions and the subsequent wear of the tool. Furthermore, the occurrence of a built-up edge leads to a situation where a layer of workpiece material on the cutting edge is, in effect, involved in the overall process. It must be stated/realized that the solubility in concept is only applicable to pure metals. Such information is not generally available for more complex *e.g.* metal/ceramic systems and this constitutes a major gap in knowledge and understanding of the coatings systems.

1.7.3 Wear surfaces

Cutting tools wear because normal loads on the wear surfaces are high, the machined chips and workpiece that apply these loads are moving rapidly over the wear surfaces. The cutting action and friction at these contact surfaces increase the temperature of the tool material, which further accelerates the physical and chemical processes associated with tool wear. Cutting tool wear is localized on specific surfaces where stress, strain, velocity and temperature are above critical levels. It is important to understand the points where these critical conditions exist and how they interact to cause tool wear.

Along the rake surface, the chip motion and high normal stress produce a wear scar called 'crater wear'. Along the clearance surface, the tool motion and high normal stress increase the area of contact between the tool and work, producing flank wear.

'Flank wear' decreases the diameter of the end mills as well as the depth of cut for a lathe tool. Both these changes in the geometry of the cutting tool produce 'out-of-tolerance' dimensions on machined parts. The edge wear and crater wear on the rake surface modify the state of stress and strain in the cutting region, thereby changing cutting forces and the mechanics associated with the machining process. Severe geometric changes that decrease the angle between the rake and clearance surfaces can weaken the tool so that the edge may suddenly fracture.

1.7.4 Metallurgical aspects of coatings

A working coating system involves two important, critical interfaces – Interface 1 between the coating and the environment or workpiece material and Interface 2 between the coating and the substrate, as depicted in Figure 1.11 [76]. The specific requirements of/at these

interfaces are strict and often contradictory. For example, in metal cutting or metal forming operations, excellent coating adherence is required at Interface 2 whereas at Interface 1 no adhesion (or welding) of work material to the tool (coating) is desirable. In the final analysis, therefore, a single coating probably cannot match these fundamentally differing requirements.

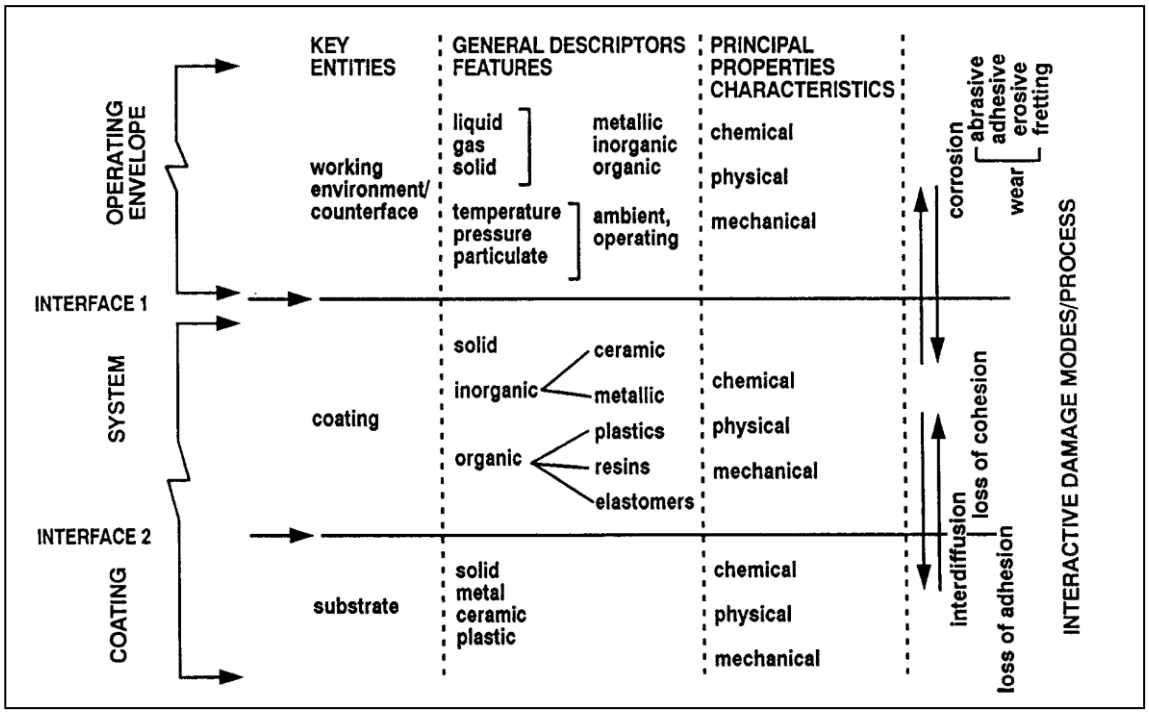

Figure 1.11. Generalized features of a working coating system [76].

As stated previously, coatings and modified surfaces are useful in combating wear of tools and components and enhancing manufacturing efficiency. In recent years PVD TiN coatings have become widely used in many applications. The success of TiN in general can be attributed to its wear resistance (associated with various key characteristics and properties) corrosion resistance and to its colour – golden yellow which serves as a very good marker. However, traditional hard coatings of TiN cannot meet the requirements, especially under extreme condition, because of relatively low hardness (~2000 Hv), high friction coefficient (> 0.4), insufficient corrosion resistance and inadequate thermal stability. Moreover, many other materials have been shown to perform equally or better than TiN [79–81].

As mentioned previously, TiN coatings are well established and have been used for a long time. New coatings such as TiAlN and TiCN are found to be harder than TiN, but lack toughness and therefore are difficult to use under certain conditions [82]. Multi-component coatings based on titanium have shown high potential due to their superior

hardness, oxidation and wear resistance [83]. However, just a few TiAlMeN coatings (Me = metal, *e.g.* Si, Cr and V) are established, in which different constituent metals play different roles. For example, Si refines the grain size, and therefore increases the hardness according to the Hall-Petch relationship, Cr improves the oxidation resistance, and vanadium provides low friction resistance at certain application temperatures [84–86]. It has also been shown that by depositing thin layers of metal nitride, less than few nanometres of coatings, such as VN, NbN, TiAlN and CrN with interlayers of TiN, leads to the growth of hard coatings which are fully cubic in structure. This interlayer, which is usually in a narrow range of 4–20 nm, is the most important parameter in affecting the hardness of the coating [87]. Several explanations have been proposed, including dislocation blocking due to layered interfaces, Hall-Petch strengthening effect, strain effects and the super modulus effect. This 'superlattice' concept is based on the deposition of a layered structure of two materials with the same crystal structures, where the interface would provide the energy barriers to the movement of dislocations [88]. These types of coatings show far superior performance as compared to single layered coatings. These coatings have been applied on carbide tools, which have been used to machine superalloys such as Inconel 718 [87].

Chromium nitride films with their good oxidation and anti-adhesive properties, have found a wide industrial use in metal cutting industries. These coatings have not been used successfully in the steel industry due to their low hardness and low abrasive wear resistance [89]. These properties have been improved by alloying with another metal – usually aluminium – to form a ternary hard coating. One of the major advantages of these ternary Al-Cr-N systems is the stabilization of the cubic AlN phase even at high aluminium concentrations of between 65–75% [90]. It has been reported that the addition of aluminium to CrN, increases the hardness in comparison to pure CrN [91]. Moreover, this not only increases the hardness, but also the wear resistance is improved in comparison to conventional TiN and TiAlN [92]. Exceeding the solubility limits of Cr, results in a hexagonal wurtzite structure and the mechanical properties degrade [93].

The modern paradigm is the use of nano-structured multi-layered coatings. These coatings have a specific structure consisting of alternate nano-layers of various compounds, which results in outstanding physico-mechanical properties, especially at high temperatures and under hard conditions [94]. The thermal barrier of these coatings is affected by the presence of interfaces between various layers [95]. Investigations of nano-layered coatings

which contain vanadium nitride, niobium nitride, tantalum nitride, chromium nitride and tungsten nitride have been carried out by various researchers [96–99]. However, limited information exists about the wear resistance of these coatings under dry machining conditions.

In the following subsections, various parameters are discussed in order to enhance the understanding of their effects on coating performance.

1.7.5 Microstructure of coatings

Coatings may be amorphous or crystalline, dense or porous, depending on the processing conditions. Generally amorphous coatings are denser than crystalline ones, and especially those with columnar morphology because of the presence of pores between the columns of the grains. A third important parameter in the PVD process is the substrate bias voltage. The average grain size of TiN coatings is less than 1 μm, often <0.1 μm. In some circumstances even sizes of 5–10 nm are not uncommon. A coating often develops a texture due to preferred direction of material growth. Texture is determined by the substrate material and parameters (surface finish, condition, composition, *etc*) and process variables (temperature, gas pressure, *etc*).

In the last two decades, attention has been focused on the potential of multi-layer coatings due to superior hardness, modulus, toughness and wear resistance [100]. Specific multi-layer coatings have been shown to perform better than their single layer constituents in metal cutting and metal forming applications. Multi-layers may involve just two layers or more than 1000 layers (although a total thickness of less than 5 μm). When individual layers are very thin (few atomic layers) the resultant entity can be considered to be similar to a modulated composition [101]. It has been demonstrated recently that by optimizing the thickness of the individual layers, the hardness of the coating can be maximized.

1.7.6 Coating hardness

The measured hardness of a coating depends on its bonding structure but also the way in which it is deformed during hardness measurement. Coating materials with high degrees of cohesive energy, covalent bonding and short bond length exhibit high inherent hardness. High cohesive energy of a coating material however does not necessarily mean higher hardness, as measured by indentation methods. This is because the hardness of a coating system depends upon other factors such as composition, microstructure, texture, substrate material, indentation load and testing method. The composition of a coating should be

controlled to appropriate stoichiometry for consistent hardness (and other properties). To achieve higher hardness, the grain size of the coating should be finer, as stated in the well-known Hall–Petch relation [102, 103], shown in Equation 1.3:

$$\sigma_y = \sigma_0 + k_y d^{-1/2} \quad \textbf{(}\text{Equation 1.3)}$$

Where, 'k_y' is the strengthening coefficient (a constant unique to each material), 'σ_o' is a materials constant for the starting stress for dislocation movement (or the resistance of the lattice to dislocation motion), 'd' is the grain diameter and 'σ_y' is the yield stress. Other possible strengthening mechanisms include compressive stresses induced during the coating process, solid solution hardening, second phase hardening by precipitates, and multi-layer (modulated structure) strengthening. Second phase hardening due to whiskers is not generally possible with PVD techniques, although it is currently employed in other coatings, for example, those developed by plasma spraying.

1.7.7 Coating roughness

The surface roughness of a material significantly influences the tribological performance of a mechanical system. If, for example, the harder member of an assembly is rough, the second face may wear by abrasion due to micro cutting or micro ploughing mechanisms. It has been clearly established that under lubricated conditions the relative dimensions of the asperities and the lubricant film thickness are critical in avoiding metal-to-metal contacts *i.e.* to efficient lubrication and lower resultant friction and wear. Rough tool surfaces are not preferred in metal forming industries for obvious reasons – the surface finish of the product generally replicates the tool surfaces.

The cost of producing smoother surfaces increases exponentially. Cost is considered to be a major factor in specifying surface roughness for a product. Generally most of the thin coatings produced by PVD techniques simply reproduce the substrate roughness. It has been shown by many workers that, the rougher the surface finish, the lower the coating adhesion, as measured by scratch testing methods. As the work material slides against a tool surface the contacting points are at the asperity levels and thus the total load is borne by these asperities. When a hard coating is on a rough surface it is more easily removed than a coated smooth surface. A primary concern then is how smooth a substrate surface should be before coating in order to obtain an optimum performance in the system.

1.7.8 Thermal properties of coatings

Thermal conductivity or thermal diffusivity of a material is considered to be important in all tribological situations as it influences strongly the temperature at the rubbing surfaces. The maximum temperature reached at the surface is not just influenced by a sliding body but also by the counter surface. This is true for both bulk and flash temperatures (the temperature experienced at the macro scale and micro scale, respectively).

Under metal cutting conditions wear occurs by many mechanisms as discussed previously. At high cutting speeds and feed rates, the temperature reached at the interface is extremely high, sometimes close to the melting point of the work material. Therefore, in these situations failure of the tool is either due to abrasion/diffusion or softening of the tool. It is generally agreed that the cutting performance of a tool is related to its high temperature hardness apart from other properties such as chemical stability (free energy of formation) and fracture toughness. A good insulating coating not only protects the substrate but also reduces the risk of cracking due to thermal expansion which is discussed below.

Thermal expansion – especially the relative values of the coating and substrate – is critically important in determining the extent of thermal stresses developed. Ideally, the coating and substrate should have similar thermal expansion coefficients. Furthermore, the actual thermal stress developed is determined by the elastic modulus and thermal expansion coefficients. Since a mismatch between the coating and the substrate may result in spalling, care should be taken in the selection of the coating and substrate materials. An intermediate layer, whose coefficient of thermal expansion lies between that of the substrate and the coating, may be useful in reducing such thermal stress problems.

As mentioned previously, the two most common coating processes are Chemical Vapour Deposition (CVD) and Physical Vapour Deposition (PVD). Both are used for depositing single and multi-layer coatings. CVD coatings are generally applied at much higher temperatures (typically 1000°C) than those used for PVD coatings (typically 500°C). CVD coatings are generally between 5 to 15 μm thick, whereas PVD coatings vary between 2 and 5 μm. In general, the metallurgical bond that is formed in CVD coatings and the tool is stronger than the mechanical bond that is produced in PVD coatings. As a result, the CVD coatings provide longer tool life when properly applied. However, the temperature requirements in CVD coatings processes reduce the range of substrate materials to which these coatings can be applied. PVD coatings are essentially free of thermal cracks that are common in CVD coatings. Generally, PVD coatings are better suited for precision HSS, HSS-Co, and solid WC tools. PVD coatings are generally fine

grained and are usually smoother than CVD coatings, which build up on sharp corners [79].

Coating/substrate compatibility can be improved by applying one or more intermediate layers between the coatings and the substrate material in order to balance the chemical bonding and thermal expansion coefficients, resulting in a multi-layer coating system which optimizes tool performance by providing resistance to several kinds of wear. Multilayer coatings are very common for turning and boring inserts because they provide the best combination of properties.

1.7.9 Coatings for metal cutting tools

Enhancing the performance of cutting tools is an economically important goal and coating technologies contribute significantly to achieving this. Surface coatings improve the tribological properties of the cutting tools in an ideal way, and therefore allow the application of tough or ductile substrate materials. The market for surface engineering in the UK in the 20th century was estimated to be in the order of at least £600 million, with the products of over £12 billion pounds being manufactured using some form of surface engineering [104]. Measured by value, more than 40% of all cutting tools are coated in modern industry today. The market share of the coated tools is growing continuously as different tools and cutting operations need different coatings [105]. The suitable coating processes for metal cutting tools are CVD and PVD technologies. Both are competing deposition technologies and permit the deposition of thin hard coatings (about 3-12 μm) on cutting tool materials. The development of these coatings has eased the machining of ferrous alloys (cast iron and steel) and were termed as "first generation" wear protective coatings. However, there were problems associated with these coatings, due to the formation of brittle phases (η-phase) at the interface, resulting in their sensitivity to impact and strain of the cutting edges. The η-phase formation was largely suppressed during the 1970s, by balancing the carbon proportion in the CVD processes. The resulting ductility had two effects: it improved the machining reliability for application conditions and permitted the increase of film thickness up to *circa* 6–7 μm, and thereby increasing the tool life. These were termed as "second generation" coatings.

In 1972, "third generation" CVD coatings were produced, and were characterized by the deposition of multi-layer and gradient structures and thereby achieved various aims. In many cases, TiC is used as a bond layer to improve adhesion, and hence takes the abrasive

loads which the softer layers could not withstand. The transition between TiC and TiN is often observed by one or more Ti(C,N)-layers arranged in steps or with graded compositions, providing a high adhesive strength between the different multi-layered coating structures. The "fourth generation" CVD coatings were developed in 1980s and consisted of many thin films, permitting a higher total coating thickness (8–12 μm) for many applications. With these complex structured CVD multi-layer coatings, improvement in cutting performance was achieved compared to uncoated tools or the tools coated with a monolayer, especially in continuous machining processes, such as turning. For high cutting speeds, these coatings with chemically inert interlayers or top layers (Al_2O_3, ZrN), are often combined with P or M grade cemented carbides as substrates. Higher requirements concerning ductility, thermal shock and abrasion resistance have to be met for more demanding cutting conditions, such as dynamically alternating cutting forces, *e.g.* milling. However, CVD coated cemented carbides were unable to become generally accepted for milling high strength steels, due the cutting edge chipping off and due to embrittlement at the coatings/substrate interface arising from the coating deposition process [106]. The operating temperatures in the CVD process are also a problem for coating other substrate materials. Ni-based cermets, like the cemented carbides, show a significant embrittlement at high coating temperatures. Moreover, in CVD processes due to the higher processing temperatures, nickel diffuses from the substrate to the coatings, which reduces coating adhesion and wear resistance. In practice, high speed steels cannot be coated with CVD or plasma activated (PA) CVD processes due to their softening temperature of around 550°C [27].

CVD has several important advantages which make it the preferred process in many cases. These can be summarized as follows:

- It is not restricted to a line-of-sight deposition which is a general characteristic of sputtering, evaporation and other PVD processes. As such, CVD has high throwing power. Deep recesses, holes, and other difficult three-dimensional configurations can usually be coated with relative ease.

- The deposition rate is high and thick coatings can be readily obtained and the process is generally competitive and, in some cases, more economical than the PVD processes.

- CVD equipment does not normally require ultra-high vacuum and generally can be adapted to many process variations. Its flexibility is such that it allows many changes in composition during deposition and the co-deposition of elements or compounds is readily achieved.

CVD coating technologies are, however not universal coating methods. They have several disadvantages, a major one being that they are most versatile at temperatures of 600°C and above, a temperature range in which many substrates are not thermally stable or where costly heat treatments would be negated. However, the development of plasma-CVD partially offers a solution for this problem. Another disadvantage is the requirement of having chemical precursors (the starter materials) with high vapour pressure which are often hazardous and at times extremely toxic. The by-products of the CVD reactions are also toxic and corrosive and must be neutralized, which can be a costly operation.
The disadvantages of the CVD, as described above, led to focus on PVD process technologies. PVD processes take place at lower temperatures, typically around 350–550°C, thus avoiding the above mentioned difficulties.

1.7.9.1 PVD-coated metal cutting tools

The first generation of PVD-coated tools featured TiN as the hard coating and was applied on tools used for interrupted cutting, such as milling. The superior performance of these PVD TiN coatings led to their applications to other machining operations such as turning and as wear resistant or protective layers on dies. The success of the first generation PVD coated tools led to the development of the second and third generation PVD coatings, such as TiCN, TiAlN, and AlCrN which offered higher productivity [107–110].
As stated previously, a very important characteristic common to all the PVD process is the low deposition temperatures compared to CVD processes. These range between 350 and 500°C and permit the coating of HSS tools without the loss of hardness in the substrate material [111]. The coating of high speed steel tools – especially drills and end mills, but also plain milling cutters, broaches, and other cutting tools – represent a wide spectrum of applications in which the PVD technology had quickly established itself during the 1980s.
Although research of PVD processes started with coating depositions on cemented carbide substrates, the significance of coating temperature for this application had not been fully recognized for a long time. On the contrary, when comparing PVD and CVD processes, the better efficiency of CVD coating processes, owing to their larger batch size and their

outstanding wear performance in smooth cutting, based on increased coating thickness and multi-layered coating structures, was placed in the foreground. Consequently, PVD coatings were practically not applied for coating cemented carbides until the 1990s. This situation changed when different studies indicated clearly that embrittlement occurred with CVD coated cemented carbides, which can be avoided with PVD coatings [112]. For PVD-coated cemented carbides, no brittle phases (η-phase) are formed at the interface or in the substrate volume and no other embrittling material changes take place due to the low coating temperatures. Furthermore, the outstanding mechanical properties of cemented carbide can only be effectively utilized through PVD coatings. The adhesion-reducing effects of hard coatings, *e.g.* TiN, prevent, in lower ranges of cutting speed, micro-weldings and the formation of built-up cutting edges and thus avoid stress peaks and mechanical overloading of the cutting edges, which will lead quickly to break-out and chip-off compared to uncoated cemented carbides. The application of PVD coatings to machining tools was restricted to TiN for a considerable time. TiN is still popular today as a coating for cutting tools (reamers, twist tools and cold forming tools). Over the last few decades, TiN coatings have been successfully applied to solid round carbide tools as well as carbide metal cutting inserts and have offered performance advantages in applications involving interrupted cuts and/or those requiring sharp edges, as well as finishing and other operations. The data on the cutting performance of coated multi-point cutting tools (such as tungsten carbide tipped bandsaws and circular saws) are sparse, but some work carried out, suggests strongly that coated multi-point tools offer improved performance and tool life when compared to uncoated cutting edges [113]. Binary hard materials, *e.g.* TiC or ZrC, cannot be deposited easily in PVD processes and show no favourable properties for practical use. However, different research studies have already shown in the mid-1980s that with ternary hard materials, *e.g.* Ti-C-N or the metastable Ti-Al-N, PVD coatings for specific applications with a superior cutting performance can be produced [114]. The high stability and increased hardness of complex hard materials compositions are due to the formation of mixed crystals by substitution, and this has positive effects on wear properties of coating materials systems. In various investigations, ternary hard materials within the system Ti-Zr-N, Ti-Hf-N, Ti-Nb-N, Ti-V-N and Ti-Cr-N show better performance compared to simple TiN [115]. This is also true for quaternary hard materials, *e.g.* Ti-Al-V-N. [116].

The residual stress state and the formation of microstructure in PVD coatings can be controlled by coating process parameters and will influence the wear behaviour. It is well

established that compressive stresses in coatings have proven to be beneficial for many wear and cutting applications. Recently, zirconium nitride (ZrN) films have attracted increasing interest for various applications in hard and wear resistant coatings, because of their favourable mechanical properties, and they have shown better results than TiN-coated tools during drilling tests [109]. A recent development in PVD-coated tools is to enhance the cutting performance of the tools by multi-layer structures, which is to increase the coatings thickness (from 3–5 μm to about 10 μm) and the deposition of multi-layer coatings containing Al_2O_3 films. Al_2O_3 is an excellent choice for incorporation in tool coatings due to its retained hardness at elevated temperatures, its low solubility in many workpiece materials, as well as high thermal and chemical stability [117]. The historical development of coatings on carbide tools is shown in Figure 1.12.

There are several advantages of PVD processes over competitive processes such as electrodeposition, CVD, and plasma spraying and they are listed below:

- Extreme versatility in composition of deposit. Virtually any metal, alloy, refractory or intermetallic compound and their mixtures can be easily deposited. In this regard, they are superior to any other deposition process.
- The ability to produce unusual microstructures and new crystallographic modifications, *e.g.* amorphous deposits.
- The substrate temperature can be varied within very wide limits from sub-zero to high temperatures.
- Ability to produce coatings or self-supported shapes at high deposition rates.
- Deposits can have very high purity.
- Excellent surface finish which can be equal to that of the substrate.
- Elimination of pollutants and effluents from the process which is a very important ecological factor.

There are, however, certain limitations of PVD deposition techniques, *viz*:

- Adhesion to substrate material is sometimes marginal (low deposition temperature)
- Thickness limitations arising from uncontrolled residual stress.
- Inability to deposit polymeric materials.
- Higher degree of sophistication is required of the processing equipment and hence a higher initial cost.

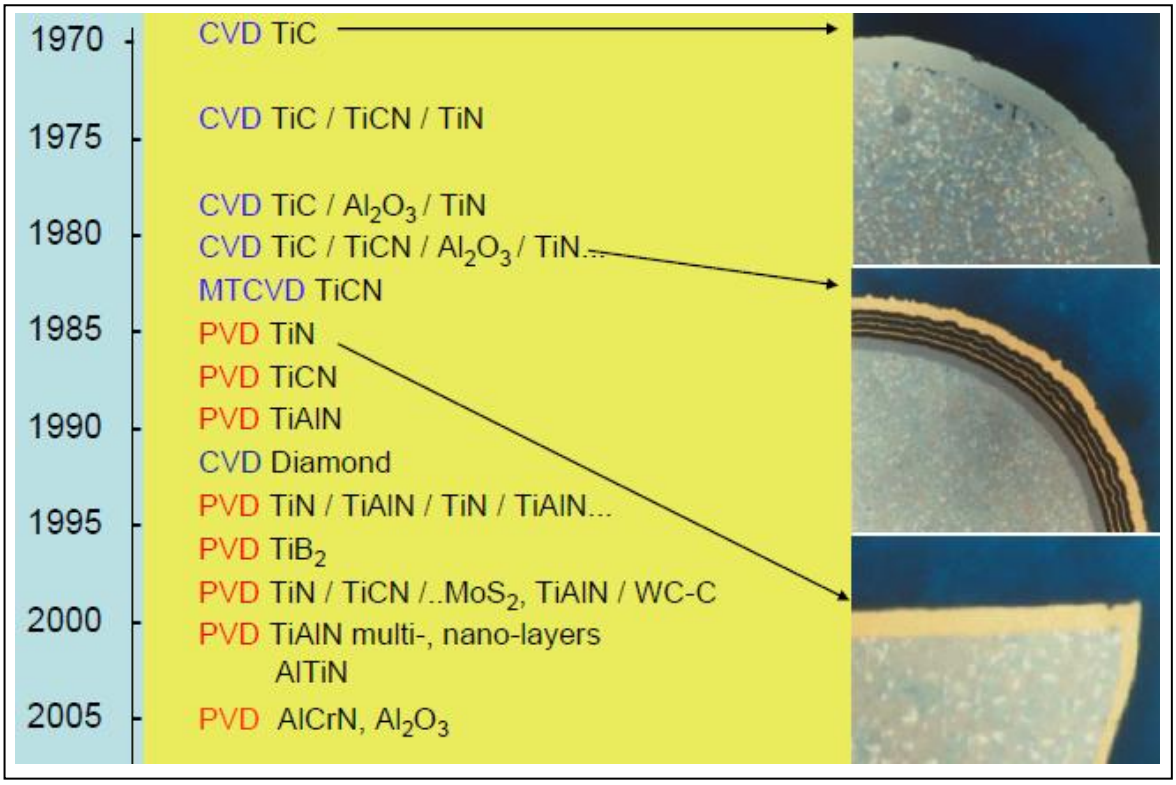

Figure 1.12. Historical coatings development on carbide tool, starting from first CVD TiC coating to first PVD TiN coating on sharp edge [79].

There are four basic types of equipment in use for depositing PVD tool coatings, and they all fall under the broad category of ion plating [118]. The four PVD hard coating techniques are:

- low voltage electron vapour deposition;
- cathodic arc deposition;
- triode high voltage electron vapour deposition; and
- magnetron sputtering.

The differences between the four types are: the way the source material is vaporized (evaporation of sputtering), the way plasma is created, and the number and the types of ions, electrons and the gas atoms that constitute the plasma [119]. Each of these techniques will be described briefly.

1.7.9.2 Low voltage electron vapour deposition

The low voltage electron beam evaporation process is very effective in ionizing the evaporating reactive gas atoms, and estimates have put the amount of ionization at 50%. Low voltage electron beam deposition is an excellent process for producing a very hard and smooth TiN, which has become the industry standard.

1.7.9.3 Cathodic arc deposition

The cathodic arc process uses an electric arc to flash evaporate material from the surface of the target or source, and the evaporating material and the reactive gas become highly ionized. It is estimated that 90% of the vaporized material is ionized and the high degree of ionization helps to promote the reaction and to form a fully dense, well-adhered coating. The problem with the conventional cathodic arc process is that it produces 'macro-particles', which are metal droplets, 1 to 10 μm in diameter, ejected from the target surface that become embedded in the coating [120, 121].

For many tooling applications, these macro-particles are not harmful, but they can be detrimental with respect to the surface finish. Variations of the arc process, such as the steered arc or the filtered arc, have been very successful in reducing the number of macro-particles in the coating, but they reduce the deposition rate during the sputter etch step, which is common to all PVD tool coating processes. All the processes use ions to bombard and clean the substrates prior to coating. All methods except the cathodic arc process use argon ions for this cleaning; but in the arc process, metal ions, many of which are usually multi-charged, are attracted at voltages of about –1000 V to the substrate surface. The metal cations not only clean the surface by sputtering the outer layer of atoms, but they also become embedded in the surface producing a very thin zone, 20-30 nm thick, of intermixed coating and substrate materials. Only the arc process produces this intermixed zone, which is beneficial for some coated tooling used in stamping and punching applications [122, 123].

1.7.9.4 High voltage electron vapour deposition

High voltage electron vapour deposition can deliver fast deposition rates, but it is not very effective in ionizing the evaporating atoms because of their small ionization cross-section in the high voltage electron beam. Electrons injected from a hot filament triode source very effectively ionize both the evaporating and reactive gas atoms, and the degree of ionization is independently controlled from the other process parameters. It has been

reported that the substrate ion current density in the triode high voltage electron beam process is typically 4 mA/cm^2 and that more than 90% of the substrate ion current is carried by the metal species [124]. Higher substrate ion current densities could be achieved in this triode system, but the limitation comes from substrate heating. A substrate ion current density of 4 mA/cm^2 results in a substrate temperature of approximately 400°C.

1.7.9.5 Magnetron sputtering

Sputtering is a method of depositing both thin metal films and insulators onto a substrate. Unlike evaporation, the material to be sputtered does not have to be heated. The deposition of alloys and insulators as composite materials are two important benefits of sputtering. Sputtering has additional benefits as a deposition technique when compared with evaporation [125, 126].

Sputtering is a physical process that can be compared to throwing steel balls at a concrete wall. Upon impact, the ball tears away fragments of the concrete, resulting in fragments which retain the chemical and physical properties of concrete. If the process is continued, surfaces in the immediate vicinity of the impact are covered with a layer of concrete dust. A schematic diagram of the sputtering process is shown in Figure 1.13.

In sputtering, the 'steel balls' are ionized atoms. The "wall" is a plate of the material to be sputtered, called a 'target'. The sputtering process takes place in an evacuated chamber. Argon is introduced, and then ionized in the chamber which contains the substrate and the target of the film material to be sputtered. The target is maintained at a negative potential relative to the positively charged argon ion. The positive ion accelerates towards the negative charge, striking the target with sufficient force to remove material. The argon atom is not embedded in the target. It slams into it like a steel ball into the wall and tears off some of the target material. Since the chamber is maintained as a vacuum, the liberated material settles on everything in the chamber, mainly the substrates. Magnetron sputtering, which has been used to deposit many different hard coatings, was not successful as a commercial tool coating process because it did not provide a high degree of ion bombardment in the substrate region. Even though there is dense plasma next to the target, this plasma is tightly confined to the face of the target, and low ion current densities are collected on the substrate. It was not until the magnetron cathode was unbalanced, that high substrate ion current densities on the order of 5 mA /cm^2, which match those found in the other successful PVD coating processes, were realized and utilized. Magnetron cathodes are unbalanced when one set of the magnets – either the inner or outer one – is

made stronger than the other. The effect of the unbalanced magnetic field is to trap the fast secondary electrons that escape from the target surface. These electrons undergo ionizing collisions with gas atoms away from the target surface and produce secondary plasma in the region of the substrate.

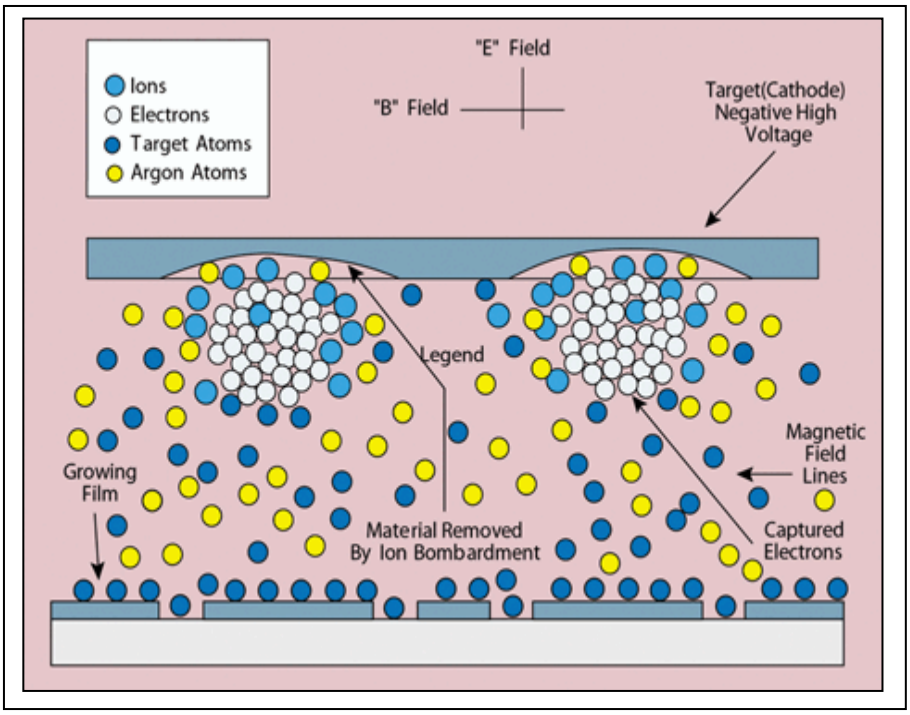

Figure 1.13. Schematic diagram of sputtering process [125].

The magnetron sputtering source addresses the electron problem by placing magnets behind, and sometimes, at the sides of the target. These magnets capture the escaping electrons and confine them to the immediate vicinity of the target. The ion current (density of ionized argon atoms hitting the target) is increased by an order of magnitude over conventional diode sputtering systems, resulting in faster deposition rates at lower pressure. The lower pressure in the chamber helps create a cleaner film. The target temperature is lower using a magnetron, thus sputtering enhances the deposition of high quality films [127].

1.8.0 Machining Titanium alloys using coated tools

Titanium alloys are machined with a coated carbide tool in the speed range between 50 to 100 m/min [128]. The coatings provide a good thermal barrier for the tool thereby arresting diffusion wear and simultaneously lowering the co-efficient of friction between the tool and the workpiece. The coating deposition technique employed will influence the

tool performance as the bonding strength between the coatings and the substrate varies with the processing technique used. Typical coatings techniques employed for the tools used for machining titanium alloys are high temperature chemical vapour deposition and lower temperature physical vapour deposition. Research carried out by Jawaid *et al* [129] who used multi-layered CVD coated (TiCN + Al_2O_3), observed that CVD coatings showed better performance than single layer PVD-coated TiN carbide tools when face milling Ti-6Al-4V alloy within the speed range of 80-100 m/min and at the feed rate of 0.1-0.15 mm per tooth: adhesion and attrition wear mechanisms were responsible for the wear of both faces. Moreover, they observed excessive chipping at the cutting edge, plus flaking and chipping on the rake face were the dominant failure modes along with plastic deformation of the cutting edge. The authors also concluded that coating delamination on the rake face and adhesions on the clearance face were responsible for the initial wear [129]. In milling, due to its intermittent cutting operation, the initial loss of coating was due to delamination. This accelerates the loss of substrate material as the result of high temperature generated due to machining operations.

A multilayered TiN/TiCN/TiN-coated tool showed similar results. A single layer TiN-coated carbide tool showed higher flank wear rate [130]. Cutting speeds up to 150 m/min have been reported by using coated carbide (straight and mixed) tools with WC-Co coatings by Fitzsimmons *et al* who carried out turning tests on Ti-6Al-4V [131]. WC-Co coatings improve the crater resistance of the tool as they suppress diffusion of the tool particles into the chip at higher speed due to the formation of a protective layer saturated with tool particles. They also concluded that the flank wear performance of the coated tools was determined by the substrate properties (straight or mixed grade carbide) while the crater wear performance was determined by the coating properties. This was attributed to the edge geometry of the tool.

Ezugwu *et al* used PVD coated TiCN and TiN carbide tool and observed that a TiCN-coated tool performed better than a TiN-coated tool while machining IMI 318 titanium alloys and concluded that flank wear was the dominant failure mode and that the performance of the coated tools is jointly controlled by wear and plastic deformation [132]. Another study carried out by Faga *et al* who compared PVD-coated TiCN and nanostructured AlSiTiN-coated carbide tools while turning titanium alloy and demonstrated that the AlSiTiN-coated carbide tool performed better than TiCN-coated carbide tool [133]. This was attributed to the nano crystalline structure, multi-layered architecture and the gradient composition of the AlSiTiN-coated carbide tool. However,

there are some publications which suggest that coated carbide tools offer no significant advantage and show increased wear rate compared to un-coated carbide tools, when machining titanium alloys [45, 62, 134].

Research on the drilling of titanium and its alloys is not widely reported. Some work has been carried out on the aspects of bur formation, tool life, chip formation, hole quality, cutting force and surface integrity [135-137]. Work carried out by Sharif *et al* concluded that TiAlN-coated carbide drills outperformed un-coated drills at all cutting speeds both in terms of tool life and surface roughness of the drilled surface while drilling Ti-6Al-4V alloys and observed that the dominant failure modes for the coated and un-coated carbide drills are non-uniform flank wear, chipping and catastrophic failure [138].

Recently, research reported by Bastruk *et al* studied the novel process of plasma boronizing on a tungsten carbide tool used to machine Ti-6al-4V alloy. They concluded that this process increases the price of the cutting tool by only 5% whereas the life of the carbide tool is enhanced three times [139].

It is considered important to give brief details about the two coatings selected for the current project.

1.8.1 Titanium Aluminium Silicon Nitride (TiAlSiN) coating

Titanium-based coatings, such as TiN and TiCN, are widely used on metal cutting tools to prolong their lifetime and enhance their working performance because of their high hardness and low co-efficient of friction *etc* [140, 141]. However, when more hostile and aggressive environments are considered, the conventional titanium-based coatings show drawbacks, especially in oxidation resistance, hardness and chemical stability. For example, at temperatures higher than 500°C, TiN starts to oxidize to TiO_2, leading to crack formation and delamination of the oxide layer and thereby causing deterioration in mechanical and tribological properties [142]. In recent years, considerable efforts have been carried out to alloy TiN-based coatings with several elements in a variety of different ways [143, 144]. Silicon and aluminium are being widely incorporated into TiN coatings, thus producing ternary coatings for a variety of cutting applications [84, 145, 146]. TiAlSiN is superior to TiN coatings not only in its resistance to high temperature degradation, but it also shows higher hardness values (greater than 30 GPa).

The TiAlSiN coatings have been prepared by using various deposition techniques, *eg* CVD, plasma enhanced CVD, and PVD technologies including electron beam ion plating and cathodic arc evaporation [84, 147–150].

1.8.2 Aluminium Titanium Nitride (AlTiN) coatings

Twenty five years ago TiN started the success story of PVD coatings in cutting tool applications. The introduction of aluminium in the FCC structure of TiN effectively enhances the hardness and thermal stability of the TiN coating [151]. A general trend in the last decade in improving the TiAlN coatings has been to increase the aluminium content in the coating, in order to promote the formation of aluminium oxide during the cutting operation being carried out by the tool, thereby forming an Al-rich TiAlN coating. These coatings are suitable for near-dry or dry high speed cutting operations, where a permanently wearing and re-growing dense Al_2O_3 top layer is responsible for the high oxidation resistance [152]. These aluminium-rich PVD coatings have shown improved tool life in machining of aerospace alloys such as austenitic stainless steels and superalloys [87, 153]. Not only do AlTiN coatings display higher hardness (greater than 30 GPa) they also exhibit superior oxidation resistance compared to TiN coatings (hardness of 20 GPa). Furthermore, these coatings have improved plasticity and fatigue fracture resistance. Therefore, during plastic deformation, the coatings have the ability to dissipate energy, which is very beneficial for the reduction of attrition wear [154]. At higher temperatures, aluminium forms a stable aluminium oxide which not only protects the underlying tool surface, but also prevents intensive sticking of the workpiece to the cutting tool [155].

1.9.0 Novel aspects of this research project

The novel aspect reported in this thesis is that these advanced coatings (deposited through PVD arc evaporation technique) have not been applied to the newly developed multi-point TCT bandsaws, although they have been applied to single-point cutting tools. These coatings (AlTiN and nano-structured TiAlSiN) will not only allow efficient bandsawing of the difficult-to-cut materials such as titanium alloy (Ti-17) and Inconel 718 (nickel-based superalloy), but would also increase the life of these bandsaws blades by arresting wear on the cutting edge.

CHAPTER 2: SINGLE TOOTH TEST RIG

2.0 Introduction

It is costly and time-consuming to test the wear of the full bandsaw products on a full-scale bandsaw machine. Therefore, it is highly desirable to devise Single Tooth Tests (STT) for force measurement and wear testing of the bandsaws. A single tooth test also needs to be representative of the full product bandsaw testing and should be able to produce scientific data which co-relate both these machining tests.

Sarwar and Thompson built a test rig using a commercially available lathe to simulate the cutting action of the hacksaw blades [158]. This was further developed and utilized by Sarwar, Bradbury and Dinsdale, in order to generate cutting data for predicting stress behaviour within bandsaw teeth [159].

The single tooth technique and instrumentation were then further developed by Doraisingam, who used this methodology for testing bi-metal bandsaw teeth in order to obtain data associated with the cutting forces and specific cutting energy when bandsawing different workpiece materials [1]. It was stated by Doraisingam that the use of this methodology allowed 75% time saving compared to the complete full bandsaw test [1]. This previous research dealt with the initial cutting action of the bandsaw teeth and related the performance of single teeth to the performance of the full bandsaw product.

This test rig was later utilized by Persson, to evaluate the wear of the bi-metal bandsaw blade and to assess the wear modes and mechanisms of the bandsaw blades [2].

This technique was subsequently modified by Antoshina, who designed a new tooth holder. Previously, only a straight tooth could be used. However, on some bandsaw blades, the 0-set teeth are chamfered, which means that they could not be used on the single tooth test. The new tooth holder allows using the left set teeth for the STT [160]. The details will be presented in the following sections.

2.1. Features of the single tooth test rig

The single tooth test rig is presented and elaborated in Figure 2.1. Workpiece (labelled 1) is mounted onto the chuck of the lathe, using M10 bolts. The chuck was held in the camlock spindle nose of the lathe. The single tooth sample (labelled 2) is installed on the tooth holder mounted on the Kistler dynamometer platform (labelled 3). The platform is

placed onto the cross-slide (labelled 4). The slide ways are operated from a computer (labelled 5), which is in serial with the control box (labelled 6). The signal from the Kistler platform is transferred *via* the charge amplifier (labelled 7) to the PC (labelled 8) and an oscilloscope (not shown).The tool holder was secured on the top of Kistler, 3-axis force dynamometer, which was fastened onto the precision cross-slide. This cross-slide was mounted on a solid platform bolted onto the lathe bed.

2.1.1 DSG lathe

The model 1609 Dean, Smith and Grace (DSG) lathe has a number of possible fixed rotational speeds. The important features of this lathe are its stiffness (in radial and axial directions) and the play of the axial bearing. This has previously been investigated, during the research carried out by Doraisingam [1]. Since the speed range was limited by the gear box settings, it was therefore, sometimes not possible to achieve desired cutting speeds by using the lathe's rotation. In this case the cutting speed was set using a combination of the preset rotation and varying the workpiece diameter. The workpiece diameter needed to achieve a desired cutting speed determined using Equation 2.1:

$$V = \frac{\pi \cdot D \cdot n}{1000} \qquad \text{(Equation 2.1)}$$

where

V = cutting speed [m/min], D = workpiece diameter [mm], n = rpm [1/min]

	Rotational speeds (rpm)
DSG lathe	20, 29, 40, 57, 80, 115, 120, 175

Since the diameter of the workpiece has a significant effect on the cutting speed, therefore, the lathe's rotational speed is used to achieve the desired cutting speeds.

2.1.2 Force measurement instrumentation

The main aim of these experiments was to measure the cutting force components under various cutting conditions. Therefore, a force measurement system with appropriate instrumentation was required to work in parallel with the precision cross-slide setup. A schematic diagram of the setup is shown in Figure 2.2.

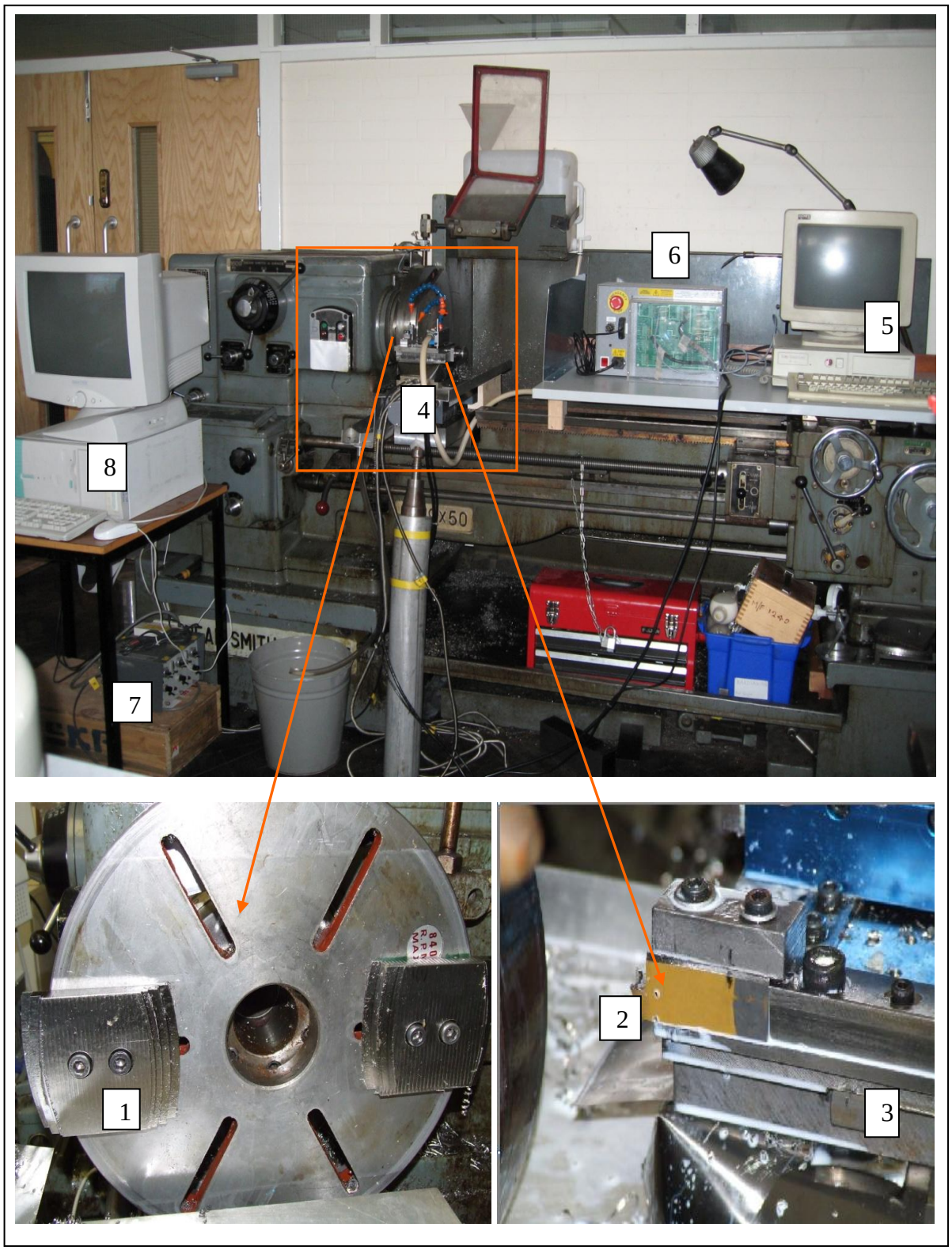

Figure 2.1. Single tooth test rig – also shown are the tooth holder and the workpiece material attached to the chuck of lathe.

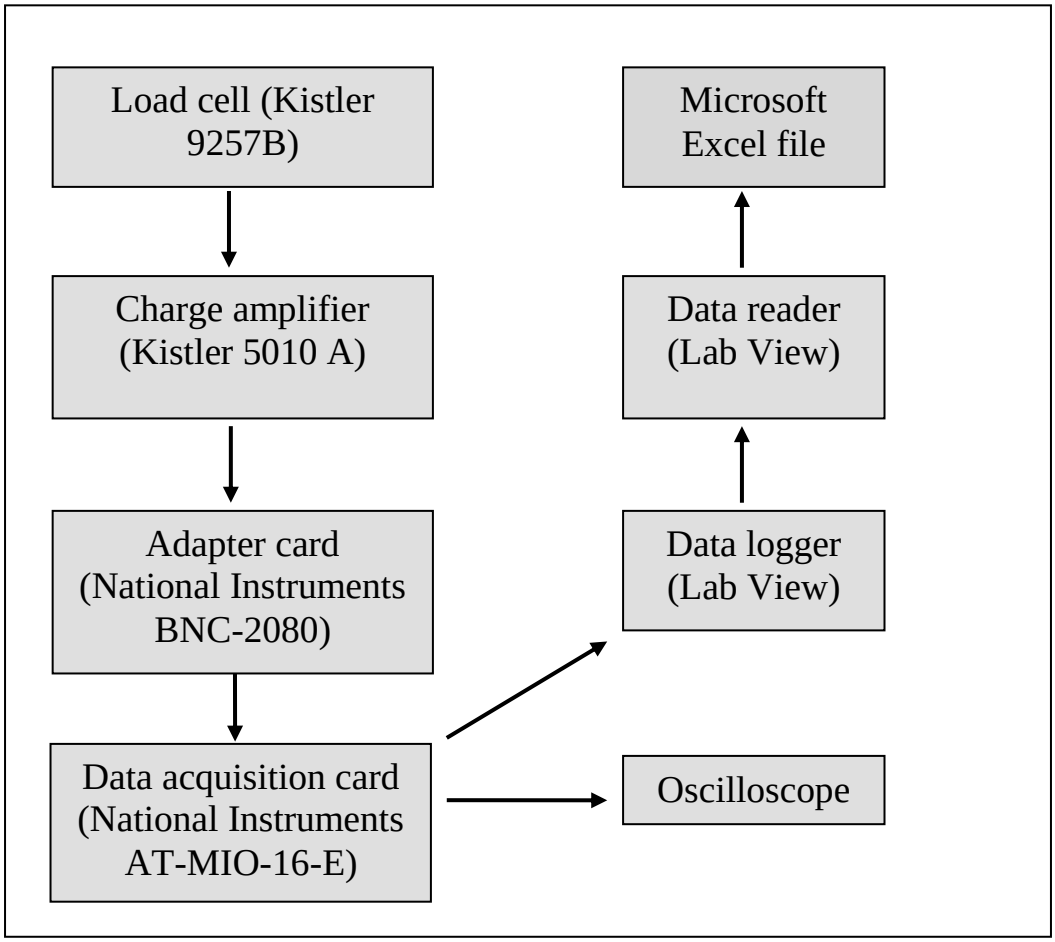

Figure 2.2. Schematic diagram of the experimental single tooth test rig.

The cutting force components [lateral (Fv), feed (Fp), vertical (Fr)] were measured using a three force component Kistler dynamometer with piezo-electric transducers. The schematic diagram of the experimental set up and the principal cutting directions are shown in Figures 2.3 and 2.4 respectively.

The piezo-electric transducers sends signals in the form of electrical charges to the charge amplifier. These charges are caused by the forces (arising from the cutting action) on the platform due to the applied load. This signal is then sent to the data acquisition card and in parallel to the oscilloscope, so that the force traces are observed while the cutting operation is taking place. These signals are stored in the computer, but can be observed directly on the of the oscilloscope as stated previously. The digital signal can then be read, analyzed and presented for visualization by LabVIEW Data Reader VI. This data reader allows storing selected data in a data file which can be opened using Microsoft Excel, allowing further processing.

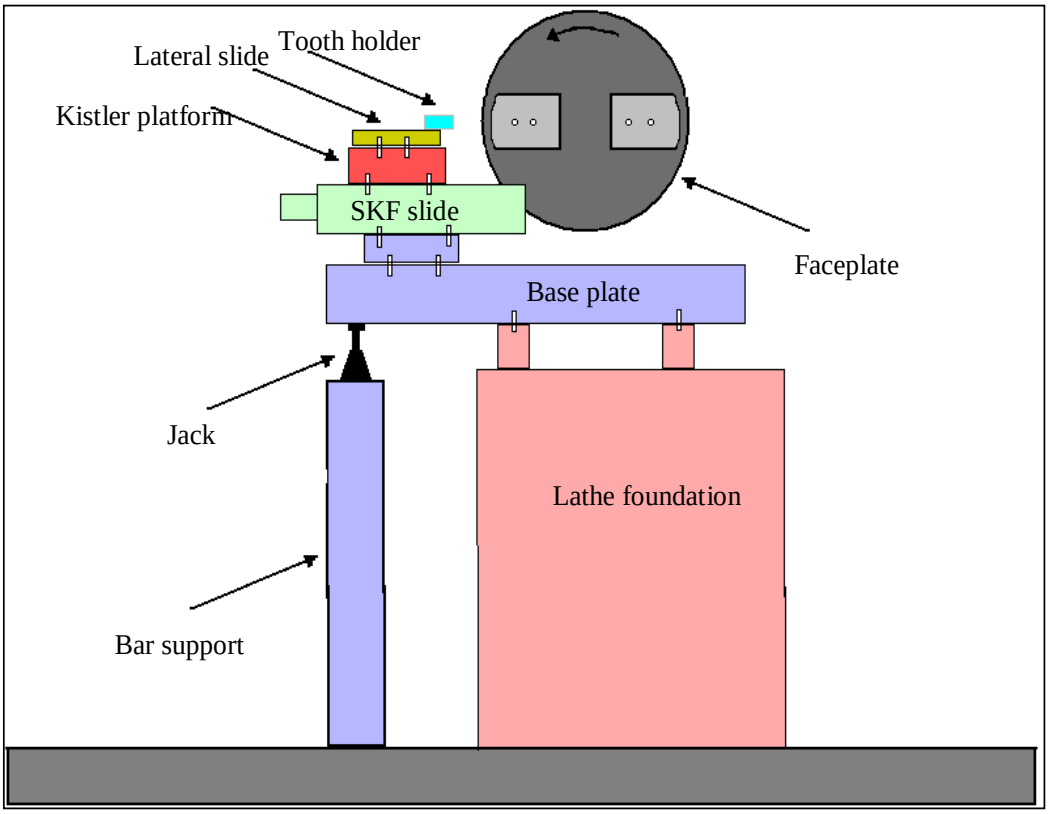

Figure 2.3. Overview of the single tooth test rig [2].

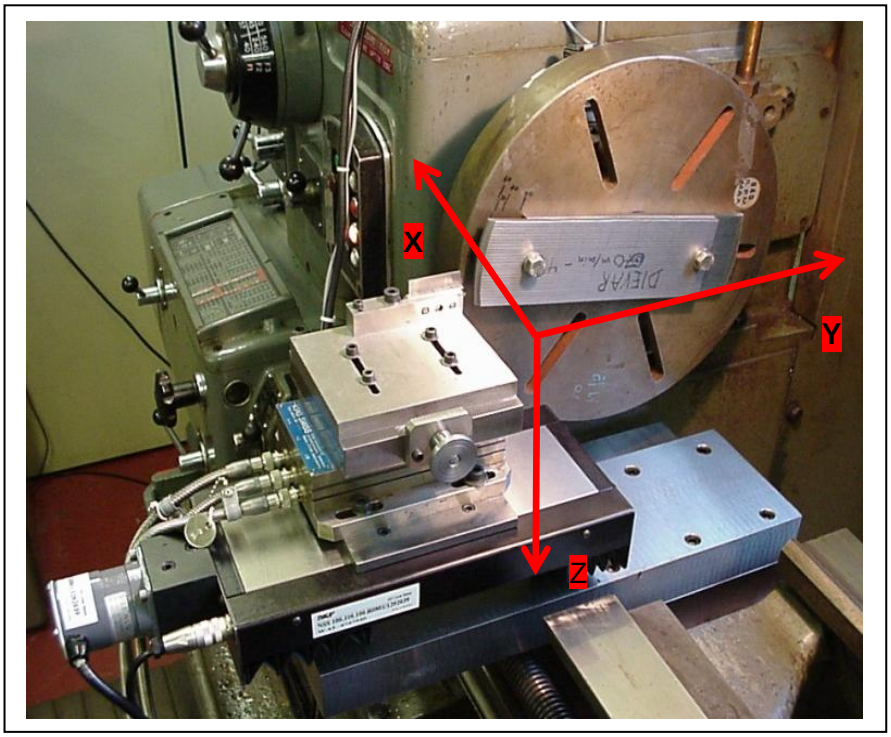

Figure 2.4. Principal directions of system: X = lateral, Y = feed, Z = vertical [2].

2.1.3 Data acquisition system

The data acquisition device is required in order to collect, analyze and present the measurements of the forces that were carried out. The DAQ (National Instruments) device is connected directly to the computer's internal bus through a plug-in slot and this hardware device converts the analogue signal into the digital signal, which was then sent to the computer to be electronically stored. This signal, in parallel, was sent to the Gould oscilloscope for immediate visual display of the forces.

2.1.4 Precision cross-slide

The precision cross-slide supplied by SKF was used to drive the cutting tool and had N-rail guides with needle roller assemblies. The cross-slide and stepper motor are shown in Figure 2.5. The cross-slide was selected for its greater dynamic load-carrying capacity (60.9 kN) and static load carrying capacity (13 kN). Furthermore, the short stroke (100 mm) and preloaded guide (3–10% of static load rating) provided high stiffness (≈ 30 N/μm) with negligible backlash, which made the cross-slide less sensitive to shocks. This is an important factor since the cross-slide would be subject to impact loading when the cutting tool engages with the workpiece in the STT. The cross-slide was equipped with preloaded planetary roller screws (1 mm pitch). The drive screws were supported at the motor end by preloaded angular contact bearings in the table endplate. The cross-slide can travel at speeds of up to 2 m/s and with acceleration of up to 10 m/sec^2. The travel speed and acceleration of the cross-slide were appropriate for working with the spindle speed of the lathe used in this STT rig.

2.1.5 Machine control hardware

The machine control hardware (MC3E) operates the stepper motor to control the motor's shaft position. The MC3E controls the linear movement by the number of steps per unit. This parameter value is the number of drive pulses or steps from the MC3E which are required to cause the machine axis to move by one whole unit. The unit used to represent the linear axis is mm. For a leadscrew of 1mm pitch directly coupled to a 1000 steps/rev, there will be 1000 steps to rotate the leadscrew by one turn and move the load by 1 mm, *i.e.* 1000 steps/unit. This cross-slide control system is illustrated in Figure 2.6.

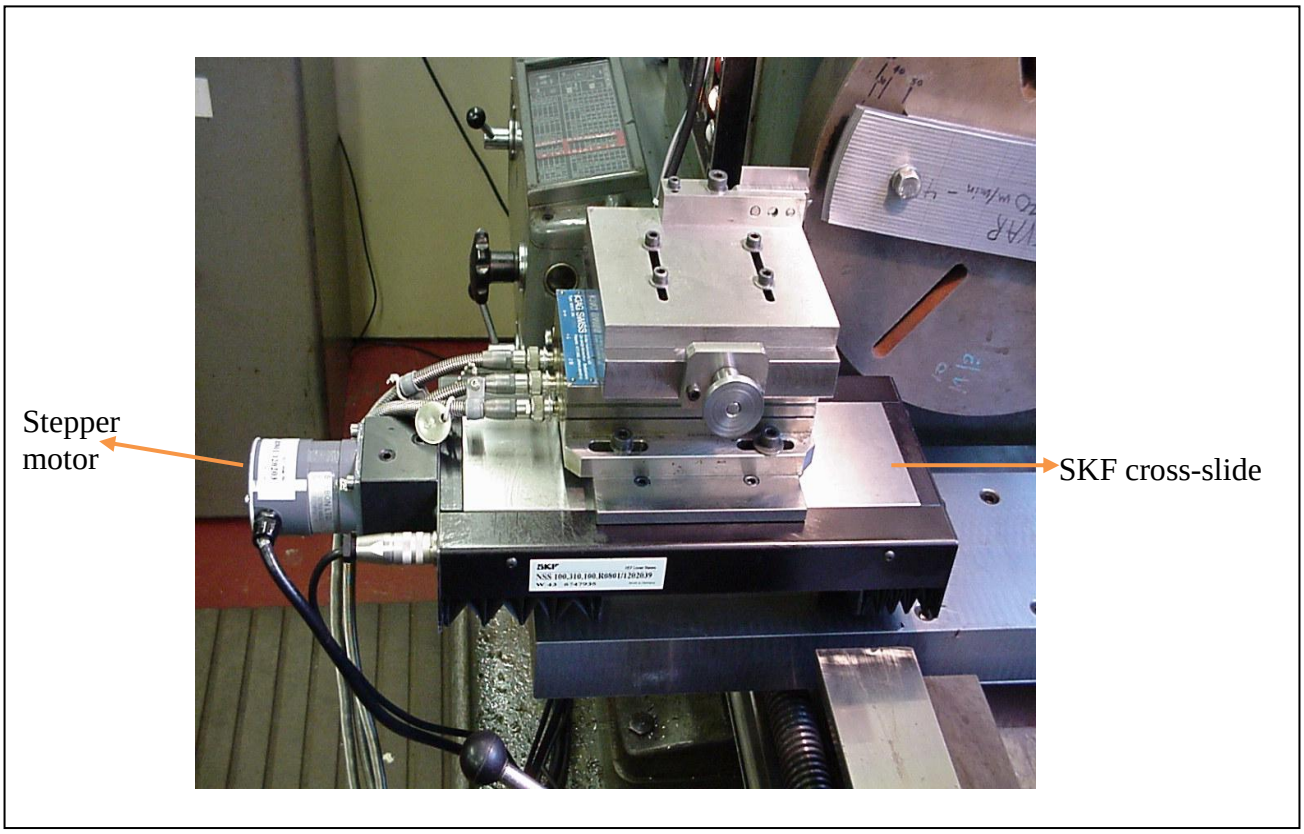

Figure 2.5. SKF cross-slide and stepper motor.

2.1.6 Proximity detector

A proximity detector was used in order to ensure that the cutting tool was fed into the workpiece at a correct time/instance during the cutting process. The proximity detector was positioned at approximately 0.5 mm from a ferrous metal plate mounted onto the back of the lathe's faceplate. The proximity detector operates as a current switch whose output current depends upon whether the ferrous metal plate is covering the detector or not. The description of the metal plate is given in [1-2].

2.1.7 Stepper motor

The stepper motor consists of a stator which has coils electrically connected to and driven by a motor drive, and a rotor which can be considered as a bar magnet and is mechanically connected to the load. When there is no power applied to the motor, the shaft magnetically locks into the pre-defined mechanical position around its rotational axis. Usually, there are 200 such positions per revolution of the motor shaft. It is the motor drive that is responsible for sequencing the current to generate rotational motion of the motor. Links on each drive allow selection of 4000, 2000, 1000 or 400 steps per motor revolution. For the purpose of the STT experiment, the motor drive was set for 1000 steps per revolution.

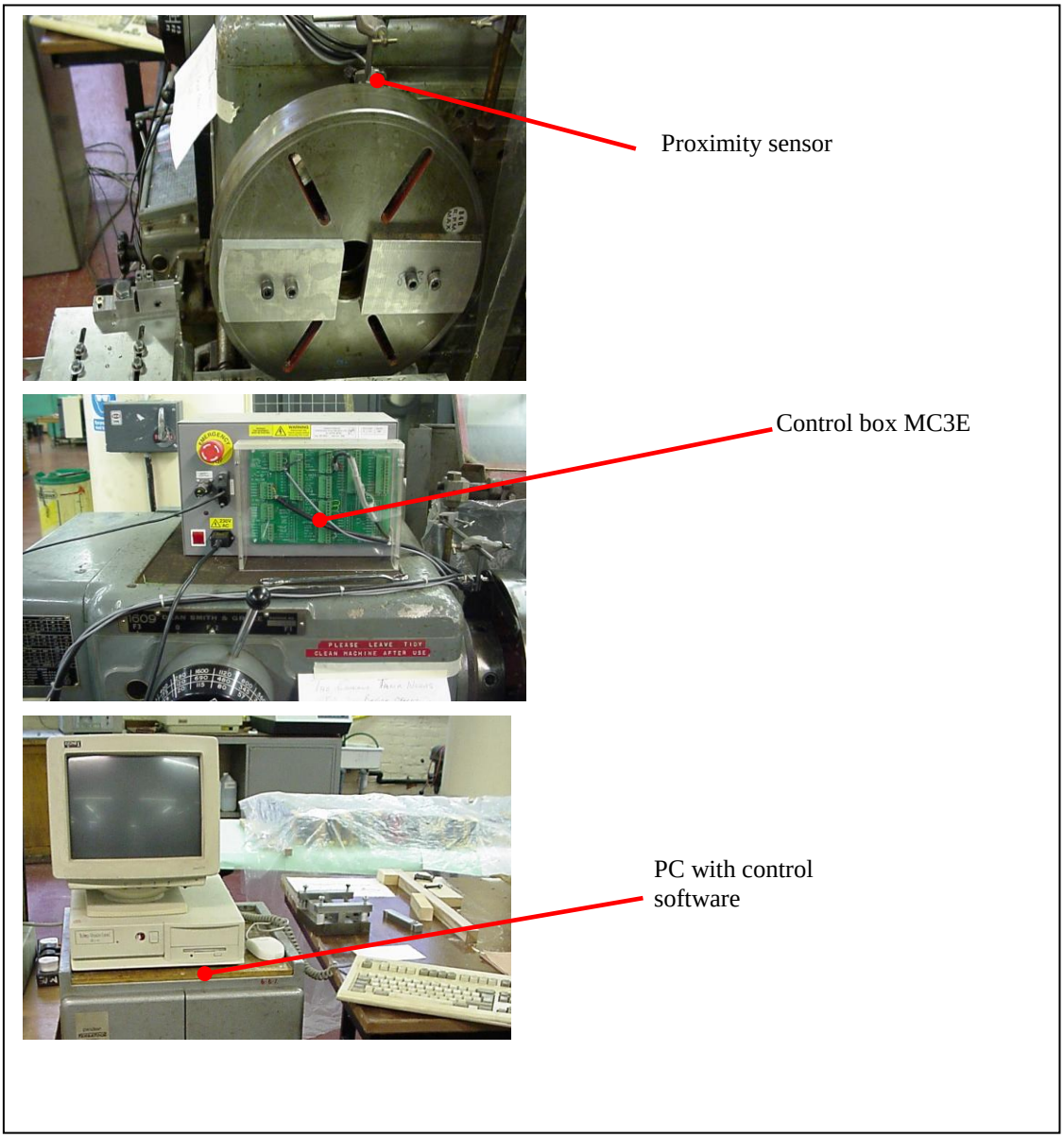

Figure 2.6. Cross-slide control systems [2].

The lead screw in the precision cross-slide has a 1 mm pitch; therefore the minimum movement can be calculated as follows:

$$\text{Minimum movement} = \frac{Leadscrew\ \ pitch}{Steps\ \ per\ revolution\ \ of\ \ motor\ drive} = \frac{1\ mm}{1000} = 1\mu m$$

2.1.8 Precision cross-slide calibration tests

In order to ensure that the precision cross-slide was working to its full capability and specifications, a series of different calibration tests was performed during previous work:

1) Stiffness test (detailed description is presented in [1]).
2) Laser interferometer test [1].

The most important feature of the STT rig is the accurate feeding of the cutting tool. In the first version of the test rig, the depth of cut was determined through calculation using the weight of the chip collected because of the inaccuracy associated with the lathe cross-slide feed system. This method was found to be time consuming and inaccurate. Therefore, it was decided that using the precision cross-slide would eliminate the need for confirming the depth of cut. For this purpose, the precision cross-slide was calibrated in order to assess its accuracy using laser interferometry. The detailed description of the laser interferometer test technique is given by Doraisingam [1].

It is important to describe and explain a parameter which will be used in evaluating the performance of the bandsaw teeth, know as Specific Cutting Energy (Esp).

2.1.9 Specific cutting energy

The specific cutting energy can be used to determine the efficiency of the metal cutting process. Esp is a measure of the energy required to remove (cut) a specific volume of workpiece material previously described by Sarwar and is measured in J/m^3 [158]. Since bandsaw teeth operate at very small values of depth of cut per tooth, it is not as efficient as most single-point cutting operations such as turning. The bandsaw tooth is also restricted since it has to accommodate the chip in a gullet of limited size. These factors lead to a high value of specific cutting energy.

The Esp is calculated using Equation 2.2:

$$Esp = F_v / A_{chip} \qquad \text{Equation 2.2}$$

where

Esp = specific cutting energy [J/m^3],

F_v = cutting force [N],

A_{chip} = chip cross-sectional area [m^2].

In order to observe the wear modes and mechanisms experienced by the un-coated carbide tooth when machining Ti-17 alloy, a large number of cuts were made. The methodology was to produce a number of cuts and then observe the tooth under the scanning electron microscope. For this purpose, a number of bandsaw teeth were used for machining. They were carefully examined under the optical and scanning electron microscope to observe if they were damaged in any way (such as chipping, scratches *etc*) before using them for machining tests.

Sarwar introduced the concept of Esp as a parameter for evaluating the efficiency of sawing processes and this parameter has been used to evaluate bandsaws, hacksaws and circular saws. The performance of uncoated and TiN coated circular saw blades while machining different steel workpieces was also evaluated by Sarwar *et al* using Esp [17].

CHAPTER 3: COATINGS CHARACTERIZATION

3.0 Introduction

This chapter focuses on the techniques used to characterize the coatings on the carbide tipped bandsaw teeth and will discuss the experimental techniques and results associated with characterization of:

- surface morphology of the coatings;
- chemical composition of coatings;
- cross-sectional analyses;
- structural characterization and grain size of coatings;
- coatings hardness; and
- coatings adhesion.

The properties mentioned above, play a significant role in the performance of the coatings. For example, without sufficient adhesion onto the tool surface, a coating of otherwise excellent properties in terms of its resistance to wear, scratches or impact would be rather useless. Usually, the failure of the hard, wear resistant coatings is not by progressive wear, but rather by the failure of adhesive bond between the coatings and the substrate. It is vital that the coatings remain attached to the substrate in order to improve the life of the component. If a hard and wear resistant coating breaks away from the tool, more severe failure can take place than if the component was uncoated. Therefore, it is crucial to measure the adhesion between the coatings and the substrate.

For the hard and wear resistant coatings, it is necessary to observe the surface and cross-section morphology of the coatings, because it reveals important information, such as porosity or voids in the coatings. Porosity and voids affect the coating properties/performance in a number of ways. For example, if the voids exist at the interface between the coatings and the substrate, they may reduce the adhesion between the coating and the substrate by decreasing the effective contact area and may provide an easy path for fracture initiation and propagation.

The hardness of the coating plays a significant role in the performance, especially when they are applied to the cutting tools. The hardness of the wear resistant coating is influenced by its grain size, phases present, microstructure *etc* as well as by the substrate properties. Therefore, for thin wear resistant coatings, the structure/property relationship is

particularly important because these properties would determine the performance and life of the tool.

Two types of coatings, namely, TiAlSiN and AlTiN coatings were deposited, using cathodic arc evaporation technique, by IonBond Limited. These coatings were deposited on the honed carbide bandsaw teeth as well as on flat carbide coupons, so that they can be characterized for their properties. No coating deposition parameters were provided, except the deposition temperature is 450°C, as they are confidential, intellectual property of IonBond.

3.1.1 Surface morphology for AlTiN coating

The scanning electron microscope is perhaps the most widely employed surface exploration technique, using electrons which probe the sample surface. The interaction of these electrons with the surface produces signals that contain information about the surface morphology, composition and other properties, such as electrical conductivity. Moreover, this is a powerful technique to observe any defects, such voids, or particles (*eg* macro particles) that have formed during the coating deposition process. These defects are formed by substrate irregularities (pits, asperities *etc*), foreign particles (dust, debris *etc*) or by the coating deposition process (incorporation of small particles and micro-droplets).

A FEI Quanta 200 ESEM electron microscope with tungsten filament was used for microscopy. Figure 3.1 shows representative SEM images of AlTiN coating at various magnifications. It can be observed that the coating is smooth and continuous over the tungsten carbide substrate. However, droplets can be seen on the surface. This is due to the technique used for depositing this coating and is typical of the cathode arc deposition technique. The cathodic arc current is localized in fragments of minute and non-stationary cathode spots, which are necessary to provide sufficient power density for plasma formation, current transport and electron emission between the anode and the cathode. Particles originate from plasma/solid interactions at these cathode spots. The formation of these particles is connected to the existence of the non-stationary cathode spots. The formation of these particles cannot be avoided unless the arc is operated in other cathode modes, such as “spotless vapour mode” or as “anodic arc” [161, 162]. Another technique that led to reduced formation of these particles is the development of a deposition technique which uses a magnetically “steered” arc [163]. It was, however considered important that these droplets be analysed in terms of their chemical composition in order to confirm that they are not “foreign” particles, but have the same chemical composition as

that of the coating materials. EDX analyses were carried out on these spots and the results for the two analysed drops are shown in Figure 3.2. The EDX analyses confirm that the droplets on the surface of the coating have the same elemental composition as that of the coatings.

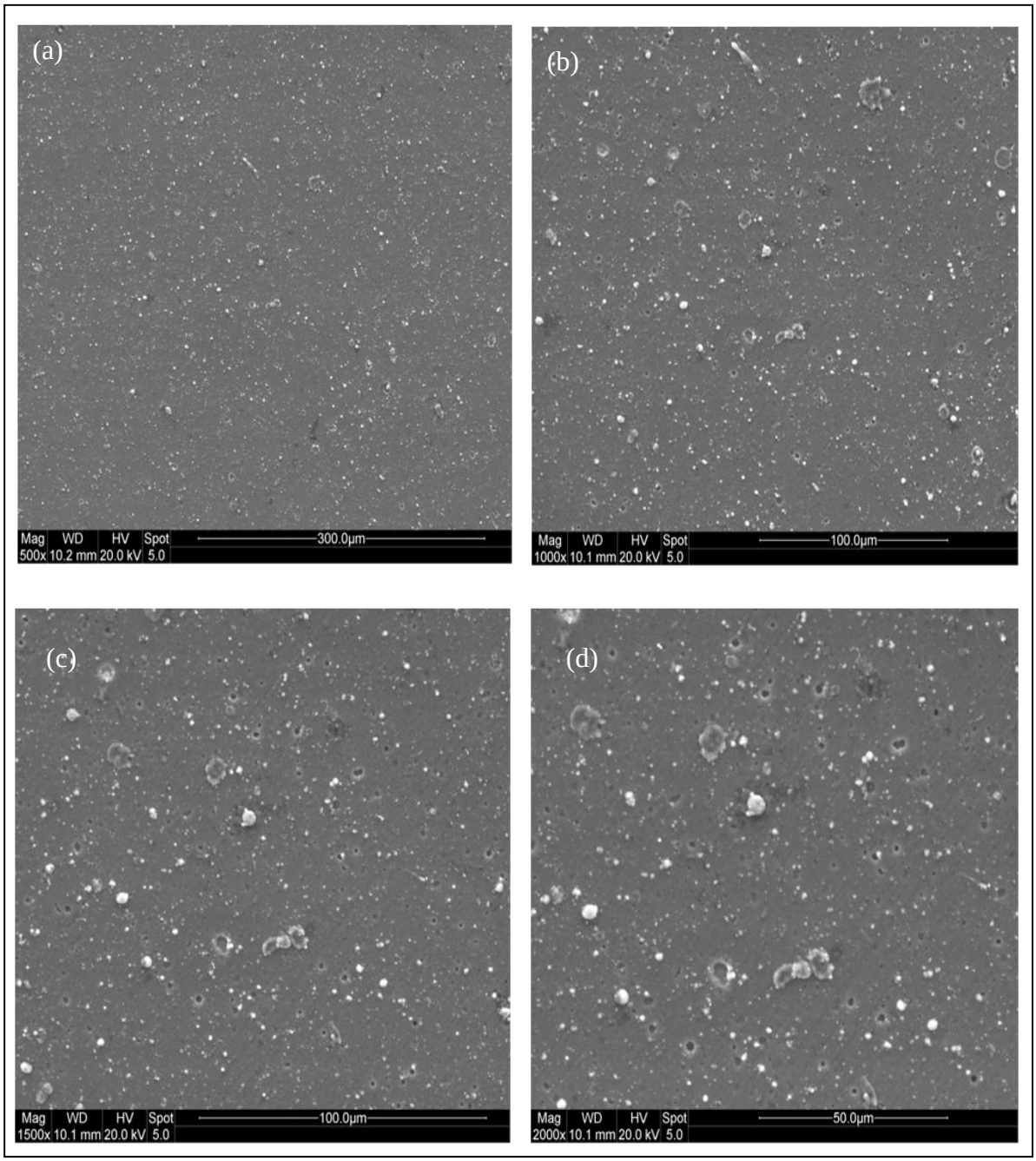

Figure 3.1. Surface morphology of AlTiN coatings (a) 500 mag, (b) 1000 mag, (c) 1500 mag. and (d) at 2000 mag.

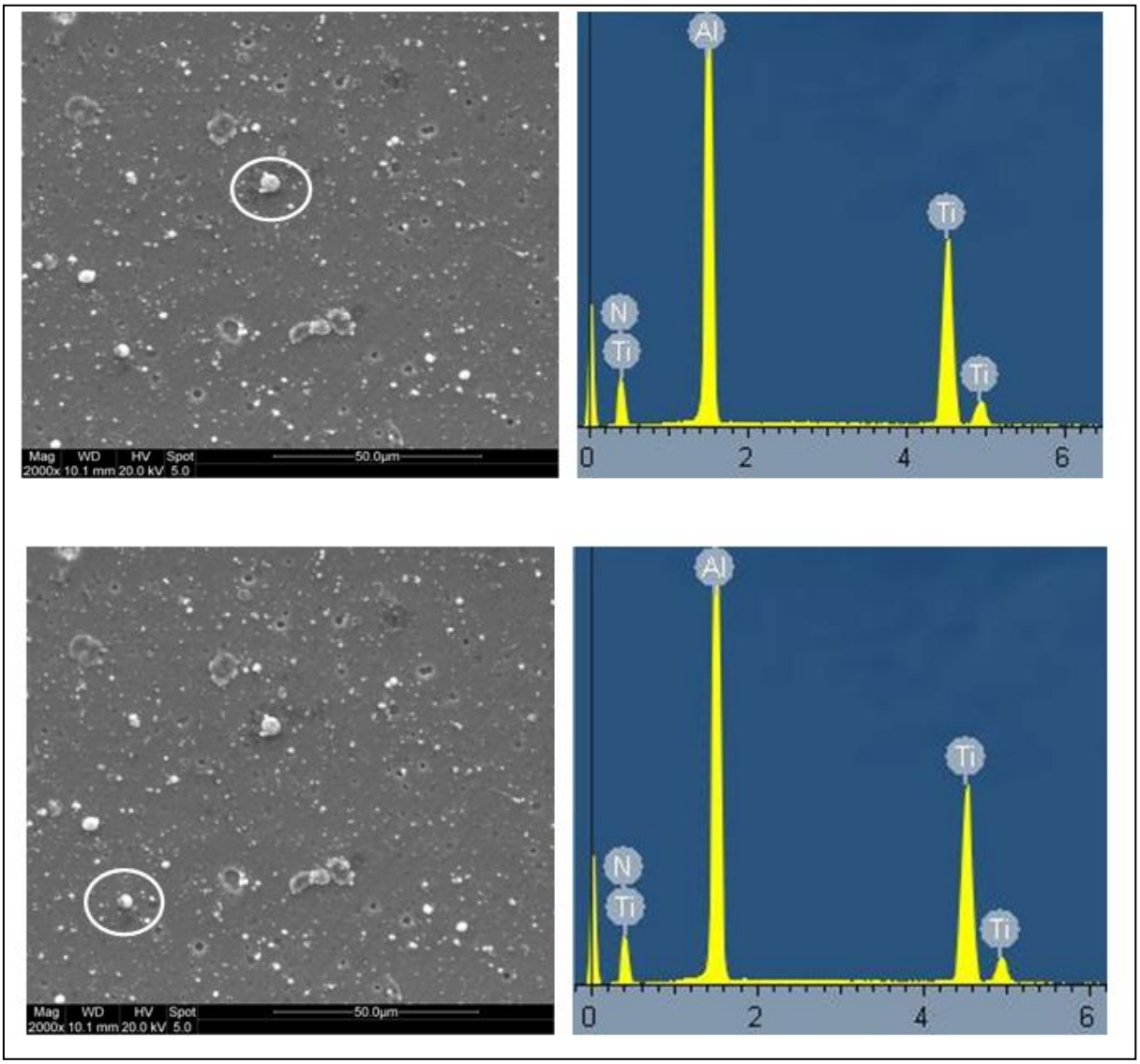

Figure 3.2. SEM image of the surface morphology of AlTiN coating showing the droplets and their corresponding EDX spectra of the droplets revealing the chemical composition of the droplets.

3.1.2 Surface morphology of TiAlSiN coating

Figure 3.3 shows the surface morphologies for TiAlSiN coatings at various magnifications. The coating appears to be smooth, continuous and adhering well to the substrate. The macroparticles (droplets) are observed on the surface, which are due to the coating deposition technique, as described previously. However, the sizes of droplets are larger whereas the number of droplets per unit area is less compared to AlTiN coating. It was considered important to analyse these droplets in terms of their chemical composition and therefore EDX analyses were carried out on them. The analyses are shown in Figure 3.4.

The EDX results show that the macroparticles or droplets have the same composition as that of the coating materials and therefore it can be concluded that these particles are formed due to plasma/solid interaction and not due to any foreign element in the coatings chamber.

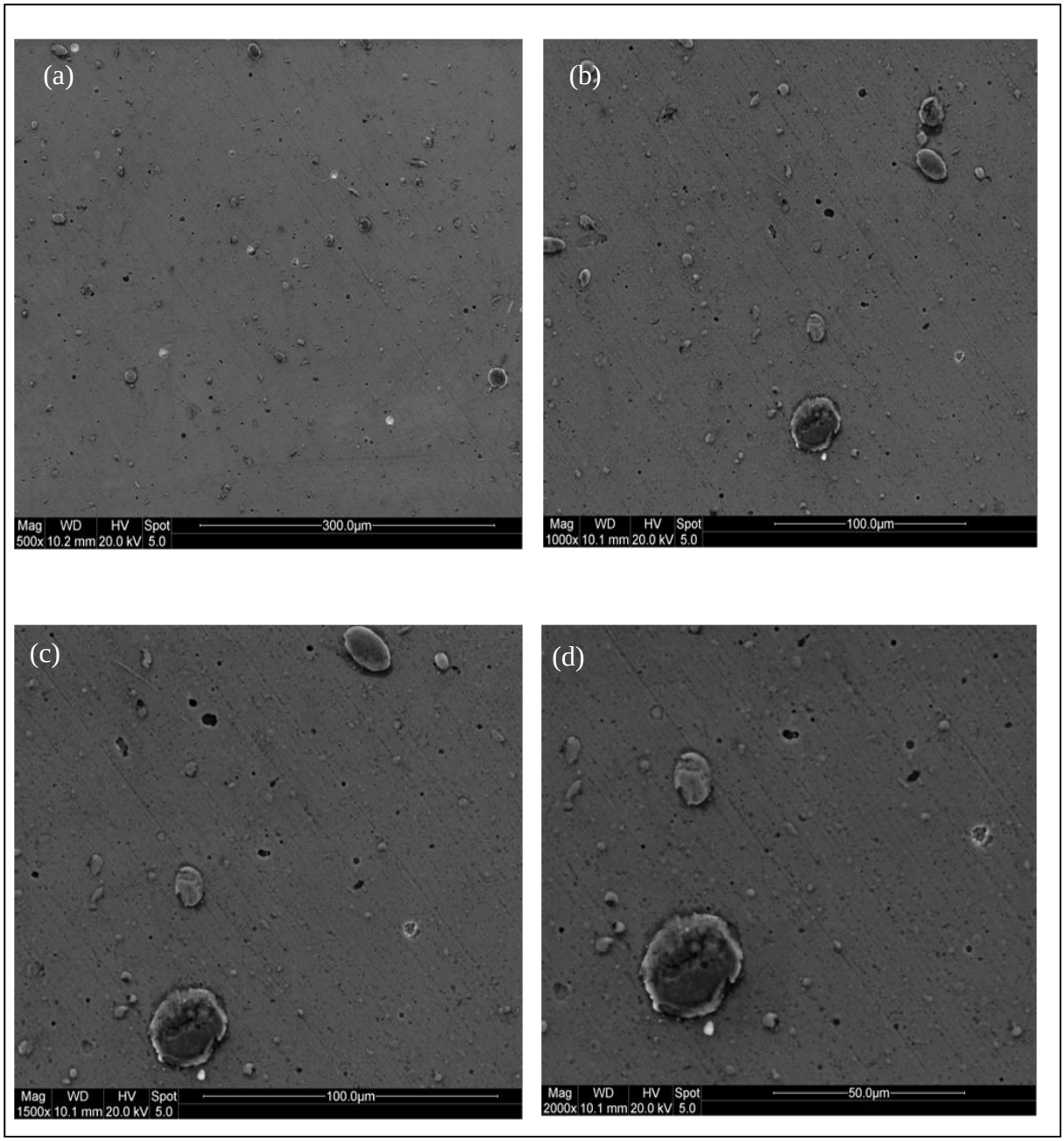

Figure 3.3. Surface morphology of TiAlSiN coatings (a) 500 mag, (b) 1000 mag, (c) 1500 mag and (d) at 2000 mag.

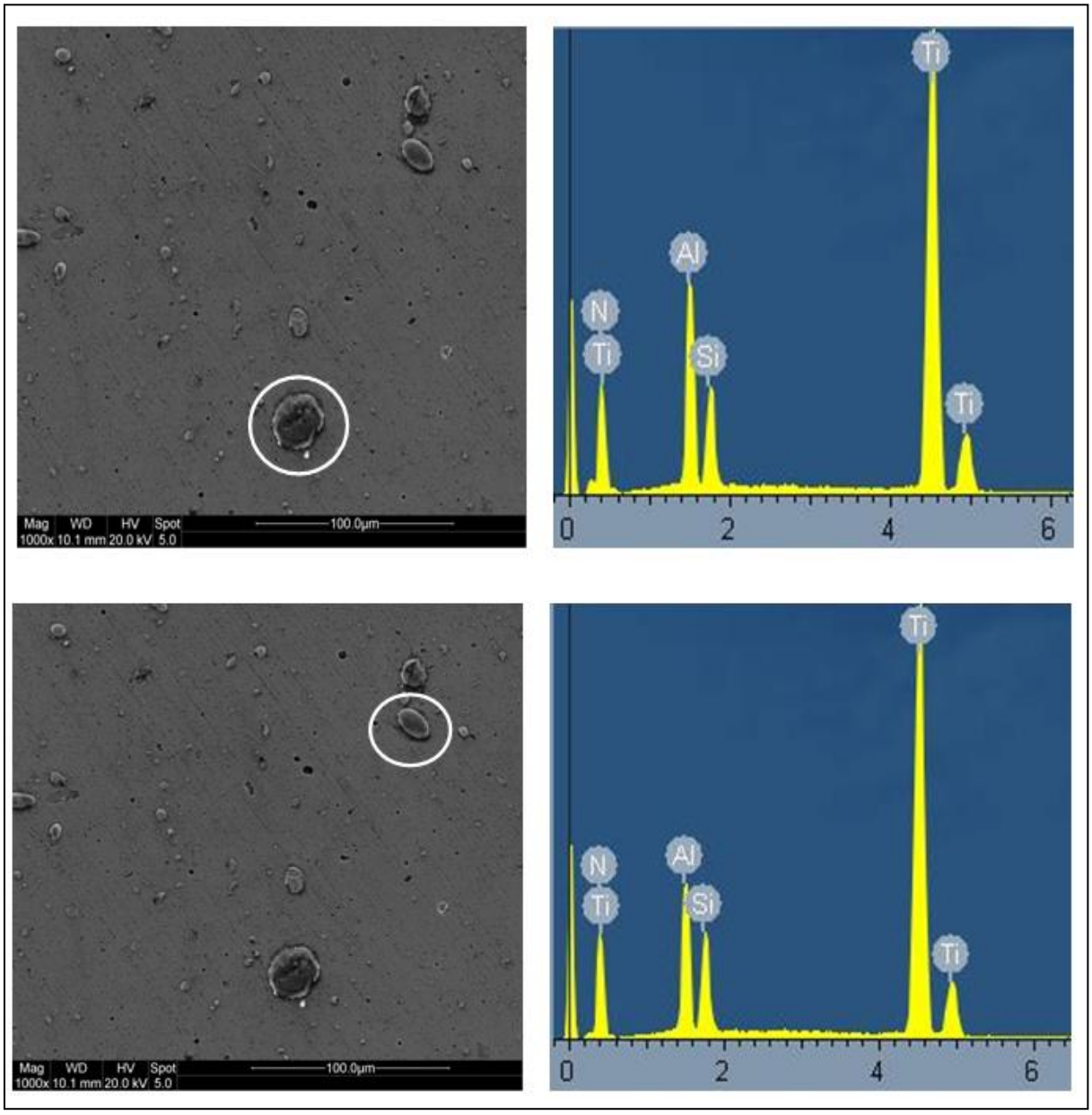

Figure 3.4. SEM image of the surface morphology of TiAlSiN coating showing the droplets and their corresponding EDX spectra indicating the elemental composition of the droplets.

3.2 Elemental composition of the coatings

The SEM uses a focused beam of high energy electrons to generate a variety of signals from the surface, which reveal information about the sample in terms of its chemical composition, texture *etc*. Energy dispersive X-ray spectroscopy (EDX or EDAX) is a powerful analytical technique used for elemental or chemical analysis of a sample. Its characterization capabilities are due to the fundamental principle that each element has a unique atomic structure, which distinguishes that element from the others. In order to ascertain the chemical composition of the coatings, EDX analyses were carried out on ten

different spots on the AlTiN and TiAlSiN coated sample. The averages of these ten values were taken and are presented in Tables 3.1 and 3.2 respectively.

Table 3.1. Elemental composition of TiAlSiN coatings, using energy dispersive spectroscopy.

Element	Average Atomic %
Nitrogen	53.75 ±0.93
Aluminium	9.899 ±0.50
Silicon	5.369 ±0.3
Titanium	30.986±0.54

Table 3.2. Elemental composition of AlTiN coatings, using energy dispersive spectroscopy.

Element	Average Atomic %
Nitrogen	49.522 ±0.98
Aluminium	31.063 ±0.52
Titanium	19.415±0.53

3.3 Cross-sectional analyses of coatings

In order to ascertain the thickness of both of the coatings, the coated flat carbide coupons (with AlTiN and TiAlSiN coating on their surface) were fractured and the cross-sections were examined using the scanning electron microscopy. Typical SEM micrographs illustrating the fracture cross-section views of TiAlSiN and AlTiN coatings are shown in Figures 3.5 and 3.6 respectively.

The thickness of both coatings was calculated to be approximately 2 μm. This measurement was carried out using the imaging software on the scanning electron microscope. From these fractured surfaces, it can be seen that there is a single layered coating on the tungsten carbide substrate. Both the coatings appear to be dense and be adhering well to the substrate. The cross-sectional SEM images of both coatings do not show any columnar or lenticular structures. For the TiAlSiN coating, it has been reported that incorporation of Si in the coating results in amorphous morphology, as this addition of silicon hinders the grain growth and probably stimulated a re-nucleation of grains [164]. The TiAlSiN coating was found to be dense and non-columnar in structure, probably due to refinement of the microstructure by the incorporation of silicon into the film. The amorphous structure of both coatings can also be explained based on the assumption that the nucleation seeds of TiN, AlN and $Ti_xAl_{1-x}N$ were not sufficient in number to induce the

crystalline growth due to the low temperature used in PVD deposition technique. Both AlTiN and TiAlSiN coatings appear to be very compact, without any visible pores or cracks and were found to adhere tightly to the substrate material.

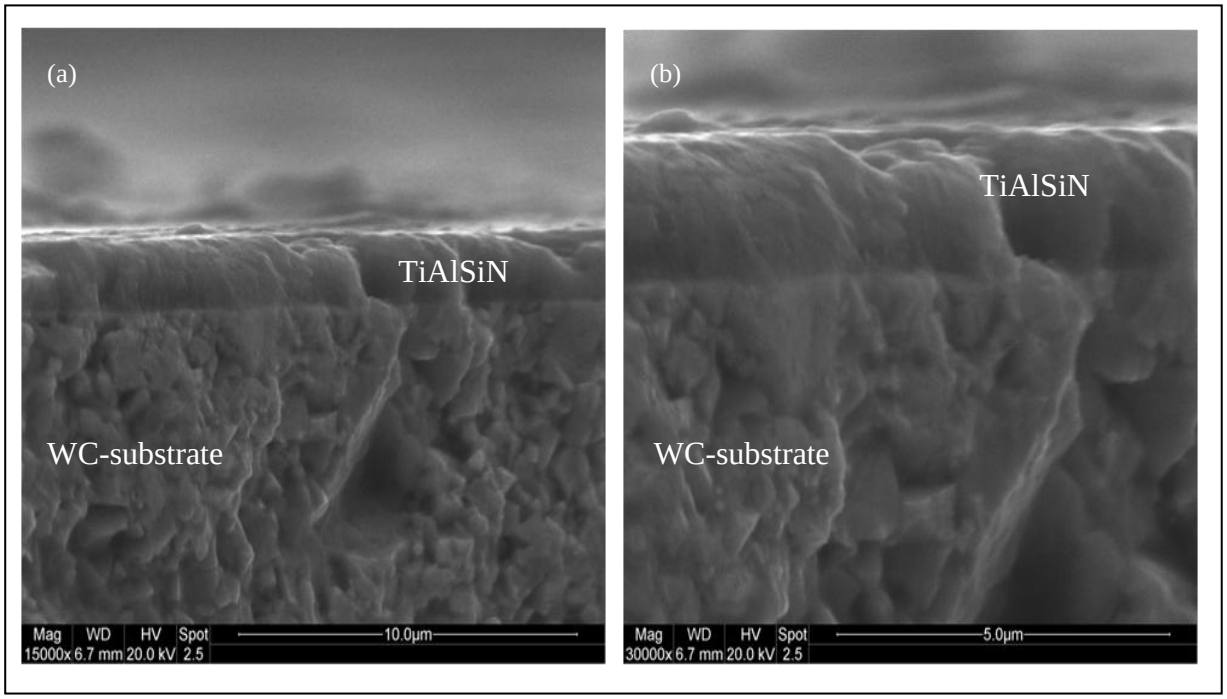

Figure 3.5. SEM photomicrographs illustrating the fracture cross-section view of TiAlSiN (a) at 15000 mag and (b) at 30000 mag.

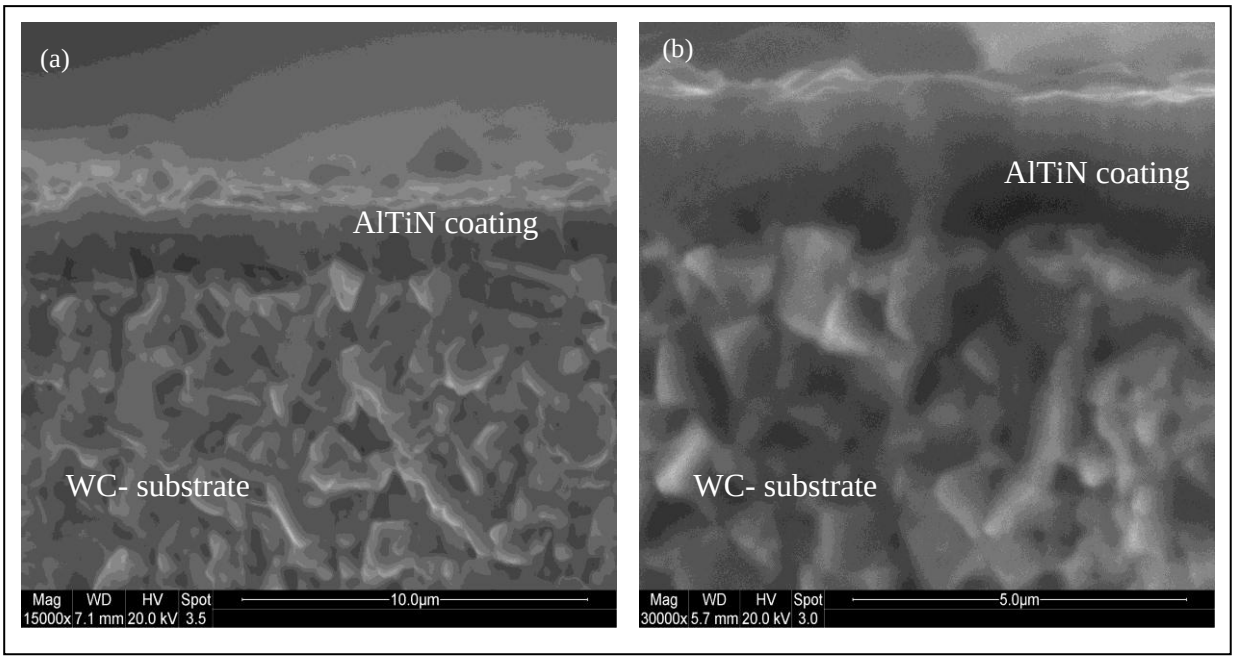

Figure 3.6. SEM photomicrographs illustrating the fracture cross-section views of AlTiN coating (a) at 15000 mag and (b) at 30000 mag.

3.4 Structural characterization and grain size

The crystal structure of both coatings was determined by glancing angle X-ray diffraction (GA-XRD) technique using an angle of incidence of 2°. A Cu-K_α radiation source (wavelength of 0.15405 nm) was used at 40 kV and 40 mA.

Figure 3.7 presents the XRD results for the TiAlSiN coatings and reveals that the coating exhibits a single phase FCC structure. The diffractogram shows a large number of peaks from the substrate *ie* tungsten carbide. There are, however, no signals from other crystals, such as Si_xN_y or titanium silicide. The only peaks observed are those of TiN, with mixed orientations of (220) and (222). No peaks associated with the AlTiN phase were observed. This is probably due to the low aluminium content in the coating. This result implied that Si is present in an amorphous phase of silicon nitride. Peak broadening is observed in the TiAlSiN XRD spectra, which is attributed to the decrease in crystalline size of the coating probably because of the incorporation of TiN in an amorphous Si_3N_4 matrix. This observation is consistent with earlier reported work [165-168]. However it should also be mentioned that distinction between TiN and TiAlSiN phases with diffraction methods is generally not feasible because of the isomorphism of these phases. In fact, the TiAlSiN is the secondary solid solution based on TiN. The average grain size of the crystallites in TiAlSiN coating was calculated from the Full Width at Half Maximum (FWHM) value for the pair of parallel plane {222} and was found to be approximately 2.8 nm. Therefore, this TiAlSiN coating can be termed as a nanostructured coating.

The XRD result for the AlTiN coating is displayed in Figure 3.8. The spectra show peaks corresponding to TiN phase as well as to the tungsten carbide substrate. It appears that the coating crystallized in a FCC TiN structure. None of the other phases, such as AlTiN or AlN were observed. This is due to the chemical composition of the coatings which does not have the required proportion of aluminium to form an AlTiN or AlN phase [152].

The average grain size of the crystallites in AlTiN coating was calculated from the FWHM value for the pair of parallel plane {111} and was found to be approximately 34.3 nm.

3.5 Coating hardness

Nanoindentation is a sensitive probing technique and is being increasingly used to reveal the mechanical properties of thin films and coatings. In these studies, indentations are made on flat surfaces or well-polished cross-sections. Ideally in nanoindentation experiments, the flat surface of sample is mounted perpendicular to the tip of the indenter.

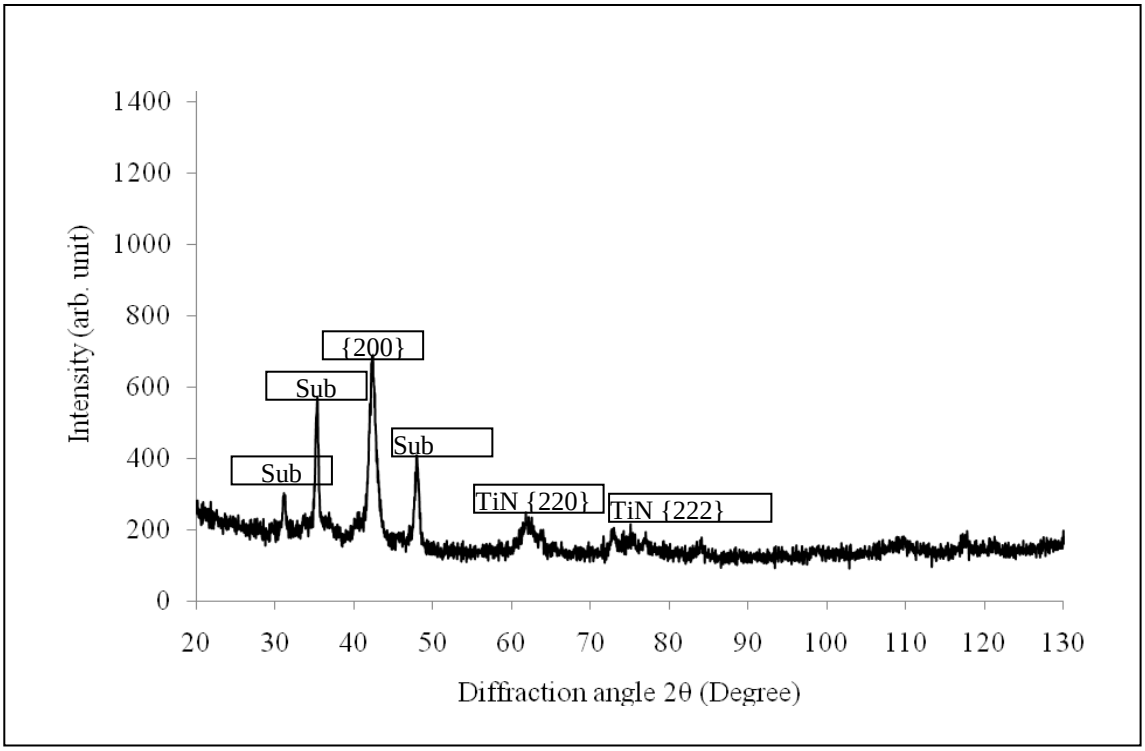

Figure 3.7. X-ray diffraction pattern of TiAlSiN coating.

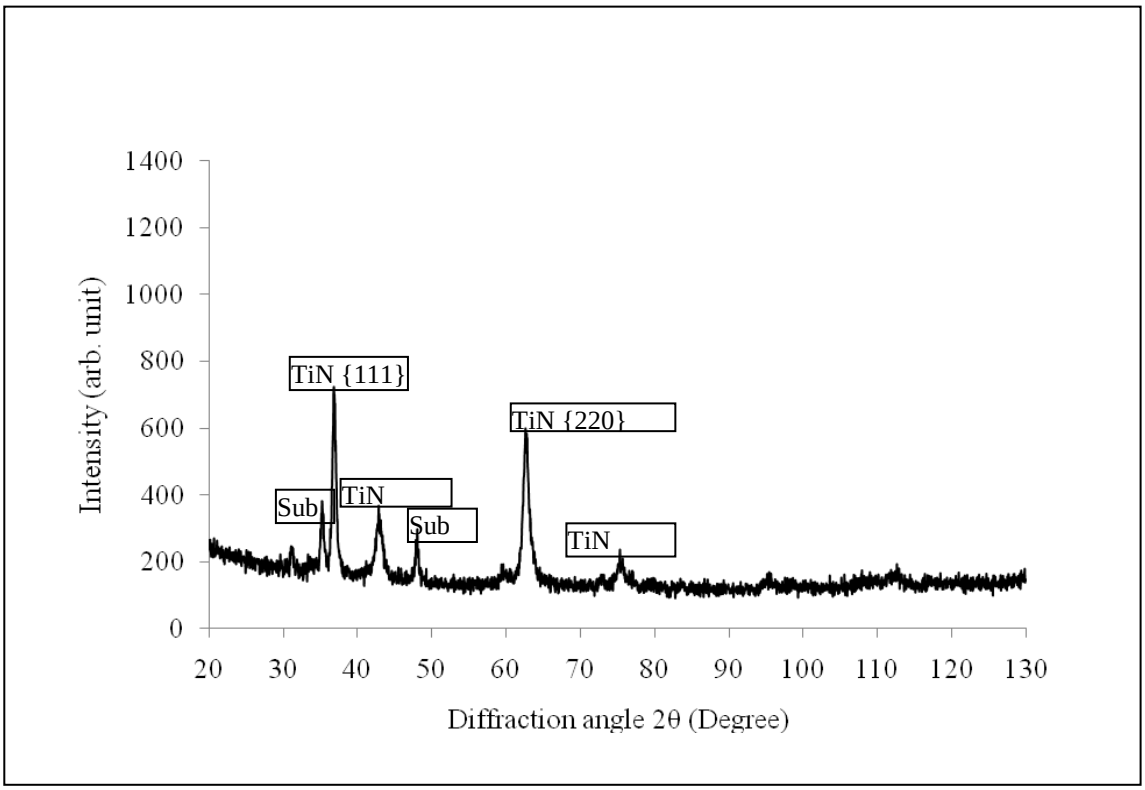

Figure 3.8. X-ray diffraction pattern of AlTiN coating.

The main objective of the nanoindentation test is to extract elastic modulus and the hardness of the coating (or any other specimen) from the experimental reading of the indenter load and the depth of penetration. In a typical test, load and depth penetration are recorded as the load is increased from zero to some maximum value and then back to zero from the maximum load value. There is a residual impression (or indent) left on the surface of the specimen if plastic deformation takes place. However, this impression is too small to be observed through optical means. The known geometry of the indenter, together with the depth of penetration provides an indirect means of measuring the area of the contact at the full load, from which the mean contact pressure and therefore the hardness may be calculated. The deformed material attempts to regain its original shape once the load is removed, but is prevented from doing so due to the plastic deformation that has taken place. There is, however, a certain degree of recovery due to the relaxation of the elastic strains in the material. The elastic modulus of the indented materials can be calculated by analysing the initial portion of this elastic unloading response.

Indentation experiments were performed using a Hysitron Triboindenter fitted with a Berkovich indenter (tip end radius or radius of curvature of 100 nm) and loaded with Triboscan 7.0 software, designed by Hysitron, Inc. Tests were done at a range of peak loads from 0.5 to 10 mN. The maximum indentation (or penetration) depth was less than 1 μm, which is less than half the thickness of either coating. The nano-indentation tests were performed under open loop control mode. The mechanical properties (hardness and elastic modulus) of the coatings were measured using the Oliver and Pharr method [169]. The load-indentation graphs for TiAlSiN and AlTiN coatings were plotted using Microsoft Excel and are shown in Figures 3.9 and 3.10 respectively. The tabulated mechanical properties of both these coatings are listed in Table 3.3.

The results presented in Table 3.3 indicate a large scattering due to the cathodic arc deposition technique. These values are in close agreement with the reported values for other TiAlSiN coatings deposited by other techniques such as reactive sputtering. Previous work carried out by Chang *et al* who deposited TiAlSiN coating on a tungsten carbide substrate, using cathodic arc evaporation technique, reported hardness of 40 GPa and Young's modulus of 365 GPa [167]. Fuentes *et al* obtained a hardness value of approximately 35 GPa and modulus of approximately 472 GPa for the TiAlSiN coating deposited by cathode arc evaporation technique on a steel substrate [170].

Mo *et al* deposited an AlTiN coating on a tungsten carbide substrate using multi-arc ion plating technique and found the hardness and elastic modulus to be 35.7 ± 9.8 GPa and 460.4 ± 80.3 GPa respectively [171]. Rabinovich *et al* deposited AlTiN coatings $(Al_{0.66}Ti_{0.34})_{0.51}N_{0.49}$ on a tungsten carbide substrate using un-balanced magnetron sputtering source and determined the hardness and Young's modulus as 22 ± 3.5 GPa and 321± 34 GPa respectively [172]. Chang *et al* deposited graded AlTiN/CrN coating on a silicon substrate using cathodic arc evaporation and stated the hardness and elastic modulus of the coating to be 31 ± 2 GPa and 420 ± 30 GPa respectively [173].

Table 3.3. Mechanical characterization results for TiAlSiN and AlTiN coatings.

Coating	Hardness [GPa]	Young's Modulus [GPa]
TiAlSiN	35.84 ± 9	348.87 ± 56
AlTiN	32.08 ± 9	372.09 ± 68.7

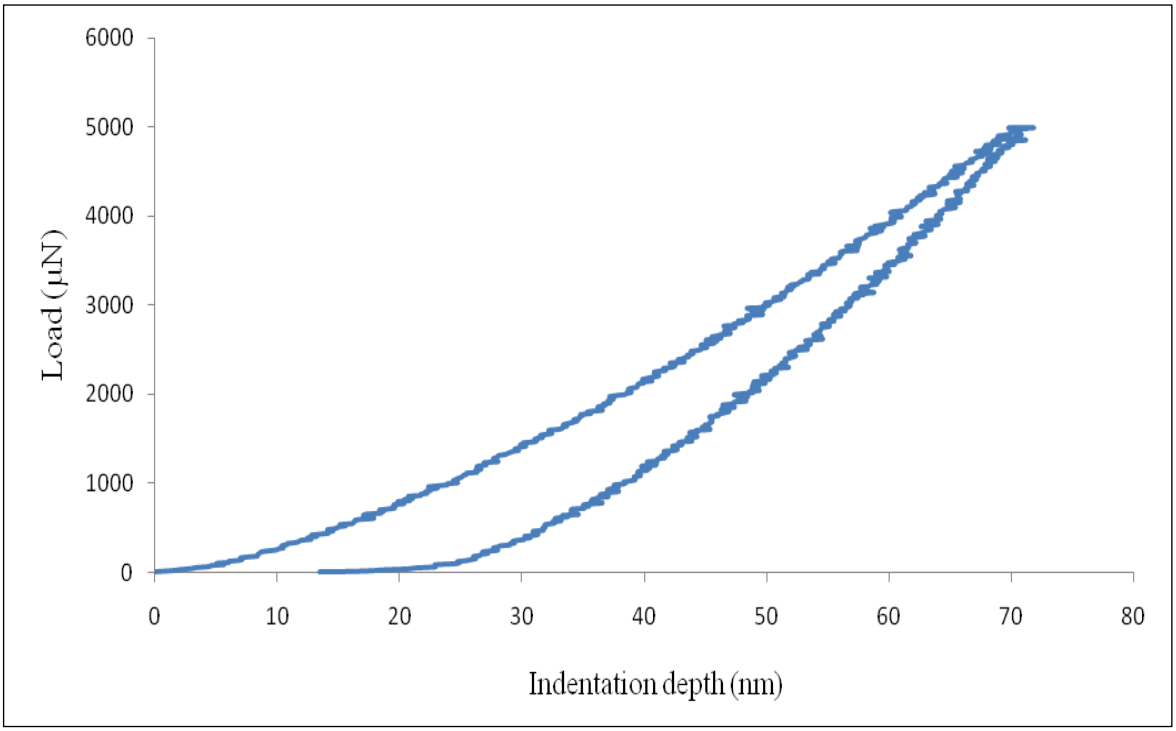

Figure 3.9. Load versus indenter displacement for TiAlSiN coating.

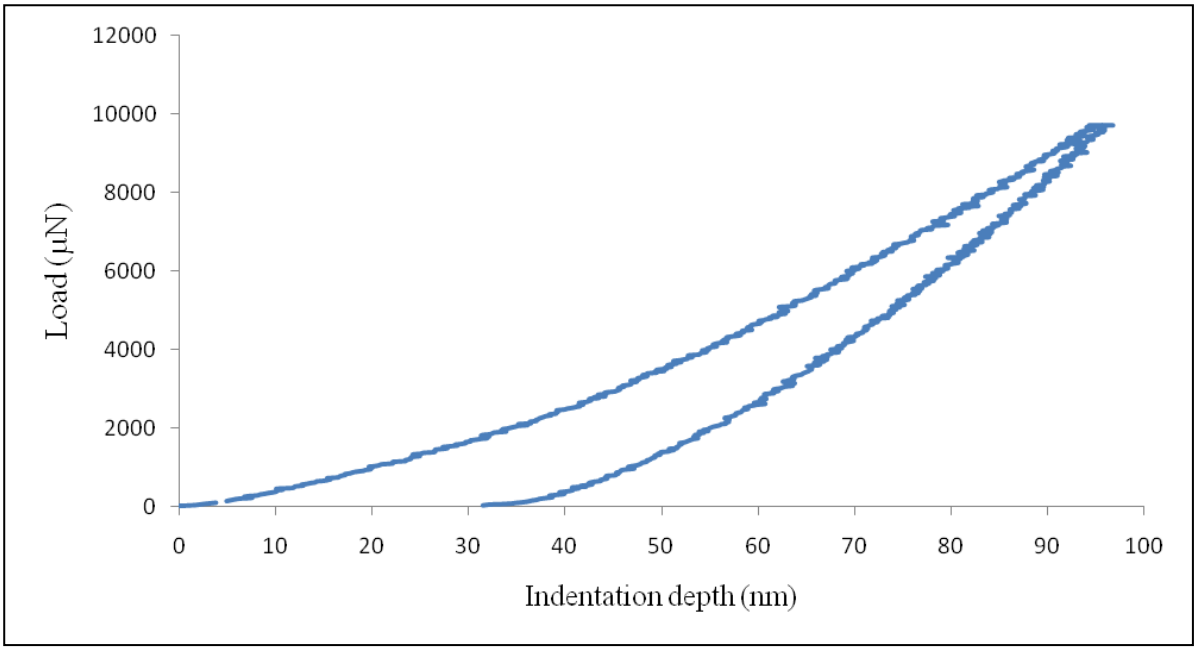

Figure 3.10. Load versus indenter displacement for AlTiN coating.

3.6 Coating adhesion

One of the basic requirements of the functional coatings is their sufficient adhesion onto the substrate. Therefore, the need for quantitative assessment of thin film or coating adhesion on the substrate is important. Many techniques for the assessment of coating/substrate adhesion have been documented and it seems to be an active area of research [174, 175]. The test procedure that is widely used is the scratch test and this has been used for many years to produce quantitative measures of the coating/substrate adhesion [176, 177]. The primary reason for using this method is the fact that this test offers an attractive compromise between easy test procedure with little specimen preparation on the one hand and accuracy of quantitative results on adhesion on the other.

In the conventional configuration of the scratch test, a diamond stylus is drawn across the coated surface under stepwise or continuously increasing normal force until some failure occurs and this load is termed as "critical failure". Many different failure modes have been observed which include coating detachment, through-thickness cracking and plastic deformation or cracking in the coating or substrate [174, 178–180]. For example, spalling of the coating at the interface would indicate adhesive failure; whereas chipping within the coatings would indicate a cohesive failure. The adhesive mechanical strength of the coatings/substrate system is characterized by the "critical load" L_c, which is defined as the

minimum load at which the first damage occurs. Several different failure modes can happen simultaneously and can complicate the interpretation of the results. The failure of the coatings can be observed using optical or electron microscopy.

A Teer Coatings ST-200 scratch tester with 200μm radius Rockwell diamond stylus was used for scratch testing. The applied normal load was ramped from 10 to 100N during the test as the stylus was drawn across the steel substrates coated with TiAlSiN and AlTiN. The loading rate was 10N/mm and the indenter transverse speed was 10mm/min. Three scratch tests were performed on the coated substrate (*i.e.* backing steel in the bandsaw teeth). This scratch test was not carried out on coated carbide teeth or on the flat coated carbide coupons, as their sizes were too small for the complete scratch track. The adhesion quality of the coatings was evaluated based on the morphology around the scratch line, using electron microscopy. Representative SEM images of the scratch test for TiAlSiN and AlTiN coatings on the steel substrate are given in Figure 3.11.

Figure 3.12 shows the magnified SEM images of the scratch line morphology of TiAlSiN and AlTiN coating on the steel substrate and reveals no significant difference. There is no evidence from these images of coating spallation. No cracking, flaking or chipping of the coating can be observed from these SEM micrographs, suggesting that TiAlSiN and AlTiN coatings adhere well to the substrate and possess good adhesive and cohesive properties.

The adhesive strengths of the AlTiN and TiAlSiN coatings were found to be approximately 75N and 69 N respectively (average of three results), therefore it can be concluded from these results that the AlTiN and TiAlSiN coatings can withstand scratching loads of 75N and 69 N without severe failures, such as flaking or cracking. It should, however be noted that the substrate plays an important role in measuring the adhesive strength of the coatings. Chen *et al* reported that TiAlSiN coating had low adhesive strength (~67 N) compared to TiAlN (~81N) on a cemented carbide substrate and attributed this to the high stress and brittleness associated with the incorporation of a Si_3N_4 phase [181].

In order to gather more information on the adhesion of the coatings, Rockwell C adhesion test was performed on the coated steel substrate. The Rockwell C-indentation tests were carried out for the steel substrate, since the test is not applicable for ceramic or hard metal substrates [182]. This test method uses a standard Rockwell hardness tester exploiting a standard Rockwell indenter tip (120° diamond cone, 200 μm radius) with a maximum applied load of 150 kgf (or 1471N). The indentation causes layer damage adjacent to the boundary of the impression. Three indentations were produced on each of the coated

samples and were evaluated using the scanning electron microscope at a magnification of 100, which is the standard magnification for this test.

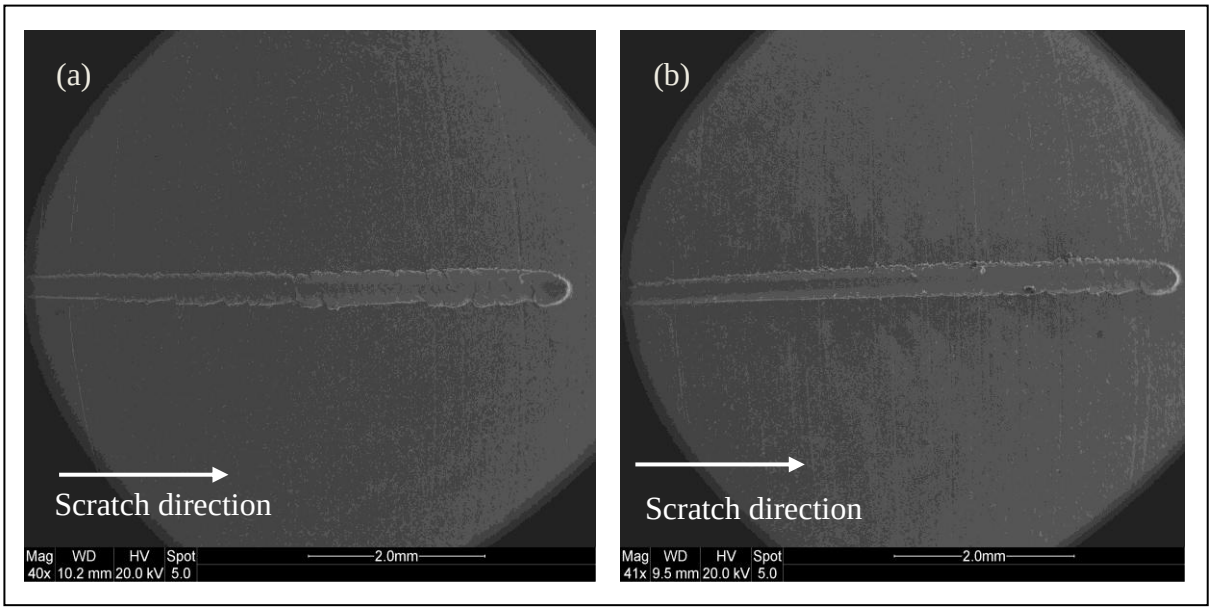

Figure 3.11. SEM micrographs for the scratch tests (a) AlTiN coatings (b) TiAlSiN coating – scratch direction is left to right.

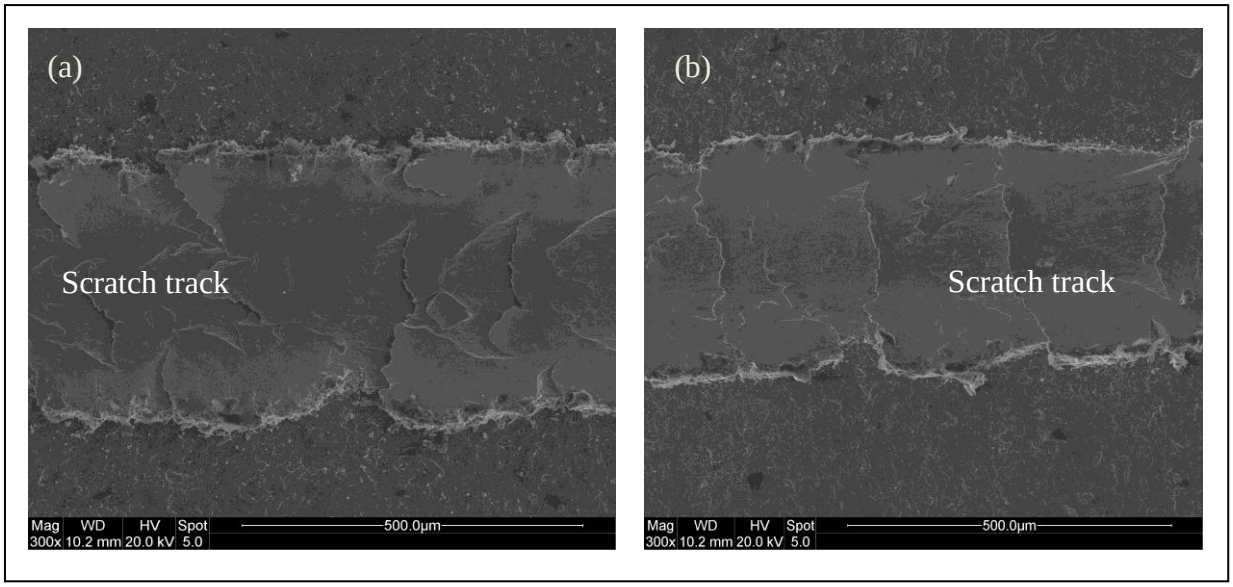

Figure 3.12. Magnified SEM micrographs for the scratch test track (a) AlTiN coatings (b) TiAlSiN coating – scratch direction is left to right.

The damage to the coatings was compared with the defined adhesion strength quality shown as Figure 3.13. The strength adhesion quality varies from HF1 to HF6. HF1 to HF4, define sufficient adhesion, whereas HF5 and HF6 indicate poor adhesion.

Typical results of the Rockwell C indentation carried out for AlTiN and TiAlSiN coatings are shown in Figures 3.14 and 3.15 respectively – both coatings displayed circular cracks

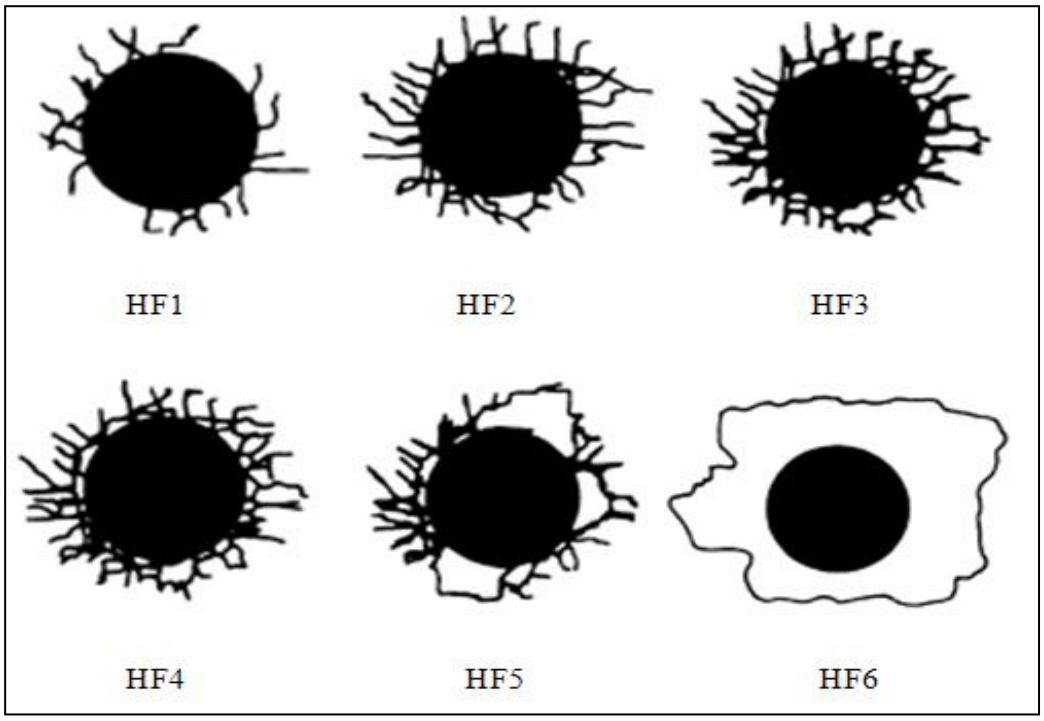

Figure 3.13. Adhesion strength quality from HF1 to HF6 [183]

around the indentation (these have not penetrated the indentation mark) and no radial cracks can be observed. On the basis of Figures 3.14 and 3.15, the adhesion level of both coatings was considered good, since no detachments of the coatings along the indentation edge can be observed. Both the coatings show adhesion strength of between HF2 and HF3. Moreover, circular cracks noticed around the indentations, in both coatings, is a feature which is typically observed in indented hard coatings and derives from the fact that the top layer is extremely hard and results in multiple cracking when indented. This phenomenon has been reported in systems where a thin hard layer of coating is deposited on a substrate with a significantly lower hardness compared to the coatings [184, 185]. This explanation correlates well to the present work, where hard, wear resistant coatings have been applied to a softer substrate (hardness of substrate 472 ± 26 Vickers or 4.6 GPa).

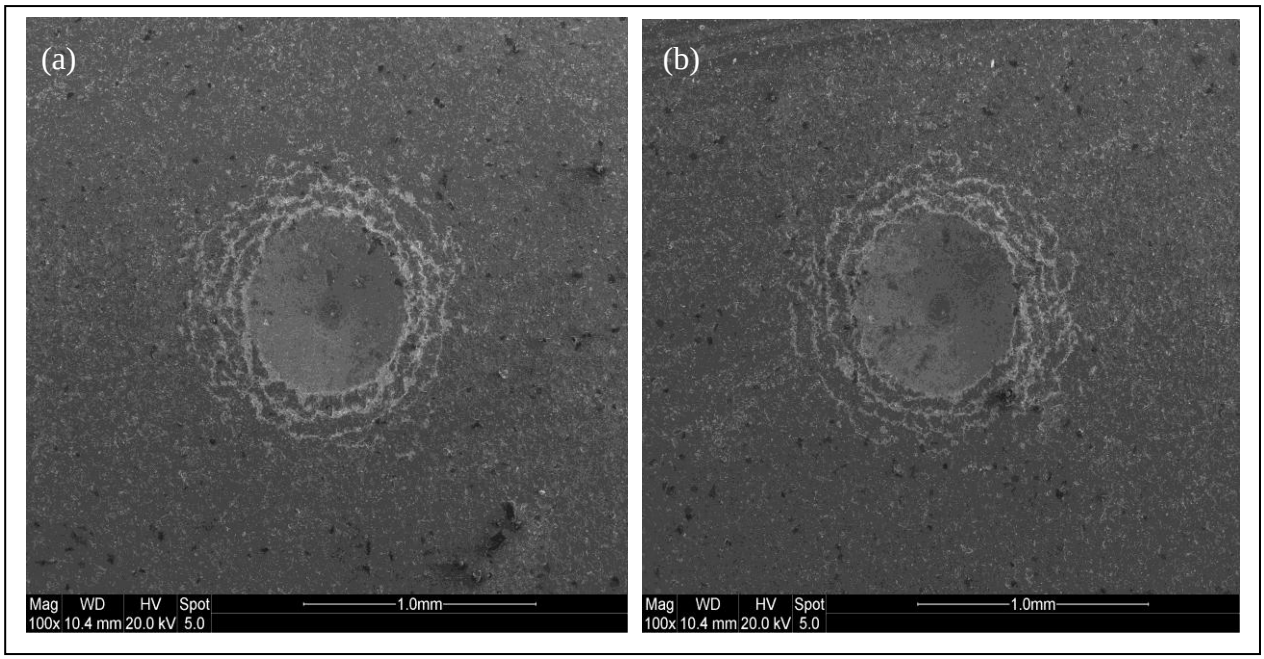

Figure 3.14. SEM micrographs of Rockwell C adhesion tests carried out on AlTiN coated substrate, showing circular cracks around the indentation.

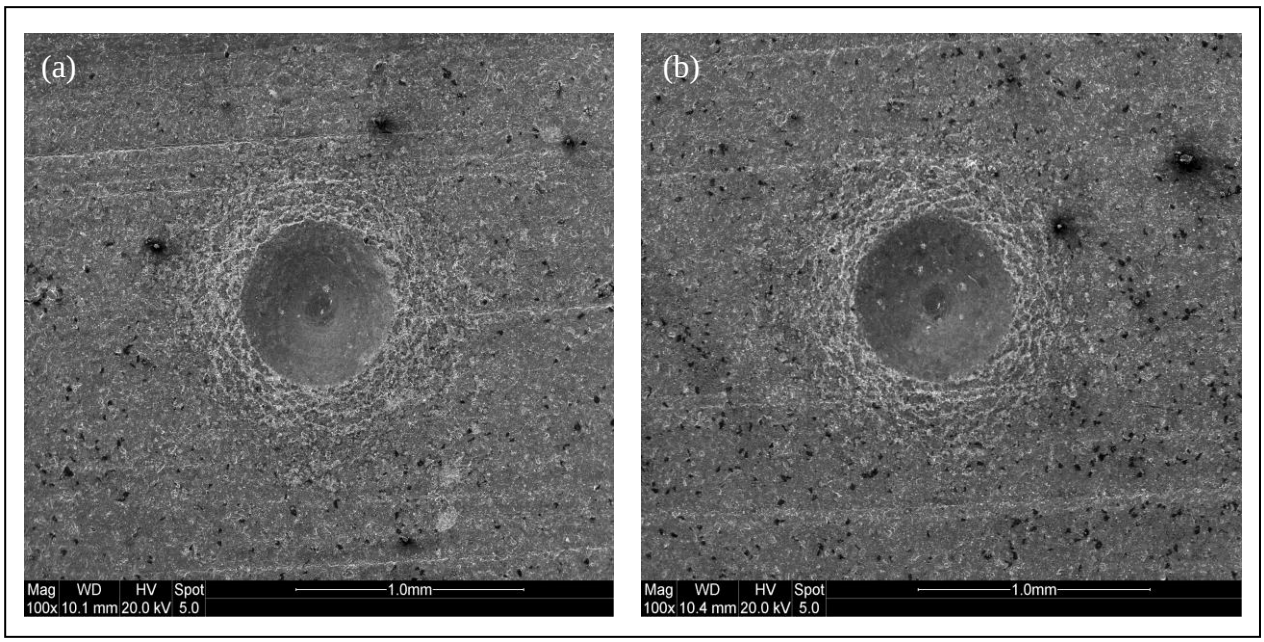

Figure 3.15. SEM micrographs of Rockwell C adhesion tests carried out on TiAlSiN coated substrate, showing circular cracks around the indentation.

CHAPTER 4: RESULTS AND DISCUSSIONS

4.0 Introduction

This chapter will focus on the results and analysis of the single tooth tests carried out on Ti-17 alloy, using un-coated and coated carbide bandsaw teeth. The results and analyses will focus on forces and specific cutting energy while machining Ti-17 alloy and the wear modes and mechanisms of the un-coated and the coated bandsaw teeth that evolve during the machining operation. Moreover, it was observed during the cutting tests using Ti-17 as the workpiece material, that the cutting force was always less than the thrust force. This behaviour is not observed, normally in other metal cutting operations (*e.g.* turning, milling) while machining titanium alloys. It was, therefore considered important to investigate this unique phenomenon by using bandsaw teeth with different honing lengths and by using different workpiece materials (Ti-17 alloy and mild steel).

It is important to consider the main physical features and chemical composition of the carbide teeth that were used to machine Ti-17 alloy.

4.1 Characteristics of carbide tipped bandsaw teeth

The main features of bandsaw tooth are presented in Figure 4.1. The nominal rake and clearance angles were measured using a Leica S6D optical microscope and were found to be 10º ±0.5º and 20 ±0.5º respectively. The average cutting edge radius of the bandsaw tooth was approximately 13 µm. Figure 4.1(a) presents a typical SEM micrograph of the bandsaw tooth, showing both the clearance and rake faces. The carbide tip can be clearly differentiated from the backing steel. Figure 4.1 (b) provides a magnified view of the cutting edge, which appears to be free of any defects, such as chipping. Horizontal grinding marks are visible on the clearance face. However, less grinding marks are observed on the rake face due to the fine face grinding operation performed during the bandsaw manufacturing process. This helps the chip to flow easily over the smooth rake face. A special operation known as "honing" is performed on carbide bandsaw teeth, in order to produce a small flat on the cutting edge. This is low-speed, controlled, sizing and surface finishing operation. In addition to removing stock, honing serves the important purpose of generating functional characteristics for surfaces and involves the correction of dimensional errors resulting from previous machining operations. Functional characteristics generated by honing include geometric accuracy (roundness and

straightness), dimensional accuracy and improves the surface character in terms of its roughness and integrity. The bandsaw teeth are honed to remove nicks and burrs, improve finish and to make minor corrections in tooth shape, such as introducing a flat on the clearance face for the coating to adhere. For the carbide bandsaw teeth, honing is carried out to produce a flat on the cutting edge in order to reduce vibrations during run-in, which is a major issue for carbide bandsaws owing to their sharpness. Moreover, honing also modifies the edge so that it does not chip at the initial contact with the workpiece material. However, the honing process cannot be substituted for a grinding operation as it is not designed for heavy stock removal.

Figure 4.2 illustrates the difference between a nominally sharp and a honed tooth.

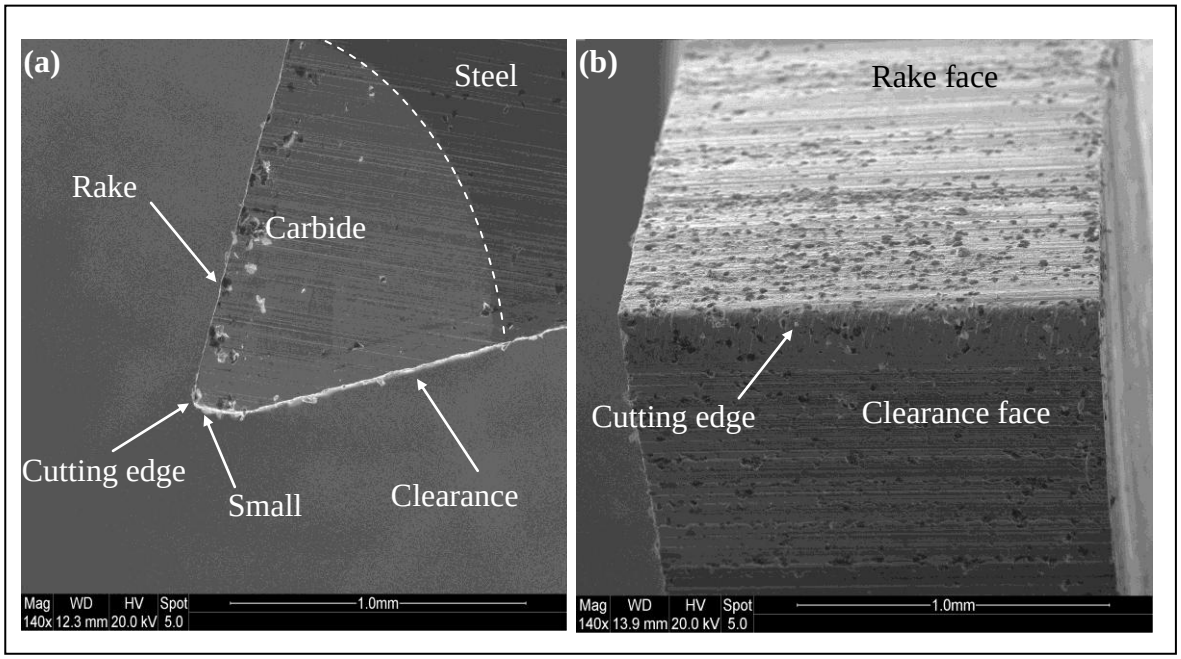

Figure 4.1. SEM micrographs of carbide tipped bandsaw tooth showing (a) tooth geometry and (b) close view of the cutting edge.

4.1.1 Elemental composition of carbide bandsaw teeth

The elemental composition of the un-coated carbide teeth (Sandvik H10F tungsten carbide) was measured using the EDX attached to the scanning electron microscope. Three different teeth were analyzed and ten different, random points were selected on each of the carbide teeth. The average of these measured values is presented in Table 4.1 and Figure 4.3. The nominal composition of H10F is shown in Table 4.2, whereas Table 4.3 presents some mechanical and physical properties of H10F.

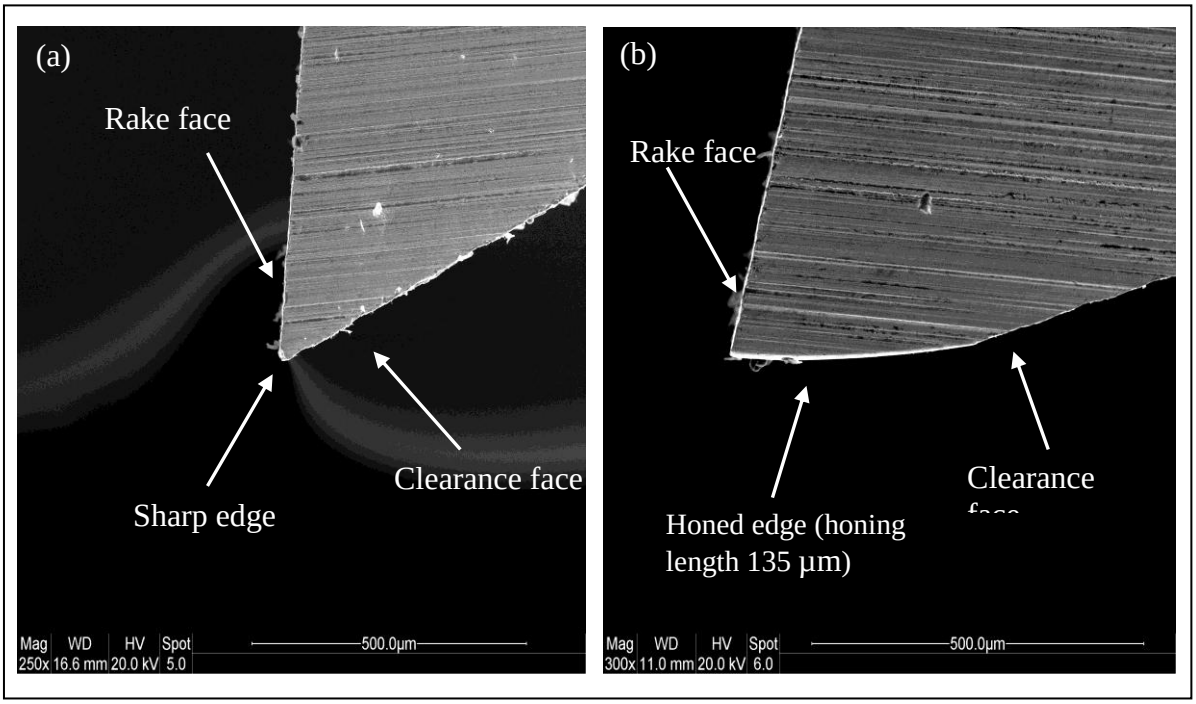

Figure 4.2. SEM images of carbide teeth (a) sharp tooth and (b) honed tooth showing a honing length.

Table 4.1. Elemental composition of the carbide bandsaw tooth as measured by EDX

Element	**Wt %**
Carbon	9.07
Cobalt	8.63
Tungsten	82.21

Table 4.2. Nominal composition of the H10F carbide

Constituent	**Wt %**
WC	89.5
Co	10
Others	0.5

Table 4.3. Some physical and mechanical properties of Sandvik H10F tungsten carbide

Binder content	10 %
Hard phase	Tungsten carbide
Young's modulus (GPa)	585
WC grain size	0.85 µm
Transverse rupture strength (MPa)	4400 (avg)
K_{1c} ($MN/m^{3/2}$)	12.7
Vicker's hardness Hv30	1585

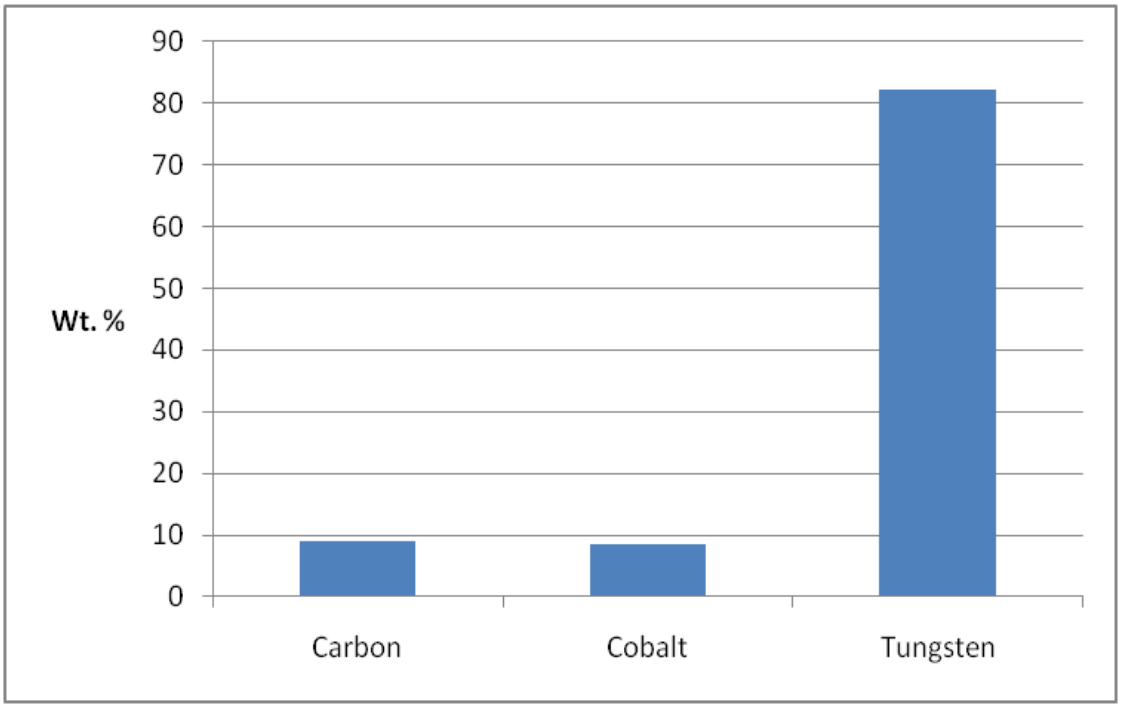

4.3. Elemental composition of the carbide teeth, measured using EDX

4.1.2 Mechanical and elemental properties of Ti-17 alloy

Ti-17 is the commercial name for Ti-5Al-2Sn-2Zr-4Mo-4Cr (wt%) alloy. It has been classified as "beta" rich alpha-beta alloy and designed primarily for application as fan and compressor disk material. Ti-17 has higher tensile and creep strengths than the well-known Ti-6Al-4V alloy and has lower density and higher modulus than most beta alloys. The mechanical properties of Ti-17 alloy are shown in Table 4.4. The elemental compositions of FIVE different points on the workpiece were measured using EDX and

their averages are shown in Table 4.5. The nominal chemical composition of Ti-17 alloy is shown in Table 4.6.

Table 4.4. Mechanical properties of Ti-17 workpiece (nominal)

Ultimate tensile strength (MPa)	Yield strength (MPa)	Hardness (HRc)
1172	1104	39

Table 4.5. Elemental composition (wt%) of Ti-17 alloy, as measured by EDX

Element	Al	Sn	Zr	Mo	Cr	Ti
Wt %	5.5	2.5	2.5	4.5	4.5	Bal

Table 4.6. Nominal elemental composition of Ti-17 alloy

Element	Al	Sn	Zr	Mo	Cr	Ti
Wt %	5	2	2	4	4	Bal

4.2.0 Machining parameters for bandsawing Ti-17 alloy

Currently, very little information is available in the public domain on the bandsawing of titanium alloys. Therefore a series of preliminary tests was carried out in order to find the optimum machining parameters (feed, speed) for bandsawing Ti-17 alloy. For these tests, width of cut for all the cutting tests was selected as 1 mm, which is less than the average tooth thickness (1.598 mm). Three cutting speeds (80 m/min, 60 m/min and 40 m/min) and four different depths of cuts (10 µm, 15 µm, 20 µm and 25 µm) were chosen for the cutting tests. These parameters were selected because industrially bandsawing of titanium alloys is carried out in this range. Forces were measured during the tests and the wear modes and mechanisms experienced by the tooth were investigated using a SEM.

4.2.1 Bandsawing life with depth of cut

Figure 4.4 presents the life of the carbide tipped bandsaw teeth in terms of number of sections cut at different depths of cut or feeds and at a constant surface cutting speed of 40 m/min. It is clear from Figure 4.4 that 10 µm is the most suitable feed for machining Ti-17 alloy *i.e.*, the tooth has a longer life in terms of its machining performance as compared to the teeth which were used at higher feeds. This can be explained by the fact that at high feed rates of 15 µm, 20 µm and 25 µm, a combination of high cutting force and heat

generated leads to rapid wear and degradation of the cutting edge. The 5 µm feed, though would make the tooth last longer, but would result in low productivity. Moreover, at 5 µm feed, the tooth will "rub" on the workpiece rather than cutting it.

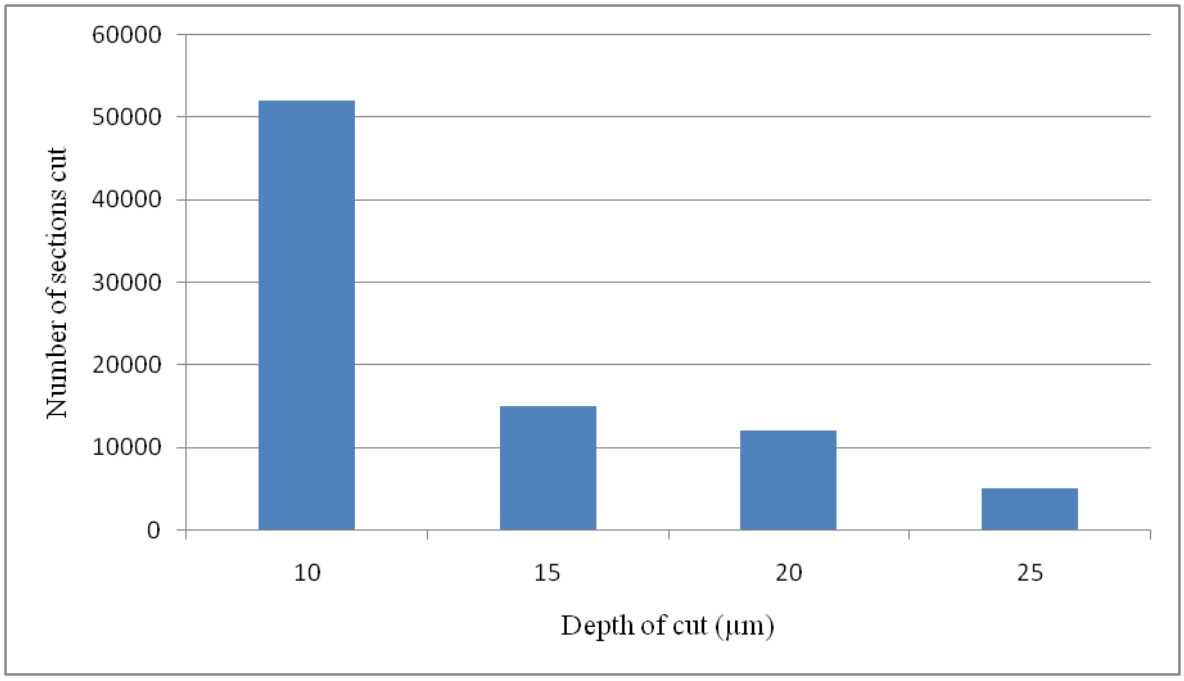

Figure 4.4. Number of workpiece sections cut at different depths of cut (feeds) while machining Ti-17 alloy using carbide teeth (cutting speed: 40 m/min, width of cut: 1 mm)

Figure 4.5 shows the variation of cutting forces with the increase in feed for the carbide tooth. It is evident from Figure 4.5 that with the increase in feed, the cutting force increases to higher magnitudes and shows a linear behaviour. At the low feed of 10 µm, the carbide tooth experienced a cutting force of 80 N and increasing the feed to 25 µm, the force value increased to approximately 110 N.

Figure 4.6 displays the conditions of the bandsaw cutting edges after they had performed a number of cuts when used at different depths of cut. In all cases, it was found that the tool life was controlled by flank wear and corner wear. The severity of the corner wear increased with the increasing depths of cut. The length of flank wear was extended to approximately half of the width of the cutting edge as the width of cut was selected as 63% of the width of cutting edge. Chipping on the rake face was characteristic of all the bandsaw teeth tested. Since the tooth engages and disengages periodically with the workpiece (intermittent operation), it can be assumed that cyclic mechanical and thermal loading on the bandsaw tooth are responsible for chipping and degradation.

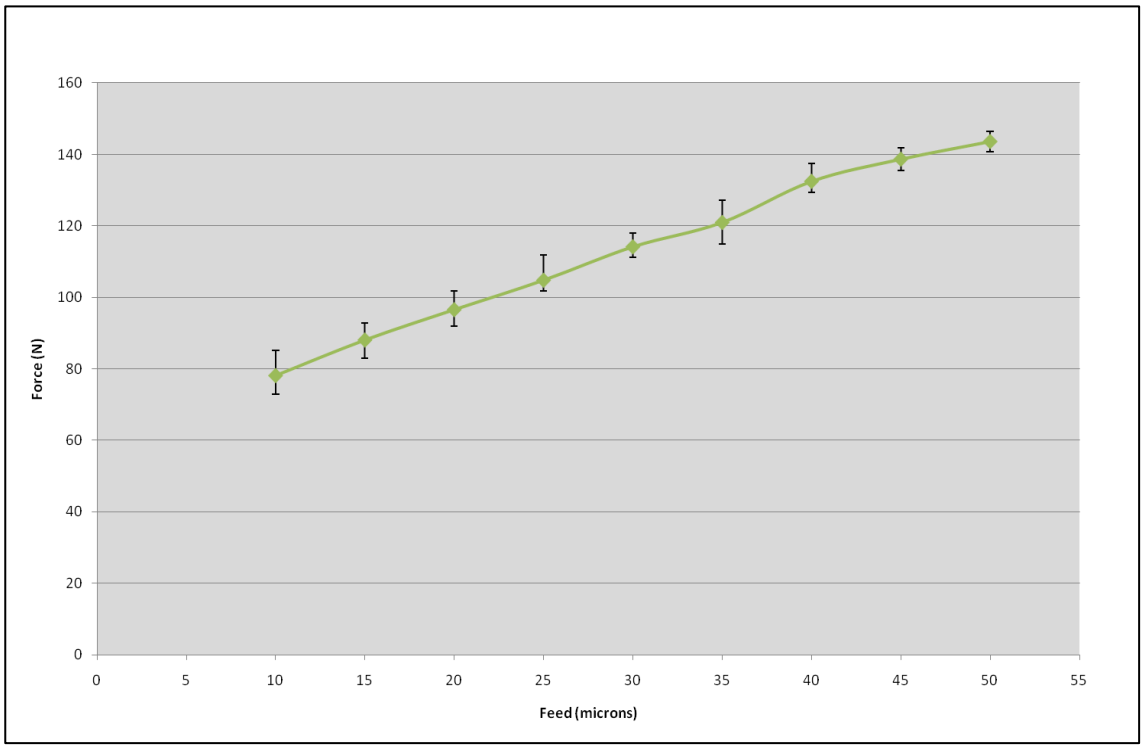

Figure 4.5. Variation in cutting force with the increase in feed for the un-coated carbide tooth (average of three cutting tests).

It is clear from Figure 4.6 that the higher feeds reduce the life of carbide bandsaw teeth while machining Ti-17 alloy. It can be concluded that the carbide teeth will perform better at low depths of cut (or feeds) when machining Ti-17 alloy. From the condition of worn carbide teeth shown in Fig. 4.6 it can be concluded that tooth will last for longer time i.e. it will produce large number of cuts and therefore it may be said that optimum feed or depth of cut for bandsawing Ti-17 alloy is 10 µm within the range of depths of cut used.

4.2.2 Bandsawing life with cutting speed

In order to find the optimum surface cutting speed for bandsawing Ti-17 alloy, another series of tests was performed. Single tooth tests were carried out, using width of cut as 1 mm, which was less than the average tooth thickness (1.59 mm). Three different cutting speeds (40 m/min, 60 m/min and 80 m/min) and a single depth of cut (10 µm) were chosen for the cutting tests to ascertain the wear/degradation of the bandsaw teeth.

Figure 4.7 presents the performance of the carbide tipped bandsaw teeth in terms of number of sections cut at different surface cutting speeds. It is clear from Figure 4.7 that 40 m/min is the most suitable cutting speed for machining Ti-17 alloy as the carbide tooth

has the longest life when used at this speed. The relatively poor performance at higher cutting speeds is attributed to the higher temperature generated, which tends to be concentrated at the cutting edge of the carbide tooth owing to the low thermal conductivity of titanium alloy. It has been reported previously that the temperatures, while machining titanium alloys can reach as high as 1000ºC [48, 49]. Therefore it can be assumed with a high level of confidence that high temperatures exist at the tool/workpiece interface and these temperatures are responsible for the poor performance at high speed. Although a low speed of 30 m/min could also have been chosen, this would have led to low productivity.

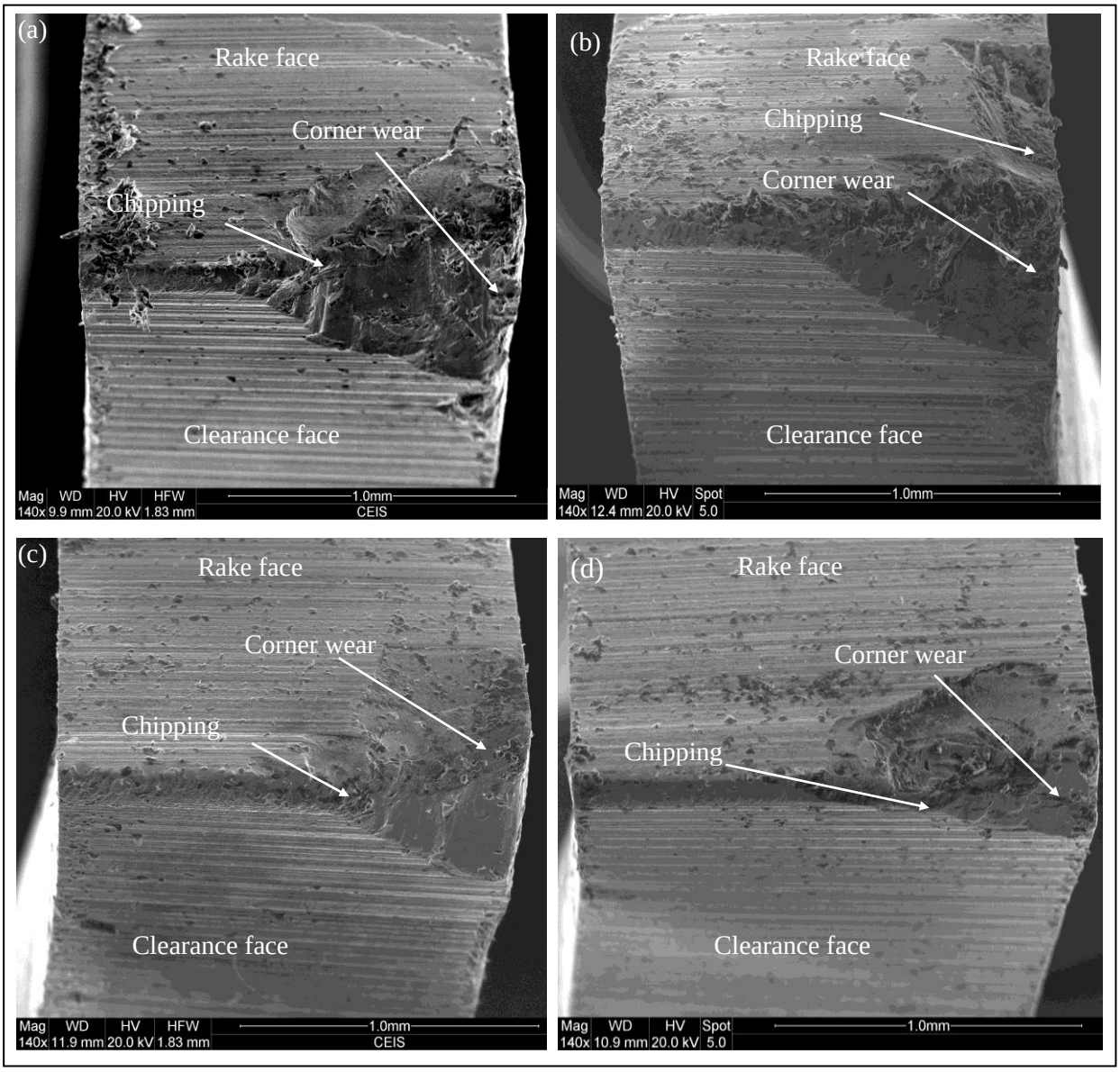

Figure 4.6. Conditions of the carbide teeth after a number of cuts (a) at 25 µm feed and after 4000 cuts, (b) 20 µm and 11000 cuts, (c) 15 µm and 15000 cuts and (d) 10 µm and 52 000 cuts, (cutting speed: 40 m/min, width of cut: 1 mm).

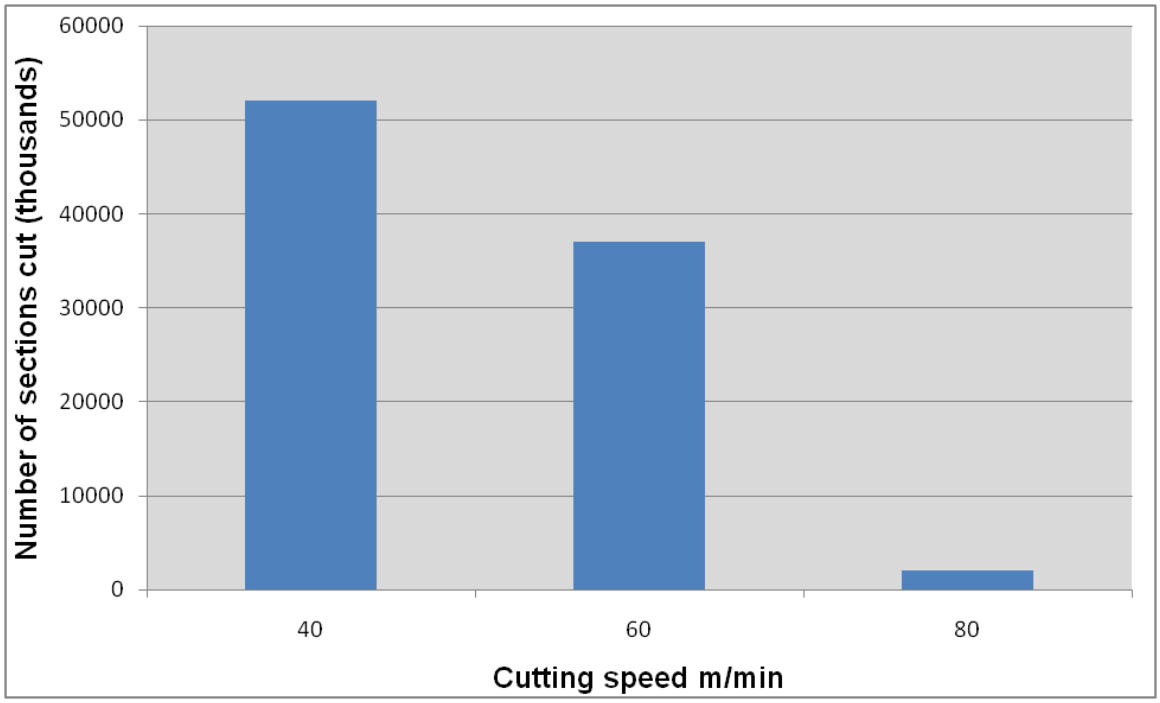

Figure 4.7. Number of workpiece sections cut at different cutting speeds, while machining Ti-17 alloy with carbide tipped bandsaw teeth (feed: 10 µm, width of cut: 1mm).

The conditions of the carbide teeth after they have performed a certain number of cuts, at different cutting speeds are presented in Figure 4.8. Although all these bandsaw teeth shown in Figure 4.8 were not used to produce the same number of cuts, however in all cases it was found that the tool life was controlled by flank and corner wear. The severity of the corner wear increased with the increase in cutting speeds. Chipping on the rake face was observed on all of the bandsaw teeth tested. It may be observed that the maximum corner wear is observed for the tooth which was used at the cutting speed of 80 m/min, followed by 60 m/min and 40 m/min. The tooth used for machining at 80 m/min showed premature failure by uncontrolled chipping and flaking.

From these results, it was concluded that higher cutting speeds reduce the life of carbide tipped bandsaw teeth during machining of Ti-17 alloy. Observing from the condition of the worn teeth, it may be concluded that the suitable cuttings speed while bandsawing Ti-17 alloy is 40 m/min within the selected speeds and at a feed of 10 µm.

4.2.3 Summary of the preliminary cutting tests

From the cutting results mentioned in the previous sections, it can be concluded that higher cutting speeds and higher feed rates affect the performance of the un-coated carbide tipped bandsaw teeth when bandsawing Ti-17 alloy. The degradation of the carbide tooth, in terms of chipping and wear increases at higher cutting speed and feeds, hence the suitable machining parameters for bandsawing Ti-17 alloy are low feed (10 µm) and low surface cutting speed (40 m/min). Therefore, it was decided that three different feeds (10µm, 15 µm, 20 µm) and a cutting speed of 40 m/min would be used as the machining parameters for further tests using both, the un-coated and coated carbide bandsaw teeth. The governing factor which led to the poor performance of the carbide teeth at higher feeds and higher speed is the poor machinibility of the Ti-17 alloy, especially their high strength (ultimate tensile strength ~1172 MPa) maintained at elevated temperatures and the low thermal conductivity (~7 Wm/K) of titanium alloys. Although less severe machining conditions *e.g.* feed of 5 µm and cutting speed of 30 m/min could be chosen, this would lead to low productivity and less efficient machining, as explained previously.

4.3.0 Performance of un-coated carbide teeth

Although a summary of preliminary results has been given in Section 4.4.3, it was considered important to mention and discuss the details of the cutting tests performed at all the parameters, *i.e.* three cutting speeds (80 m/min, 60 m/min and 40 m/min) and four different feeds (25 µm, 20 µm, 15 µm, and 10 µm). The width of the cut for these tests was set to 1 mm, which is less than the width of bandsaw tooth (average width of carbide tooth is 1.6 mm). These parameters were chosen in order to observe the forces and the wear of the un-coated carbide bandsaw teeth at the extreme machining parameters (highest and lowest) in terms of feeds and speeds.

4.3.1 Machining tests at 80 m/min cutting speed

Extremely high forces were the result of the cutting test carried out at the high cutting speed of 80 m/min and 25 µm feed, which led to the catastrophic failure of the carbide tooth. This in turn triggered the automatic safety system incorporated in the test rig, which resulted in the stoppage of machining.

Figure 4.9 shows the force trace for the un-coated carbide tooth that was used to machine Ti-17 alloy at the feed of 20 µm and a cutting speed of 80 m/min. It appears from Figure 4.9 that the tooth started wearing quickly from the corner of the cutting edge during the

initial stage of the cutting operation, leading to the side force becoming higher than the cutting force, after performing 500 cuts and therefore it will not machine the workpiece in an effective manner.

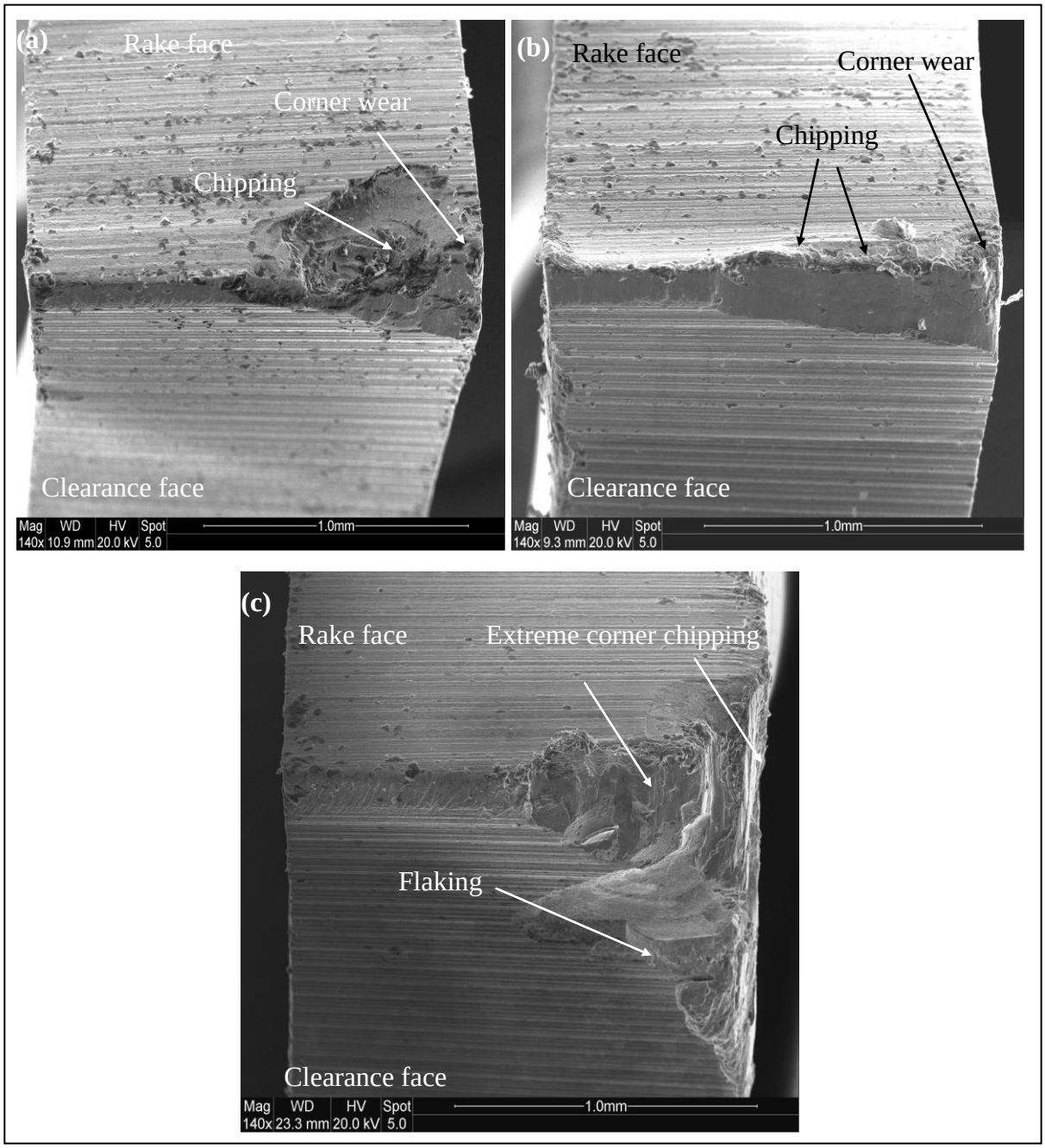

Figure 4.8. Conditions of the bandsaw teeth after performing number of cuts at (a) 40 m/min and 52 000 cuts, (b) 60 m/min and 37 000 cuts and (c) 80 m/min and 1000 cuts (feed: 10 µm, width of cut: 1 mm).

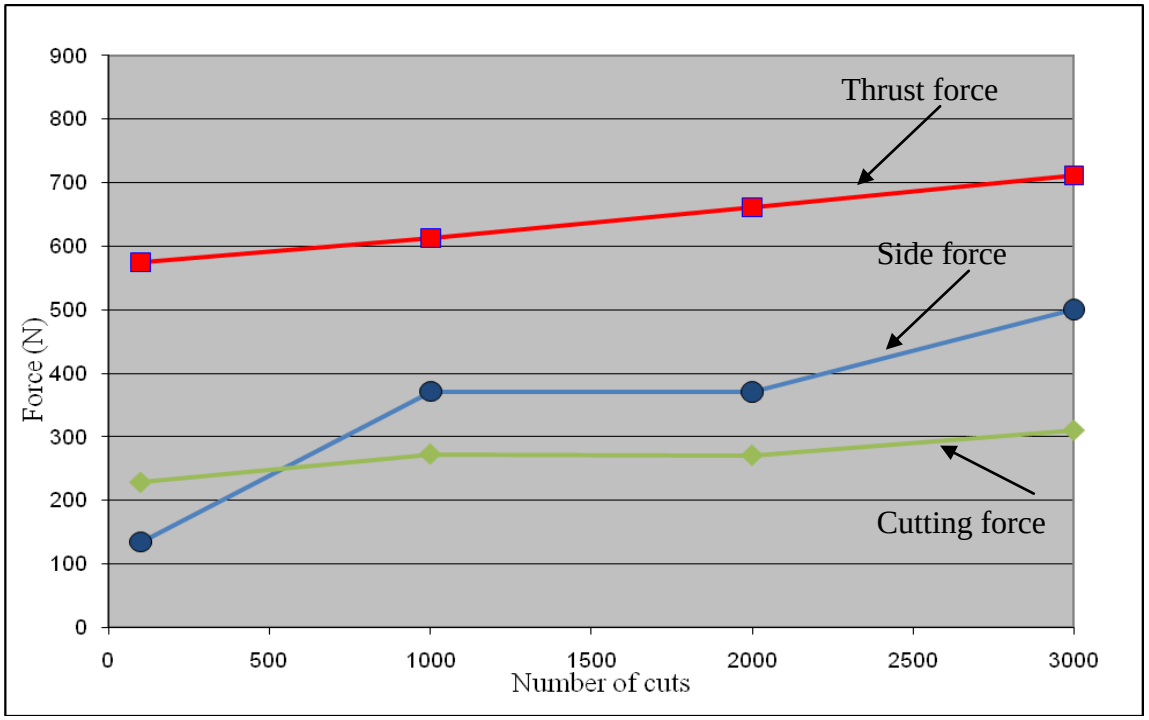

Figure 4.9. Force against number of cuts for the un-coated bandsaw tooth (feed: 20 µm, speed: 80 m/min, width of cut: 1mm, length of one cut: 0.6 m).

The condition of the bandsaw tooth is shown in Figure 4.10. Figure 4.10 (a) presents the front view of the carbide tooth, which indicates extreme chipping at both the flank and the rake faces. The chipping is dominant on one side of the tooth, because it is in contact with the workpiece during the machining operation. Figure 4.10 (b) displays the side view of the carbide tooth, which shows the chipped corner of the carbide tooth. It can be concluded that the forces are too high (approximately 100 N as shown in Figure 4.5) under these machining conditions and therefore these are not suitable parameters for bandsawing Ti-17 alloy. The variation in Esp for the cutting test is given in Figure 4.11. It can be seen that the Esp has a very high initial value (approximately 11 GJ/m^3) and increases to approximately 15.5 GJ/m^3 by the end of the test, suggesting that the cutting process at these machining parameters requires high energy and is therefore not efficient (low value of Esp is indicative of efficient cutting). The initial and final chips formed while machining at 20 µm feed and 80 m/min cutting speed are shown in Figure 4.12.

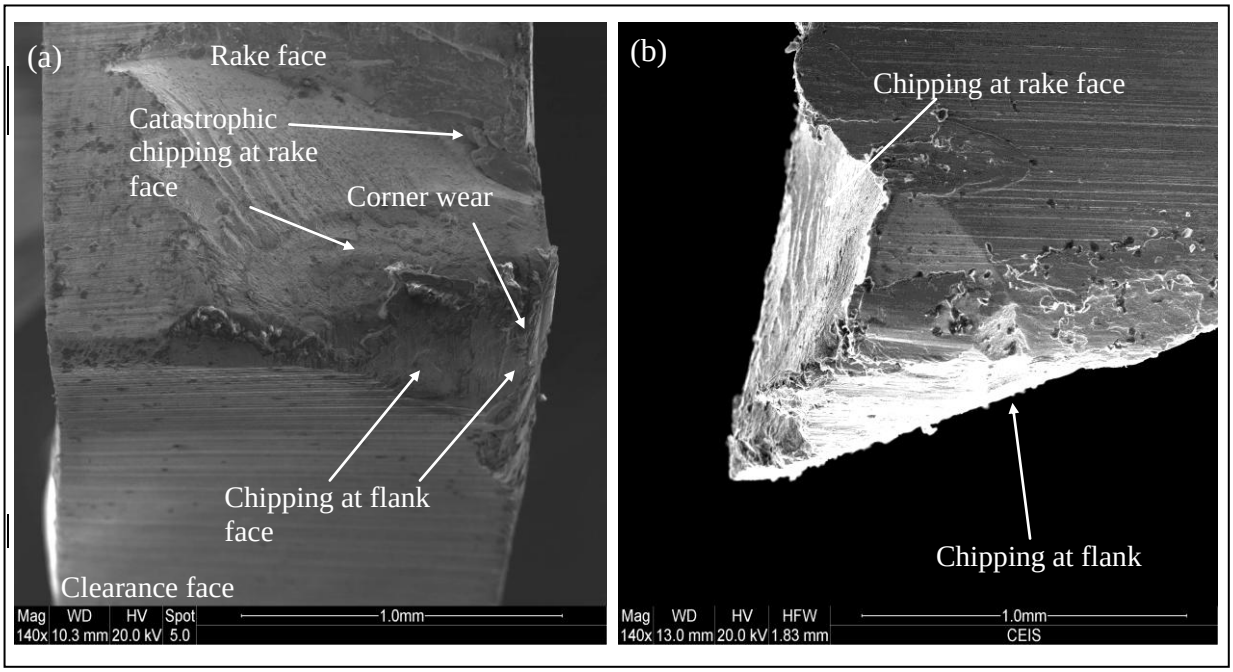

Figure 4.10. Condition of carbide bandsaw tooth used at 20 µm feed and at a cutting speed of 80 m/min (a) front view (b) side view.

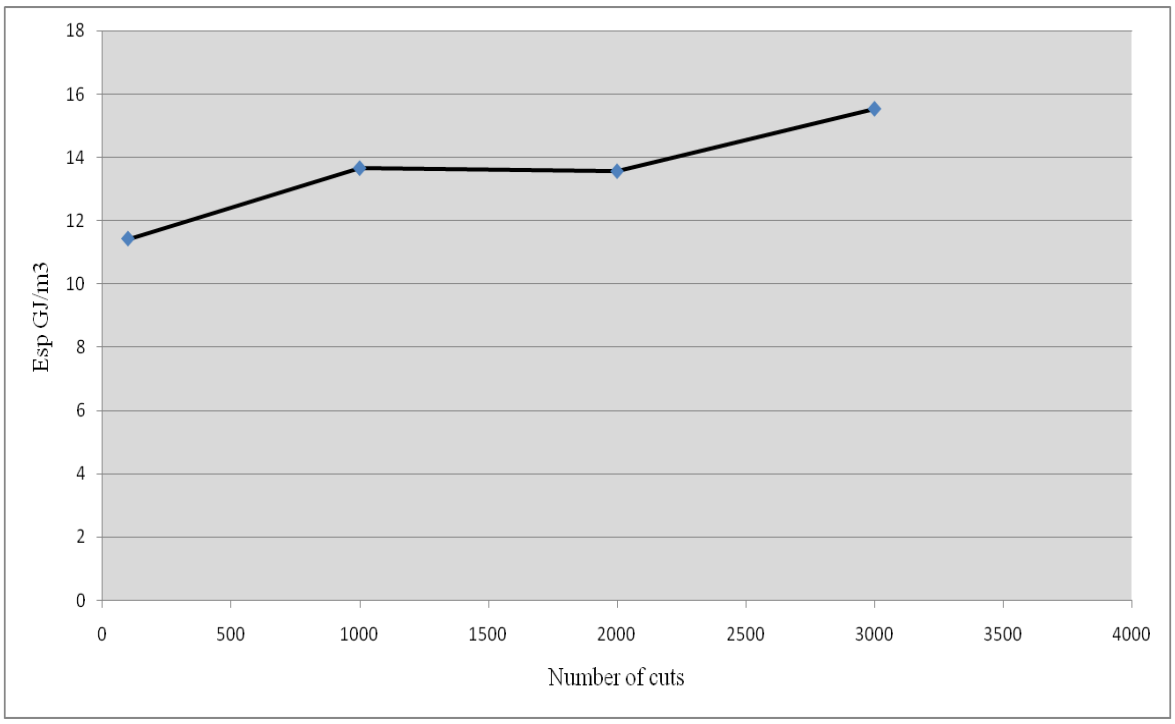

Figure 4.11. Variation in Esp with the number of cuts for un-coated carbide tooth (feed: 20 µm, cutting speed: 80 m/min, width of cut: 1mm, length of one cut: 0.6 m).

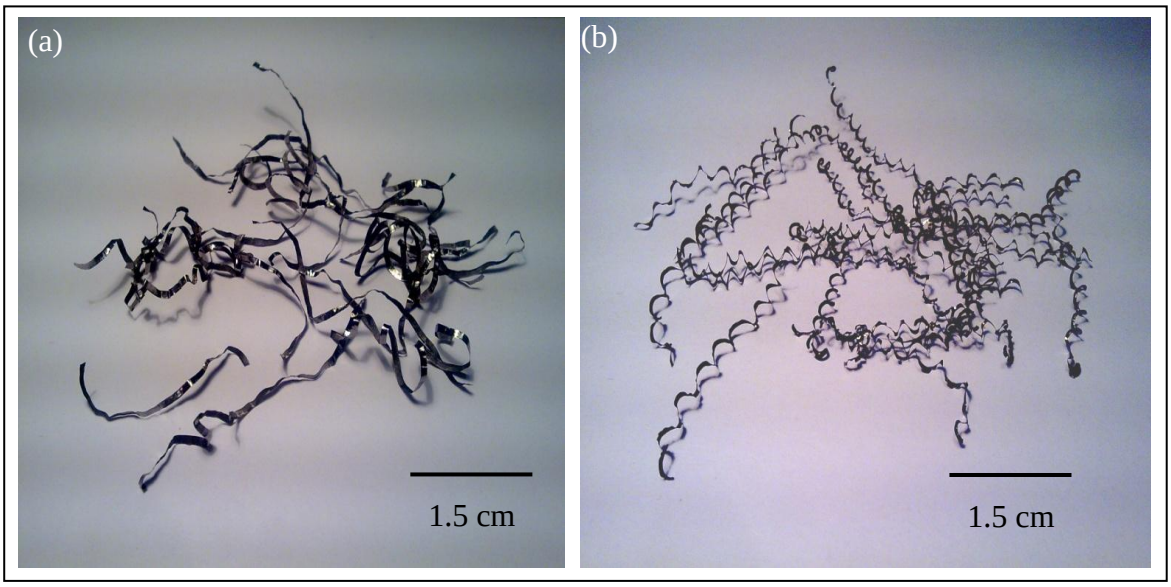

Figure 4.12. Characteristics of the chips formed at cutting speed of 80 m/min and feed of 20 µm (a) initial chips, (b) final chips.

The variation of forces while machining Ti-17 alloy at 15 µm feed and at the cutting speed of 80 m/min are shown in Figure 4.13. All the forces start from a high level and the side force becomes equal to the cutting force after the tooth has performed approximately 4000 cuts, suggesting that the corner of the carbide tooth has degraded quickly and hence the increase in the side force. However, the corner of the tooth experiences severe chipping after it has performed approximately 12000 cuts. The variation in Esp *vs* the number of cuts for this cutting test is shown in Figure 4.14. It can be observed that the Esp follows the same trend as that of the cutting force and rises considerably in the beginning of the test, but increases to a high value of 16 GJ/m^3 at the end of test. The condition of the carbide tooth at the end of the test is illustrated in Figure 4.15. The tooth has chipped at the flank and rake faces. The corner of the cutting edge which is engaged with the workpiece displays extreme chipping. Figure 4.15 (b) shows the chipping of the side even more clearly. The high forces, Esp and the SEM images indicate that these are severe machining parameters for machining Ti-17 alloy with the un-coated carbide tooth and under these conditions the bandsaw teeth will degrade quickly and therefore will have low life in terms of its performance.

The initial and final chips formed while machining at 15 µm feed and 80 m/min cutting speed are shown in Figure 4.16.

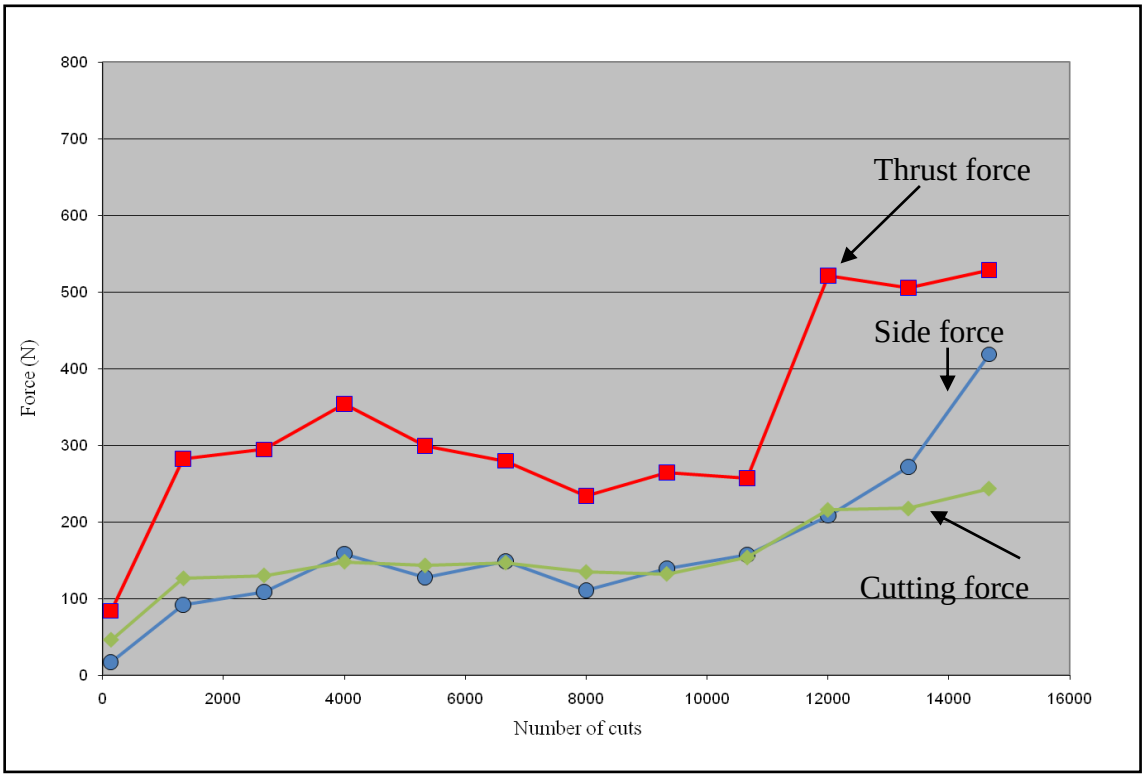

Figure 4.13. Force against number of cuts for un-coated bandsaw tooth (feed: 15 µm, speed: 80 m/min, width of cut: 1 mm).

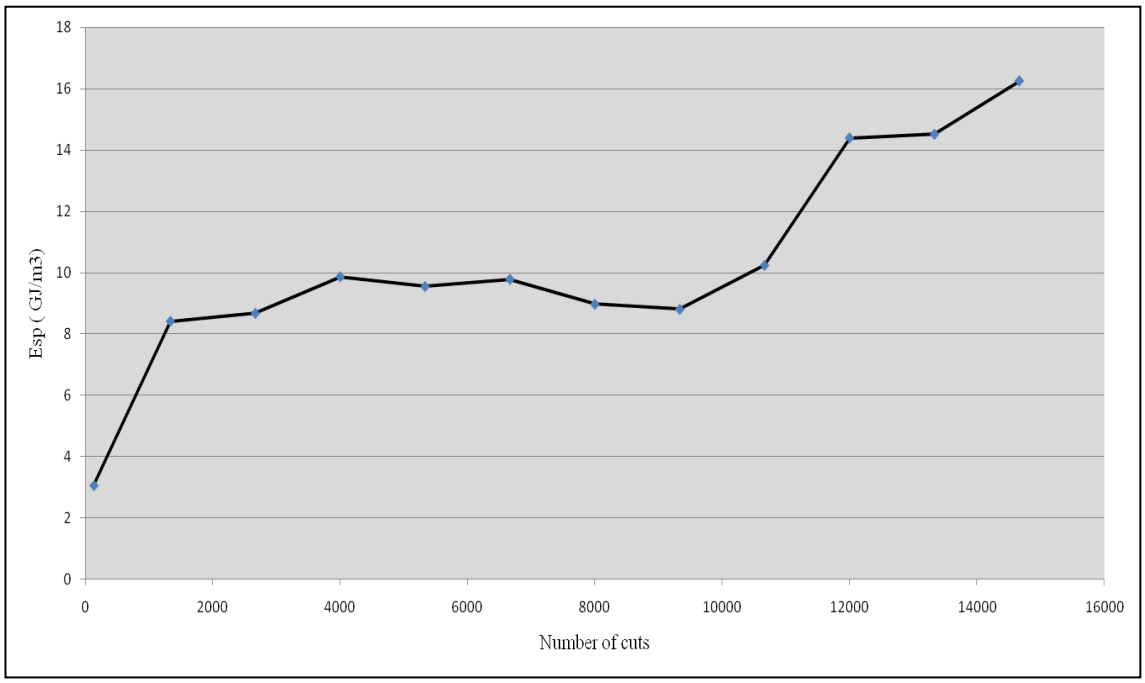

Figure 4.14. Variation of Esp with the number of cuts for un-coated carbide tooth (feed: 15 µm, speed: 80 m/min, width of cut: 1 mm, length of one cut: 0.6 m).

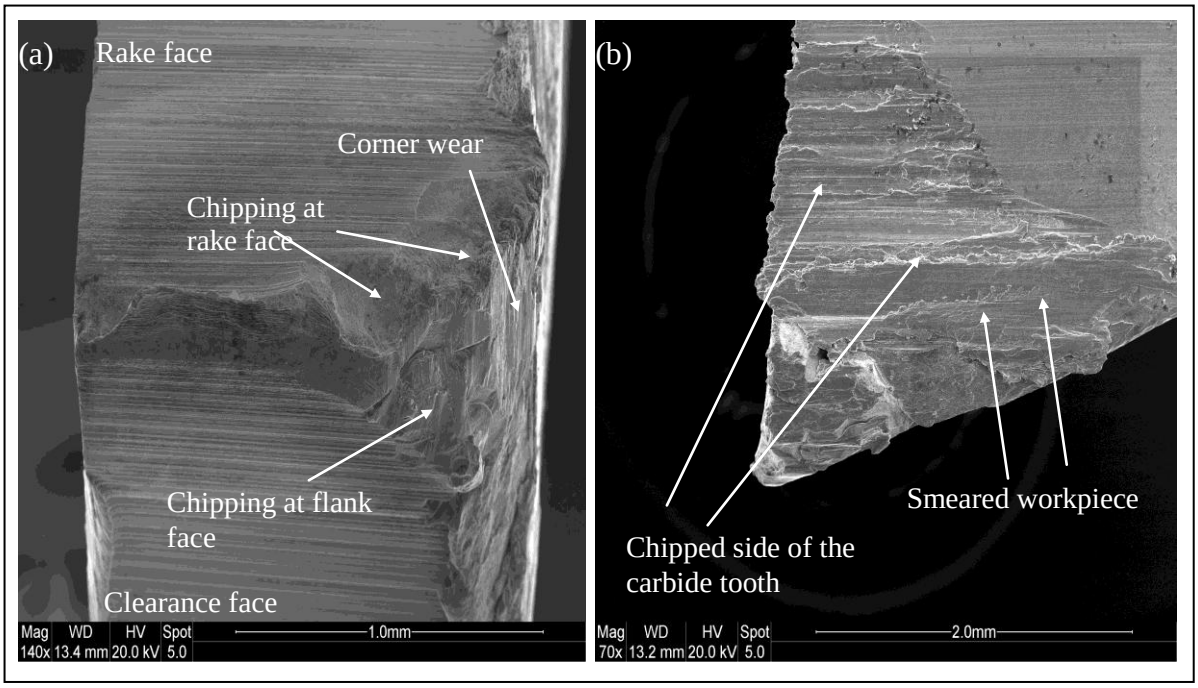

Figure 4.15. SEM images of the carbide tooth used at a feed of 15 µm and cutting speed of 80 m/min, showing excessive chipping at the corner (a) and (b) side view of the carbide tooth.

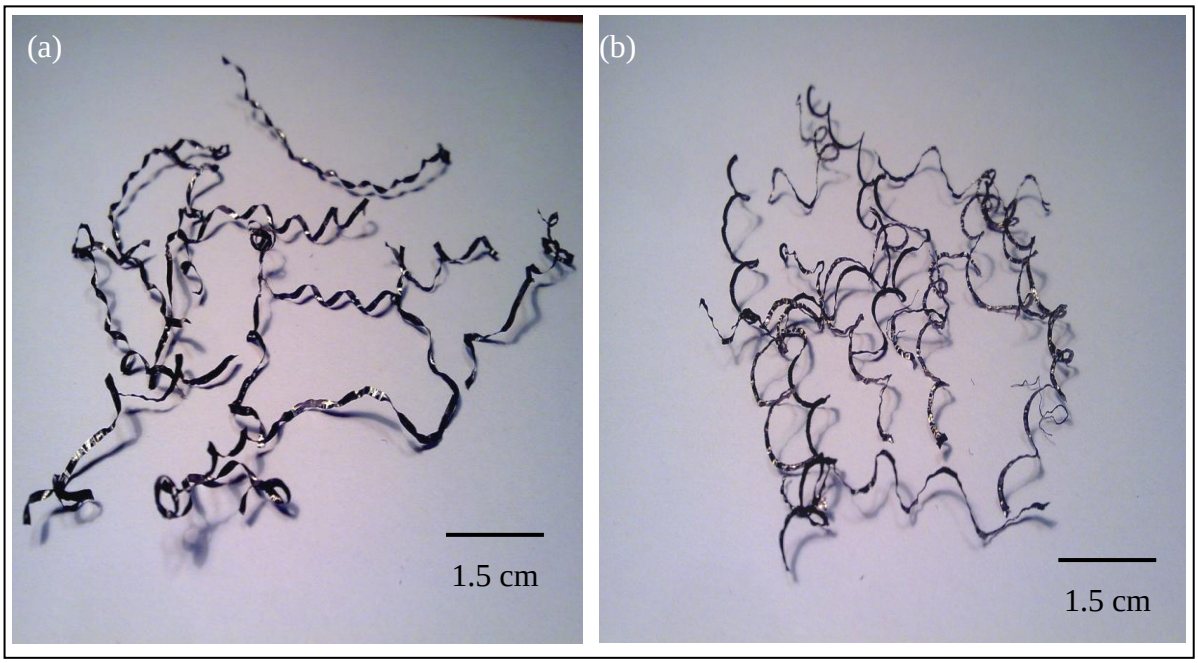

Figure 4.16. Characteristics of the chips formed at cutting speed of 80 m/min and feed of 15 µm (a) initial chips and (b) final chips.

Figure 4.17 shows the variation in forces while machining Ti-17 alloy at a low feed of 10 µm and at a cutting speed of 80 m/min. From the force graph, it appears that the tooth geometry starts to modify from its corner due to wear after performing 2000 cuts, owing to excessive force at the tool/workpiece interface. The condition of the carbide tooth at the end of its life is shown in Figure 4.18. It is apparent from these SEM micrographs that the cutting edge has chipped. Furthermore, it is clear that the maximum wear has taken place at the corner of the tooth and the corner may have plastically deformed due to excessive load.

The variation in Esp for machining at these parameters is presented in Figure 4.19 and shows that Esp increases throughout the machining session. It starts with a high value of 10 GJ/m^3 and reaches 18 GJ/m^3 at the end of the test, thereby indicating that the machining at these parameters is not efficient. Characteristic chips formed during the machining operation are displayed in Figure 4.20.

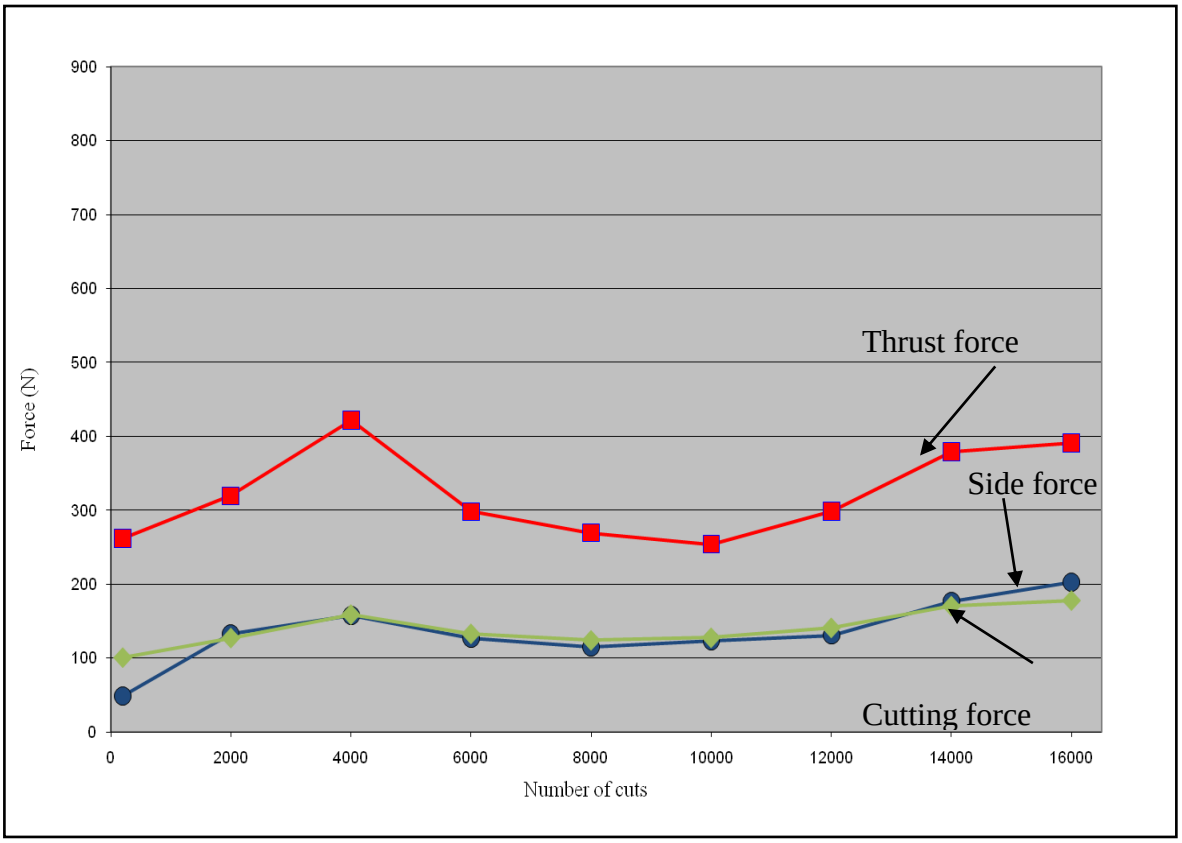

Figure 4.17. Forces against number of cuts for the un-coated bandsaw tooth (feed: 10 µm, speed: 80 m/min, width of cut: 1 mm, length of one cut: 0.6 m).

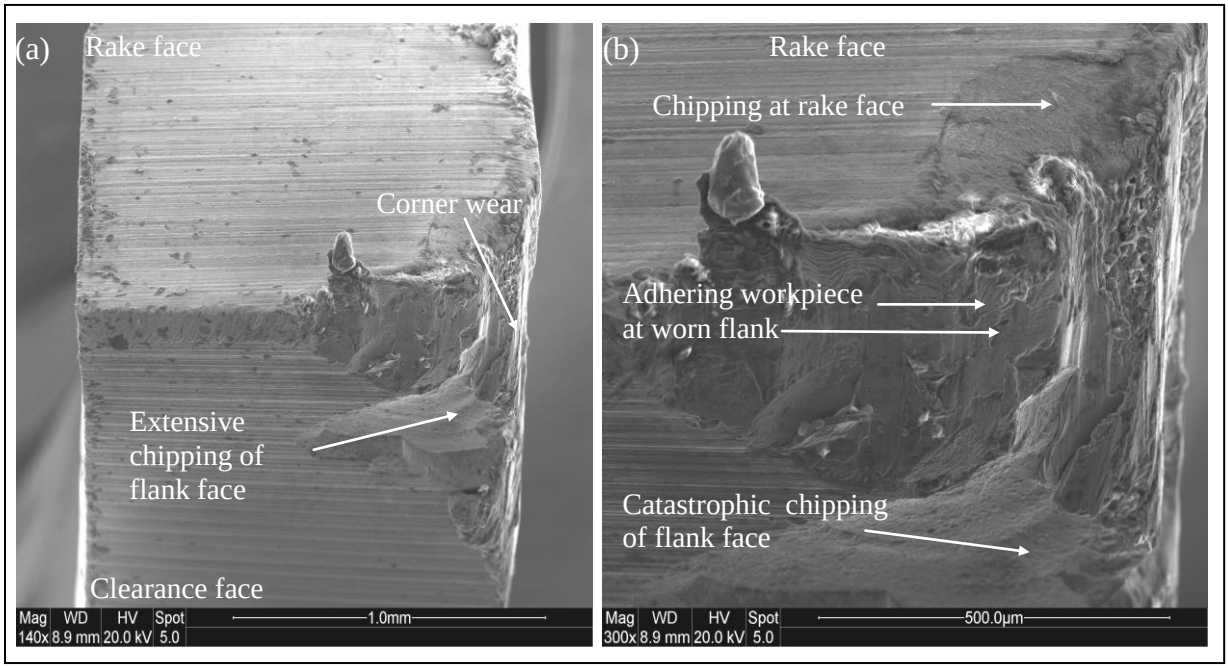

Figure 4.18. Condition of the carbide tooth at the end of its life (a), used at feed of 10 µm and cutting speed of 80 m/min and (b) magnified image of the corner of the tooth.

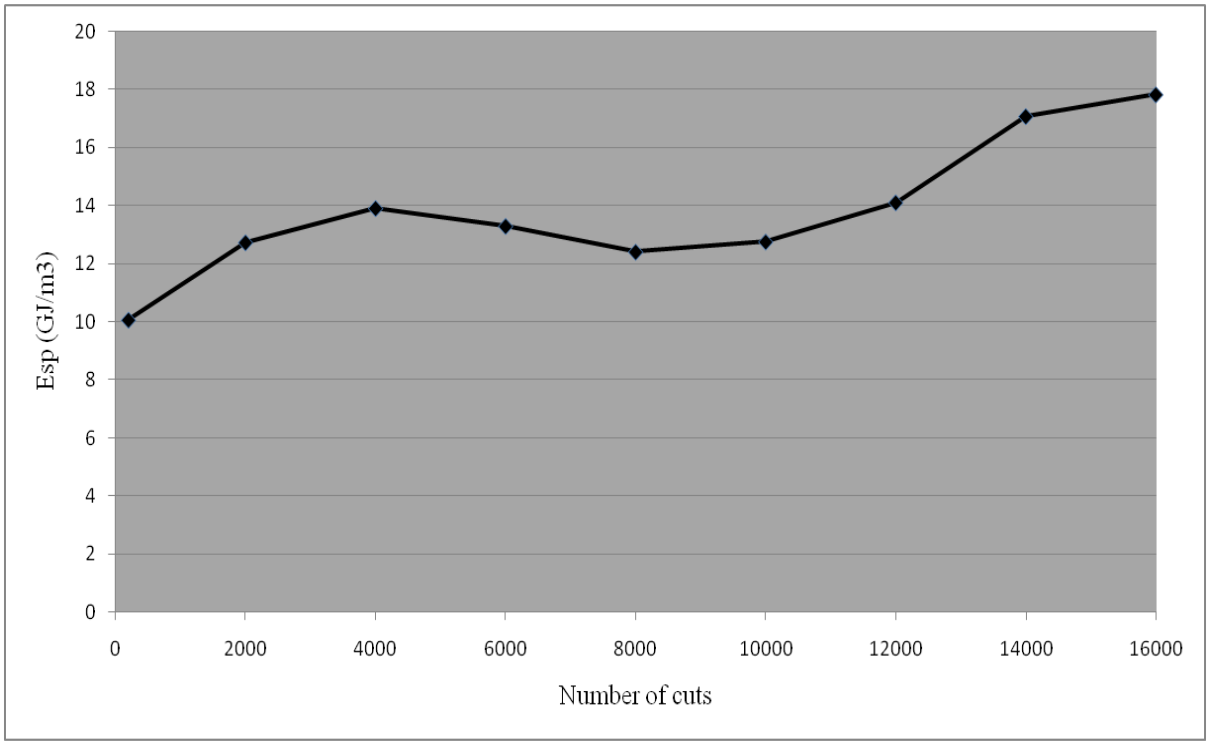

Figure 4.19. Variation of Esp with the number of cuts for the carbide tooth (feed: 10 µm, cutting speed: 80 m/min, width of cut: 1 mm µm, length of 1 cut: 0.6 m).

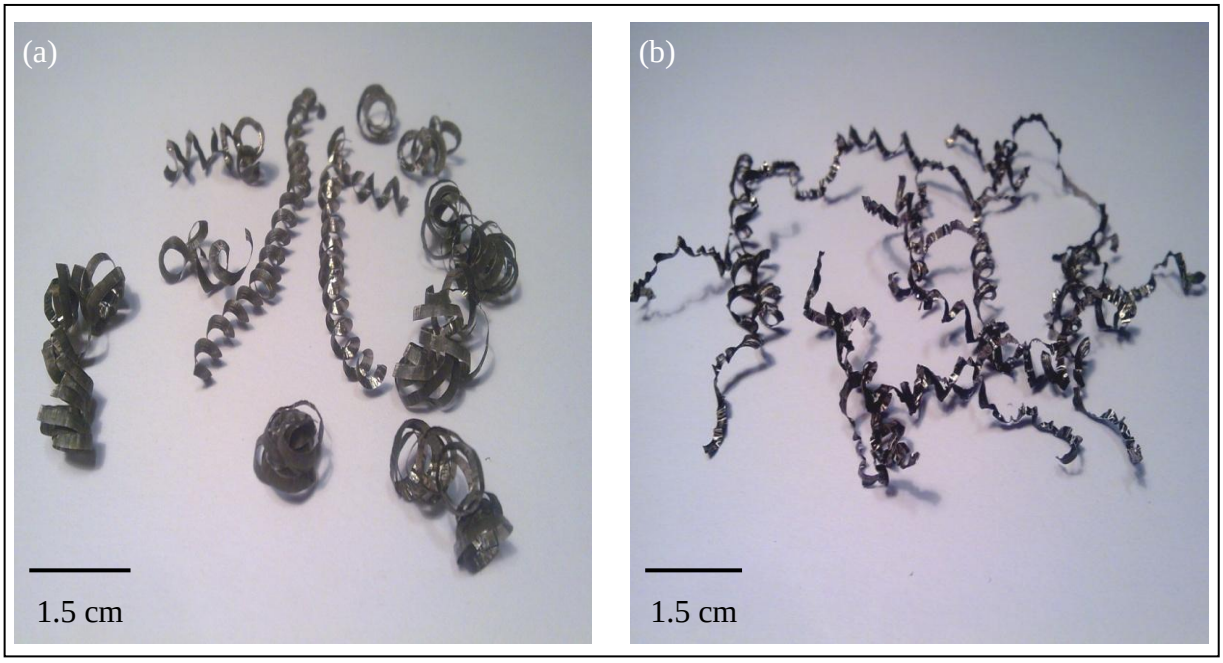

Figure 4.20. Characteristics of the chips formed at cutting speed of 80 m/min and feed of 10 µm (a) initial chips and (b) final chips.

4.3.2 Machining tests at 60 m/min cutting speed

For further tests, the cutting speed was reduced from 80 m/min to 60 m/min and the depths of cut (or feed) were varied from 25 µm to 10 µm, with 5 µm intervals. Therefore the following feeds were used, keeping the cutting speed constant at 60 m/min.

4.7. Machining parameters for cutting tests carried out at 60 m/min

Feed (µm)	10	15	20	25
Cutting speed (m/min)	60	60	60	60

The force experienced by the carbide tooth while machining at 25 µm feed was high enough to trigger the automatic safety system which led to the machine backing-off from further machining. The condition of the carbide tooth is provided in Figure 4.21. Figure 4.21 (a) shows both the faces of carbide tooth, whilst the magnified image of the corner of the carbide tooth is shown in Figure 4.21 (b). The images clearly reveal that the tooth has chipped from both rake and the flank faces, more on the rake face. The side view of the carbide tooth is presented in Figure 4.21 (c), which clearly shows chipping of the tool on both the faces as well as from the corner, which was engaging with the workpiece. The maximum chipping can be observed at the cutting edge corner that is engaged with the

workpiece and gradually decreased across the width of the cutting edge. As previously stated, this could be attributed to the engagement of the cutting edge at an angle with the workpiece as a consequence of set geometry of the bandsaw tooth as well as to the corner of the tooth being relatively weak compared to the rest of the tooth.

The characteristics of the chips formed while machining at a cutting speed of 60 m/min and at the feed of 25 µm are exhibited in Figure 4.22. It is clear from Figure 4.22 (b), which shows the final chips formed during machining Ti-17 alloy, that this is the end of the tooth life as thin chips are being formed because the corner has worn and therefore less area of the cutting edge is actually involved in machining. In order to observe the effect of the feed, the depth of cut (or feed) was reduced to 20 µm, while maintaining the cutting speed at 60 m/min. The force graph of machining at 20 µm feed and 60 m/min is provided in Figure 4.23. It can be observed that the tooth started wearing from the corner after performing 1200 cuts – this is apparent from the side force becoming higher than the cutting force. Moreover, the thrust force increased to a high value, suggesting wear of the flank surface of the tooth. Therefore the cutting edge has degraded from the corner as well as from the flank face. The SEM images of the carbide tooth are given in Figure 4.24. The images in Figure 4.24 show chipping on the rake and flank face as well as on the corner of the cutting edge. It is likely that plastic deformation took place at the rake face and probably more so at the corner.

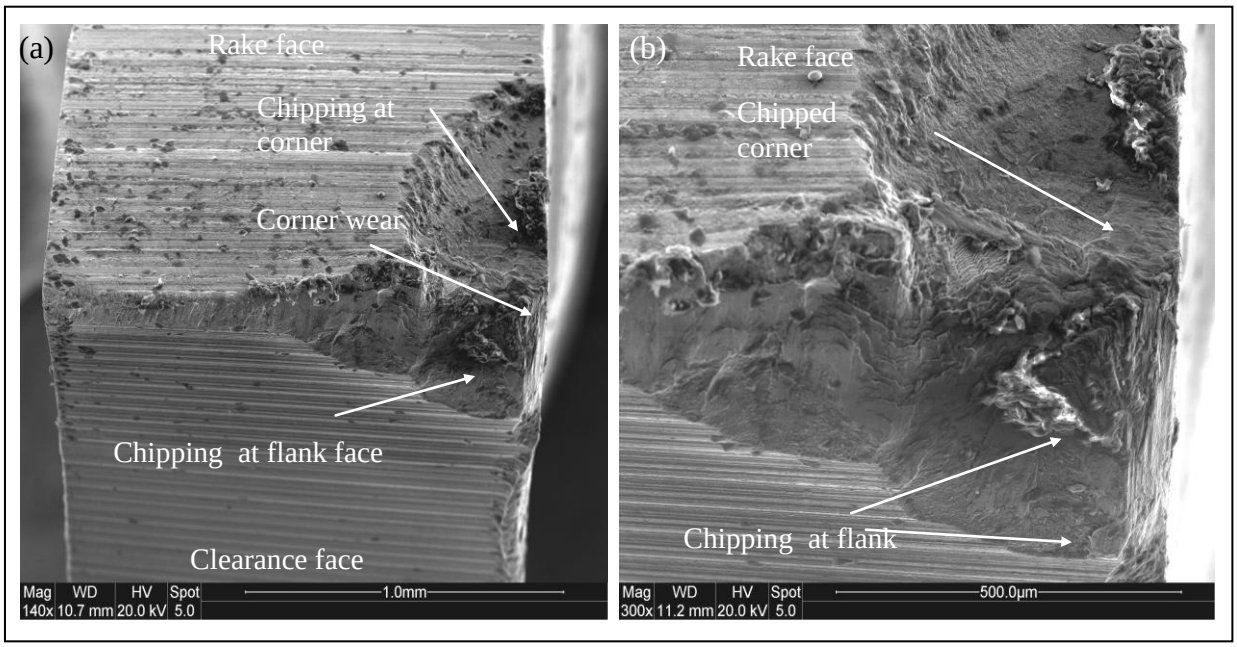

Figure 4.21. SEM photomicrographs of the carbide tooth (a) used at 25 µm feed and 60 m/min cutting speed, (b) magnified image of the corner

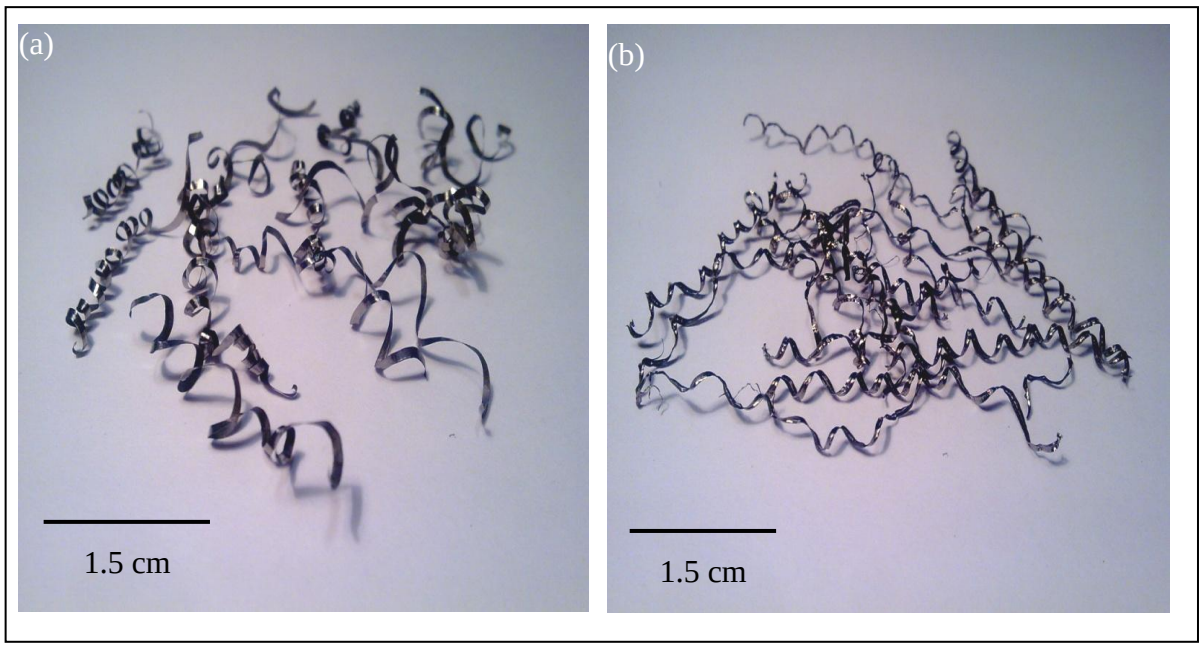

Figure 4.22. Characteristics of the chips formed at cutting speed of 60 m/min and feed of 25 µm (a) initial chips and (b) final chips.

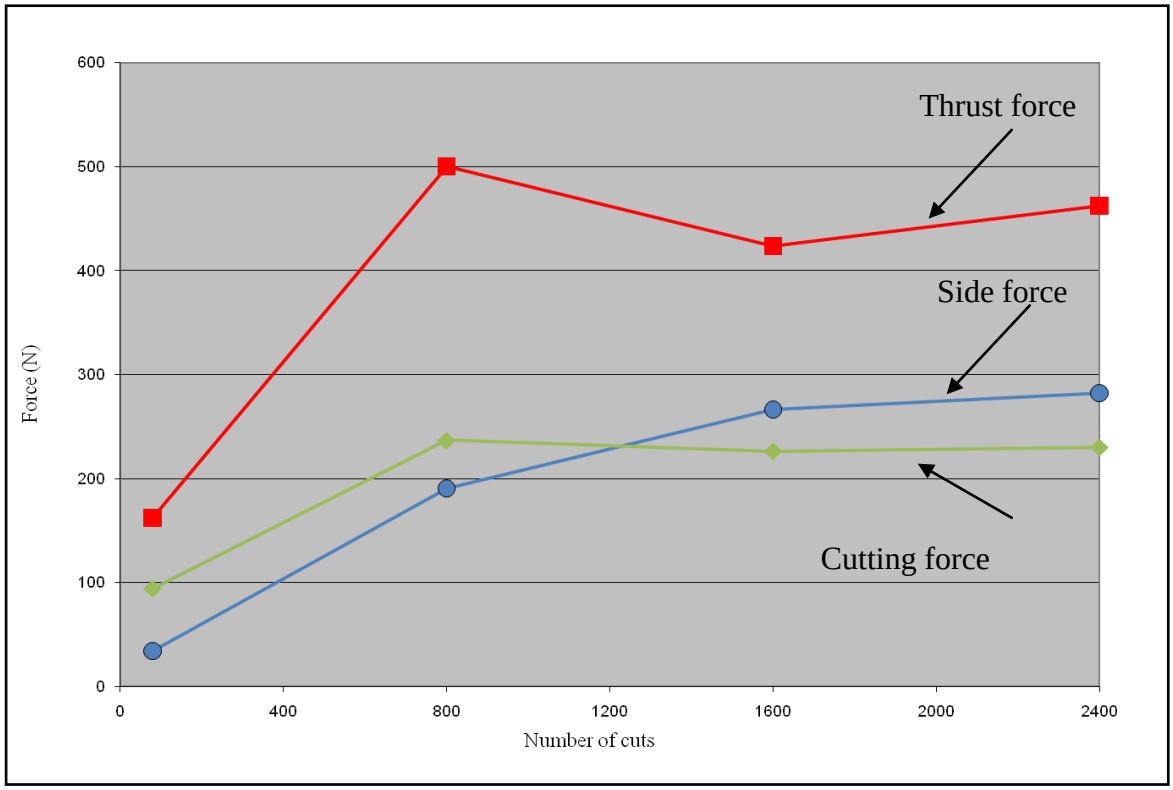

Figure 4.23. Forces against number of cuts for the un-coated bandsaw tooth (feed: 20 µm, speed: 60 m/min, width of cut: 1 mm, length of one cut: 0.6 m).

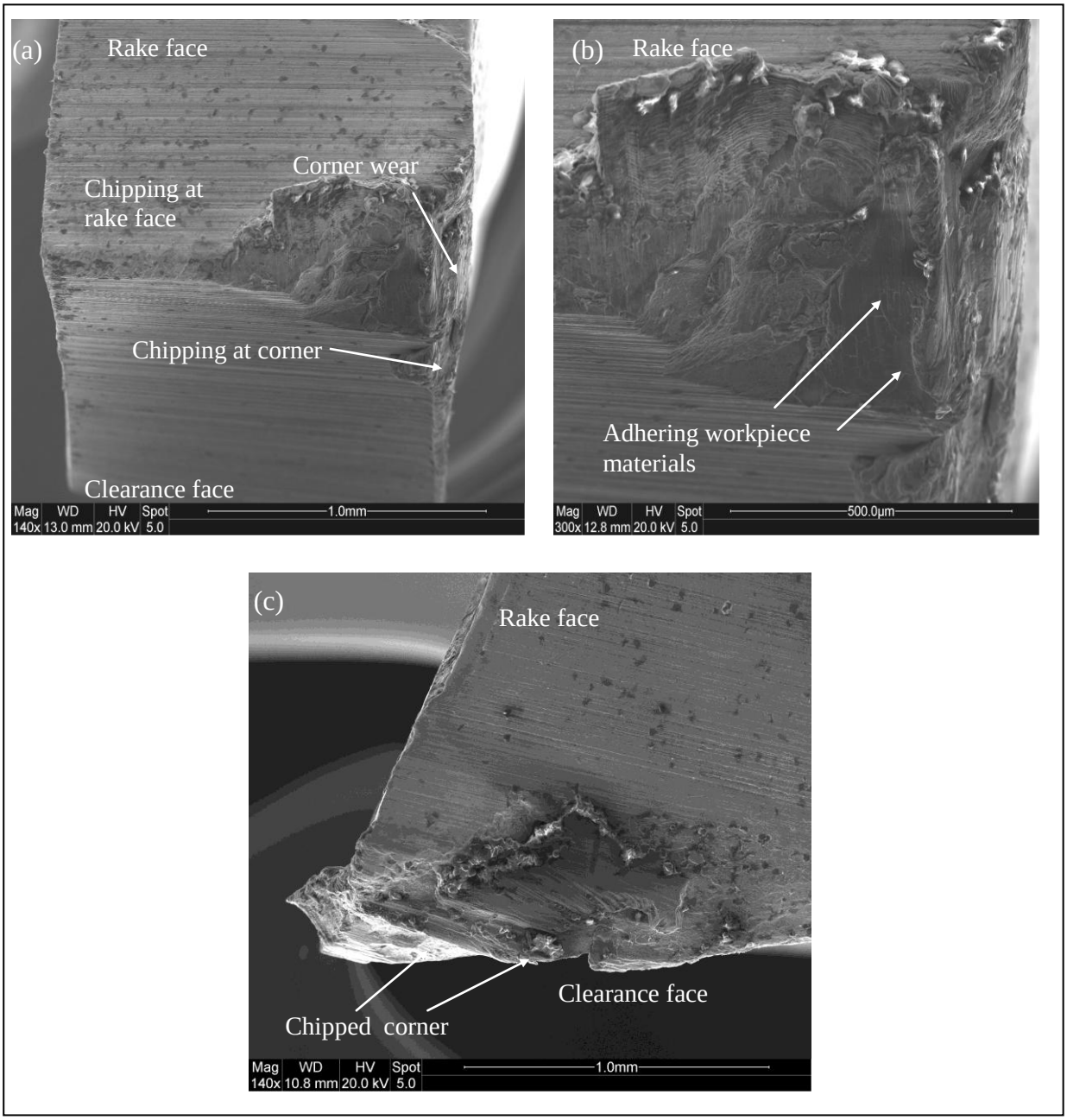

Figure 4.24. SEM images of the carbide tooth (a) used at 20 µm feed and at 60 m/min cutting speed, (b) magnified view of the corner and (c) side view.

The variation in Esp for the machining test carried out at 60 m/min cutting speed and at a feed of 20 µm is provided in Figure 4.25. It can be observed from Figure 4.25 that the value of Esp quickly rises from 4 GJ/m^3 to 10 GJ/m^3, after performing approximately 700 cuts, suggesting that the geometry of the tooth has been modified during this time.

The characteristics of the chips formed while machining Ti-17 alloy at the feed of 20 µm and at the surface cutting speed of 60 m/min are shown in Figure 4.26. It is evident from the image of the final chips [Figure 4.26 (b)] that this is the end of the tooth life due to

chipping as thin chips are being formed because less of the cutting edge is performing the cutting operation.

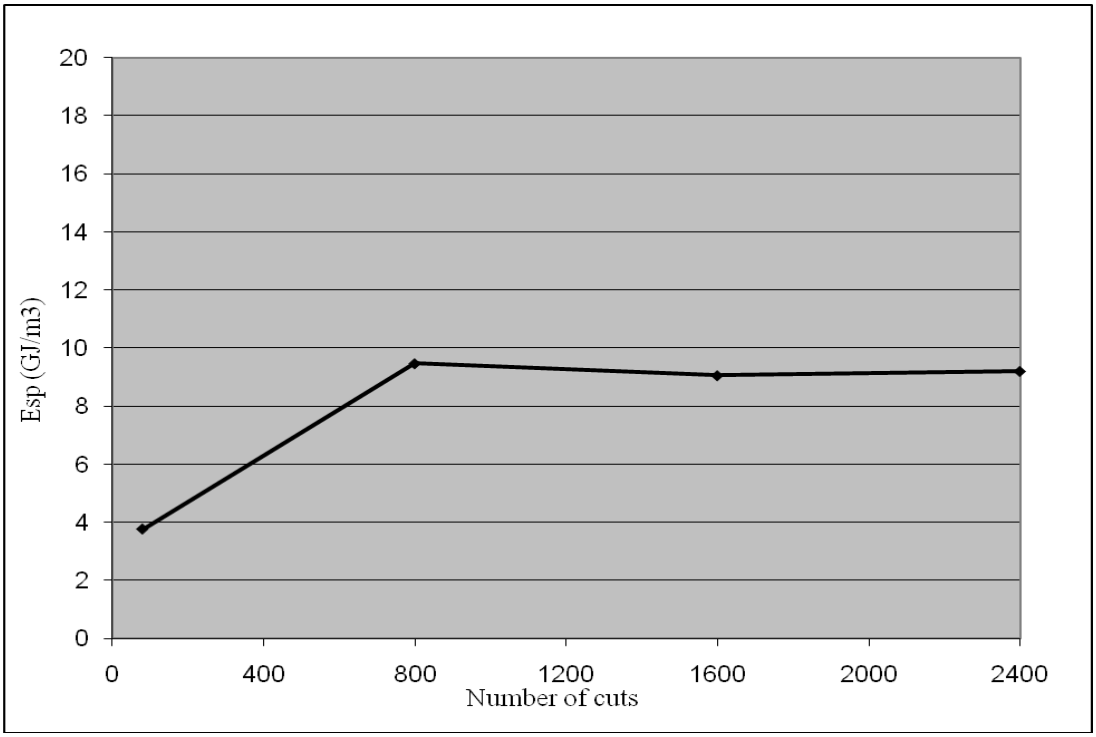

Figure 4.25. Variation in Esp with the number of cuts for un-coated tooth (feed: 20 µm, cutting speed: 60 m/min, width of cut: 1 mm µm, length of one cut: 0.6 m).

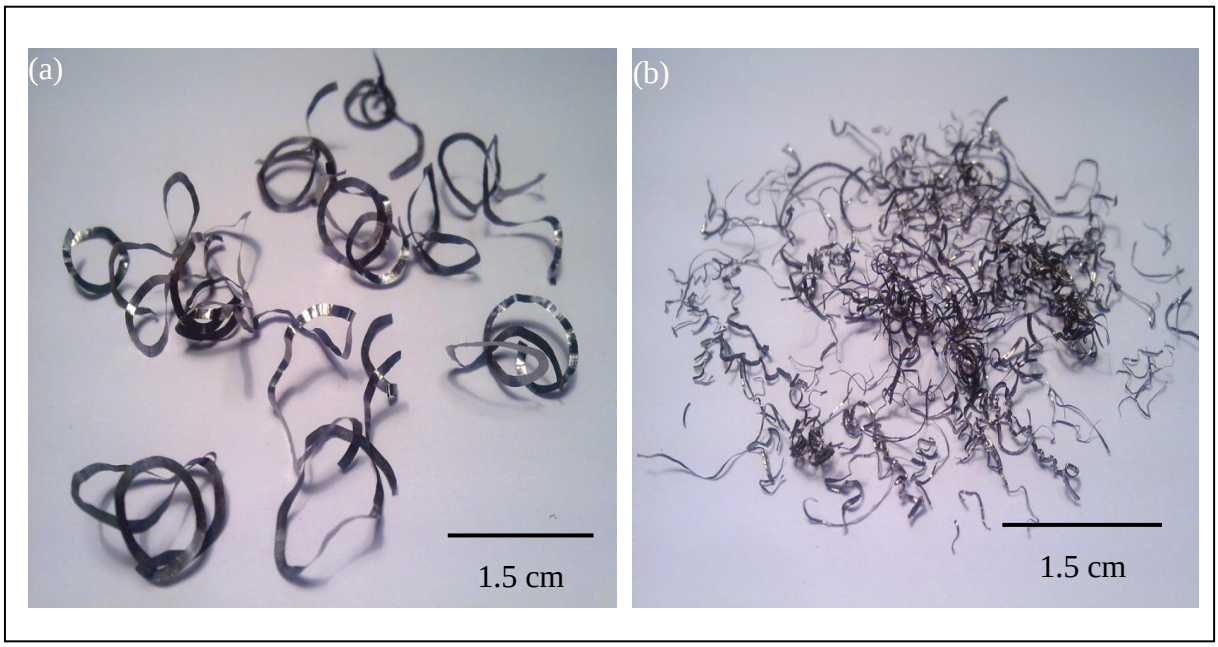

Figure 4.26. Characteristics of the chips formed at cutting speed of 60 m/min and feed of 20 µm (a) initial chips and (b) final chips.

In order to observe the effect of further reducing the feed on the wear and forces, the depth of cut (or feed) was reduced to 15 µm while maintaining the cutting speed at 60 m/min. The graph for the variation of forces against the number of cuts for the cutting test is presented in Figure 4.27. It can be observed from Figure 4.27 that the side force becomes higher than the cutting force, after the tooth has performed approximately 6500 cuts. This is the indication of the wear taking place at the corner of the carbide tooth. Moreover, the high magnitude of the thrust force also suggests flank wear. The variation in Esp for the carbide tooth used at cutting speed of 60 m/min and feed of 15 µm is given in Figure 4.28. From Figure 4.28, it can be seen that the value of Esp starts from approximately 6 GJ/m^3 and rises to 14 GJ/m^3 at the end of the cutting session, indicating progressive wear. However, the high value of Esp at the end of the test reveals that the physical geometry of the cutting edge has been modified and therefore the high value of Esp.

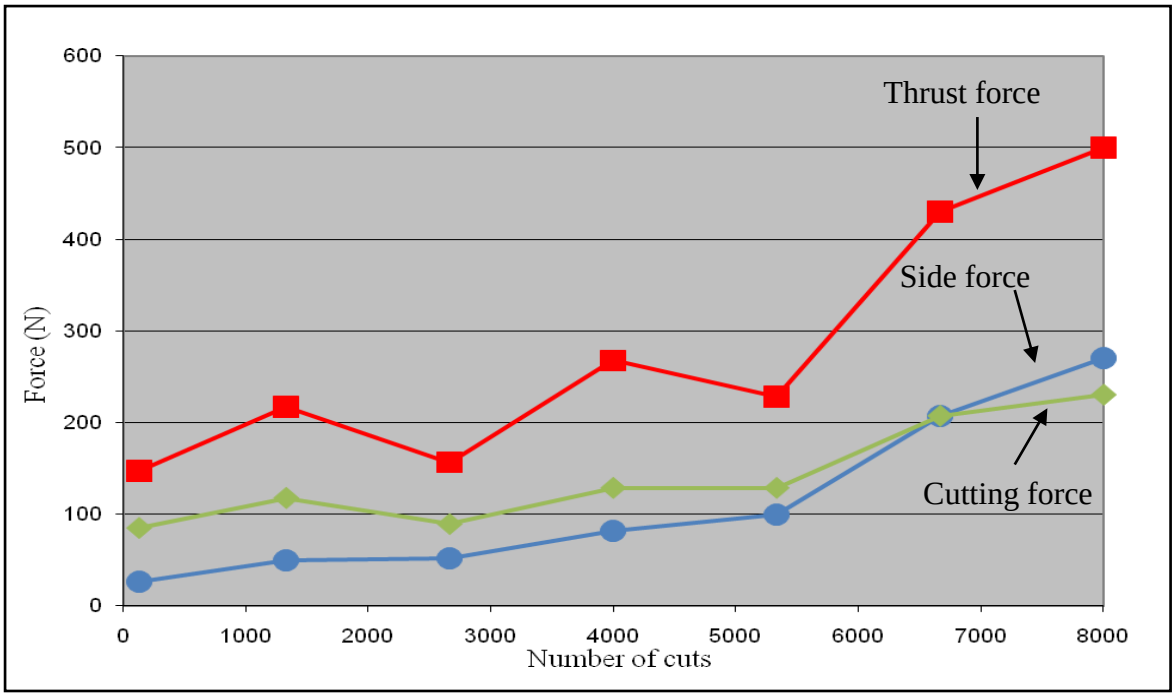

Figure 4.27. Variation in forces for the un-coated tooth (feed: 15 µm, cutting speed: 60 m/min, width of cut: 1 mm, length of one cut: 0.6 m).

The SEM images in Figure 4.29 shows chipping at the rake and flank faces, especially at the corner of the edge. The rake face has chipped at a distance from the corner of the carbide tooth which is engaging with the workpiece material, during the machining operation. The side view of the carbide tooth is presented in Figure 4.29 (c) and shows that the tooth has

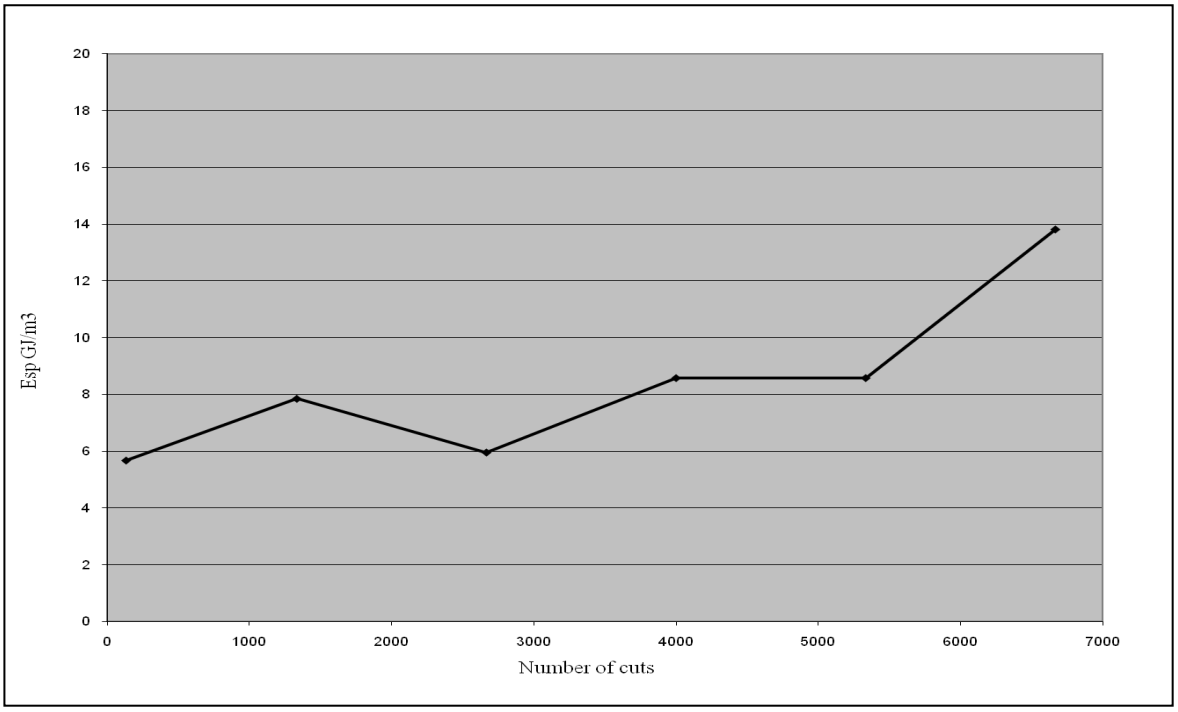

Figure 4.28. Variation in Esp for the un-coated tooth (feed: 15 μm, cutting speed: 60 m/min, width of cut: 1 mm, length of one cut: 0.6 m).

developed a wear flat on its side. However, this wear flat is at the corner only and becomes less pronounced across the cutting edge.

A feed of 10 μm was chosen for another test in order to observe the behaviour of the carbide tooth at the minimum feed while the cutting speed was maintained at 60 m/min. The graph for the variation of forces against the number of cuts for the cutting test carried out at 10 μm feed and at the cutting speed of 60 m/min is shown in Figure 4.30. The carbide tooth lasted much longer compared to the tests carried out earlier, which were at higher feed. The progressive increase in forces is an indication of progressive wear taking place at the cutting edge.

The curves for side and cutting force reveal a smooth trend throughout the cutting session, except at the end of the test, where there is an abrupt increase in all the force values, indicating that the physical geometry of the tooth has been modified. It was interesting to note that in case of machining at 60 m/min, cutting forces varied in a cyclic pattern with the general trend of increasing cutting force with the number of cuts. This was probably due to periodic adherence and removal of workpiece material on the flank face as shown in Figure 4.31. When the adhering material was building-up, the force increased and when it was removed after attaining a critical size, the forces decreased. In Figure 4.31, chipping can be observed on the carbide tooth at both the rake and the flank faces.

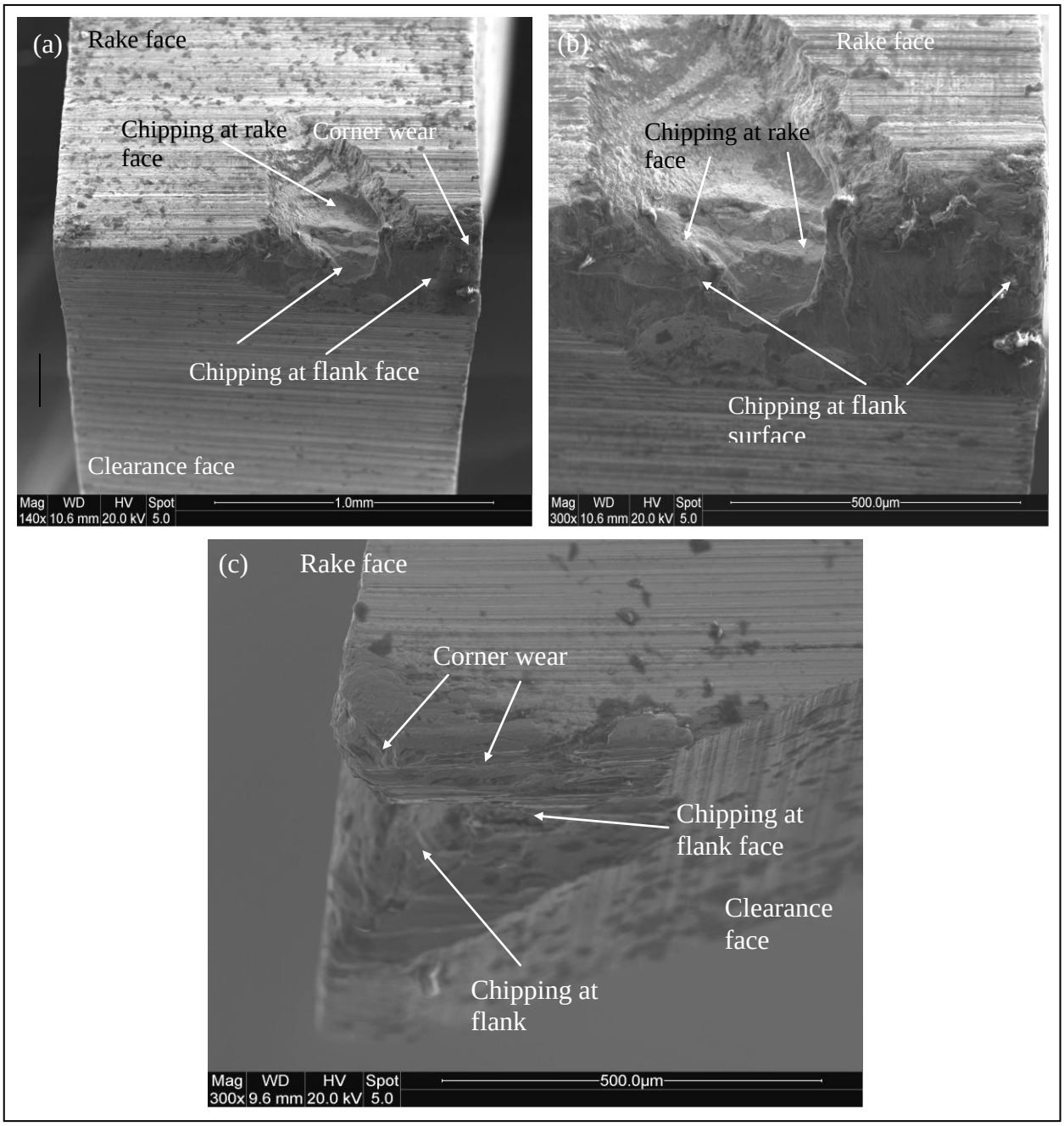

Figure 4.29. (a) SEM images of the carbide tooth used at 60 m/min cutting speed and 15 µm feed at the end of its life, (b) magnified image of the corner showing chipped corner of the cutting edge and (c) side view of the tooth showing the wear flat.

The maximum wear is distinguished at the corner of the tooth, due to the set geometry of the carbide tooth as well as due to the corner of the carbide being less strong compared with the rest of the tooth. Cyclic mechanical and thermal loading on the bandsaw tooth due to the periodic engagement and disengagement of the tooth with the workpiece during

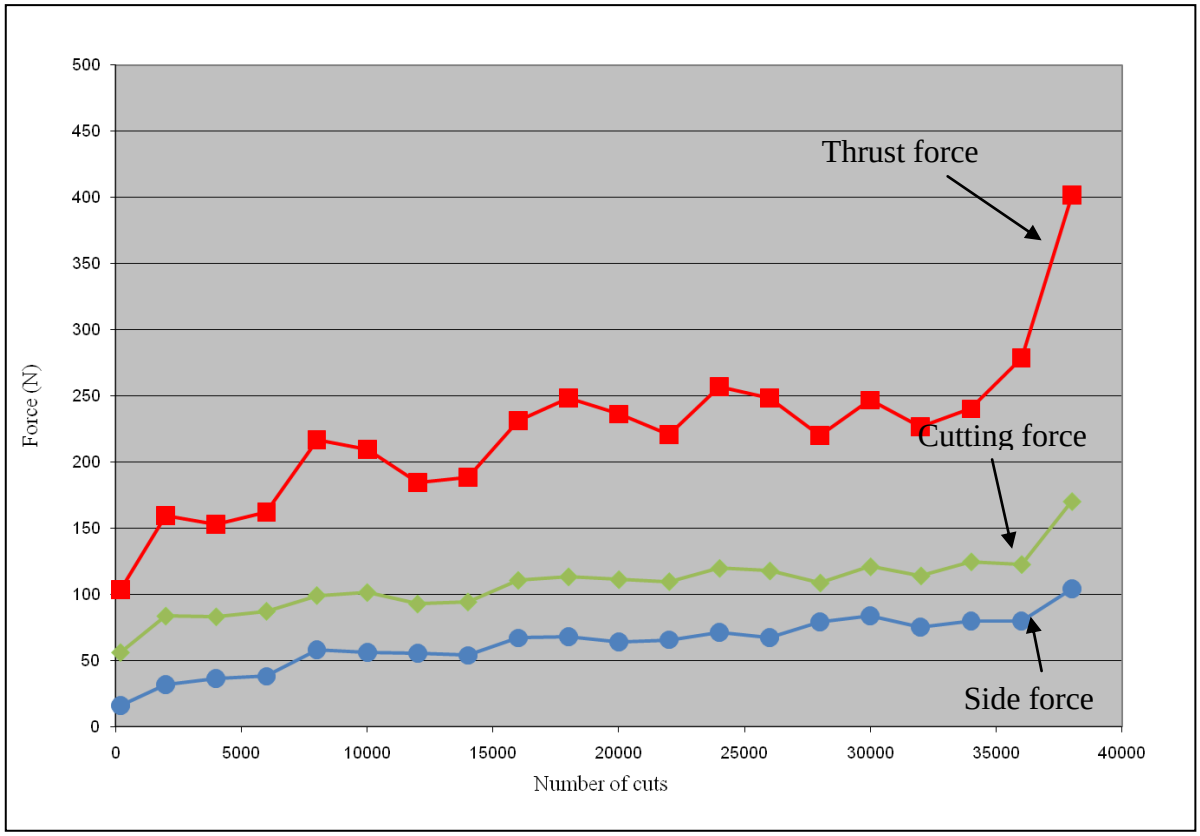

Figure 4.30. Variation of forces for the carbide tooth (feed: 10 µm, cutting speed: 60 m/min, width of cut: 1 mm, length of one cut: 0.6 m).

machining are the factors responsible. The wear gradually decreases along the width of the cutting tool owing to the fact that the width of the cut is set to 1 mm for the machining operation. Plastic deformation may have taken place on rake and flank faces due to the excessive force experienced by the carbide tooth during machining. The side view of the carbide tooth is provided in Figure 4.31 c. Wear at the edge of the corner can be clearly seen from Figure 4.31 and it can also be observed that the flank face experiences more degradation in terms of wear.

The variation in Esp with the number of cuts for the carbide tooth used at 60 m/min and at feed of 10 µm is displayed in Figure 4.32. The variation of Esp values with the number of sections cut reveal a similar trend as the cutting force (Figure 4.30). The Esp values start from approximately 6 GJ/m^3 and quickly increased to 8 GJ/m^3. After this abrupt rise to 8 GJ/m^3, the Esp values varied in a cyclic pattern, with a general increasing trend. Esp values increased with the number of sections cut due to the progressive wear in the cutting edge. Therefore at the end of the test, the high value of Esp (17 GJ/m^3), indicates that the carbide tooth had worn.

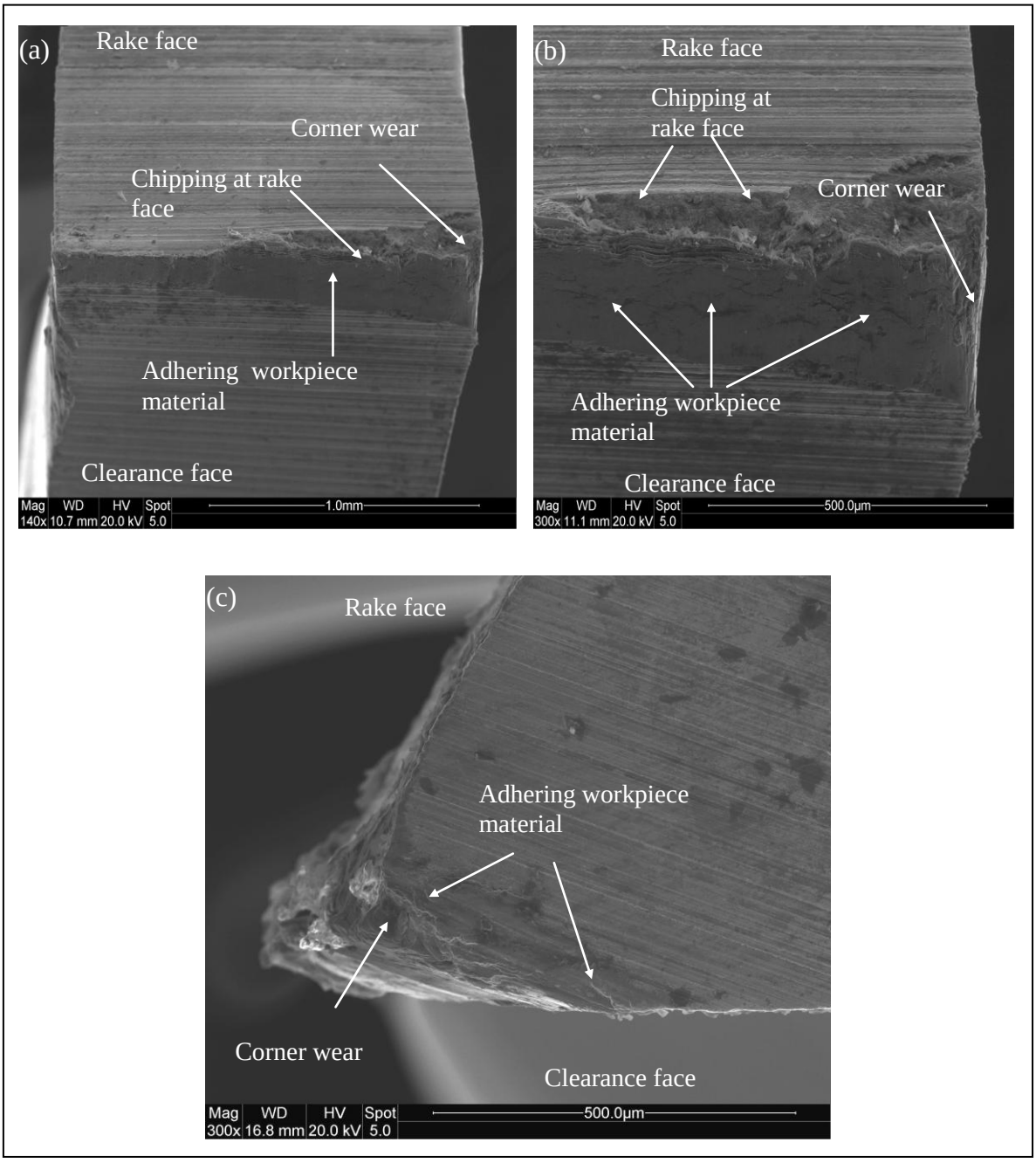

Figure 4.31. (a) Condition of the carbide tooth after performing 38 000 cuts at a feed of 10 µm and at cutting speed of 60 m/min, (b) magnified image of the corner and (c) side view of the carbide tooth showing corner wear.

The initial and final chips formed while machining Ti-17 alloy at a cutting speed of 60 m/min and at a feed of 10 µm are illustrated in Figure 4.33. The chips that are formed during the initial cutting action are straight, indicating an unworn carbide bandsaw tooth. However, the chips that are formed in the final stage of cutting are curled as can be seen in

Figure 4.33 (b), indicating that the geometry of the tooth has been modified due to wear at the cutting edge.

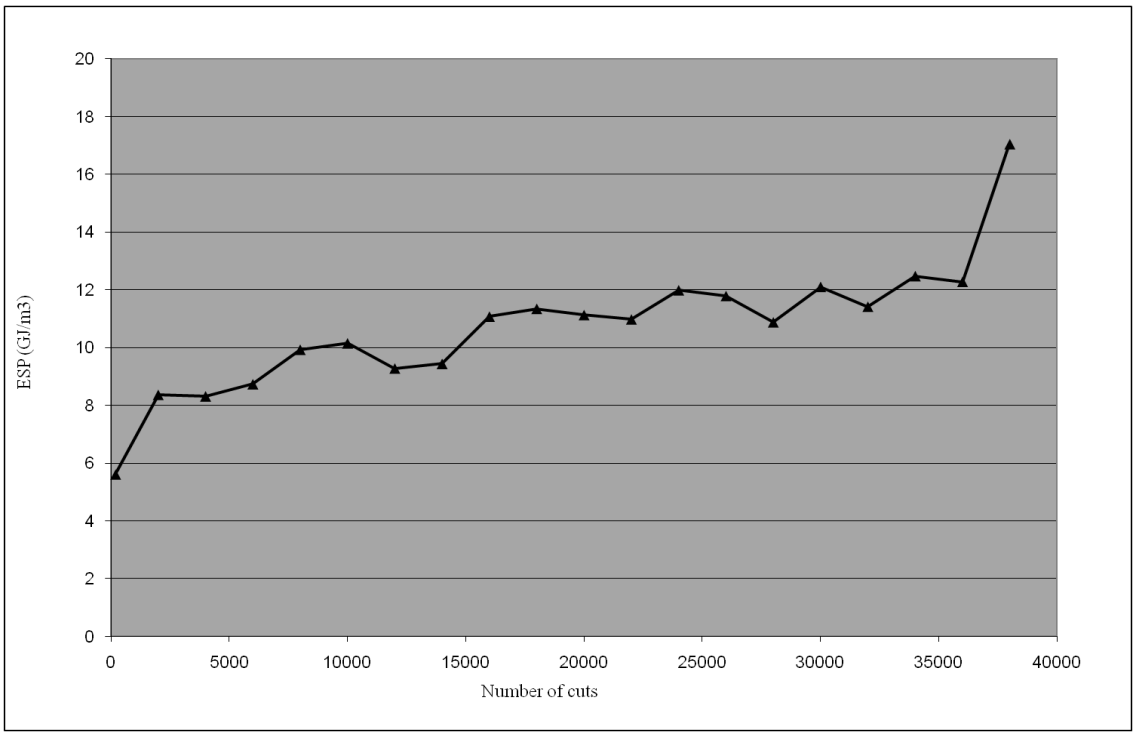

Figure 4.32. Variation in Esp for the carbide tooth used (feed: 10 µm, cutting speed: 60 m/min, width of cut: 1 mm, length of one cut: 0.6 m)

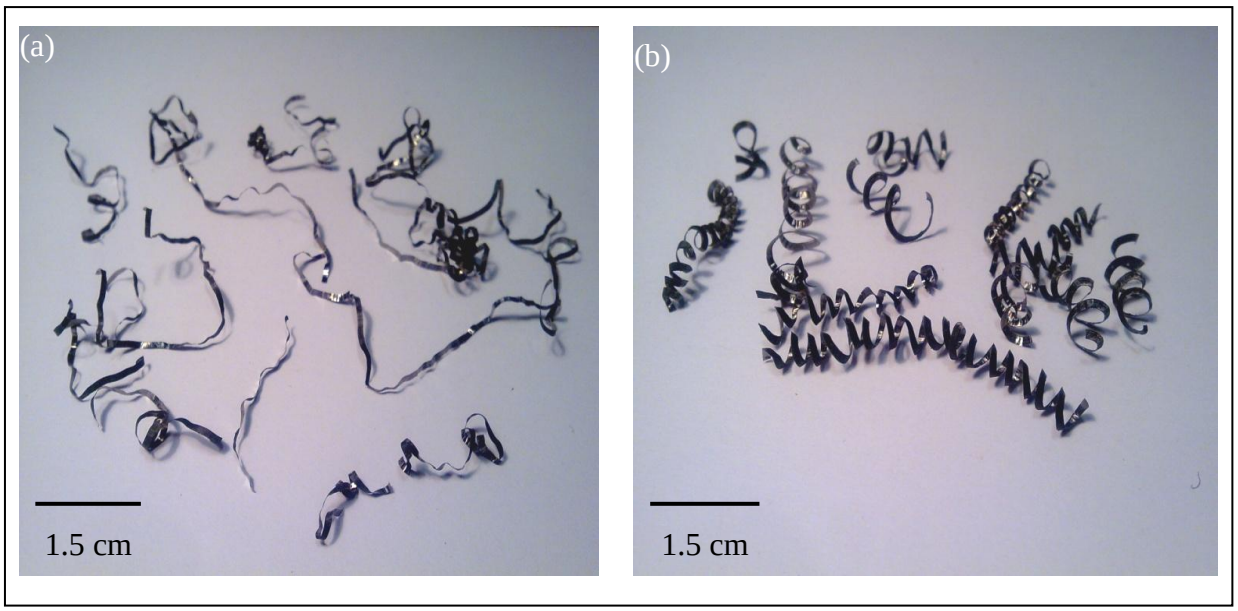

Figure 4.33. Characteristics of the chips formed at 60 m/min cutting speed and at feed of 10 µm (a) initial chips and (b) final chips.

4.3.3 Machining tests at 40 m/min cutting speed

In order to observe the wear and degradation of the carbide bandsaw tooth at low speeds, a series of tests was carried out at the cutting speed of 40 m/min. The machining parameters for the tests are listed in Table 4.8.

Table 4.8. Machining parameters for cutting tests carried out at 40 m/min

Feed (µm)	10	15	20	25
Cutting speed (m/min)	40	40	40	40

The variation of force with the number of cuts for the cutting test carried out at the cutting speed of 40 m/min and at the feed of 25 µm is shown in Figure 4.34. It was interesting to note that although the forces are high, they did not trigger the safety mechanism of the test rig to stop measuring forces, as was the case when measuring the forces while machining at 25 µm but at higher speeds of 60 m/min and 80 m/min. From Figure 4.34, it can be observed that the forces are increasing with the increase in the number of sections of Ti-17 alloy being machined and this increase becomes steeper after the tooth has performed approximately 1500 cuts. The side force becomes higher than the cutting force after the tooth has performed approximately 5500 cuts, suggesting that the corner of the carbide tooth is experiencing gradual wear. Moreover, the high thrust force is also an indication that the tooth is wearing on its flank surface.

The variation in Esp for the carbide tooth used at 25 µm feed and 40 m/min cutting speed is displayed in Figure 4.35. It can be observed that the Esp follows the same trend as that of the cutting force. It starts from 4 GJ/m^3 and increases to approximately 10 GJ/m^3 at the end of the trial. Since Esp also takes into account the area of the tooth, therefore the increased value of Esp indicates rapid wear of the cutting edge. The condition of the carbide tooth at the end of its life after being used at 25 µm feed and 40 m/min is shown in Figure 4.36. The carbide tooth appears to have chipped from both the rake and flank face and the wear is dominant on the corner of the cutting edge. Moreover, the carbide tooth might be plastically deformed at the cutting edge, due to excessive load experienced by the tooth. The side view of the carbide tooth is provided in Figure 4.36c and it clearly reveals that the corner has chipped and a wear flat has developed on the corner of the cutting edge.

The physical characteristics of the chips formed while machining Ti-17 alloy at a cutting speed of 40 m/min and at 25 µm are shown in Figure 4.37. The chips formed during the

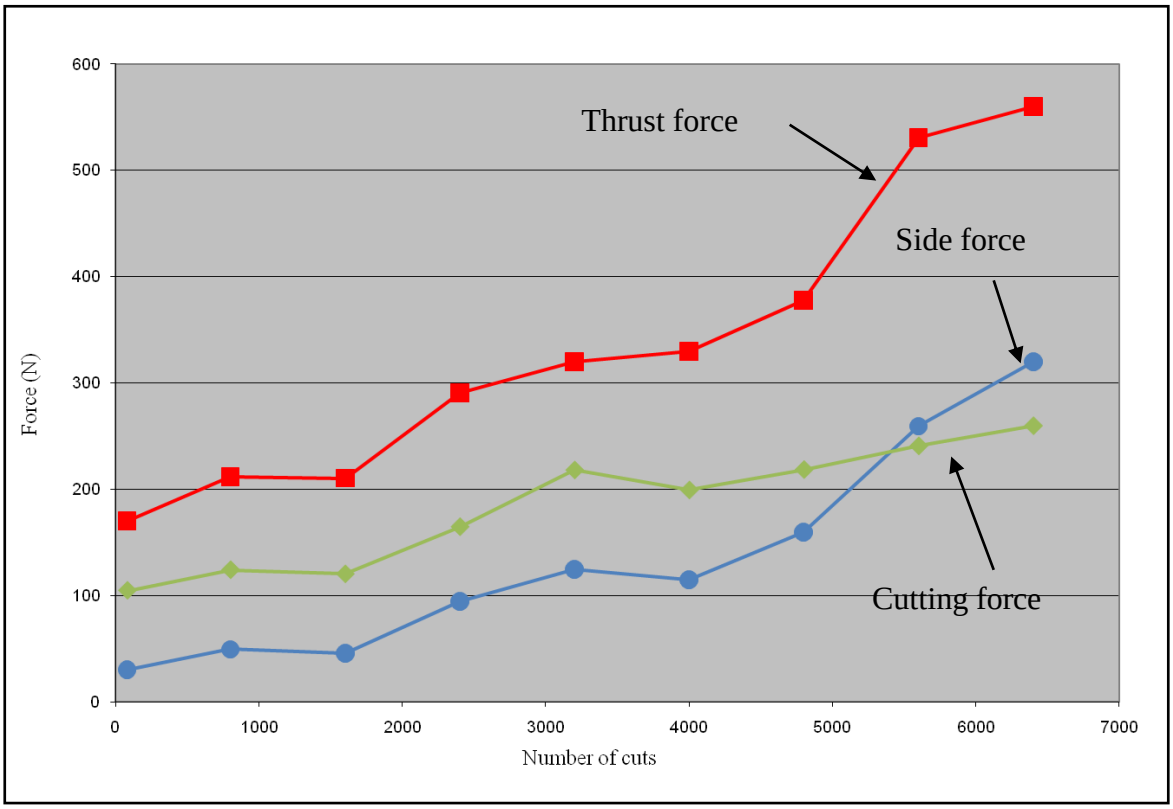

Figure 4.34. Variation in forces for un-coated carbide tooth (feed: 25 µm, cutting speed: 40 m/min, width of cut: 1 mm, length of one cut: 0.6 m).

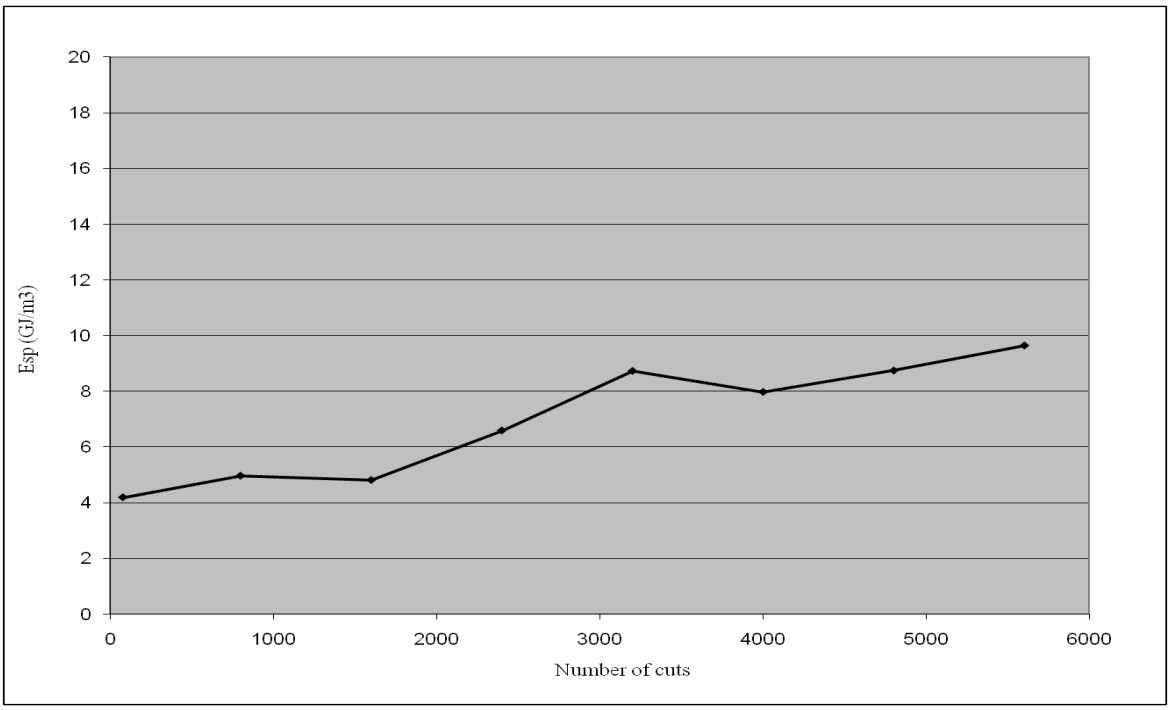

Figure 4.35. Variation of Esp with the number of cuts for the carbide (feed: 25 µm, cutting speed: 40 m/min, width of cut: 1 mm, length of one cut: 0.6 m).

initial cutting operation were found to be longer compared to the chips that were formed at the end of the machining operation, suggesting that the geometry of the cutting edge has been modified during the machining trial.

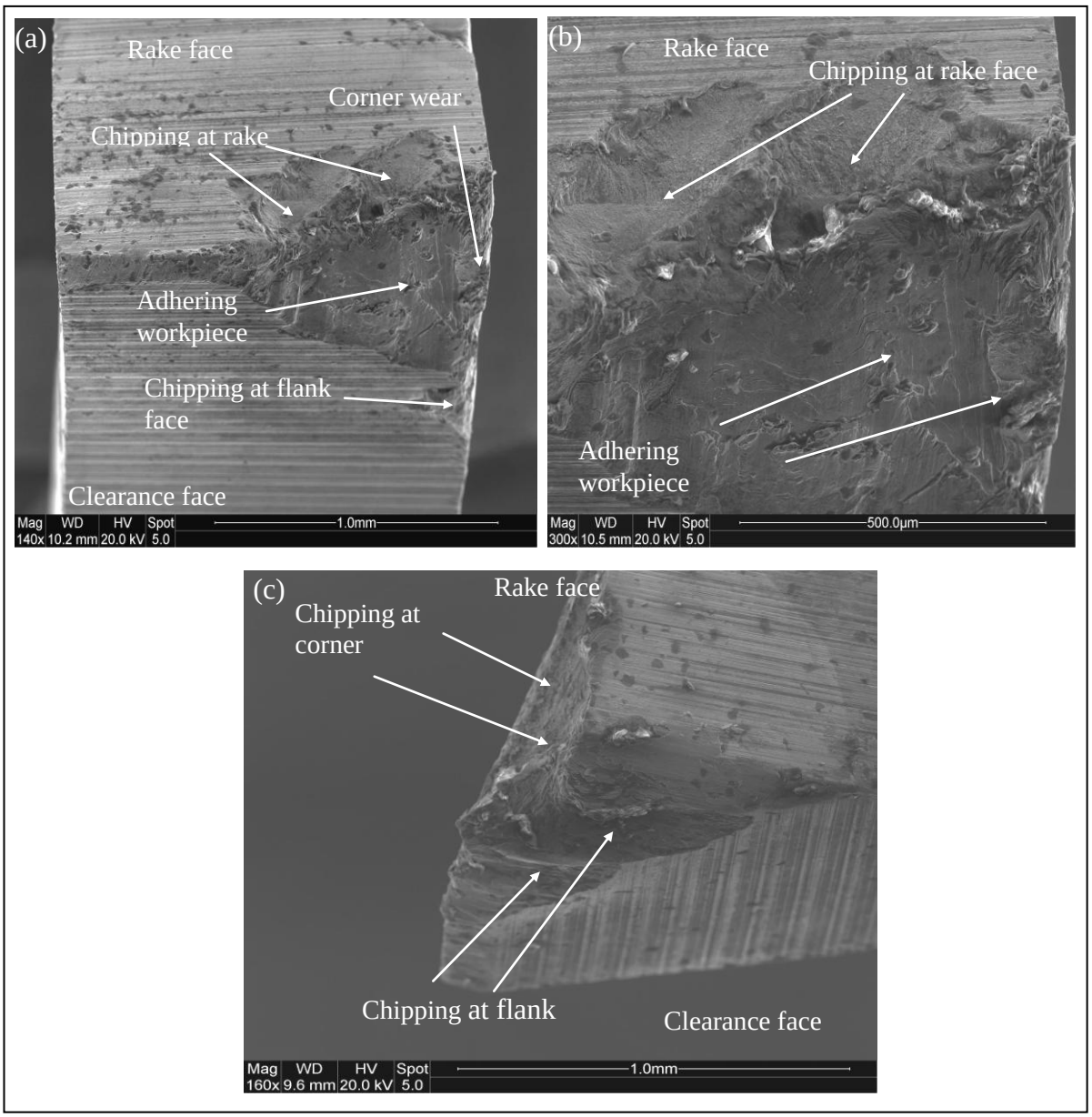

Figure 4.36. SEM images of (a) the carbide tooth used at a cutting speed of 40 m/min and feed of 25 µm, (b) magnified image of the corner of tooth and (c) side view of the tooth showing chipped cutting edge.

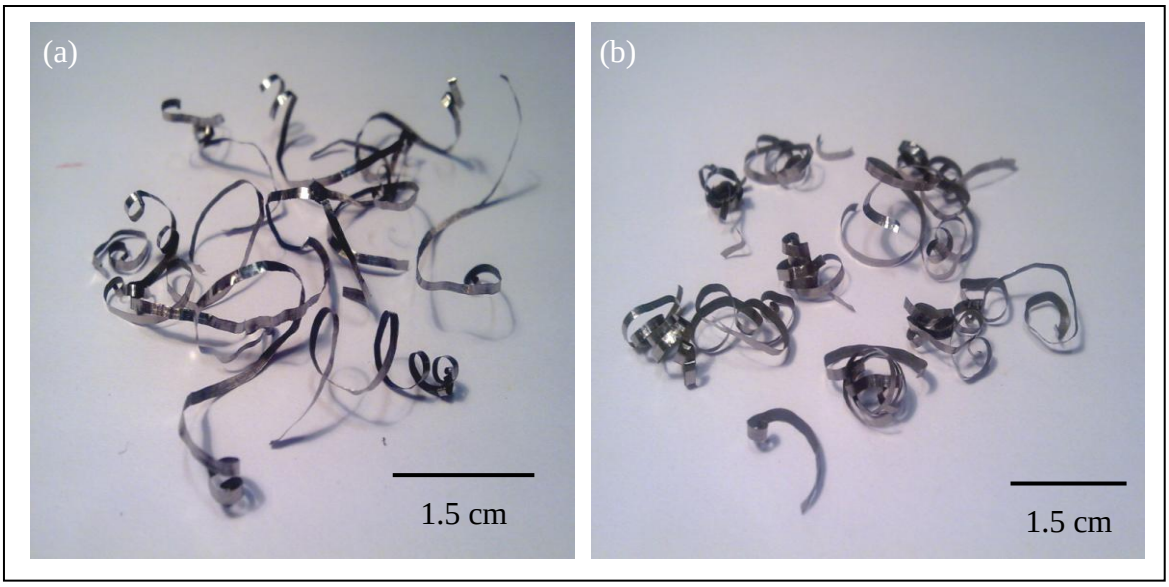

Figure 4.37. Physical characteristics of the chips formed at a cutting speed of 40 m/min and at a feed of 25 µm (a) initial chips and (b) final chips.

In order to observe the effect of feed on the degradation of the carbide tooth, the feed was reduced to 20 µm, while maintaining the cutting speed at 40 m/min. The variation of forces with the number of cuts for the carbide tooth used at a feed of 20 µm and at a cutting speed of 40 m/min is shown in Figure 4.38. From the Figure 4.38, it can be observed that the tooth has started to wear from the corner after it has performed approximately 6000 cuts.

After 6000 cuts, there is a steady increase in the side force and it crosses the cutting force after the tooth has performed 9000 cuts, suggesting an increase in the wear at the side of the carbide tooth. All the forces show an increasing trend, however, the increase in side force is much higher, which indicates that the corner of the carbide tooth is wearing at a higher rate.

The variation in Esp for the carbide tooth used to machine Ti-17 alloy at a feed of 20 µm and at a cutting speed of 40 m/min is shown in Figure 4.39. The Esp values start from 5 GJ/m^3 and remain almost constant up till 500 cuts and then rise to approximately 10.5 GJ/m^3 at the end of the test. Since Esp is related to the wear of the cutting edge, therefore an increase in the Esp values at the end is an indication of rapid wear taking place at the end of the machining session.

The condition of the carbide tooth at the end of the test is given in Figure 4.40. Figure 4.40 (a), shows the magnified image of the corner of the cutting edge, where chipping can be

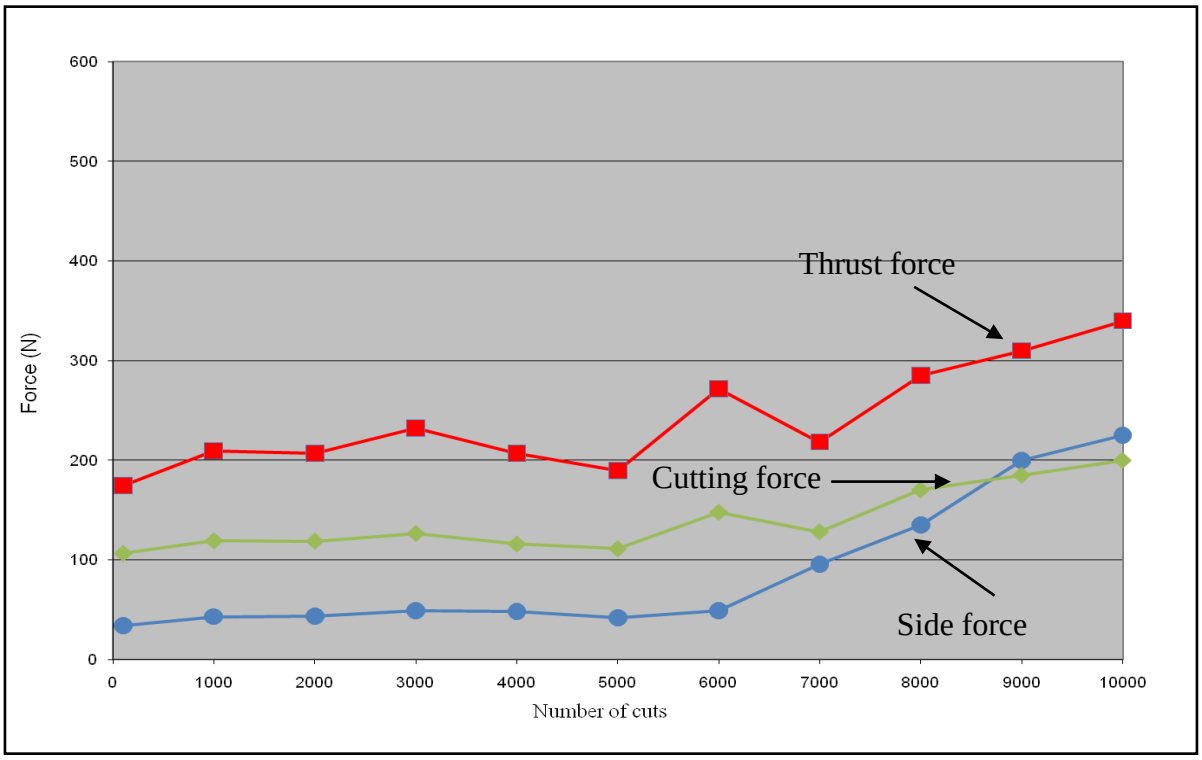

Figure 4.38. Variation in forces for the carbide tooth (feed: 20 µm, cutting speed: 40 m/min, width of cut: 1 mm, length of one cut: 0.6 m)

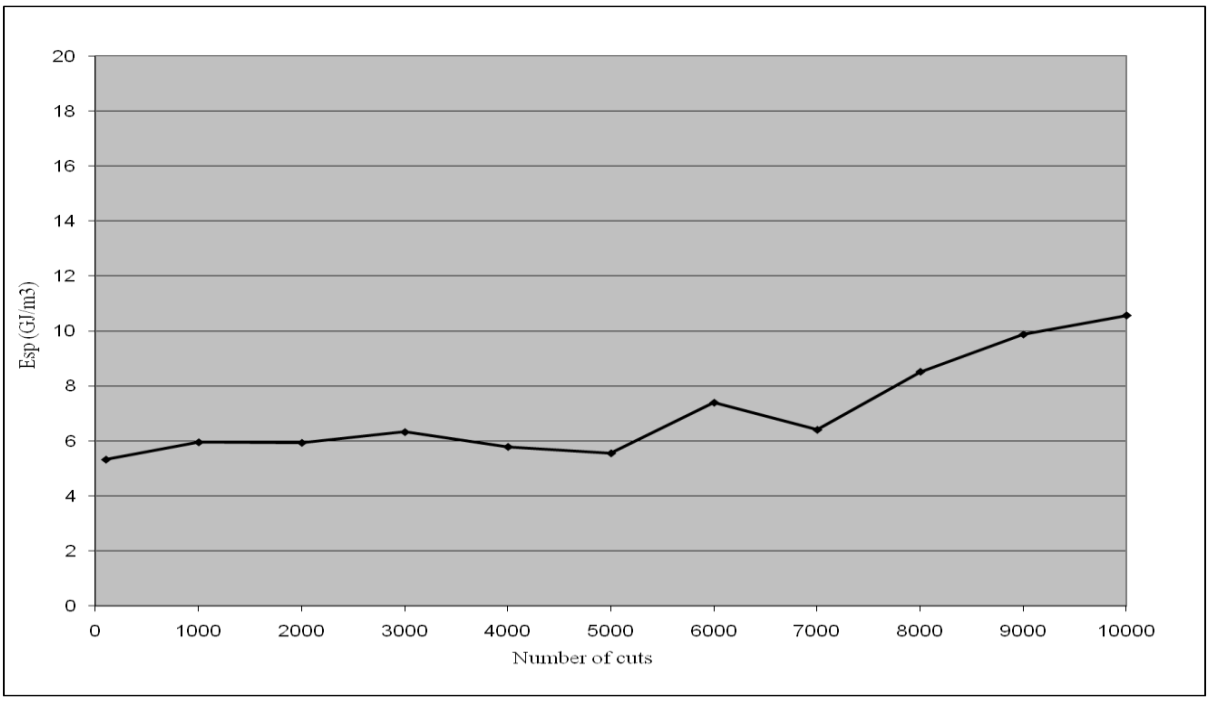

Figure 4.39. Variation in Esp with the number of cuts for un-coated carbide tooth (feed: 20 µm, cutting speed: 40 m/min, width of cut: 1 mm, length of one: cut 0.6 m).

observed on the flank and rake faces. Figure 4.40 (b) is the side view of the carbide tooth and further shows chipping of the corner as well as the chipping of rake and flank faces.

The physical characteristics of the chips formed while machining Ti-17 alloy at a cutting speed of 40 m/min and at 20 µm are shown in Figure 4.41. The chips formed during the initial cutting operation were found to be straighter compared to the chips that were formed at the end of the machining operation which are curled, suggesting that the geometry of the cutting edge has been modified due to wear.

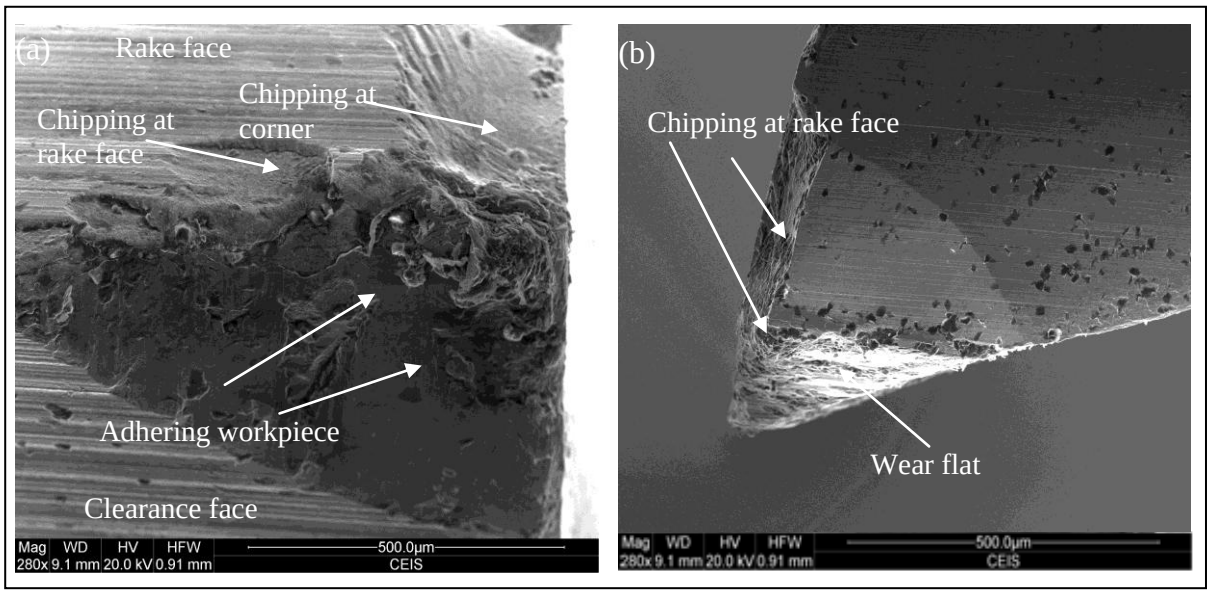

Figure 4.40. Condition of the carbide tooth at (a) the end of its life after being used at 20 µm feed and a cutting speed of 40 m/min and (b) side view of the carbide tooth showing the chipped corner and cutting edge.

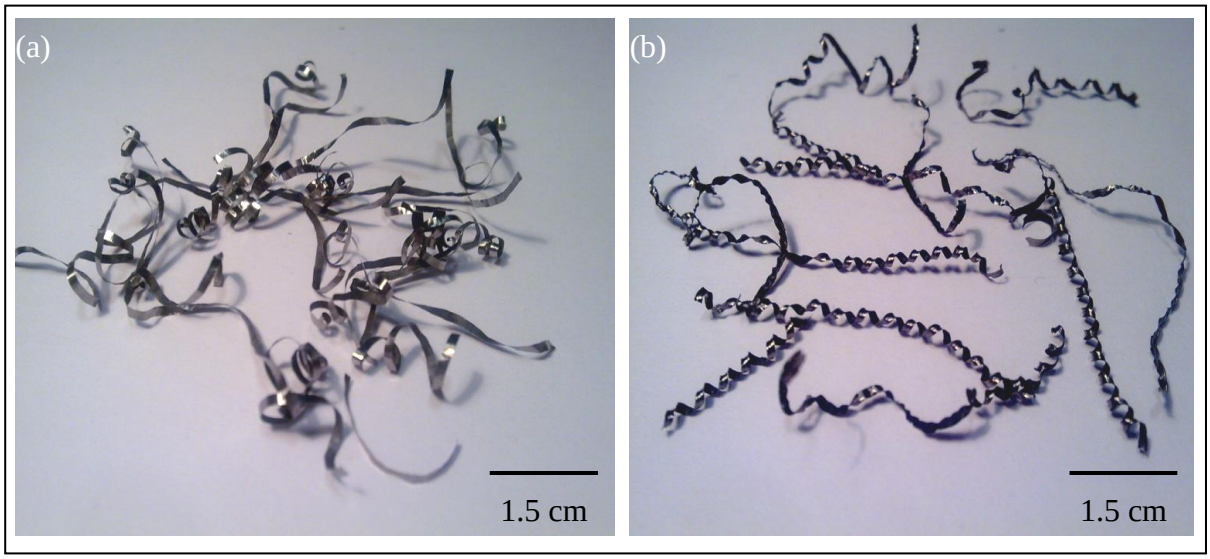

Figure 4.41. Physical characteristics of the chips formed at a cutting speed of 40 m/min and at a feed of 20 µm (a) initial chips and (b) final chips.

The feed was further reduced to 15 µm in order to examine the effect of reducing the feed on the performance of the carbide bandsaw tooth while maintaining the cutting speed at 40 m/min. The variation of forces with the number of cuts for the carbide tooth used to machine Ti-17 alloy at a feed of 15 µm and cutting speed of 40 m/min is shown in Figure 4.42. From Figure 4.41, it can be observed that the carbide tooth lasted longer than the previous cases in which the feed was higher *ie* 20 and 25 µm. It appears from the force graph that the corner of the carbide tooth has started degrading in terms of its original geometry, after it has performed approximately 15000 cuts and degrades further with more machining. After performing 16000 cuts, the side force becomes higher than the cutting force, indicating high rate of wear of the corner of the carbide tooth. The variation of Esp with the number of cuts is displayed in Figure 4.43. It is apparent from Figure 4.43 that Esp follows the same trend as that of cutting force, starting from approximately 7 GJ/m^3 and climbing to 16 GJ/m^3 at the end of the test, indicating the degradation of the cutting edge, especially at the end of the machining test.

The condition of the carbide tooth at the end of machining is illustrated in Figure 4.44. It is clear from Figures 4.44 (a) and 4.44 (b), that the tooth has chipped from the rake face and worn flank surface can be observed. Figure 4.44 (c), which provides the side view of the carbide tooth at the end of its life, shows a better view of the worn flank along with smeared workpiece material.

The physical characteristics of the chips formed while machining Ti-17 alloy at a cutting speed of 40 m/min and at 15 µm are displayed in Figure 4.45. The chips formed during the initial cutting operation were found to be straighter and longer as compared to the chips that were formed at the end of the machining operation which are shorter and rounded, suggesting that the physical geometry of the cutting edge has been modified due to wear and thereby accounting for the difference in the appearance of the chips.

The feed was reduced further to 10 µm, which is the lowest feed in the chosen range, while maintaining the cutting speed at 40 m/min. This was done to investigate the variation of forces (and Esp) and the wear of the carbide tooth at a low feed of 10 µm. The variation of forces with the number of cuts made is shown in Figure 4.46. From Figure 4.46 it can be seen that the forces remain constant throughout the machining and the values decrease and increase after performing approximately 37000 cuts. This is due to the fact that the tooth has reached the end of the length of the workpiece and was brought back to its original starting position and realigned to a width of 1 mm. This was reconfirmed by performing the test again and the results are given in Figure 4.47.

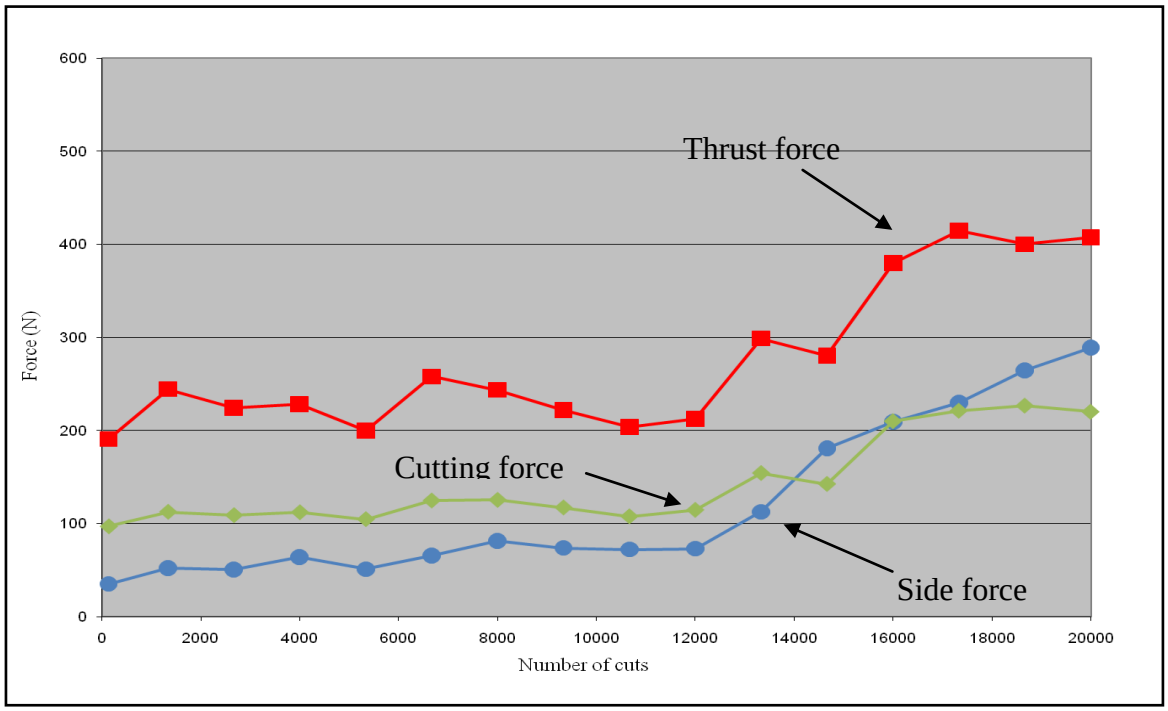

Figure 4.42. Variation in forces for the carbide tooth (feed: 15 µm, cutting speed: 40 m/min, width of cut: 1 mm, length of one cut: 0.6 m).

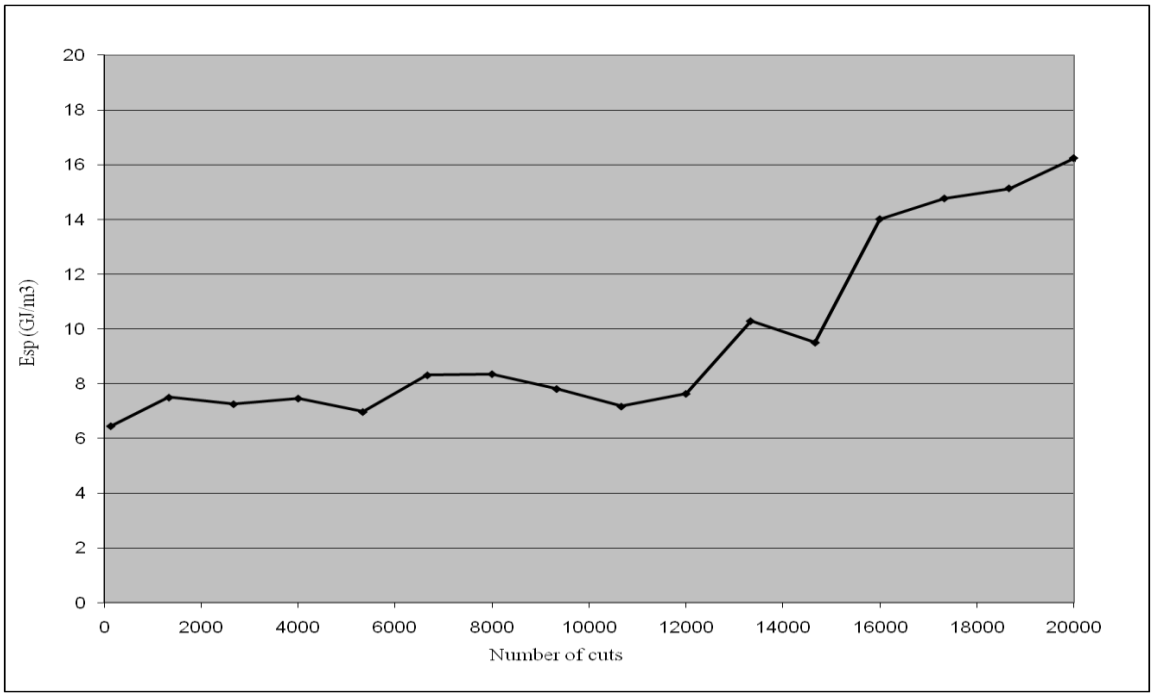

Figure 4.43. Variation in Esp with the number of cuts for un-coated carbide tooth (feed: 15 µm, cutting speed: 40 m/min, width of cut: 1 mm, length of one cut: 0.6 m).

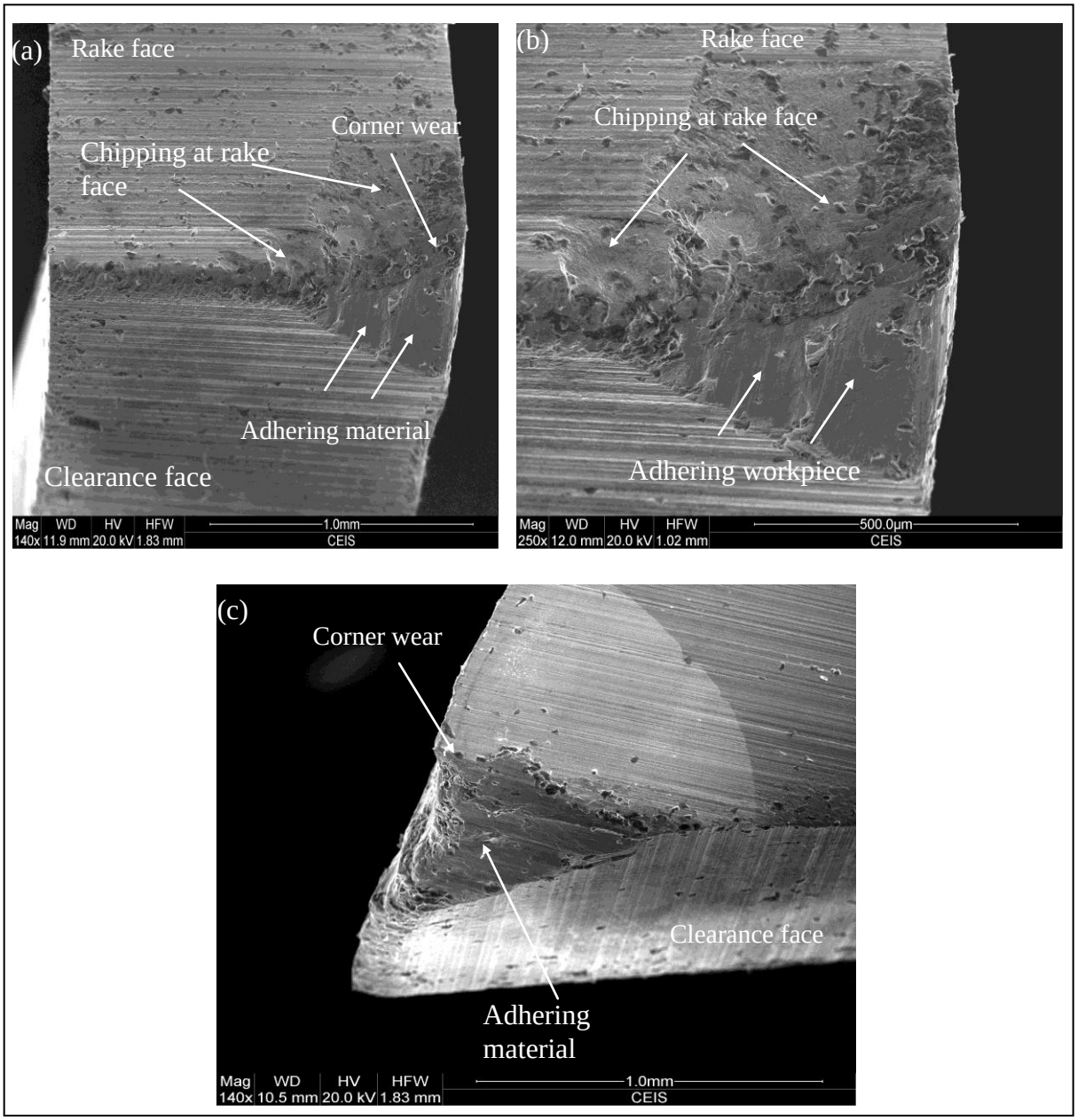

Figure 4.44. Condition of (a) the carbide tooth at the end of its life after being used at 15 µm feed and cutting speed of 40 m/min, (b) side view of the carbide tooth showing the chipped corner and cutting edge and (c) side view.

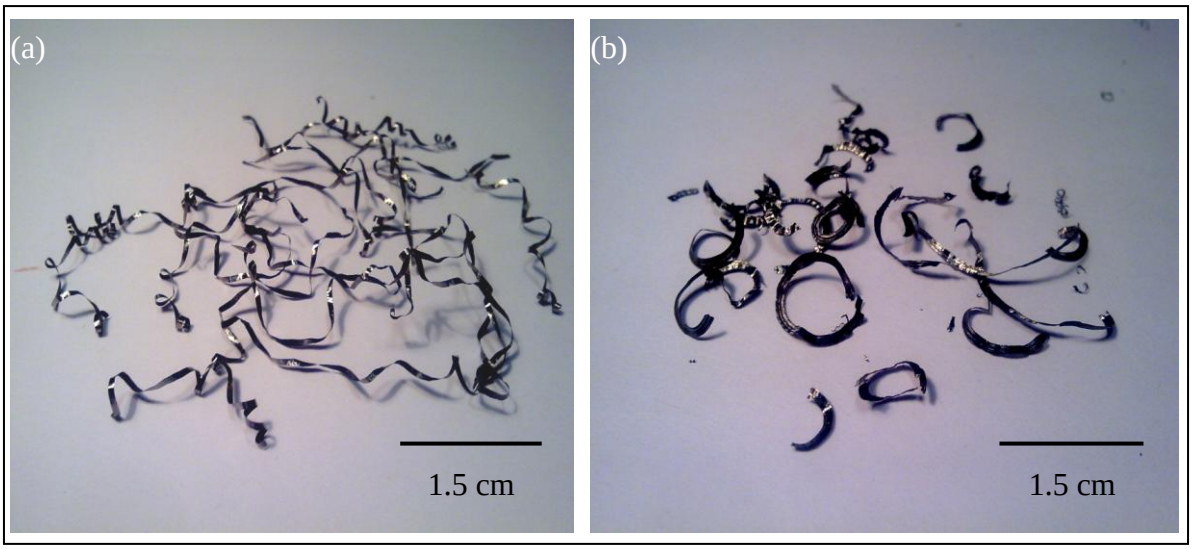

Figure 4.45. Characteristics of the chips formed at a cutting speed of 40 m/min and at a feed of 15 µm, (a) initial chips and (b) final chips

From Figure 4.46 and Figure 4.47, it can be observed that the force levels remain constant with further machining. The low level of forces indicates that the tooth geometry has not been modified to a large extent. This further suggests that the machining conditions are "mild" and that gradual, uniform wear is taking place at the cutting edge.

The variations of Esp for these machining tests are shown in Figures 4.48 and 4.49 respectively. It can be observed from Figure 4.48 that Esp follows the same trend as that of the cutting force when machining Ti-17 alloy at a feed of 10 µm and at the cutting speed of 40 m/min. The Esp values start from approximately 8 GJ/m^3 and reach to approximately 11 GJ/m^3 at the end of the machining trial, *i.e.* after performing 52000 cuts. The smooth increase in the Esp curve is indicative of uniform wear taking place at the cutting edge along with easy cutting conditions.

The SEM images of the carbide tooth used to machine Ti-17 alloy at the cutting speed of 40 m/min and at a feed of 10 µm are revealed in Figure 4.50. It appears from the Figures 4.50 (a) and 4.50 (b) that the corner of the tooth has worn, whereas it appears that the small section of rake face has chipped. It appears from Figure 4.51 (c), that the cutting edge has developed a wear flat. This is probably during the last stage of machining, where due to attrition wear, the cobalt matrix has weakened and hence the chipping. The attrition wear will be discussed later.

The physical characteristics of the chips formed while machining Ti-17 alloy at a cutting speed of 40 m/min and at 10 µm are shown in Figure 4.51. The chips formed during the

initial cutting operation were found to be almost identical to the chips formed at the end of the machining operation, suggesting that the physical geometry of the carbide bandsaw tooth has not deteriorated significantly, which can also be confirmed by observing the SEM images of the tooth.

In order to further investigate the wear and the degradation of the carbide tooth at the cutting speed on 40 m/min and at the feed of 10 µm, a number of different carbide teeth, with same physical features (such as rake angle, clearance angle) were used to machine Ti-17 alloy and to make a certain number of cuts (10000, 25000 and 40000 cuts). The teeth were then observed under the SEM to assess their progressive degradation in terms of wear, after they had performed a specified number of cuts.

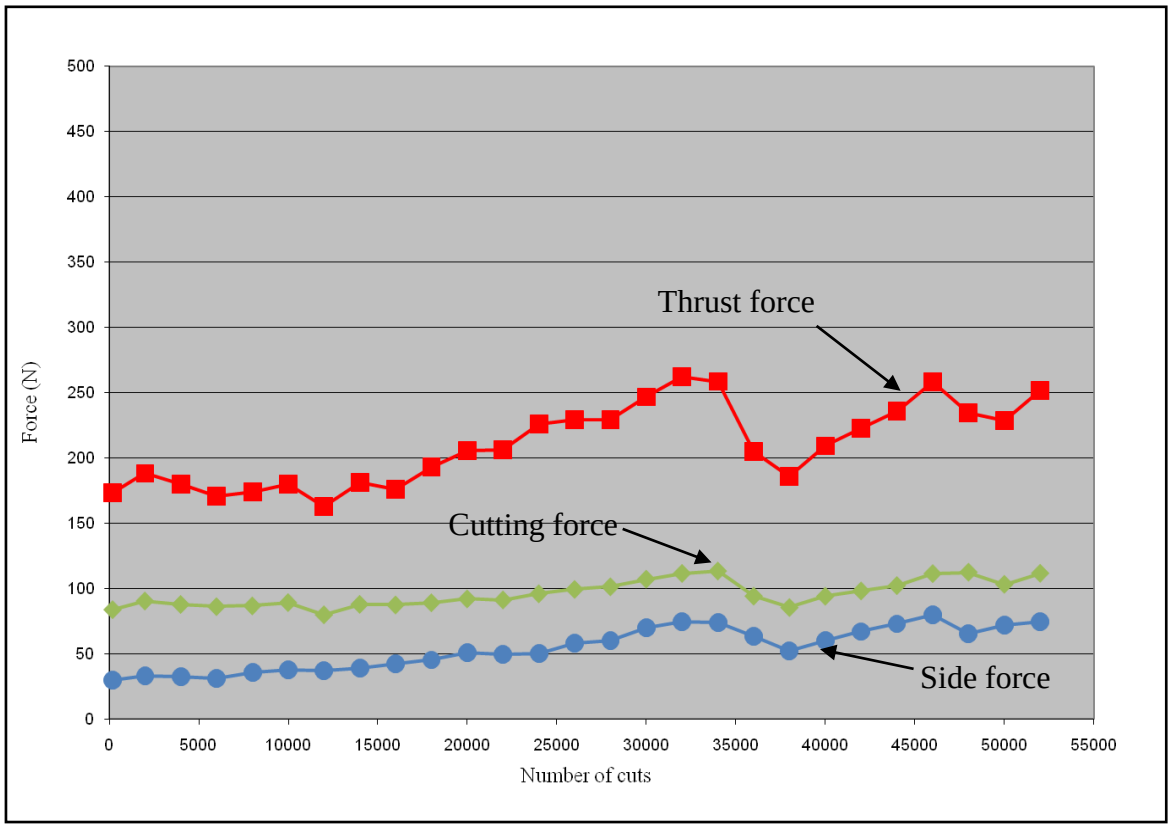

Figure 4.46. Variation of forces for un-coated carbide tooth (feed: 10 µm, cutting speed: 40 m/min, width of cut: 1 mm, length of one cut: 0.6 m).

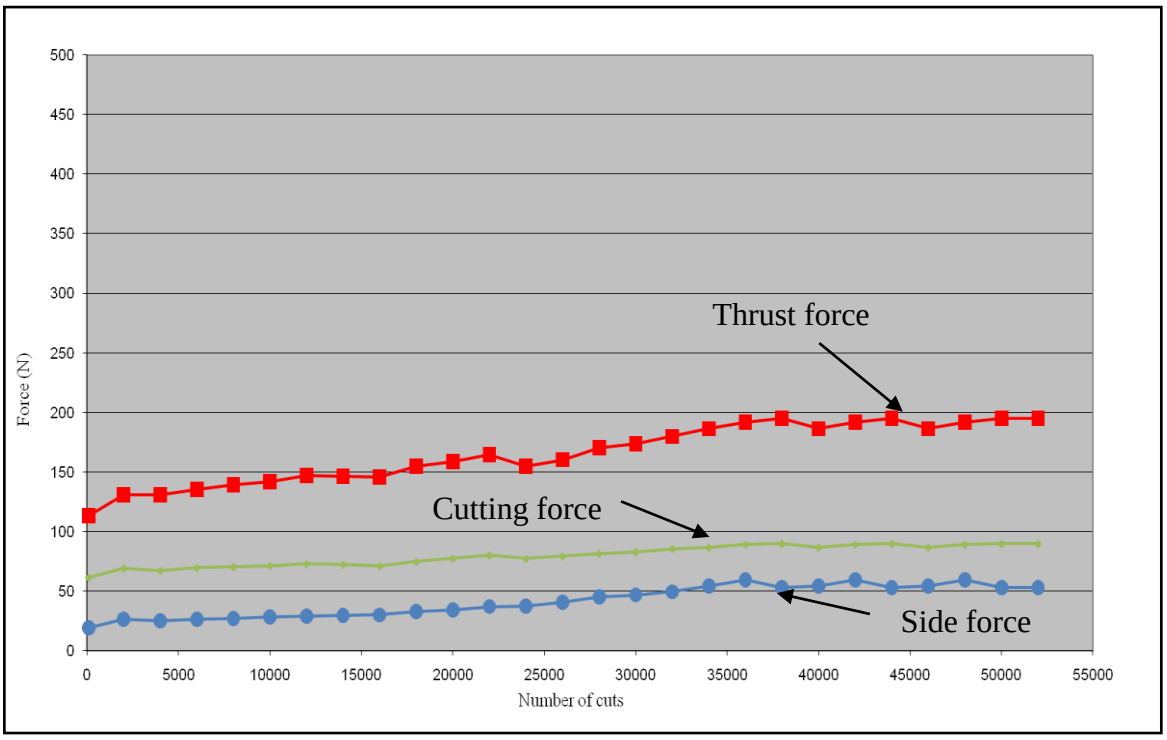

Figure 4.47. Variation of forces for the carbide tooth (feed: 10 µm, cutting speed: 40 m/min, width of cut: 1 mm, length of one cut: 0.6 m) (repeat test).

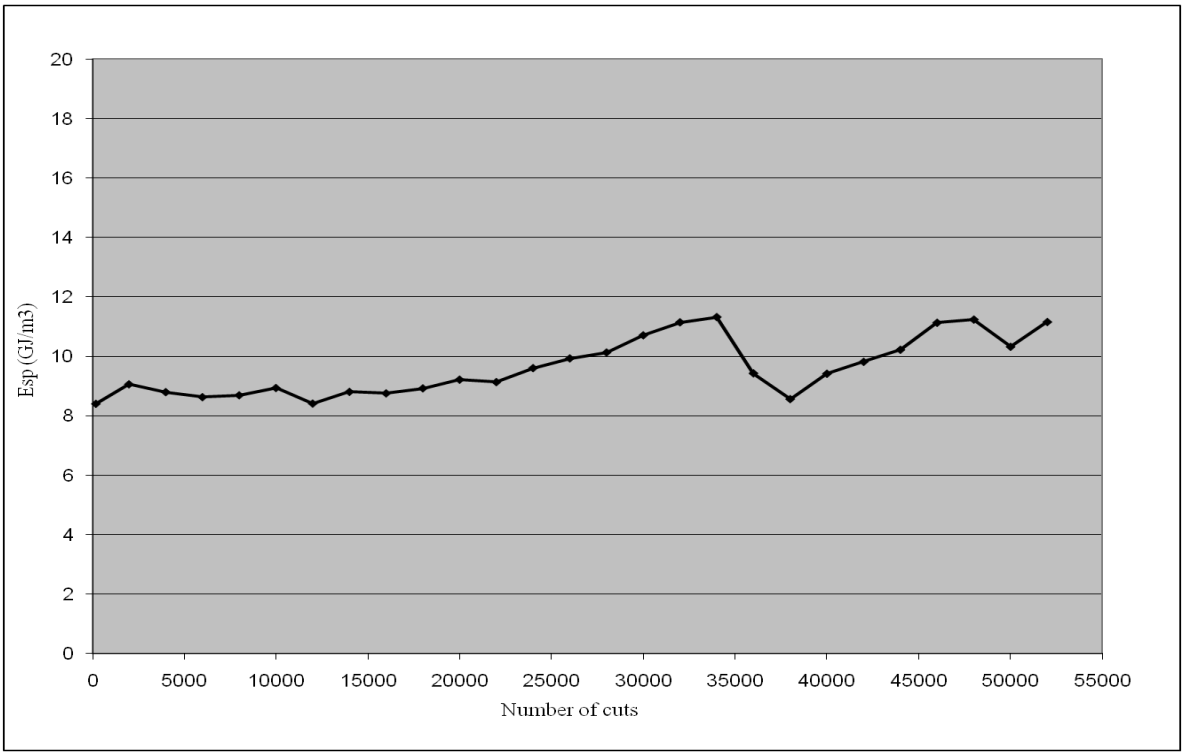

Figure 4.48. Variation in Esp with the number of cuts for the un-coated carbide tooth (feed: 10 µm, cutting speed: 40 m/min, width of cut: 1 mm, length of one cut: 0.6 m).

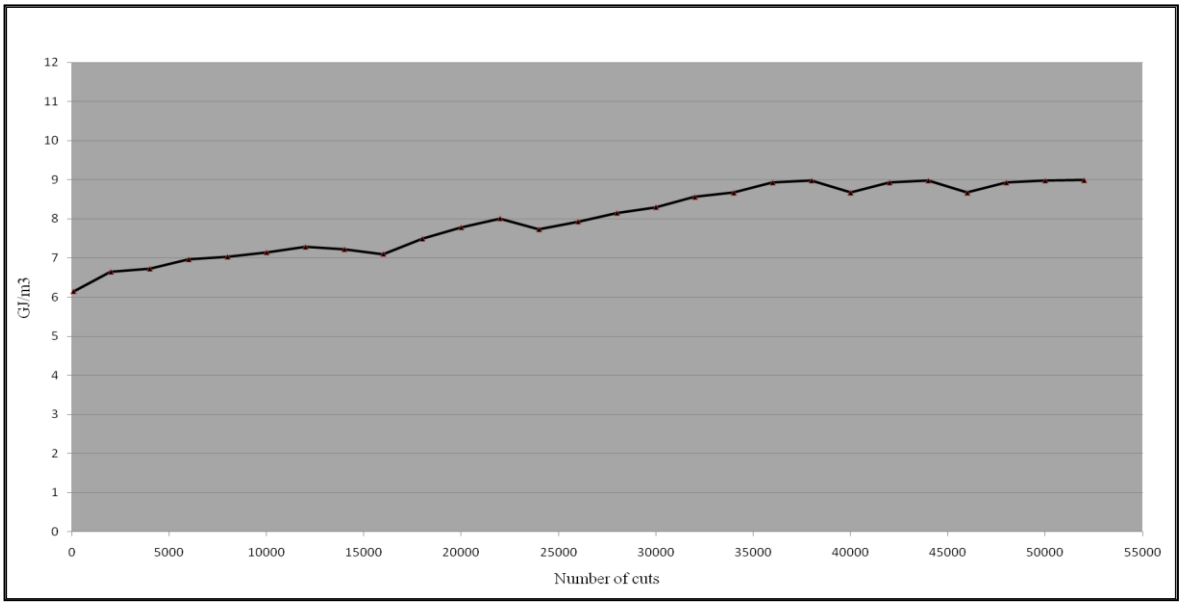

Figure 4.49. Variation in Esp with the number of cuts for un-coated carbide (feed 10 µm, cutting speed: 40 m/min, width of cut: 1 mm, length of one cut: 0.6 m, repeat test).

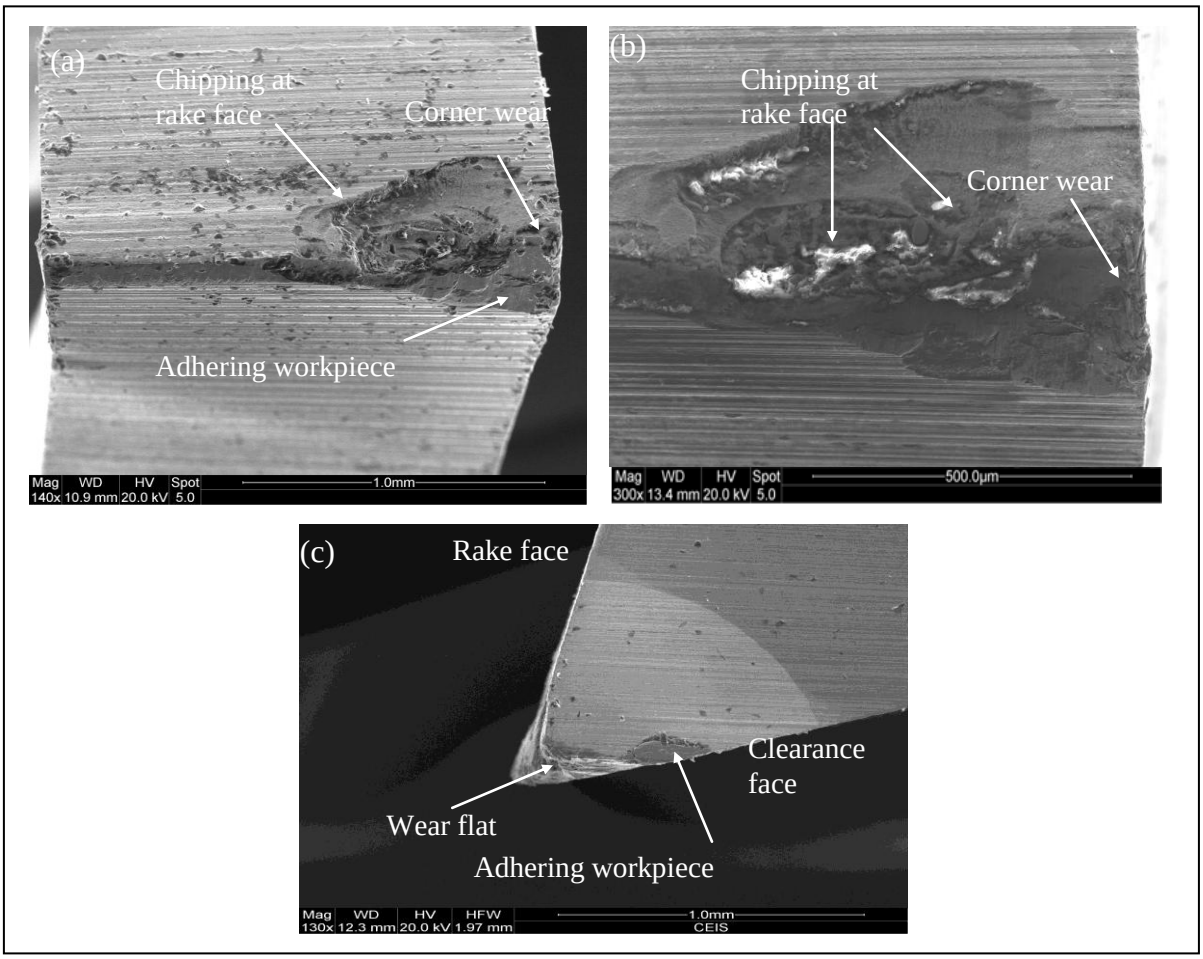

Figure 4.50. SEM micrographs of (a) the carbide tooth used at 10 µm feed and at 40 m/min cutting speed, (b) magnified view of the corner of the cutting edge showing a chipped rake face and (c) side view of the tooth.

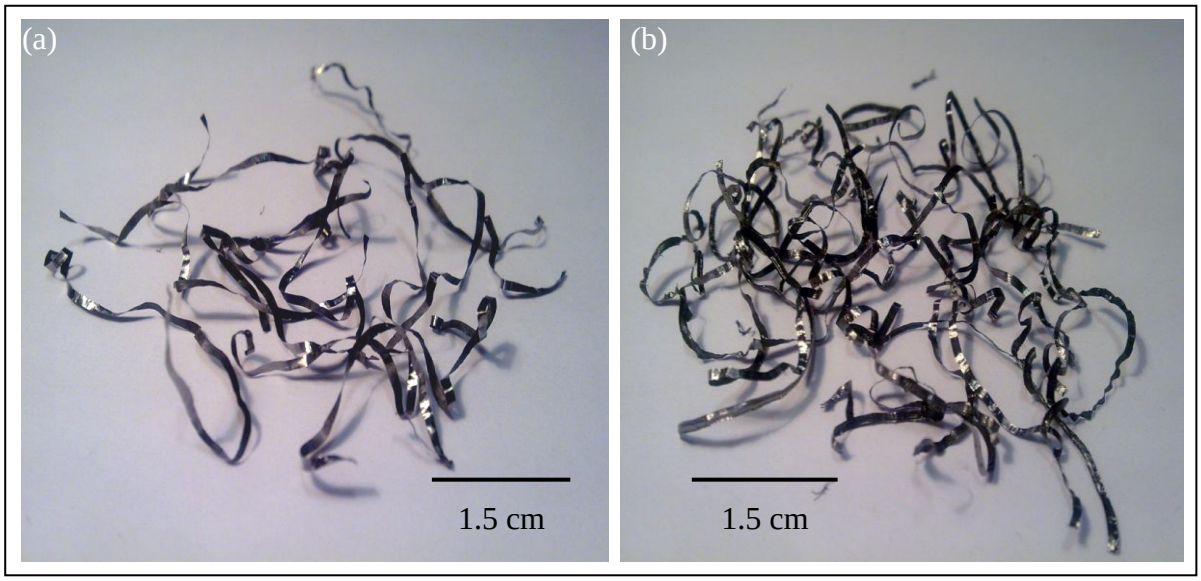

Figure 4.51. Characteristics of the chips formed while machining at 10 µm feed and 40 m/min cutting speed, (a) initial chips and (b) final chips.

The condition of the carbide tooth after it has performed 10,000 cuts is provided in Figure 4.52. It can be observed that the tooth has started to wear, especially at the corner and has begun to chip slightly at the rake face. Figure 4.52 (c) is a magnified image of the corner of the cutting edge which clearly demonstrates chipping at the rake face.

Figure 4.53 presents the condition of the carbide bandsaw tooth after it has performed 25000 cuts. It appears from these images that cutting edge had deteriorated further due to chipping at the rake face. Figure 4.53 (b) presents the magnified view of the corner of the cutting edge. Figure 4.53 (b) clearly shows the chipping at the rake face, which is predominantly higher than the chipping at the flank face. Figure 4.53 provides a side view of the same carbide tooth and shows that the cutting edge has developed a wear flat that has chipped at the corner as well as beneath the cutting edge.

Another carbide tooth was used to machine Ti-17 alloy – the test was stopped after the tooth had performed 42,000 cuts, in order to observe the condition of the tooth. The SEM images of this carbide tooth are presented in Figure 4.55. Figure 4.55 (a) shows that both faces of the cutting edge have chipped, probably due to excessive heat generated as well as due to stresses experienced by the tooth. The magnified image of the corner of the carbide tooth is given in Figure 4.55 (b), while Figure 4.55 (c) shows the degradation of the corner of the carbide tooth. Chipping at the rake face can be observed clearly from Figure 4.55 (b). The development of the wear flat (or wear land) on the corner of the cutting edge is displayed in Figure 4.55 (c). This image shows that the side of the tooth has worn and

further implies the development of uneven flat wear land on the tooth. It must, however be noted that this is a side view of the carbide tooth and the condition of the carbide tooth at a distance from the corner of the cutting edge will be different compared to the corner.

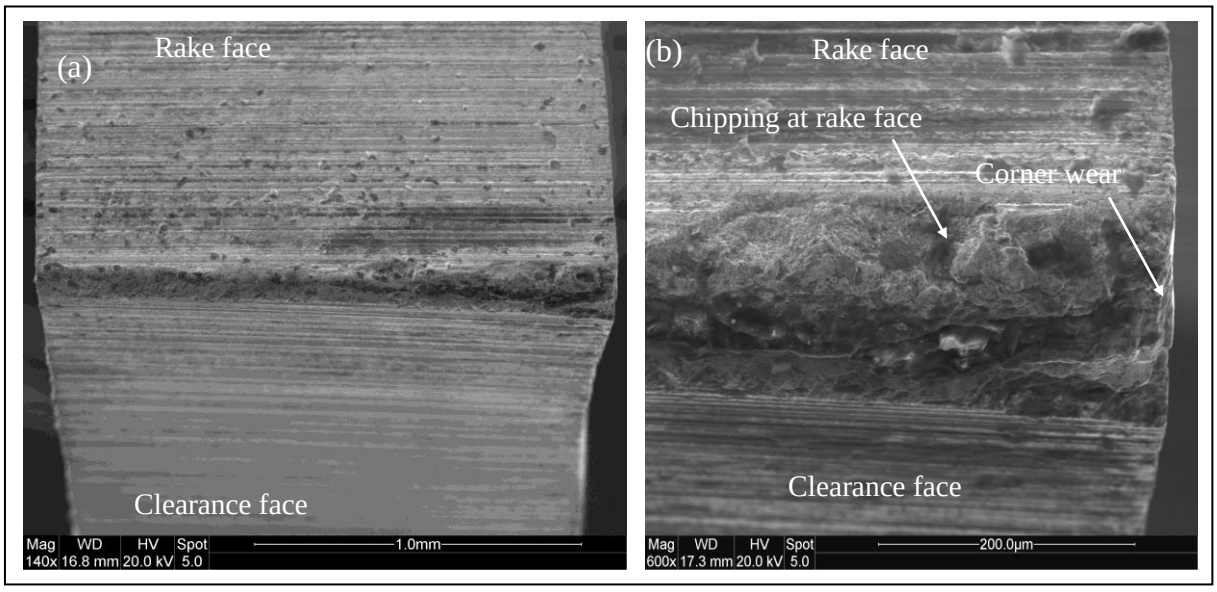

Figure 4.52. (a) Condition of the carbide tooth after performing 10 000 cuts at a cutting speed of 40 m/min and 10 µm feed and (b) magnified view of the corner.

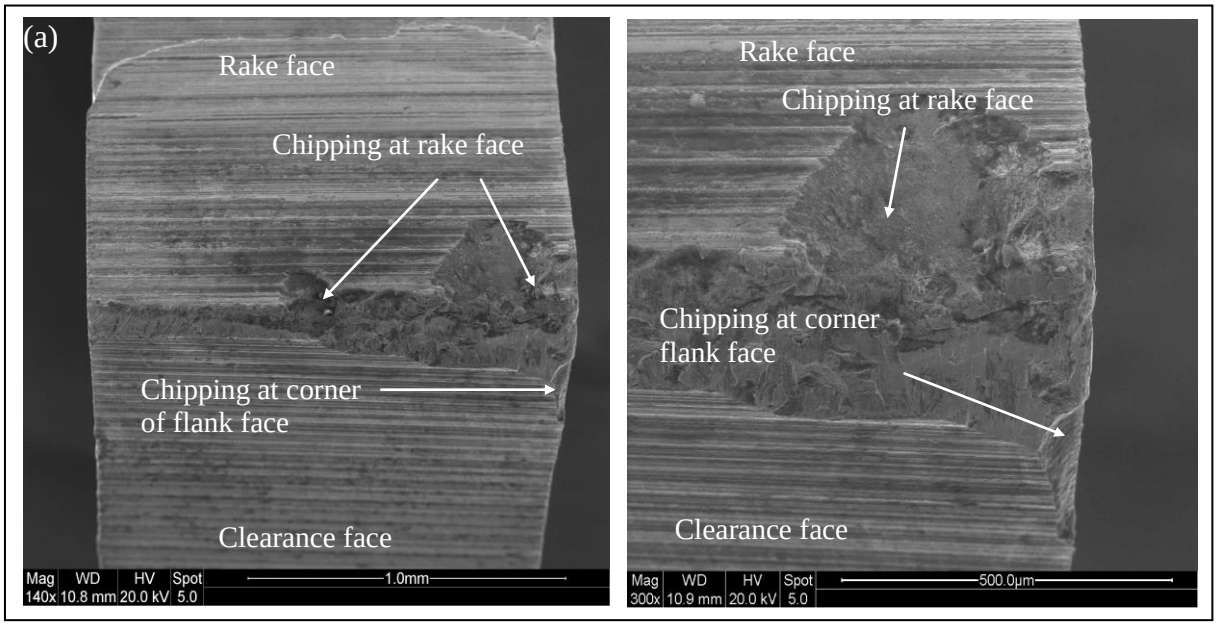

Figure 4.53. (a) Condition of the carbide tooth after performing 25 000 cuts at a cutting speed of 40 m/min and 10 µm feed and (b) magnified view of the corner.

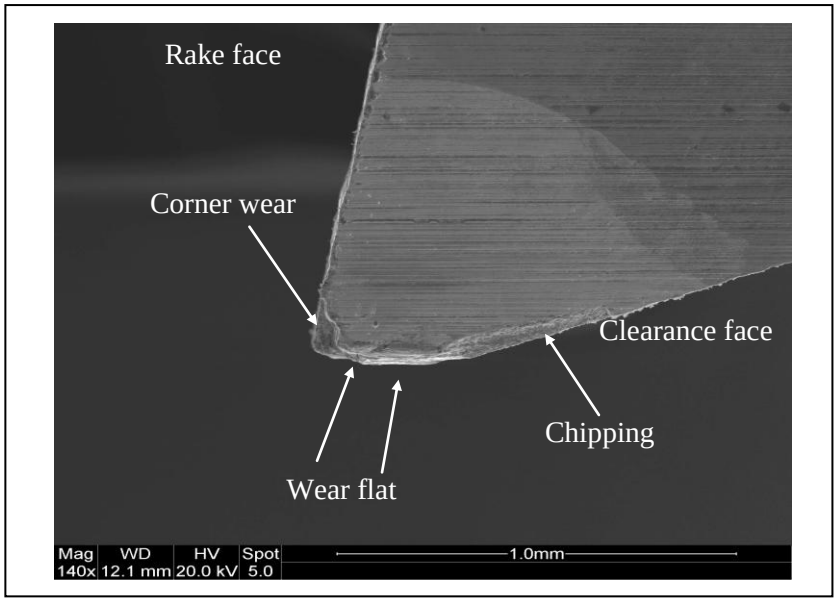

Figure 4.54. Side view of the carbide tooth after 25 000 cuts, showing a wear flat on the cutting edge as well as chipping on the corner.

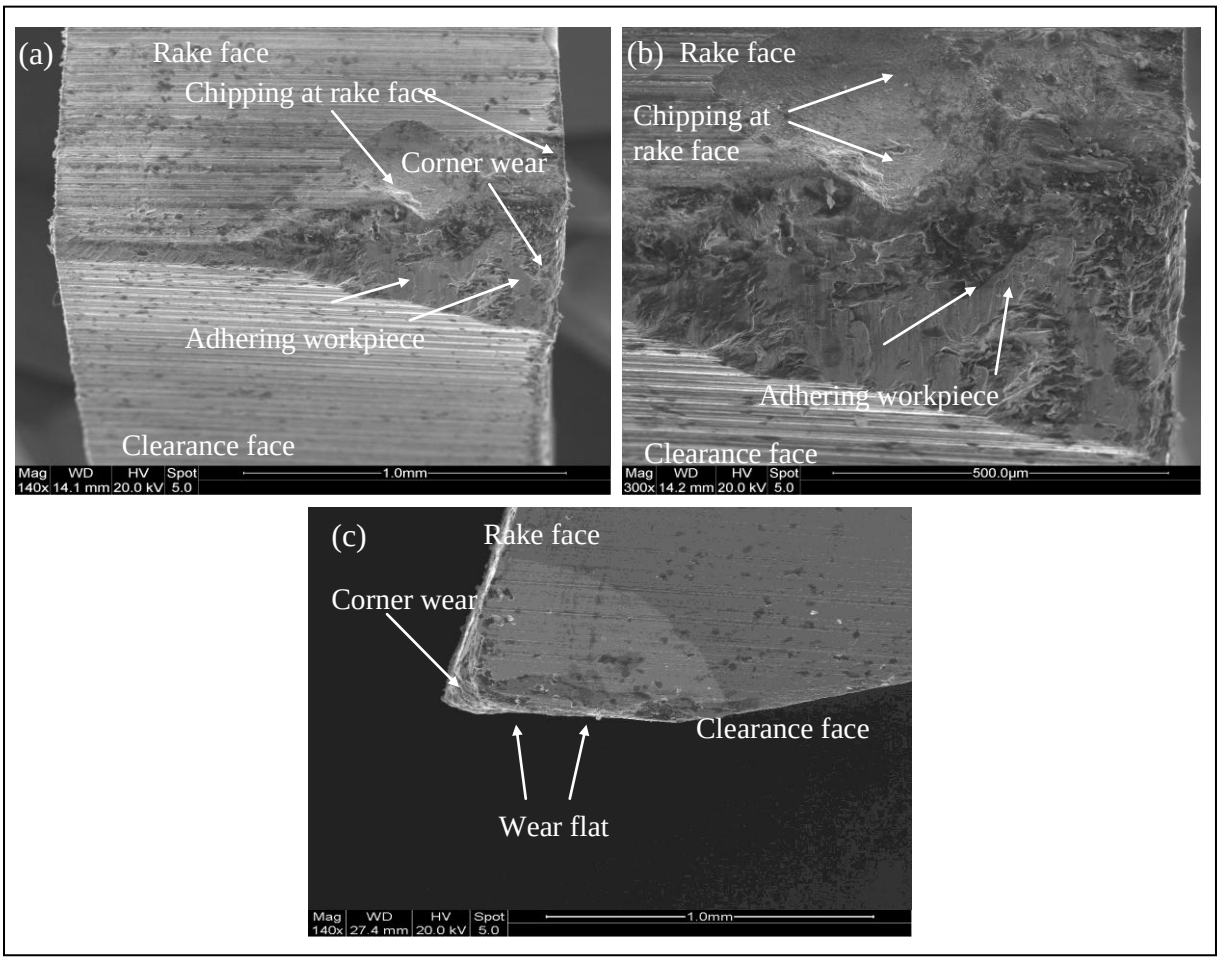

Figure 4.55. Condition of (a) the carbide tooth after 42 000 cuts, (b) magnified view of the corner of the carbide tooth showing a chipped cutting edge and (c) side view of the bandsaw tooth illustrating a wear flat.

4.4.0 Wear modes and mechanisms for un-coated teeth

In order to observe the wear modes and mechanisms, the worn carbide teeth were analysed under the scanning electron microscope, using different methods and functions such as Back Scattered Electron (BSE) mode and X-ray mapping.

Back scattered electrons are beam electrons that are the elastically scattered from the surface of the sample. BSE are used in analytical SEM along with the spectra made from the characteristic X-rays. Since the intensity of the BSE signal is strongly related to the atomic number (Z) of the specimen, BSE images provide information about the distribution of different elements on the surface of the sample. The heavy elements (with high atomic number) backscatter electrons more strongly than light elements *i.e.* the elements with low atomic number appear brighter in the image. Back scattered electrons are used to detect contrast between areas with different chemical compositions. X-ray mapping is a powerful technique employed to observe the distribution of the elements on the surface. X-ray maps are formed by collecting characteristic X-rays from elements in the specimen as a focused electron beam is scanned in a raster across the specimen.

All the worn carbide teeth revealed workpiece materials adhering to the cutting edge, especially at the flank face. This adhering workpiece material can be observed in Figure 4.56, which shows the magnified view of the corner of the cutting edges after the bandsaw tooth has been used to machine Ti-17 alloy at various machining parameters.

The magnified SEM images of the worn bandsaw teeth present clear evidence of the workpiece material adhering to the cutting edge as can be seen in Figure 4.56. The high temperature and stress generated during machining caused the welding of the workpiece material to the cutting edge. In order to further investigate this phenomenon, these samples were analysed using the BSE mode of the SEM. This was done in order to clearly identify and ascertain the amount of adhering workpiece material. Further analyses were carried out using EDX analyses on different areas of the adhering materials, in order to ascertain its elemental composition.

Figure 4.57 (a) shows the magnified image of the corner of the carbide tooth after it has performed 42 000 cuts at a cutting speed of 40 m/min and at a feed of 10 µm. The BSE image of the same area is displayed in Figure 4.57 (b). The contrast observed in Figure 4.57 (b) clearly indicates that material is adhering to the tooth.

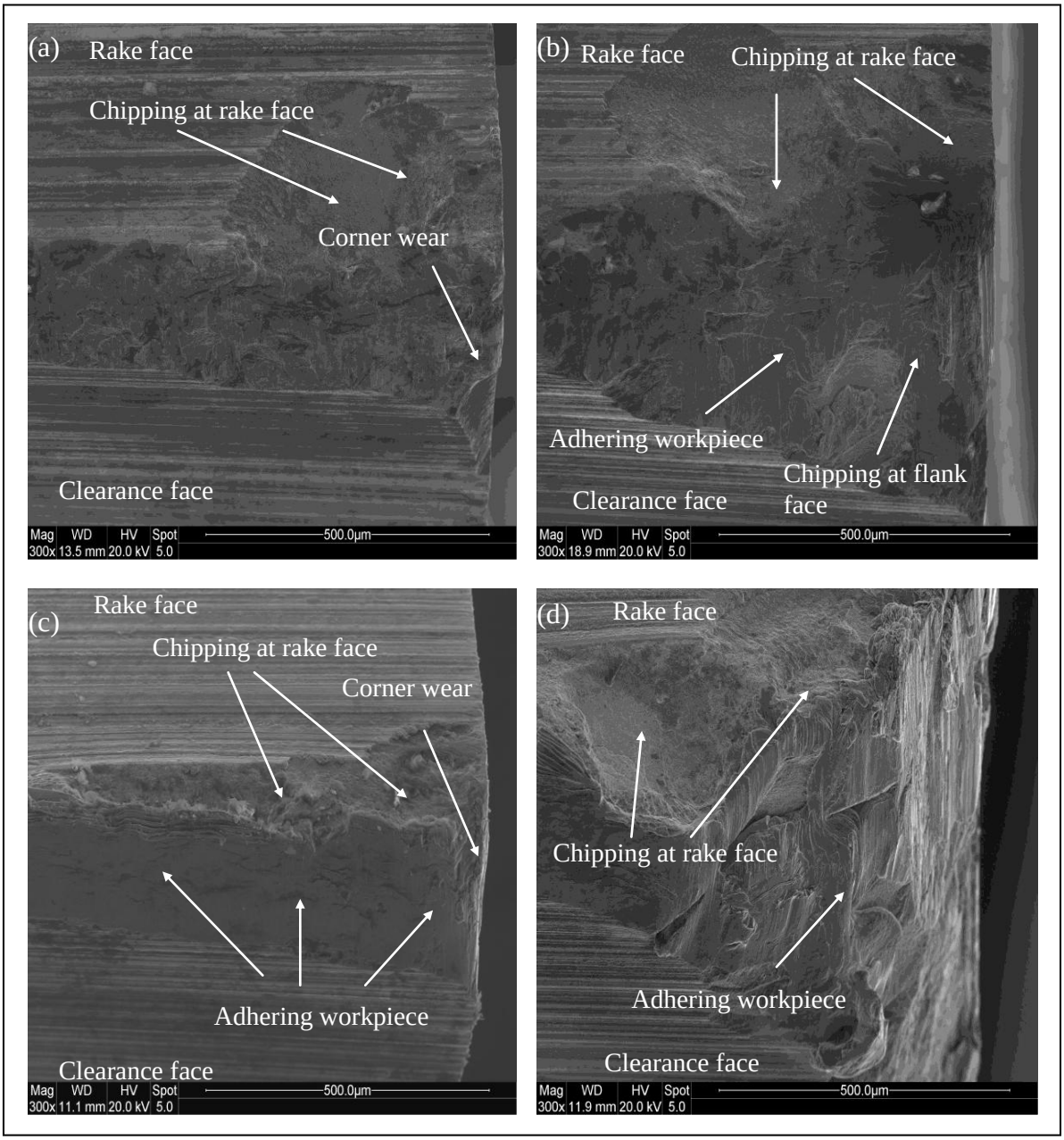

Figure 4.56. Magnified views of the corner of the carbide teeth (a) after 25 000 cuts at cutting speed of 40 m/min and feed of 10 µm, (b) after 42 000 cuts at 40 m/min and 10 µm feed, (c) end of tooth life at 60 m/min speed and 10 µm feed and (d) end of tooth life after machining at 80 m/min and 15 µm feed.

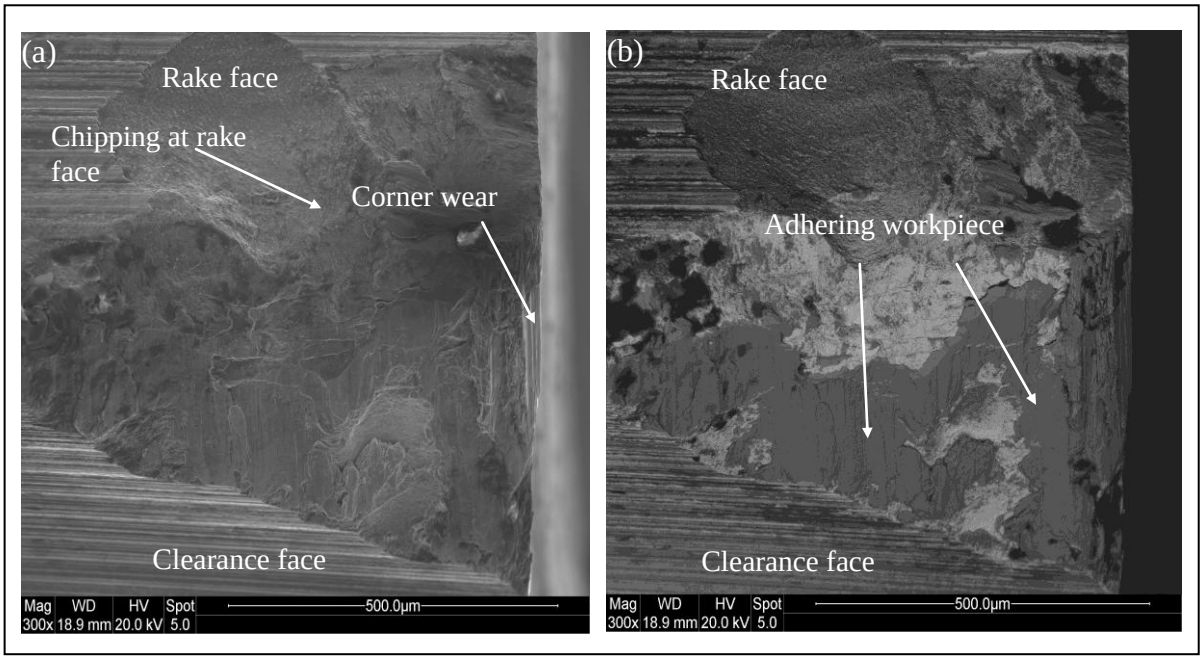

Figure 4.57. Magnified view of (a) the corner for the carbide tooth after performing 42,000 cuts at a cutting speed of 40 m/min and at 10 µm feed and (b) BSE image showing adhering workpiece material.

Figure 4.58 (a) shows the magnified view of the corner of the carbide tooth used at a cutting speed of 80 m/min and a feed of 15 µm. The same area in BSE mode is shown in Figure 4.58 (b) and this image presents clear evidence of the material adhering to the flank face. In order to confirm that the adhesion takes place at all cutting speeds, the same analysis was carried out on the tooth which was used at a cutting speed of 60 m/min and is presented in Figure 4.59. It was observed that the workpiece not only adheres to the flank face of the carbide bandsaw tooth, but also on the side of the cutting edge. This can be observed in Figure 4.60, which displays the side of the carbide tooth used at a cutting speed of 60 m/min and at the feed of 10 µm. The BSE image clearly reveals adhering material on the side of bandsaw tooth.

In order to further confirm the presence of the adhering material on the carbide teeth, X-ray mapping was carried out on some of the worn carbide teeth. Figure 4.61 (a) shows the corner of the carbide tooth which was used at a cutting speed of 60 m/min and at the feed of 10 µm. The corresponding X-ray mapping of titanium element is provided in Figure 4.61 (b).

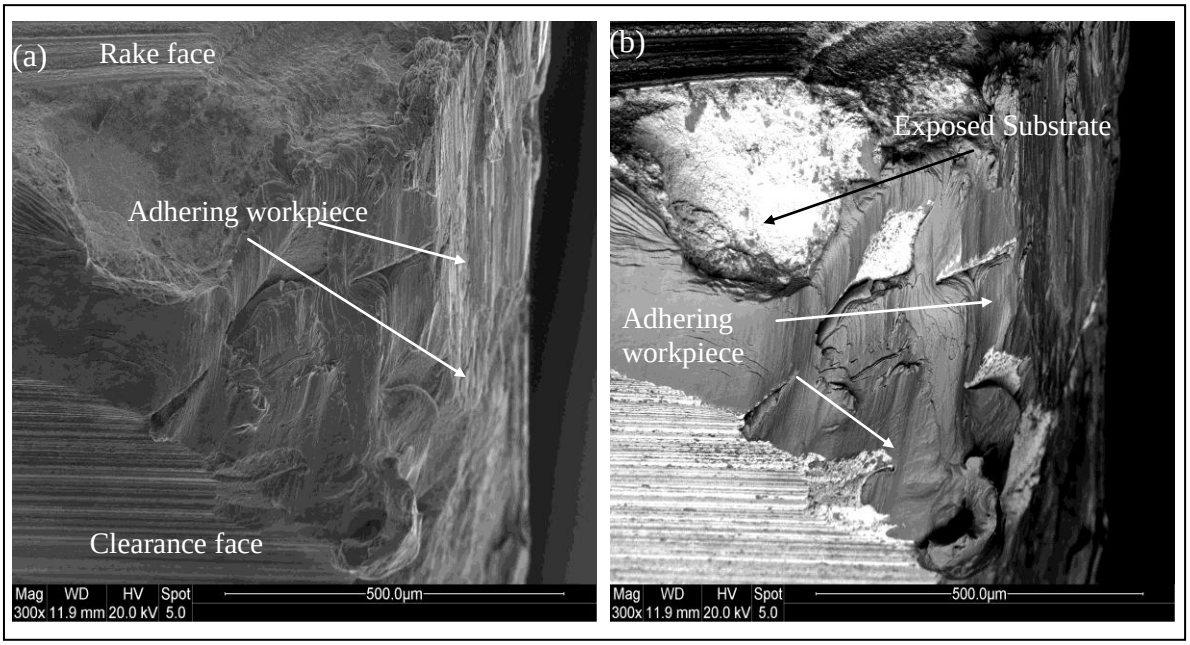

Figure 4.58. Magnified view of (a) the corner for the carbide tooth used at a cutting speed of 80 m/min and at a feed of 15 µm and (b) BSE image of the same area showing adhering workpiece material

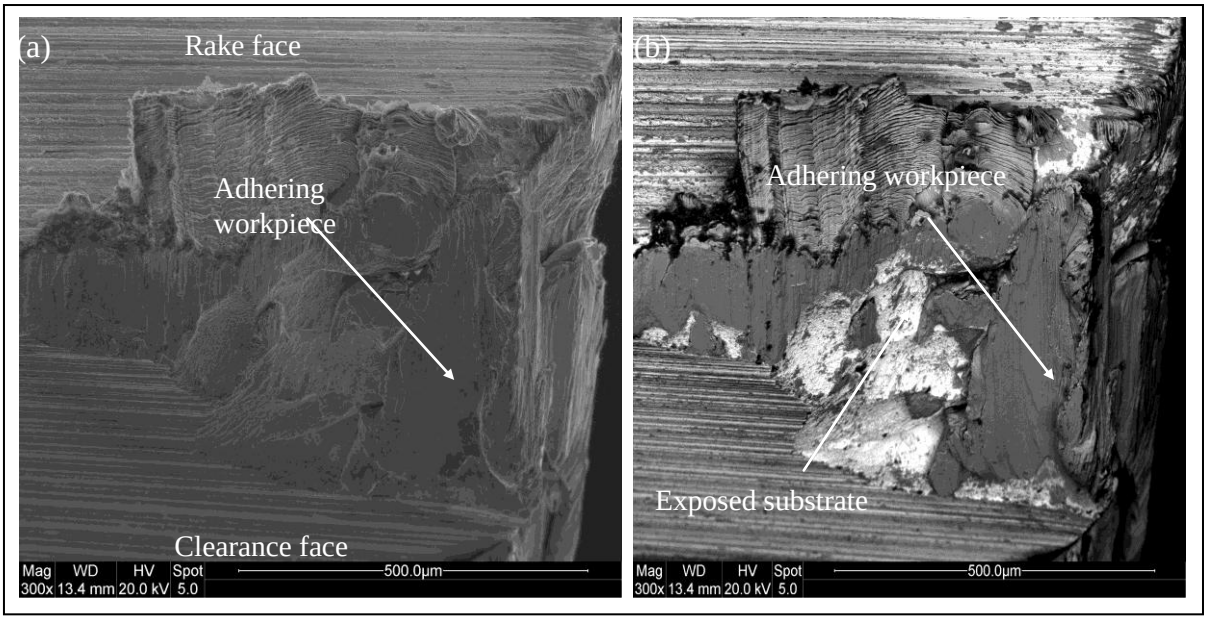

Figure 4.59. Magnified view of (a) the carbide tooth used at 60 m/min and feed of 20 µm and (b) BSE image.

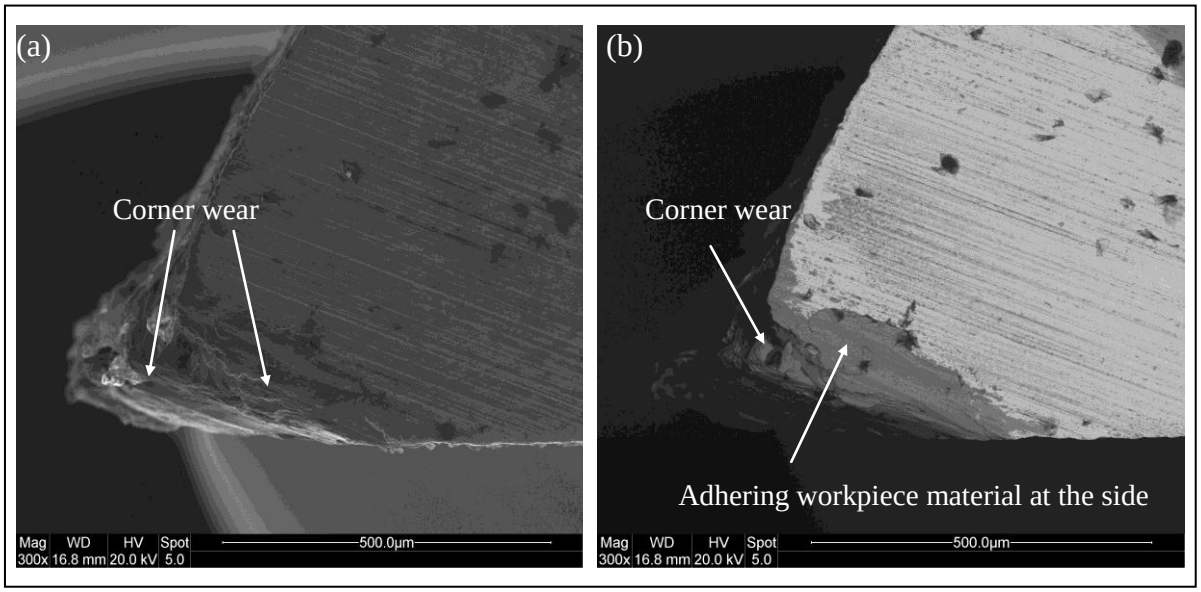

Figure 4.60. Side view of (a) the carbide tooth after being used at 60 m/min and 10 µm feed and (b) BSE image of the same area showing the adhering material.

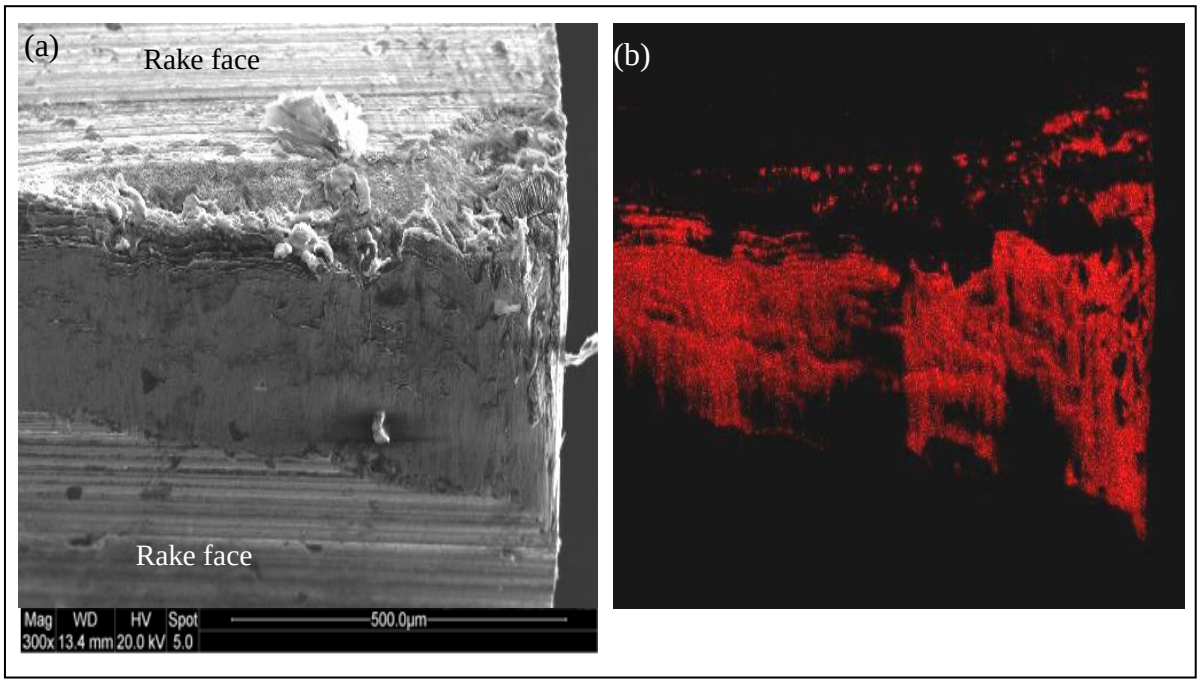

Figure 4.61. SEM image (a) of the adhering workpiece material on the cutting edge and (b) the corresponding X-ray mapping of titanium element (cutting speed: 60 m/min, width of cut: 1 mm, feed: 10 µm).

It was considered important to carry out X-ray mapping of the carbide tooth that was used at a low cutting speed, therefore X-ray mapping was performed on the carbide tooth that was used at a cutting speed of 40 m/min and at a feed of 10 µm. The magnified image of the carbide tooth corner and its corresponding X-ray mapping of titanium is shown in Figure 4.62.

X-ray mapping of the worn carbide bandsaw tooth further confirmed the presence of the adhering material on the worn bandsaw teeth, predominantly at the flank face.

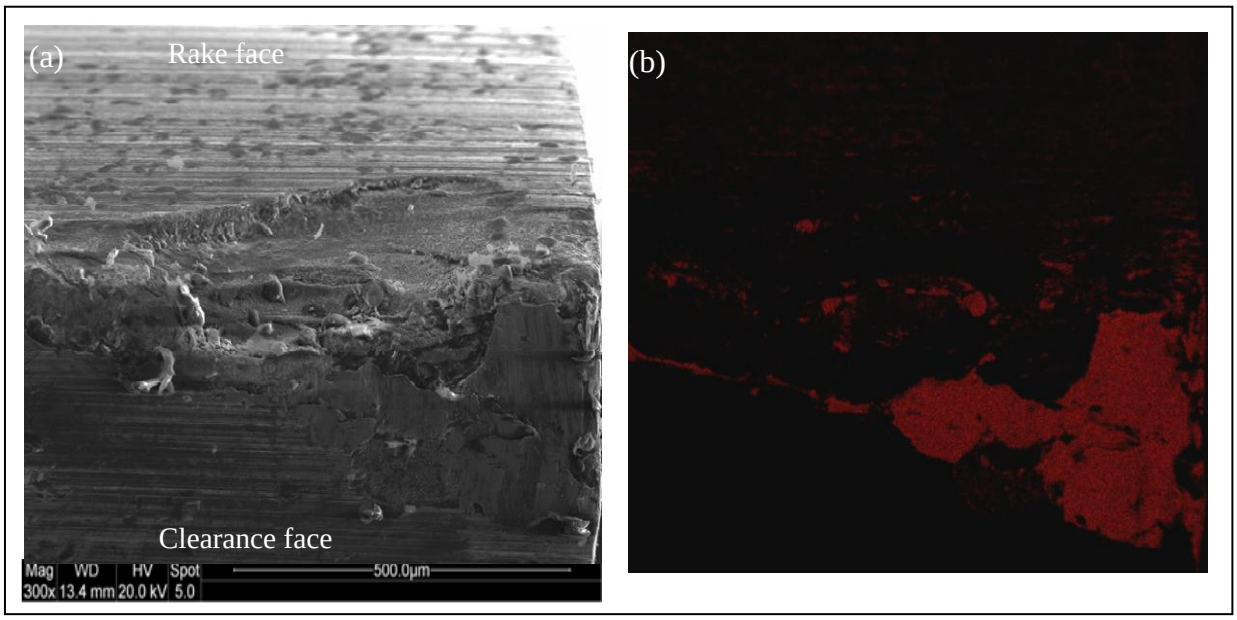

Figure 4.62. SEM image of (a) the adhering workpiece material on the cutting edge and (b) the corresponding X-ray mapping of titanium element (cutting speed: 40 m/min, width of cut: 1 mm, feed: 10 µm)

Further analysis of the adhering material required its elemental composition. Therefore, EDX analyses were carried out at various places on the adhered material and its detailed analyses gave interesting results. The adhering material was found to have the same chemical composition as that of the Ti-17 workpiece material. The SEM image of the analysed area and the corresponding EDX spectrum are displayed in Figure 4.63.

The EDX analyses were carried out on 10 different points that were chosen on the adhering workpiece material, on three different worn teeth and the average values are presented in Table 4.9.

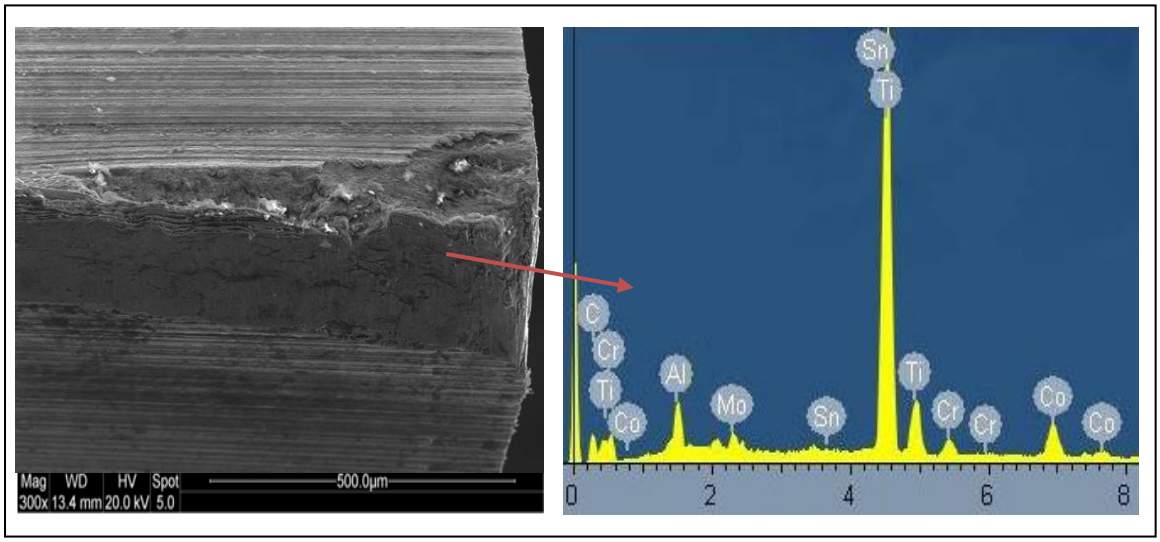

Figure 4.63. SEM image (a) of the adhering Ti-17 workpiece material on the cutting edge and (b) the corresponding EDX spectrum (cutting speed: 60 m/min, width of cut: 1 mm, feed: 10 µm).

Table 4.9. Elemental composition of the adhering T-17 workpiece material

Element	C	Mo	Al	Co	Cr	Sn	Ti
Wt %	6.98	3.3	2.5	2.72	4.13	1.22	Bal

The presence of carbon and cobalt in the adhered material indicates that the diffusion of carbon and cobalt from the carbide tool into the adhering workpiece material has taken place at the tool/chip interface, therefore confirming diffusive wear. Further evidence of diffusion of the elements from the tool into the adhering workpiece material is provided by the line scan analyses done on the adhered material. The technique gives the distribution of the elements on a line sketched on the surface of the image. The line scan images for the elements carbon and cobalt are provided in Figure 4.64.

It has been reported in the literature that under moderate cutting conditions the temperature at the tool edge could exceed 800ºC when machining titanium alloy with carbide tools [66]. This temperature is high enough to cause diffusion between the tool and the workpiece material. In the event of diffusion, lighter elements from the carbide tooth (C and Co) diffuse into the workpiece material and results in a weakened tooth which is susceptible to enhanced wear. At higher cutting speeds, the temperature at the tooth edge

increases causing the diffusion and tool weakening at a higher rate and hence an accelerated wear in the tooth.

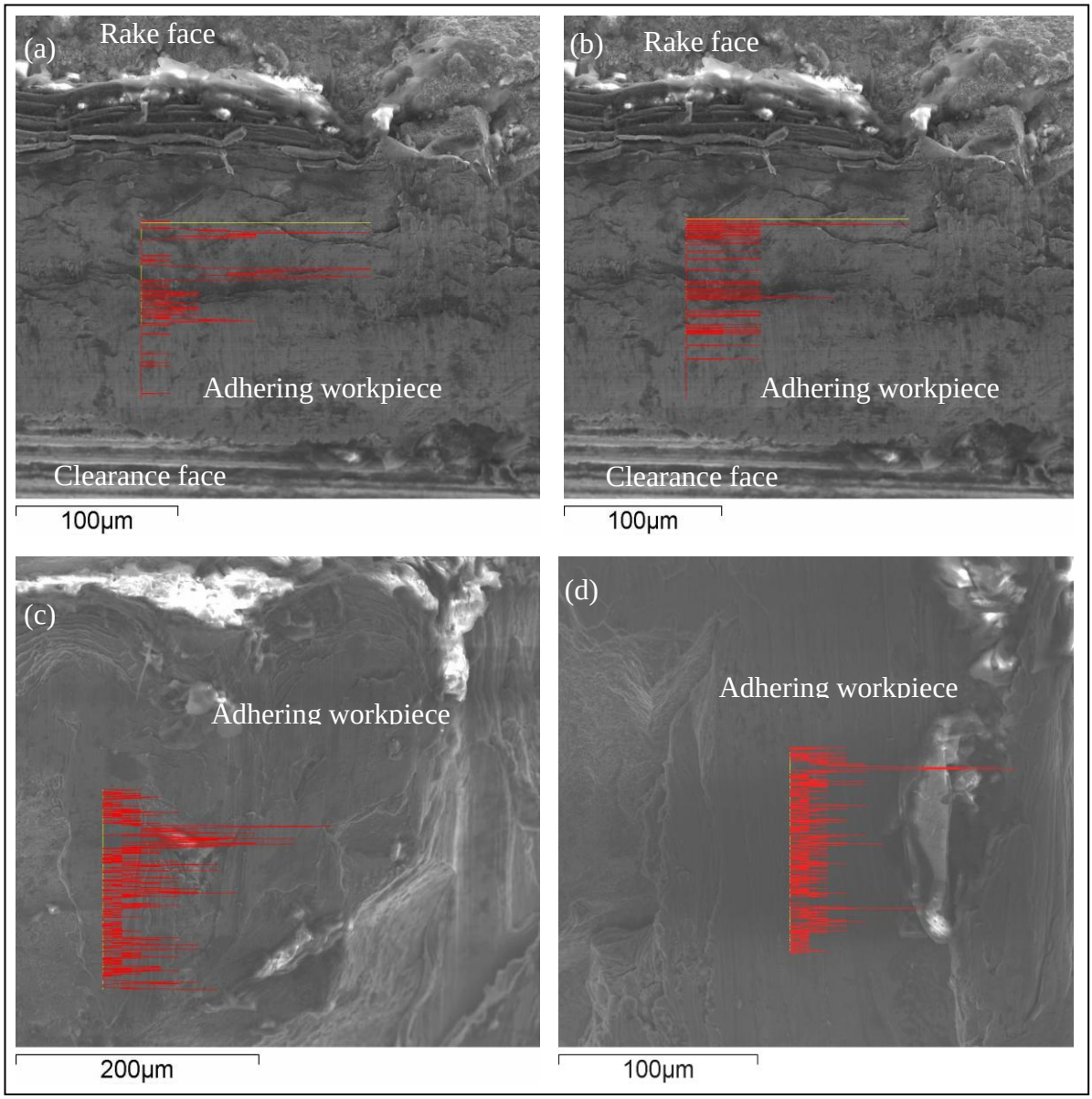

Figure 4.64. SEM linescan images for (a) carbon for the carbide tooth used at 60 m/min, (b) cobalt for the carbide tooth used at 60 m/min, (c) carbon for 80 m/min and (d) cobalt for 80 m/min (feed: 10 µm, width of cut: 1 mm).

As previously stated, the high temperature and stress generated during machining caused the welding of the workpiece material to the cutting edge. The adhering workpiece maintains a close contact with the workpiece while the machining operation is taking place. When the adhered workpiece layer attained a critical size, it will detach from the

cutting edge and will be removed with the flowing chip. This process leads to "plucking" of the hard particles from the tool, therefore causing a gradual increase in the flank wear. There was also evidence of attrition wear, which removed the tool material in the form of particles or grains due to the sliding interaction between the tool and the workpiece material as shown in Figure 4.65.

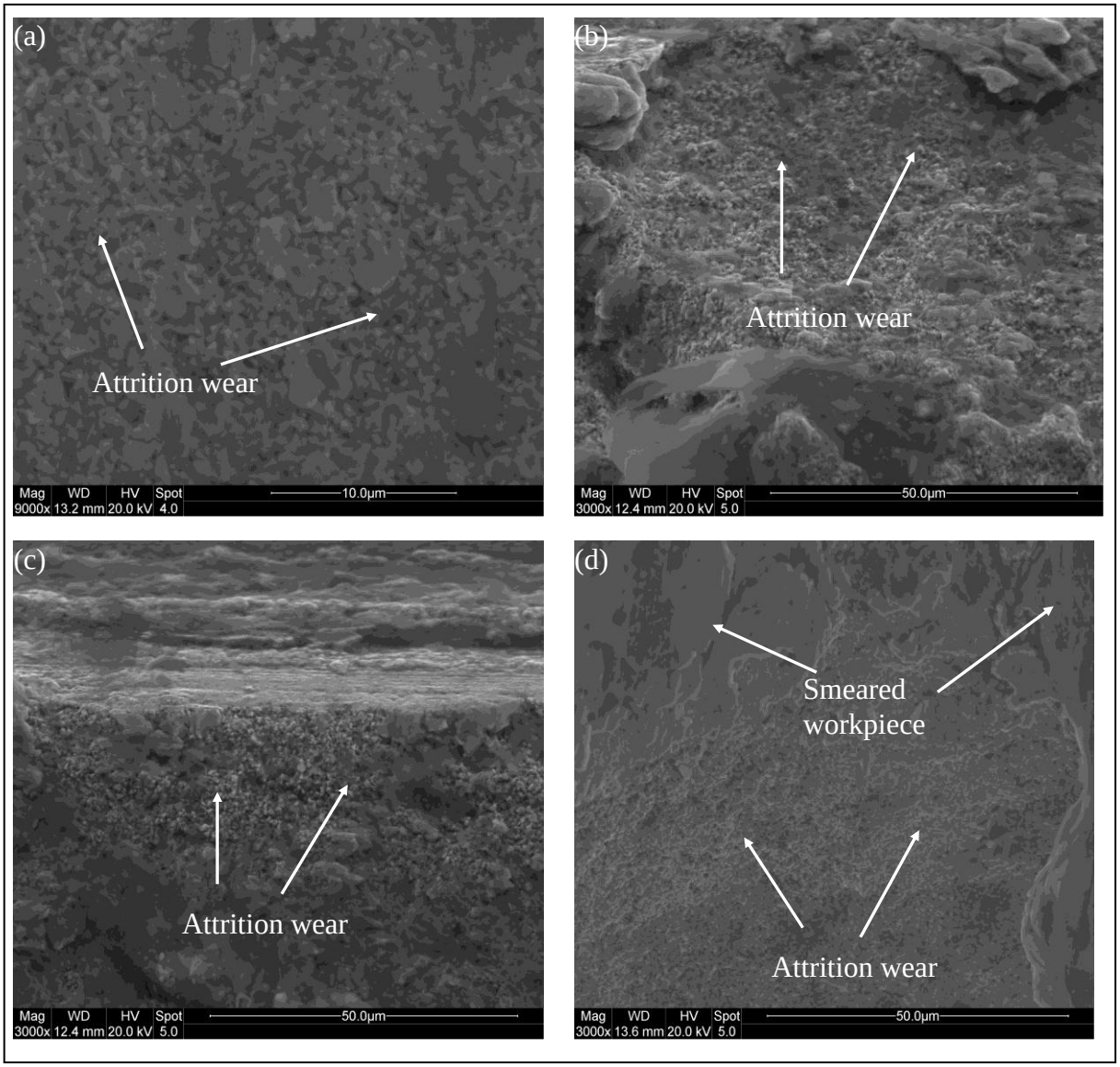

Figure 4.65. SEM micrographs of the worn edges highlighting attrition wear mechanism, (a) cutting speed: 60 m/min, width of cut: 1 mm, feed: 10 µm, (b) cutting speed: 60 m/min, width of cut: 1 mm, feed: 15 µm, (c) cutting speed: 40 m/min, width of cut: 1 mm, feed: 20 µm (d) cutting speed: 40 m/min, width of cut: 1 mm, feed: 10 µm.

4.4.1 Summary of the cutting tests for un-coated teeth

Flank wear, deformation at the corner and chipping at both the rake and flank faces were identified as the wear modes which controlled the life of carbide bandsaw tooth. More degradation of the flank face was observed in terms of wear compared to the rake face. Shorter tool life was observed for the un-coated carbide tool at high cutting speeds and feeds due to rapid tool wear, which eventually led to the severe chipping and flaking at the cutting edge of the bandsaw teeth. Uneven wear on the tool faces could be observed which suggested that the diffusion and attrition wear took place at the cutting edge. The carbide teeth may have plastically deformed, especially the ones used at higher feeds and speed and this may have contributed partly to the tool failure. Cyclic mechanical and thermal loading on the bandsaw tooth due to the periodic engagement and disengagement of the tooth with the workpiece during machining are probable reasons. All the worn carbide bandsaw teeth showed workpiece material (*i.e.* Ti-17 alloy) adhering to the cutting edge, especially at the flank. This is owing to the temperatures generated at the tool/workpiece interface, due to the low thermal conductivity of titanium alloy as well as to the general tendency of titanium alloys to "stick" to the cutting edge of the carbide teeth. Moreover, it has been suggested by Trent that increase in speeds and feeds leads to a rise in temperature at the tool flank [18]. However, it may partly be due to the high strength of titanium alloys, which is maintained at elevated temperatures. There is a possibility that this adhered material could/would have led to initiation of chipping and finally to breakage of the carbide teeth since this adhered material will be hit and be squashed by the tool on its re-entry into the workpiece material. In almost all cases, the adhering material was found on the flank face rather than on the rake face, which suggested that the adhered material on the rake face had been removed at the underside of the flowing chip, which led to chipping of the carbide tooth.

Another important factor is the interrupted nature of bandsawing operation, which imposed cyclic impacts and stresses on the carbide teeth. The periodic engagement and disengagement of the carbide teeth during the test led to fluctuating temperatures at the tool/workpiece interface, which may lead to the modification of the stress distribution in the cutting region of the carbide tooth.

The comparison of initial cutting forces experienced by the carbide teeth at different feeds, but at a constant cutting speed of 80 m/min is shown in Figure4.66. It can be observed that the cutting force is very high for the feed of 20 µm, whereas it is reduced at lower feeds.

For the high feed of 20 µm, it appears that the tooth degraded in terms of its physical geometry soon after machining started.

A comparison of the cutting forces at different feeds, but at a constant surface cutting speed of 60 m/min is provided in Figure 4.67. It is apparent that the trend is very similar to the trend observed at the cutting speed of 80 m/min; however the magnitude of the cutting force is reduced. The highest cutting force observed is for the feed of 20 µm and probably the tooth chipped as soon as machining started.

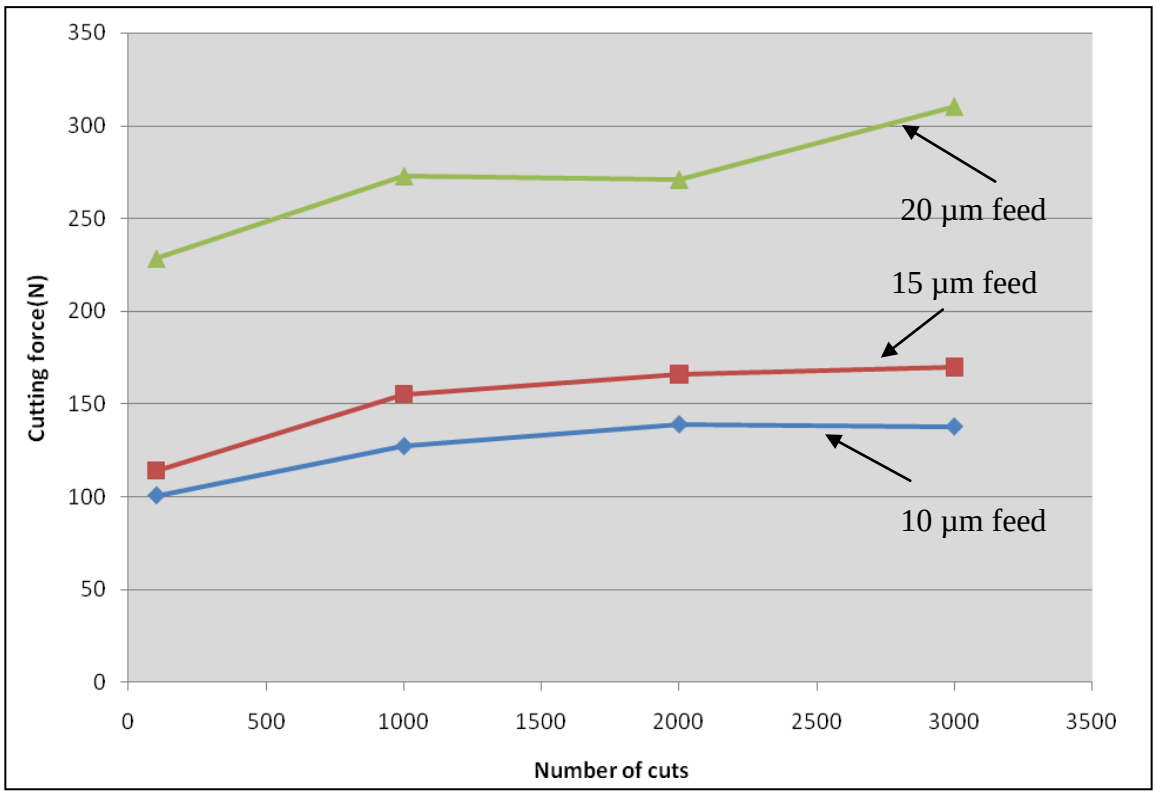

Figure 4.66. Comparison of cutting forces at different feeds (cutting speed: 80 m/min, width of cut: 1 mm, length of one cut: 0.6 m).

The forces for the feeds at 15 and 10 µm, display a sudden increase during the initial period, suggesting initial stages of wear. However, the cutting forces become constant after some time with a general increasing trend.

The comparison of cutting forces of the different feeds, but at a constant cutting speed of 40 m/min is shown in Figure 4.68. It appears from Figure 4.68 that with the increase in feed, the cutting forces increase, whereas at the feed of 25 µm, the cutting force remains constant until the tooth has performed 4,000 cuts. The forces for the higher feed show a generally increasing trend, except for the 25 µm feed, where the increase in force is very

rapid, suggesting a swift change in the geometry of the carbide tooth compared to the teeth used at low feeds.

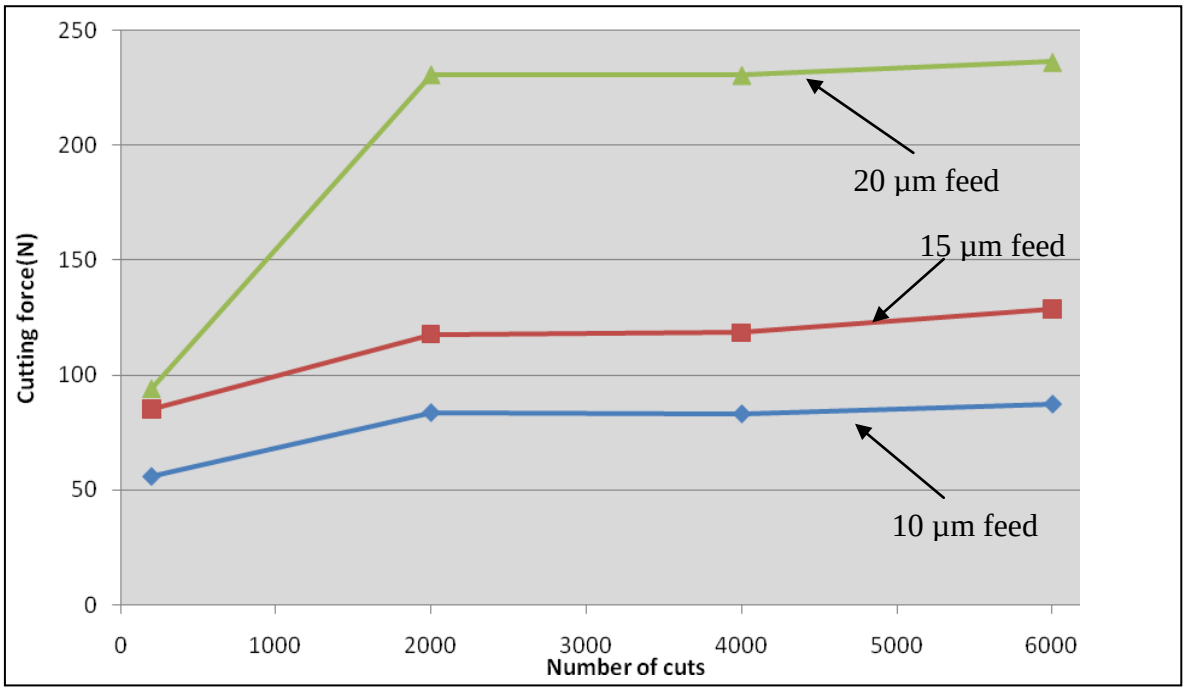

Figure 4.67. Comparison of cutting forces at different feeds (cutting speed: 60 m/min, width of cut: 1 mm, length of one cut: 0.6 m).

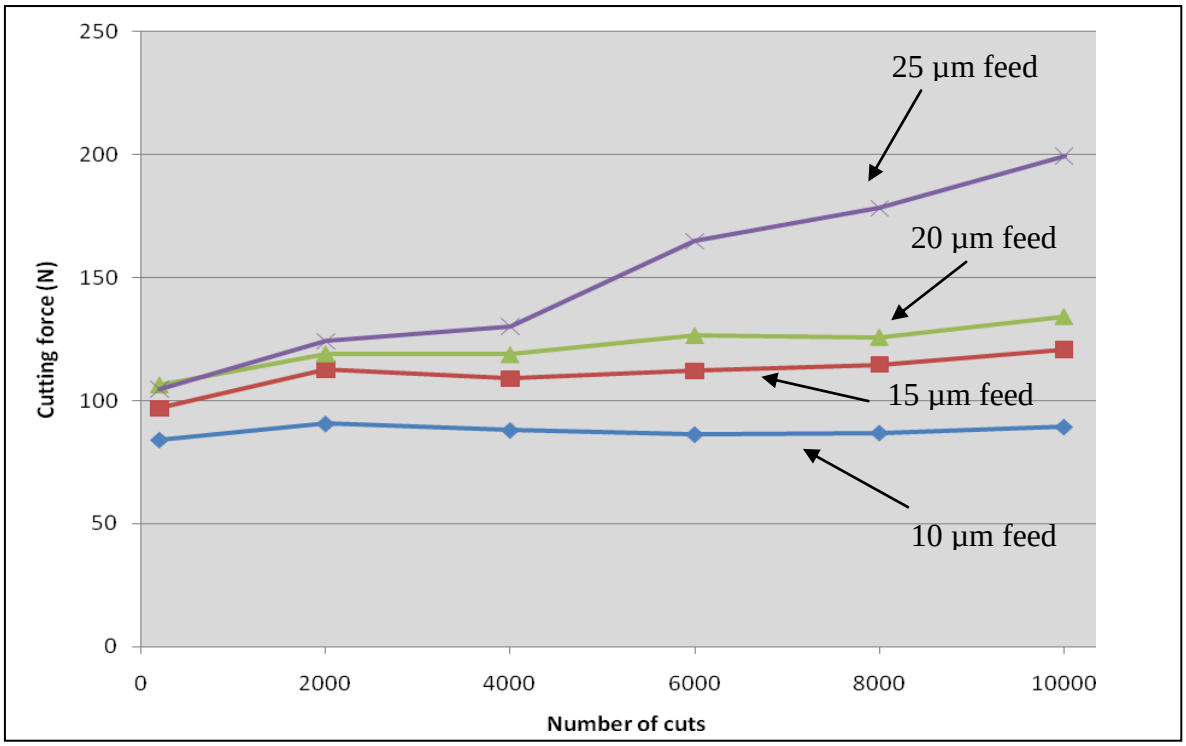

Figure 4.68. Comparison of cutting forces at different feeds (cutting speed: 40 m/min, width of cut: 1mm, length of one cut: 0.6 m).

The trend in forces shown in Fig. 4.66, Fig. 4.67 and Fig. 4.68, is almost similar at the three different speeds, with the exception of the tooth used at 80 m/min and 20 microns. This may be due to the extreme chipping which took place as soon as the carbide tooth came into contact with the workpeice (combination of high temperatures/force). The other possibility, however, can also be measurement/experimental error. The variation in Esp with the feed for the un-coated carbide tooth is displayed in Figure 4.69. It appears from Figure 4.69 that the bandsawing operation becomes more efficient if at higher feeds *i.e.* it requires less energy at higher feeds compared to the low feeds.

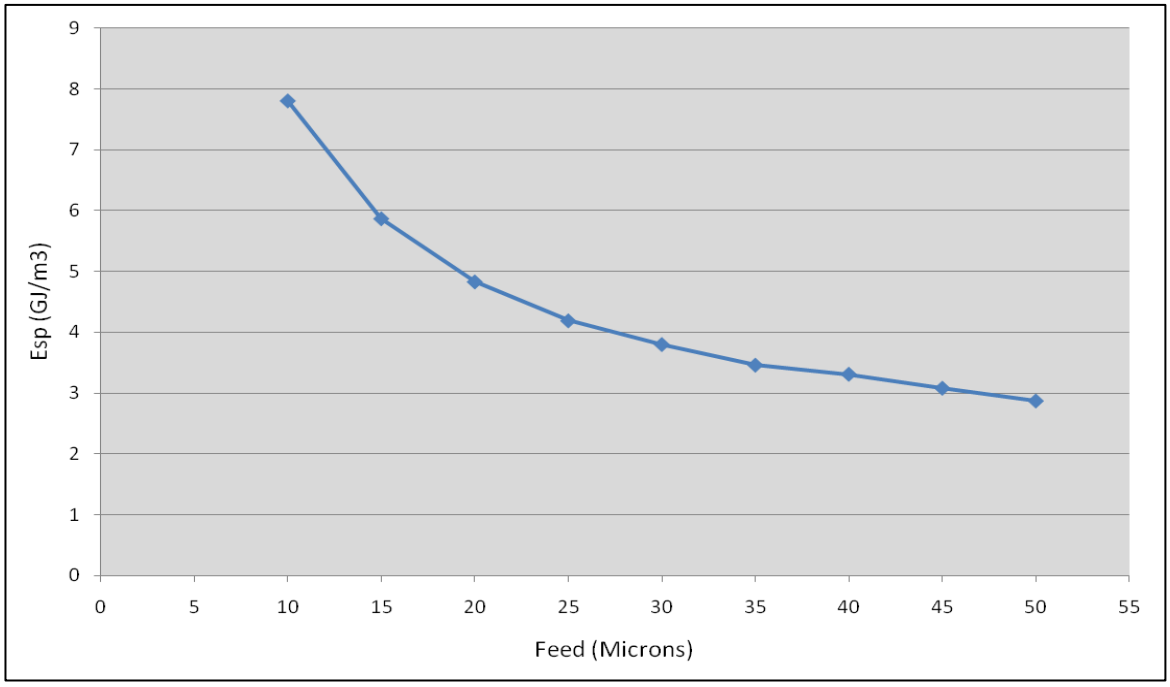

Figure 4.69. Variation in Esp with the depth of cut (width of cut: 1 mm, cutting speed: 30 m/min, feed: variable).

The dominant wear mechanisms in carbide bandsaw teeth are adhesion and attrition at the cutting edge. Diffusion wear mechanism was also identified by the presence of carbon and cobalt elements in the adhered workpiece on the cutting edge when analysed by EDX. The ensuing high temperature and the low thermal conductivity of Ti-17 alloy make the chip/tool interface a very conducive environment for diffusion to take place. During the machining process, the atoms inside the carbide tooth, such as carbon and cobalt, diffused towards the workpiece, under the action of thermal gradient. However, it is reasonable to assume that the diffusion layer is very thin and very close to the tool/workpiece interface. The relative motion between the carbide tooth and workpiece and high relative stresses

would further increase the temperature at this interface, thus making the environment even more conducive for enhanced diffusion.

The EDX method has certain associated limitations, *e.g.* it is generally suitable for detecting elements of higher atomic numbers and can be troublesome in detecting elements of low atomic numbers. However, some published papers actually use this technique in order to confirm the diffusion mechanism in machining titanium alloys [186, 187]. Furthermore, the electron beam used in EDX can actually penetrate deep into the specimen and thus analyse the material beneath the adhering material. If this were the case, tungsten would be present in the spectra obtained, which was not the case. Therefore it can be assumed that the electron beam has not penetrated deep into the underlying tool material and is analyzing only the adhering workpiece.

The mechanical properties of tungsten carbide depend critically on its final composition and structure. As mentioned previously, tungsten carbide is the main metallic hard material; whereas the role of cobalt is to provide a ductile bonding matrix for the tungsten carbide particles. The diffusion of carbon and cobalt out of the tool would lead to decrease in hardness and wear resistance of the tool material. The diffusion of cobalt from the tool resulted in weakening the strength of tungsten carbide and the brittle particles of tungsten carbide probably fractured as soon as exposed and eventually pulled out or "plucked" by the flowing chip. It may be stated with a high degree of confidence that this removal of tungsten carbide particles due to cobalt diffusion is very detrimental to the hardness and wear resistance of carbide bandsaw teeth. As the cutting test proceeded, more atoms diffused out from the tool and hence more tungsten carbide particles were plucked and taken away by the flowing chips.

Thermal cracks were observed at the cutting edge when machining Ti-17 alloy at high speeds as shown in the Figure 4.70. It appears that these cracks initiated some distance behind the cutting edge along the rake face. The plucking of carbide particles by attrition mechanism became much easier owing to the diffusion of cobalt atoms into the adhering workpiece. The formation of thermal cracks is very typical in machining of titanium alloys, especially in operations such as milling, due to fluctuating temperatures at the tool/chip interface. The cyclic heating and cooling at the cutting edge, along with the poor thermal conductivity resulted in the generation of thermal cracks.

As stated previously, the carbide teeth may have plastically deformed during the machining operation. This deformation may also have partly contributed to the formation of cracks at the cutting edge.

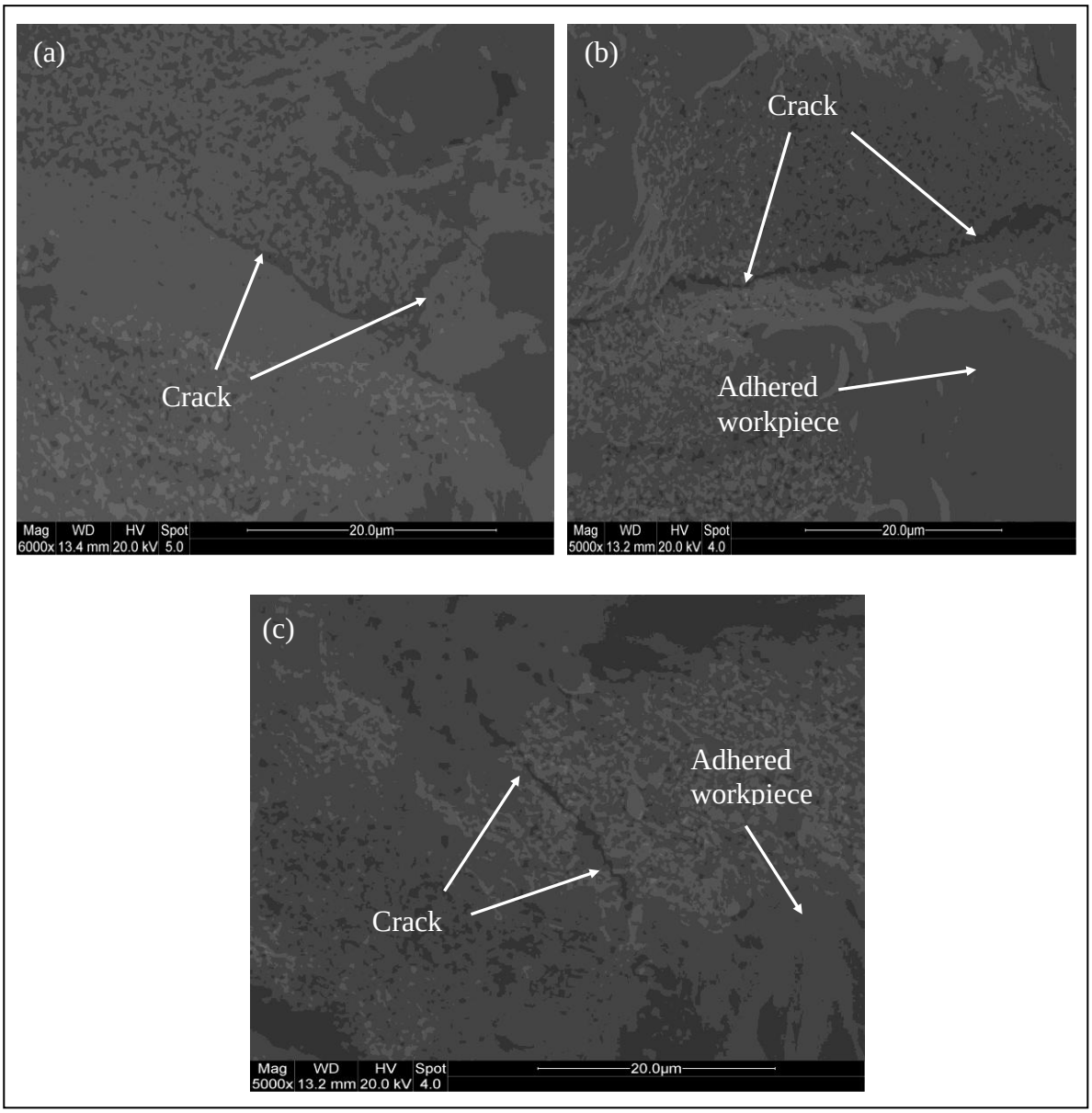

Figure 4.70. Cracks on the cutting edge of the un-coated worn carbide teeth, (a) cutting speed: 60 m/min, width of cut: 1 mm, feed: 10 µm, (b) cutting speed: 60 m/min, width of cut: 1 mm, feed: 15 µm, (c) cutting speed: 40 m/min, width of cut: 1 mm, feed: 20 µm.

4.5.0 Performance of coated carbide teeth while bandsawing Ti-17 alloy

Previous sections dealt with the evaluation and performance of the un-coated, honed carbide teeth while bandsawing Ti-17 alloy. This section deals with the evaluation and performance of coated tungsten carbide bandsaw teeth. Several bandsaw teeth were coated with two different types of coatings, deposited by arc evaporation technique. These coatings were deposited by IonBond. These two different types of coatings, namely AlTiN

and TiAlSiN, were selected owing to their different properties, which is mainly due to their chemical composition and structure. TiAlSiN coating is nano-structured in terms of its structure, while AlTiN can be termed a conventional coating.

From the results of the performance of the un-coated carbide bandsaw teeth, while machining Ti-17 alloy, it was concluded that the carbide teeth performed well at low cutting speeds and low feeds. Therefore, it was decided to evaluate the performance of the coated carbide teeth at low feeds and speeds. The machining parameters (feed and speed) used to evaluate the coated bandsaw teeth are listed in Table 4.10.

Table 4.10. Machining parameters for evaluating coated bandsaw teeth

Feed (µm)	10	15	20
Cutting speed (m/min)	40	40	40

The nominal rake and clearance angles of bandsaw teeth were $10^{o}\pm0.5^{o}$ and $20^{o}\pm0.3$ respectively, with the average cutting edge radius of approximately 13 µm. Width of cut for all cutting tests was 1 mm as it was for evaluating the performance of the un-coated carbide bandsaw teeth. The width of cut used, *i.e.* 1 mm, is less than the average tooth thickness (1.59 mm). The same methodology which was used to evaluate the un-coated teeth was employed to evaluate the coated teeth, *i.e.* force measurement, specific cutting energy and observing the condition of the worn coated carbide tooth under the SEM to assess the wear and degradation modes.

4.5.1 Performance of TiAlSiN coated carbide teeth

An SEM micrograph of the un-used TiAlSiN coated carbide tooth is provided in Figure 4.71. The coating appears to be smooth and continuous over the carbide tooth and the honed edge can be easily observed.

Before starting the complete tests, it was considered important to measure the cutting forces using a new TiAlSiN coated carbide tooth while machining within the bandsawing range *i.e.* 10 to 50 µm. Figure 4.72 displays the variation of cutting force for a TiAlSiN coated tooth with the increase in feed. It appears that the cutting force increases linearly with the increase in feed.

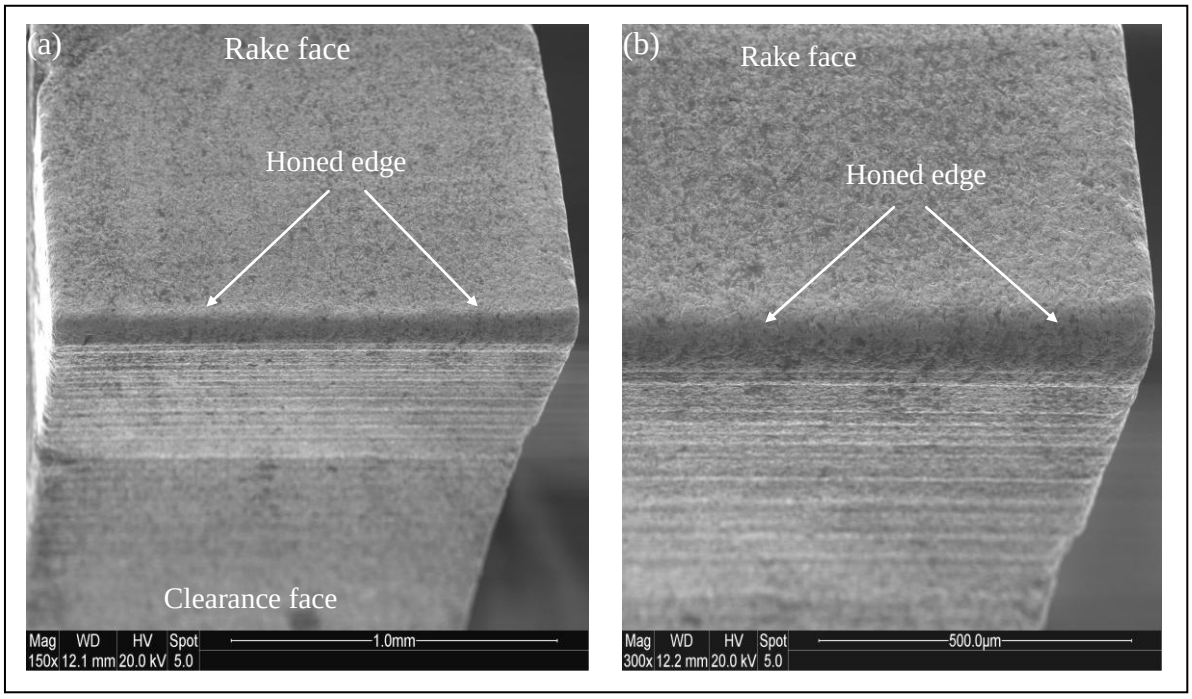

Figure 4.71. New TiAlSiN coated carbide tooth showing (a) both faces of the cutting edge and (b) magnified view of the corner of the tooth.

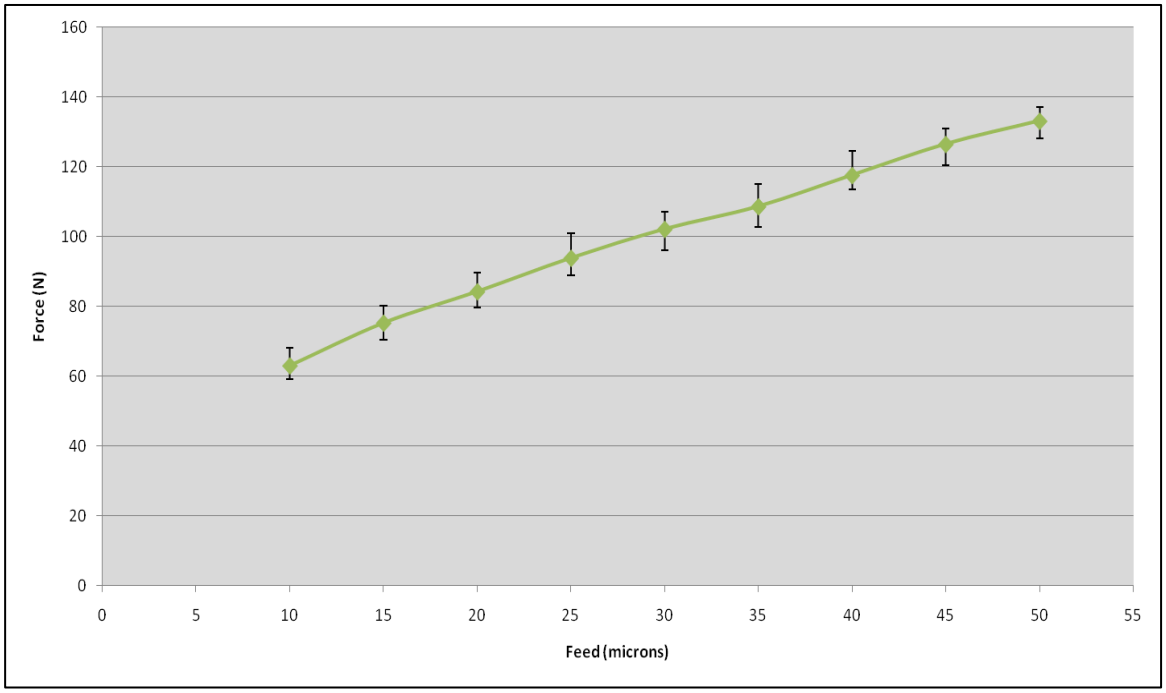

Figure 4.72. Variation in cutting force with increase in feed for the new TiAlSiN coated tooth (cutting speed: 30 min, feed: variable, width of cut: 1 mm).

The variation of all the forces against the number of cuts for the coated TiAlSiN used at 20 µm feed and at 40 m/min cutting speed is shown in Figure 4.73. It appears from Figure 4.73 that the tooth geometry was modified after performing 1000 cuts and then uniform wear took place on the cutting edge. However, the corner of the tooth started to degrade after performing 8000 cuts and the severity of the corner wear increased and therefore the side force crossed the cutting force after performing 13000 cuts. The increase in thrust force is an indication of the degradation of the flank face of the cutting edge of the bandsaw carbide tooth. This force graph indicates the end of life of the TiAlSiN coated carbide tooth used at the cutting speed of 40 m/min and at a feed of 20 µm.

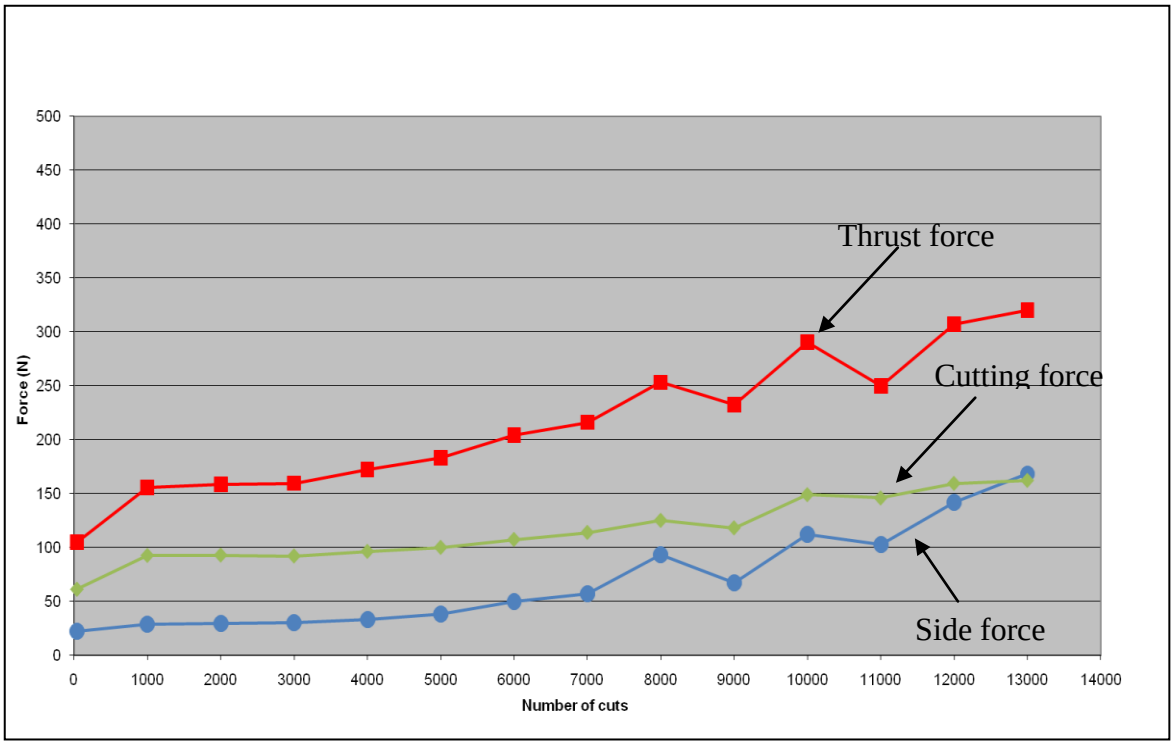

Figure 4.73. Variation of forces for TiAlSiN coated carbide tooth (cutting speed: 40 m/min, feed: 20 µm, width of cut: 1 mm, length of one cut: 0.6 m).

The variation in Esp for the TiAlSiN coated carbide bandsaw tooth used at a cutting speed of 40 m/min and at the feed of 20 µm is depicted in Figure 4.74. The value of Esp starts at 3 GJ/m^3 and quickly reaches 4.75 GJ/m^3, indicating that the geometry of the tooth has changed during this initial cutting process. However, the value of Esp continues to rise towards the end of the cutting session suggesting that the tooth is wearing and the maximum value attained is 8 GJ/m^3 towards the end of the test.

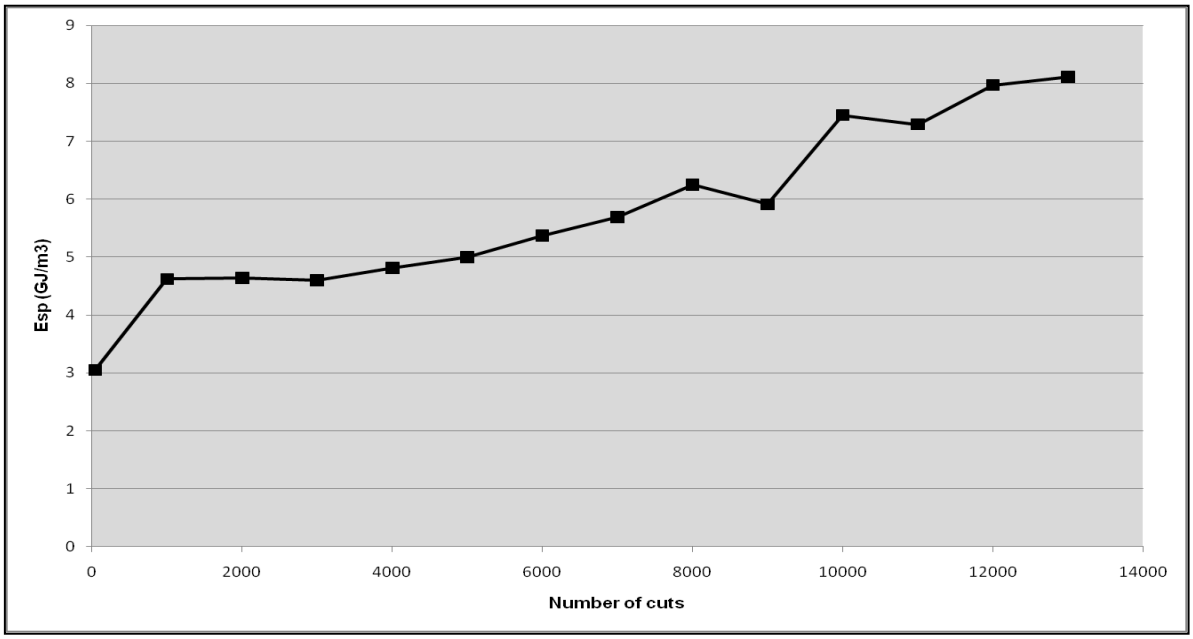

Figure 4.74. Variation in Esp for TiAlSiN coated carbide tooth (cutting speed: 40 m/min, feed: 20 µm, width of cut: 1 mm, length of one cut: 0.6 m).

The condition of the TiAlSiN coated carbide tooth at the end of its life is shown in Figure 4.75. It clearly reveals chipping at both the faces of the cutting edge. This chipping of the cutting edge can be clearly observed in Figure 4.75 (b), which provides the magnified image of the corner of the carbide tooth. The side view of the worn TiAlSiN coated carbide tooth is shown in Figure 4.75 (c). This image displays the chipping of the cutting edge from a different angle and clearly shows the chipping of both the rake and flank faces. The same images were taken in Back Scattered Electron mode using the SEM and are shown in Figure 4.76. It is clear from Figures 4.75 and 4.76 that workpiece material is adhering to the worn flank face as well as at the side of the carbide tooth. Substrate material (*i.e.* tungsten carbide) can be observed at the portion of the cutting edge which has not chipped and is at a distance from the corner of the carbide tooth.

The adhering material was analysed at ten different points, using EDS (energy dispersive spectroscopy) and it was found to have the same elemental composition as that of the Ti-17 alloy and also showed the presence of carbon and cobalt, suggesting that diffusion took place between the tooth and adhering workpiece. The initial and the final chips formed while machining Ti-17 alloy using TiAlSiN coated carbide tooth are displayed in Figure 4.77. It appears from Figure 4.77 that the chips formed during the initial machining are circular and smoother compared to the chips that are formed during the final stages of machining, which seem to be straight and appear to have a rough surface.

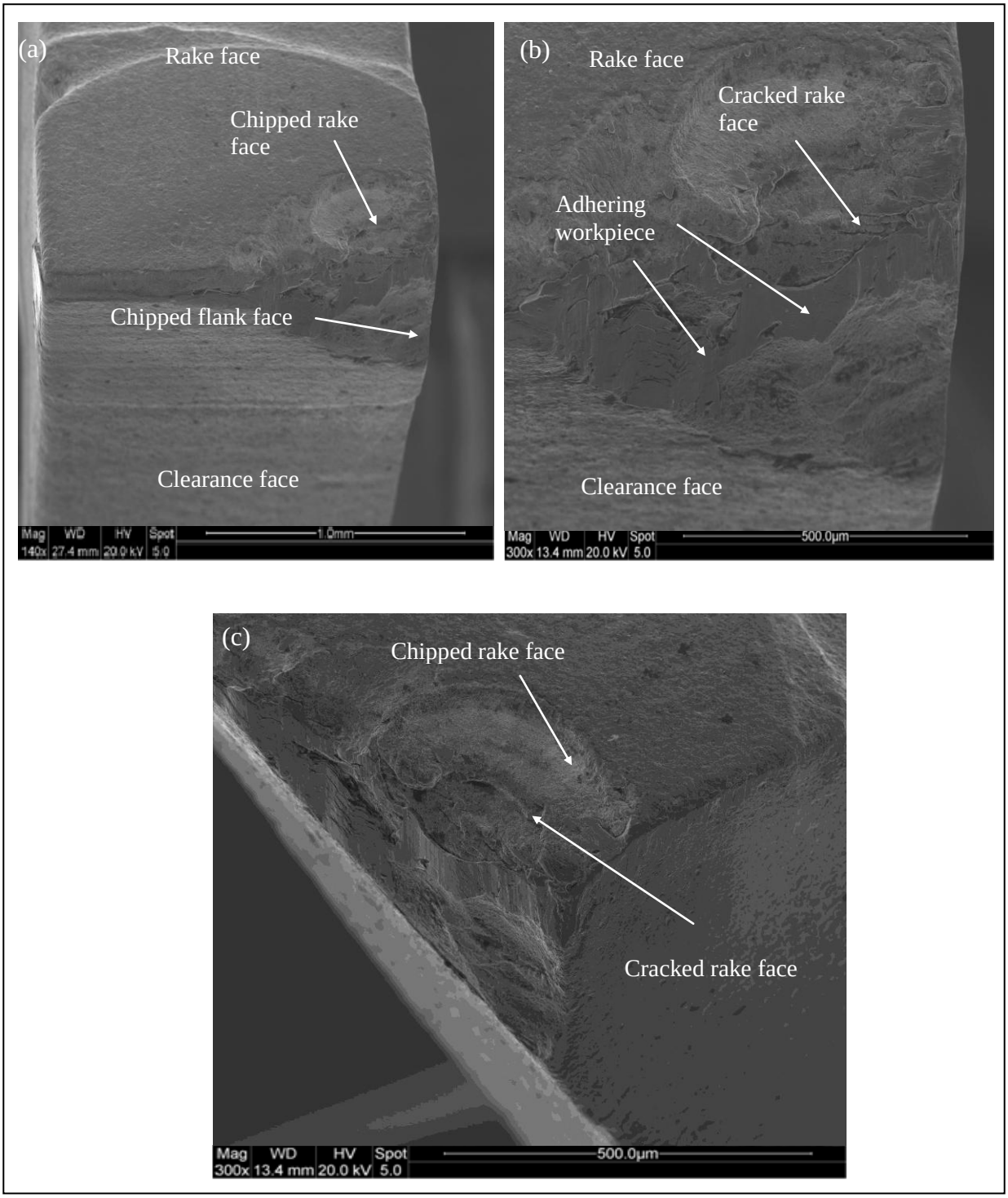

Figure 4.75. Condition of the TiAlSiN coated carbide tooth at (a) the end of its life, (b) magnified view of the corner of the tooth and (c) side view of the coated tooth (cutting speed: 40 m/min, feed: 20 µm, width of cut: 1 mm).

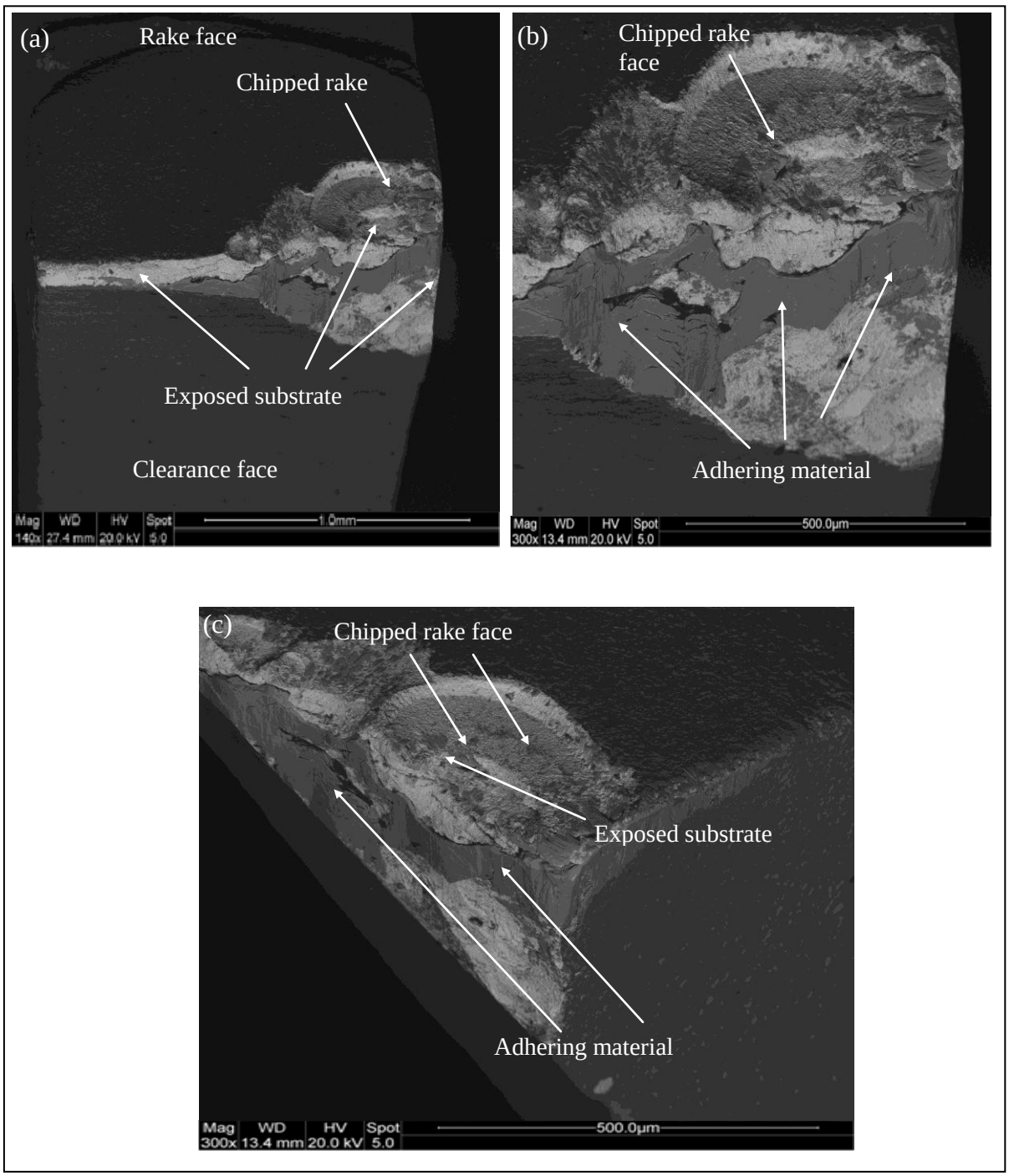

Figure 4.76. SEM micrographs taken in BSE mode showing (a) the condition of the TiAlSiN coated carbide tooth at the end of its life, (b) magnified view of the corner of the tooth and (c) side view of the coated tooth (cutting speed: 40 m/min, feed: 20 µm, width of cut: 1 mm).

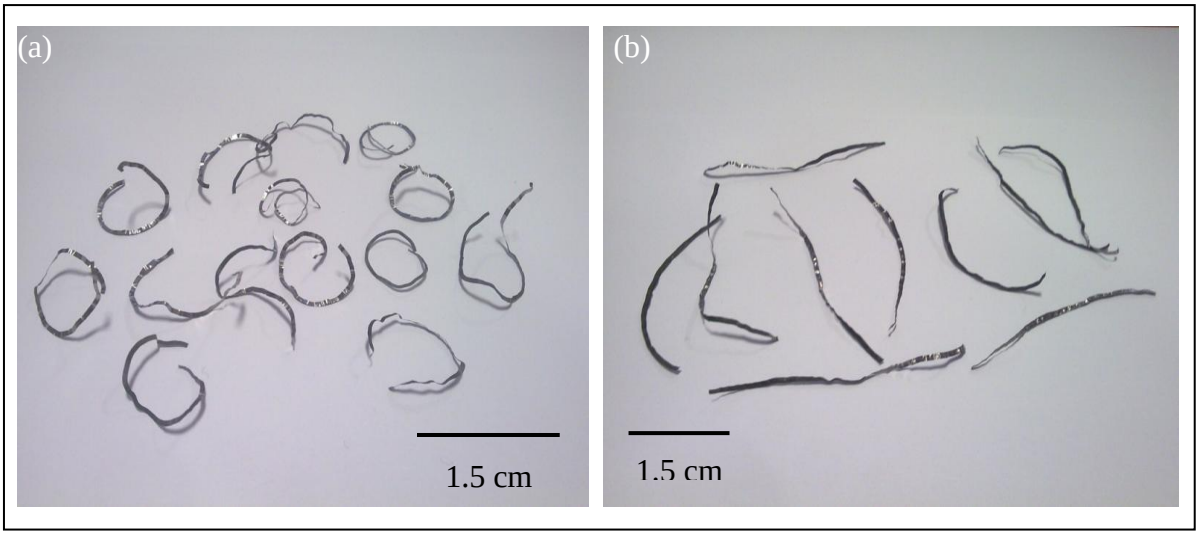

Figure 4.77. Characteristics of (a) initial and (b) final chips formed using TiAlSiN coated carbide tooth (cutting speed: 40 m/min, feed: 20 µm, width of cut: 1 mm, length of one cut: 0.6 m)

Reducing the feed to 15 µm and keeping the cutting speed at 40 m/min led the tooth to last longer than it did at a feed of 20 µm. The variation of forces along with the number of cuts is shown in Figure 4.78. From Figure 4.78, it appears that the coated carbide tooth is wearing uniformly until it performs 9000 cuts. After this point, the corner starts to wear at a faster rate compared to the rest of the cutting edge which is engaged in the machining operation. The corner wear increases with more machining and there is a sudden increase in the side force after the tooth has performed 19000 cuts – it chips, leading to the side force becoming higher than the cutting force, indicating that this is the end of the life for the TiAlSiN coated carbide tooth. The variation of Esp for the carbide tooth that is used at a cutting speed of 40 m/min and the feed of 15 µm is given in Figure 4.79. From Figure 4.79 it appears that the Esp follows the same trend as that of the cutting force shown in Figure 4.78. The Esp starts at 5.5 GJ/m^3 and slowly increases to 7.5 GJ/m^3 indicating a uniform wear taking place on the cutting edge. The maximum value of Esp from Figure4.79 is found to be 10 GJ/m^3 approximately, which is indicating that the tooth is not cutting effectively, since a high value of Esp is indication of the inefficiency of the cutting process. The condition of the TiAlSiN coated carbide tooth at the end of its life is revealed in Figure 4.80. Figure 4.80 (b), which is the magnified image of the corner of the tooth, shows chipping of the both the faces of the cutting edge and therefore the change in the physical geometry of the coated carbide tooth.

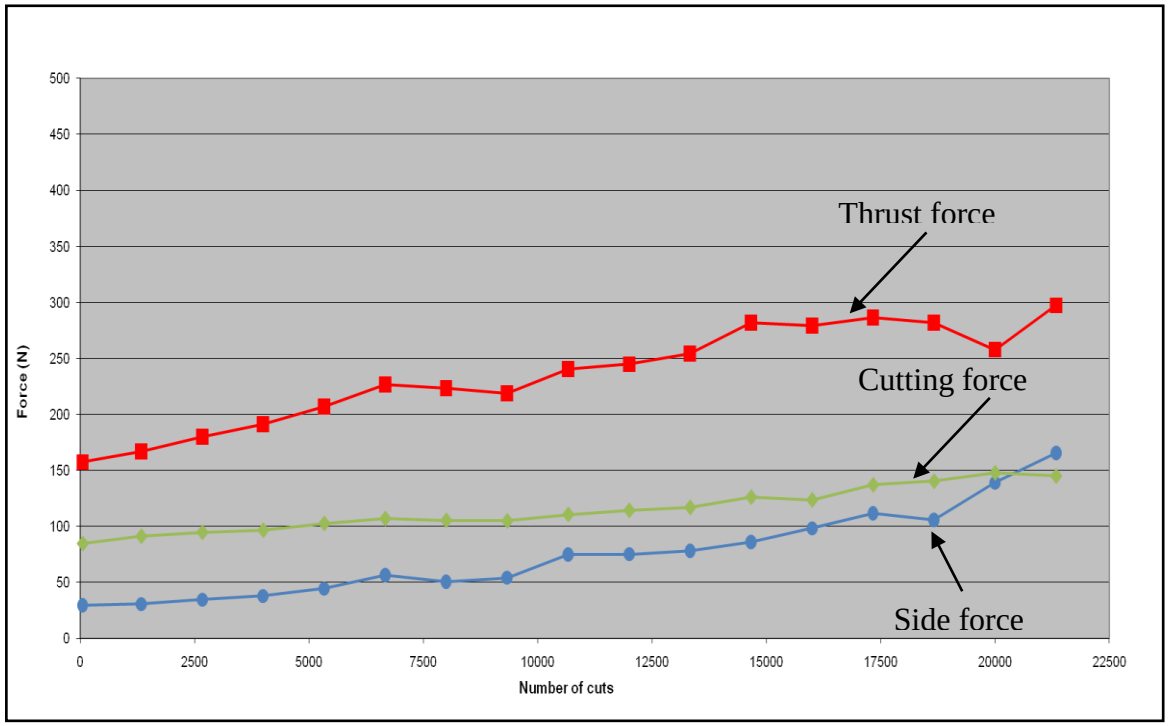

Figure 4.78. Variation of forces for TiAlSiN coated bandsaw tooth (feed: 15 µm, cutting speed: 40 m/min, width of cut: 1 mm, length of one cut: 0.6 m).

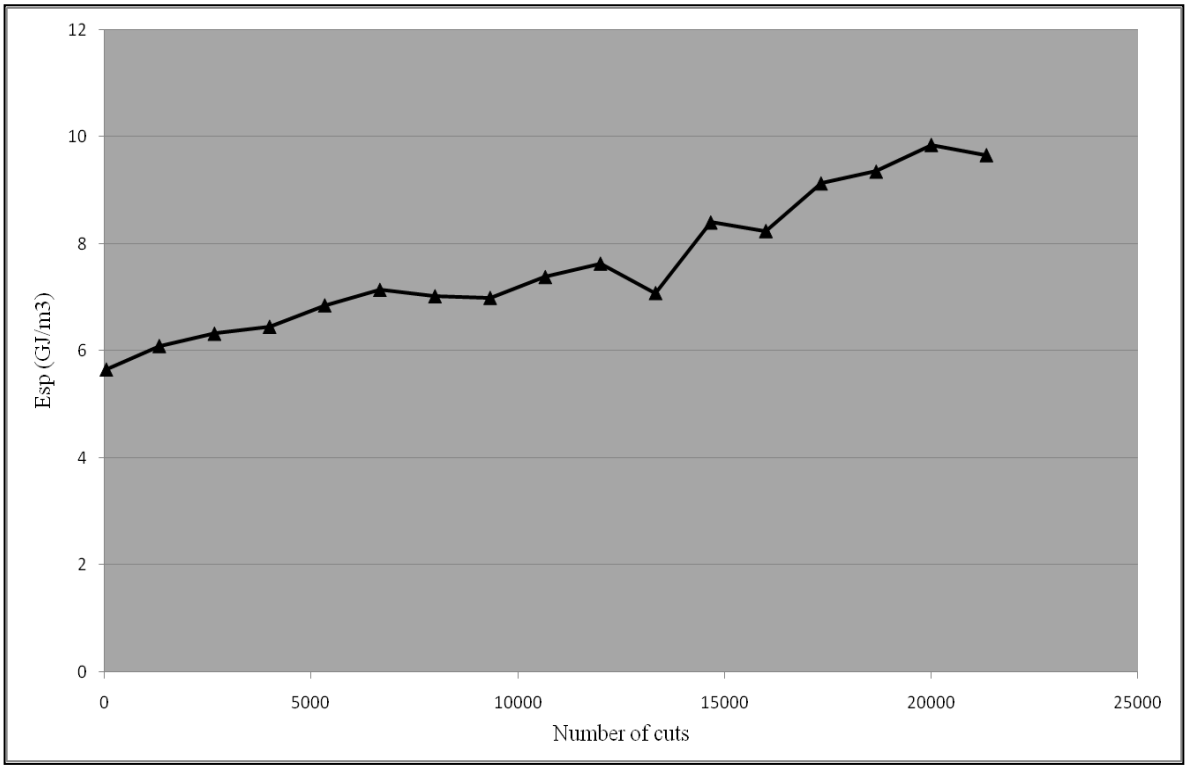

Figure 4.79. Variation of Esp for TiAlSiN coated bandsaw tooth (cutting speed: 40 m/min, feed: 15 µm, width of cut: 1 mm).

The high stress generated, along with high temperatures that exist at the tool chip interface while machining titanium alloys are responsible for this chipping of the cutting edge. The modification of the tooth geometry can be observed even more clearly from Figure 4.80, which shows the condition of the worn tooth from a different view.

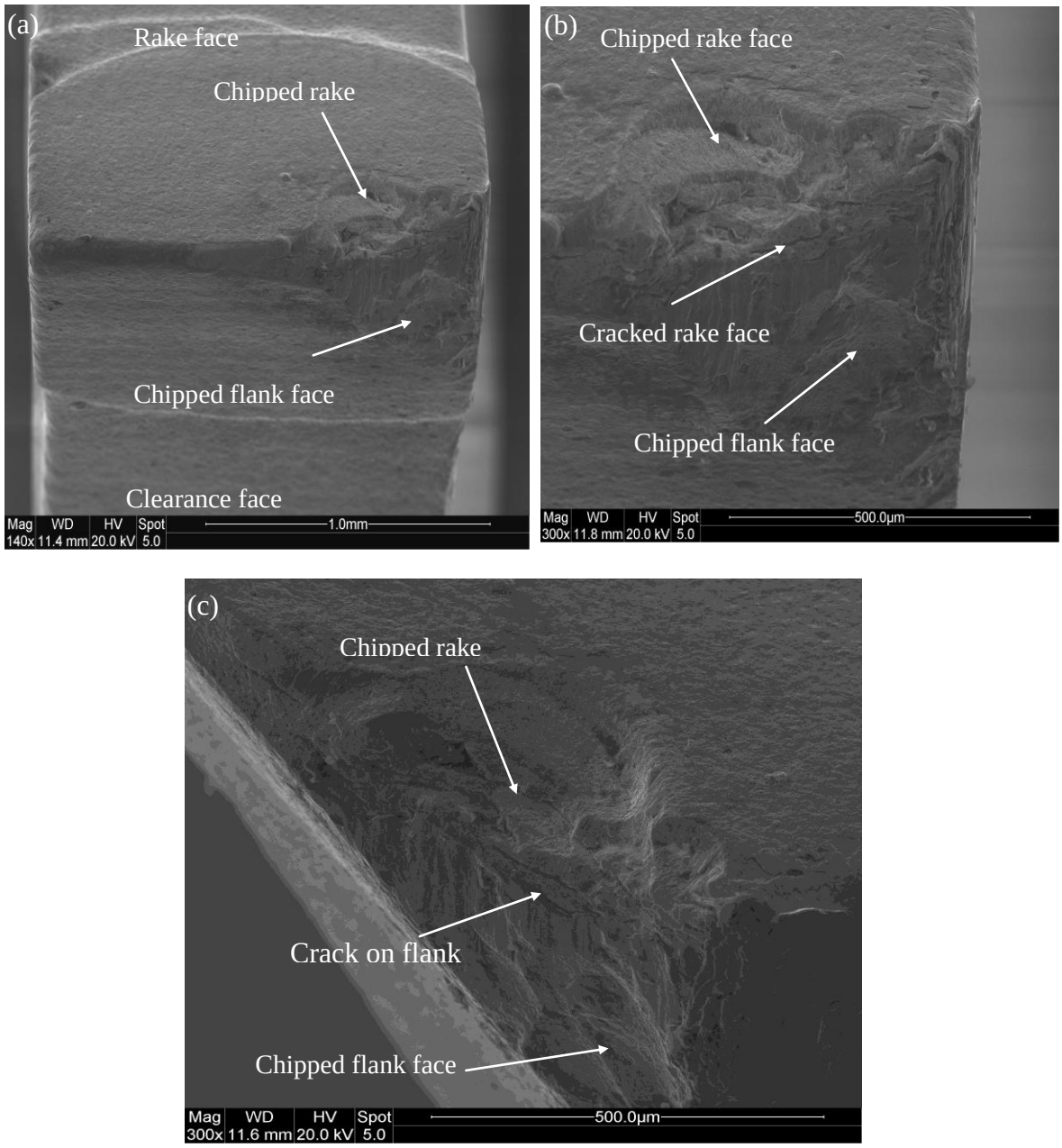

Figure 4.80. Condition of (a) the TiAlSiN coated carbide tooth at the end of its life, (b) magnified view of the corner of the tooth and (c) side view of the coated tooth (cutting speed: 40 m/min, feed: 15 µm, width of cut: 1 mm, length of one cut: 0.6 m)

The same SEM images of the worn TiAlSiN coated taken in BSE mode are provided in Figure 4.81. It can be seen from Figures 4.80 and 4.81that the coated tooth has chipped from both the faces of the cutting edge and the severity of chipping increases towards the corner of the tooth which is engaging with the side of the workpiece material. Moreover, adhering material can be observed on the worn flank, which after EDS analysis was found to have the same elemental composition as that of the workpiece materials, *i.e.* Ti-17 alloy.

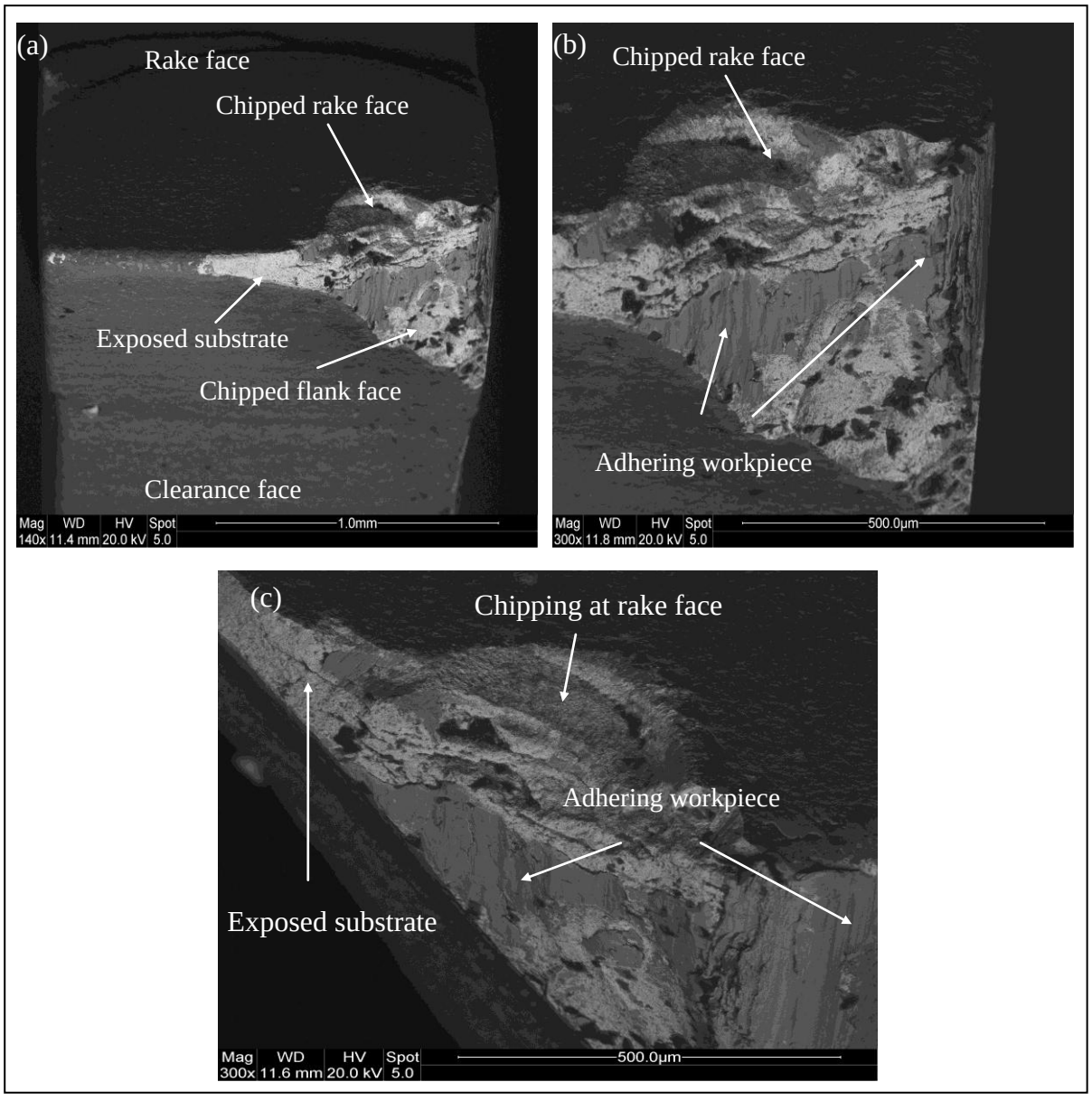

Figure 4.81. SEM micrographs taken in BSE mode showing (a) the condition of the TiAlSiN coated carbide tooth at the end of its life, (b) magnified view of the corner of the tooth and (c) side view of the coated tooth (cutting speed: 40 m/min, feed: 15 µm, width of cut: 1 mm).

The side view of the worn carbide tooth is displayed in Figure 4.81 (c) and it clearly reveals adhering workpiece material not only at the worn flank but also on the side of the tooth, suggesting that side of the tooth has been modified by the removal of a small part of the tool. The volume of material removed from the tooth is filled by the adhering workpiece material. It can also be inferred from these images that the adhering material, during the cutting action, would have maintained a close and continuous contact with the moving workpiece.

Moreover, it may be inferred that once this adhering material attained a critical size, it will be removed from the cutting edge with the flowing chip, leading to the further degradation of the carbide tooth. Furthermore, it can be observed that more workpiece material is attached to the worn flank surface compared to the rake face.

The initial and final chips formed while machining Ti-17 alloy using a TiAlSiN coated carbide tooth, at a cutting speed of 40 m/min and a feed of 15 µm are shown in Figure 4.82. From Figure 4.82, it appears that the initial chips formed during machining operation are long, smooth and shiny compared to the chips developed at the end of machining test, which appear to be shorter and seem to be curled – an indication of a worn cutting edge.

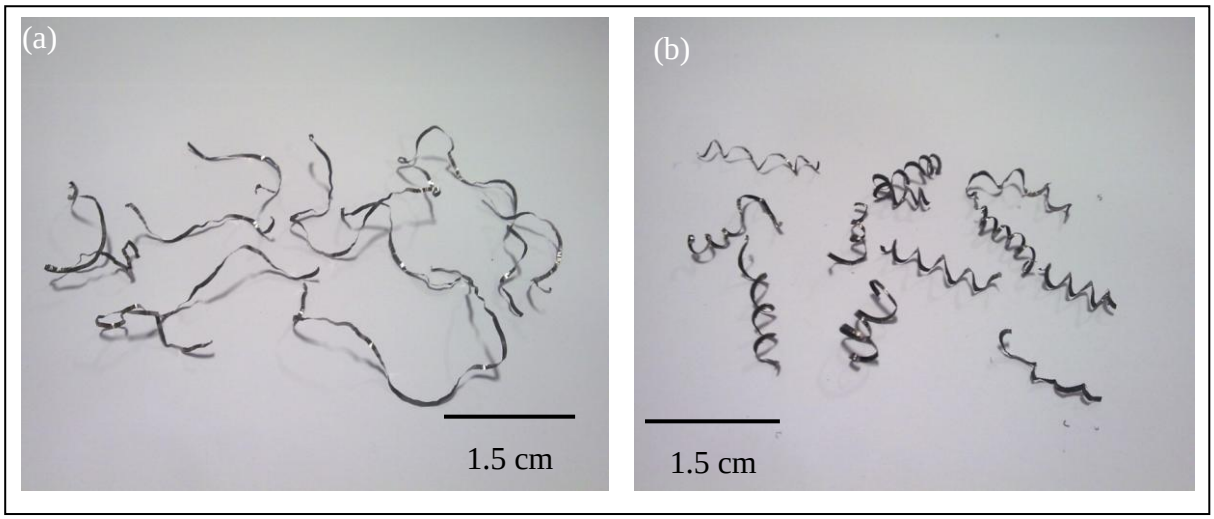

Figure 4.82. Characteristics of (a) initial and (b) final chips formed using TiAlSiN coated carbide tooth (cutting speed: 40 m/min, feed: 15 µm, width of cut: 1 mm)

The feed was further reduced to the low level of 10 µm while maintaining the cutting speed at 40 m/min. The variation of forces while machining Ti-17 alloy using TiAlSiN coated bandsaw tooth at a cutting speed of 40 m/min and at a feed of 10 µm is represented in Figure 4.83. It appears from Figure 4.83 that the cutting force increases steadily

throughout the machining test. However, the thrust force and side force show several abrupt increases in their trend, which is probably due to minute chipping taking place on the flank face as well as at the corner of the cutting edge. The relatively smooth increase in the forces is indicative of smooth wear occurring on the cutting edge. This is, however, not the end of the tooth life.

The variation in Esp for the carbide tooth used at a cutting speed of 40 m/min and at a feed of 10 µm is drawn in Figure 4.84. The increase in Esp values is similar to that shown by cutting force. However, since Esp takes into account the contact area of the bandsaw tooth, therefore it is more sensitive, which can be observed from Figure 4.84. The gradual increase in the values of Esp indicates that the tooth is wearing

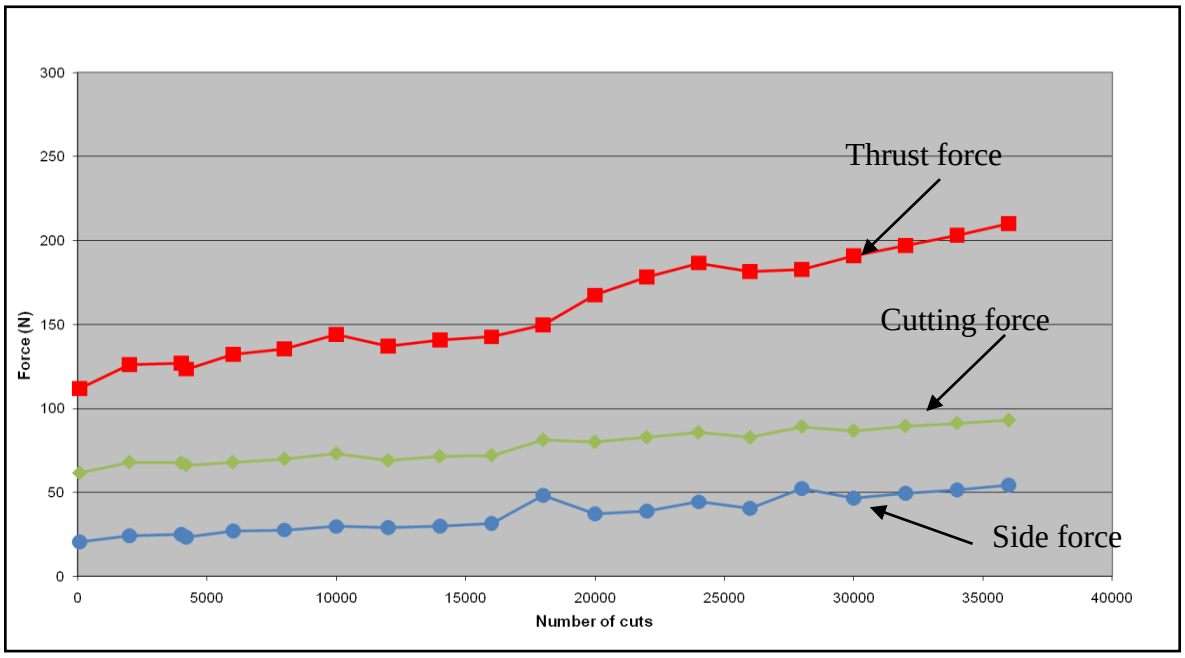

Figure 4.83. Variation of forces for TiAlSiN coated bandsaw tooth (cutting speed: 40 m/min, feed: 10 µm, width of cut: 1 mm, length of one cut: 0.6 m).

in a uniform way. The Esp values start from 6.25 GJ/m^3 during the initial part of the cutting operation and increase steadily to 9.5 GJ/m^3 at the end of the test.

The SEM micrographs of the worn TiAlSiN coated carbide tooth are shown in Figure 4.85. It appears from the images that the rake face at the corner of the tooth has chipped. However, most of the cutting edge has maintained its structural integrity. The magnified view of the corner of the TiAlSiN coated carbide tooth is shown in Figure 4.85 (b) and chipping at the rake face is evident from this image. The side view of the worn tooth is

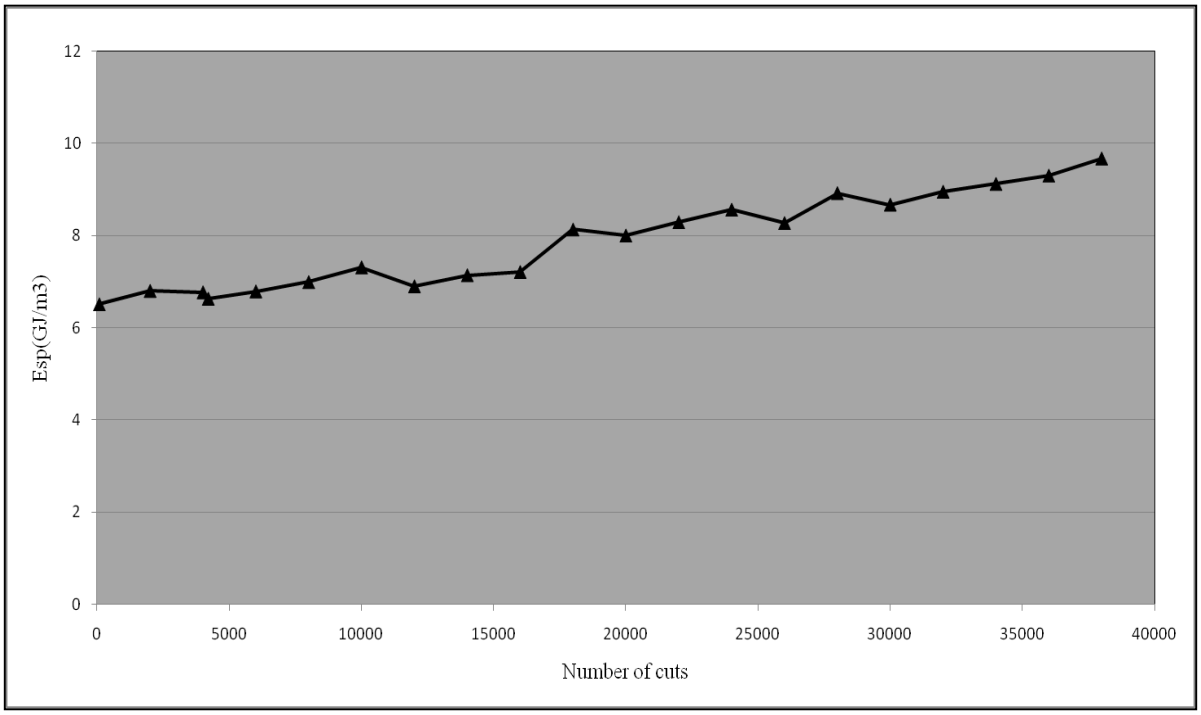

Figure 4.84. Variation in Esp for TiAlSiN coated bandsaw tooth (cutting speed: 40 m/min, feed: 10 µm, width of cut: 1 mm, length of one cut: 0.6 m).

provided in Figure 4.85 (b) and gives the perspective of wear from a different view. It appears from these images that less workpiece material is adhering onto the worn flank compared to the amount which was found on the un-coated carbide tooth used under the same cutting conditions. The same SEM images taken in BSE mode are displayed in Figure 4.86. It appears from Figure 4.86 (a), that the coating has been removed from all the area of the cutting edge that was in contact with the workpiece material while machining. Less adhering material is visible on the cutting edge, especially at the flank face. The side view represented in Figure 4.86 (c), shows that less of the workpiece material is adhering to the side of the coated carbide tooth, indicating low wear at the side of the tooth. The major degradation of the TiAlSiN coated carbide tooth used at a feed of 10 µm and at a cutting speed of 40 m/min is the chipping of the rake face at the corner of the cutting edge. The magnified image of the intact cutting edge, along with the BSE image is shown in Figure 4.87 and it is clear from these images that less workpiece material seems to be adhering to the flank, due to the TiAlSiN coating.

It is also evident that cracks have begun to form at the corner of the edge. This could be due to the high temperatures generated at the corner of the tooth, since the tooth has a set geometry. Moreover, these high temperatures are also due to the low thermal conductivity

of titanium alloys, which leads to the generation of high temperatures at the tool/workpiece interface, eventually leading to the chipping of the cutting edge. Therefore, it may be stated that further chipping will take place at the cracks observed in Figure 4.86 (b). The initial and final chips formed while machining Ti-17 alloy using TiAlSiN coated carbide tooth at a cutting speed of 40 m/min and at a feed of 10 µm are shown in Figure 4.88. It appears from Figure 4.88, that the chips formed during the initial cutting process are longer and straighter in contrast to the chips formed at the end of machining test, which are not only shorter but are curved, showing that they were formed from a tooth which had different physical geometry compared to the initial chips, which were generated from a new tooth.

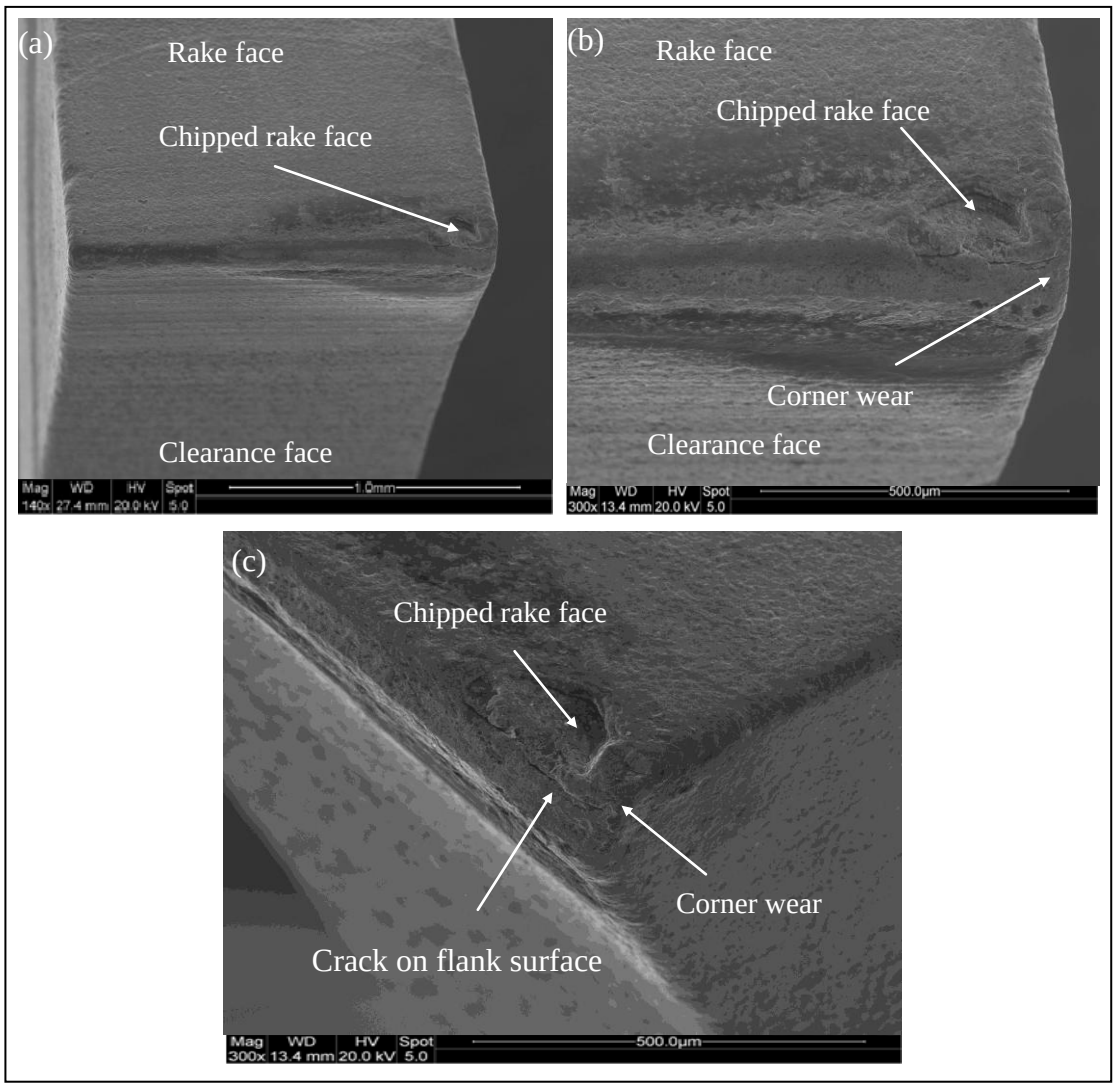

Figure 4.85. Condition of (a) the TiAlSiN coated carbide tooth, (b) magnified view of the corner and (c) view from the side (cutting speed: 40 m/min, feed: 10 µm, width of cut: 1 mm, length of one cut: 0.6 m).

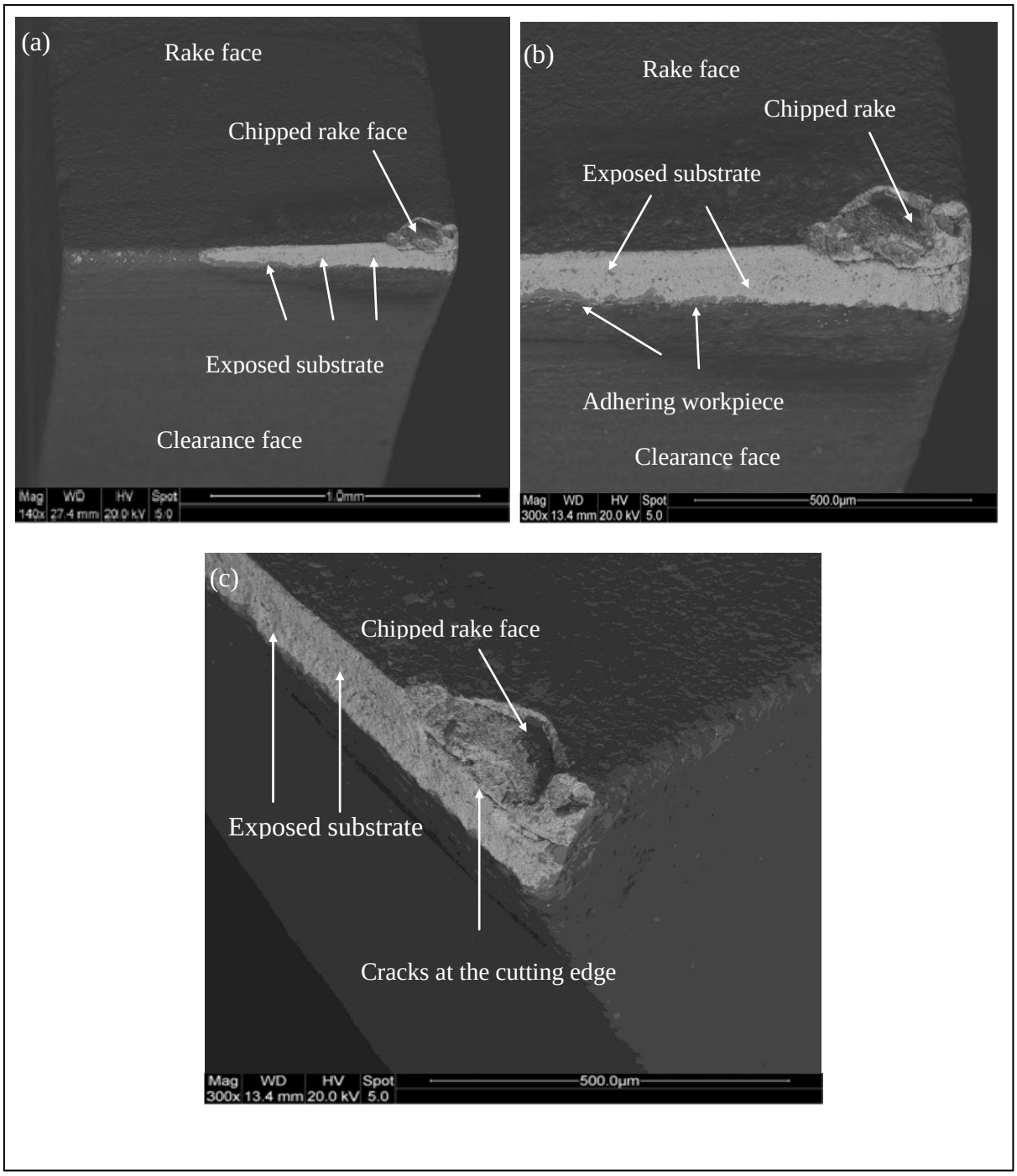

Figure 4.86. SEM micrographs of (a) the TiAlSiN coated carbide tooth in BSE mode, (b) magnified view of the corner and (c) view from the side (cutting speed: 40 m/min, feed: 10 µm, width of cut: 1 mm).

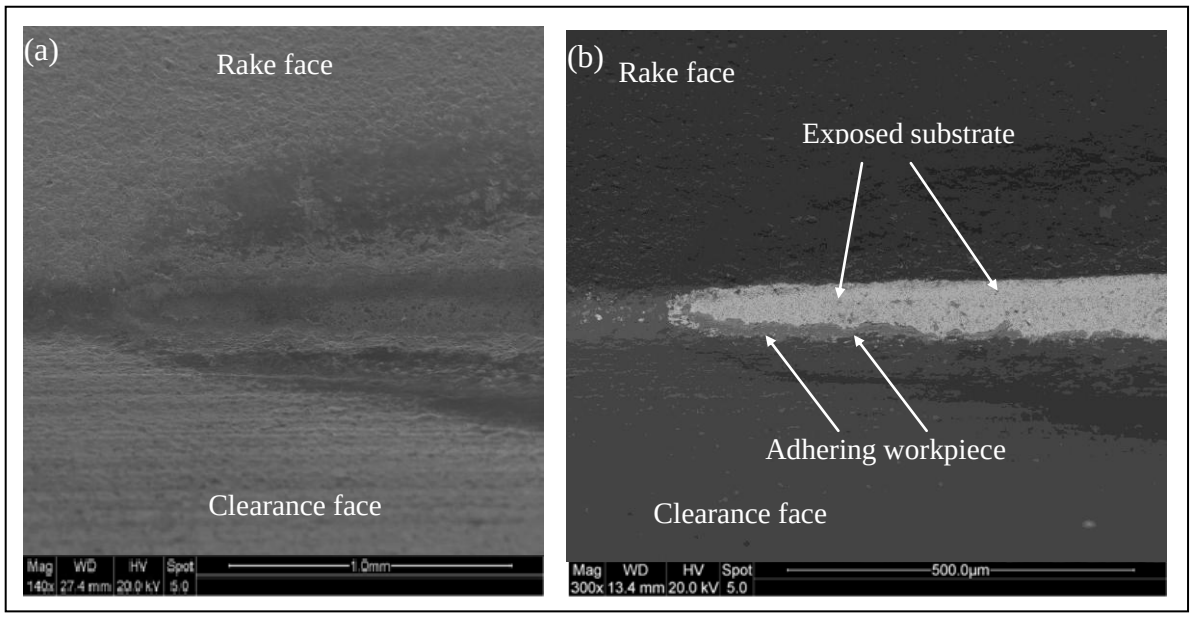

4.87. SEM images of (a) the cutting edge area exposed to the workpiece during machining operation and (b) BSE image of the same area showing the exposed substrate as well as the small quantity of the adhering workpiece (cutting speed: 40 m/min, feed: 10 µm, width of cut: 1 mm)

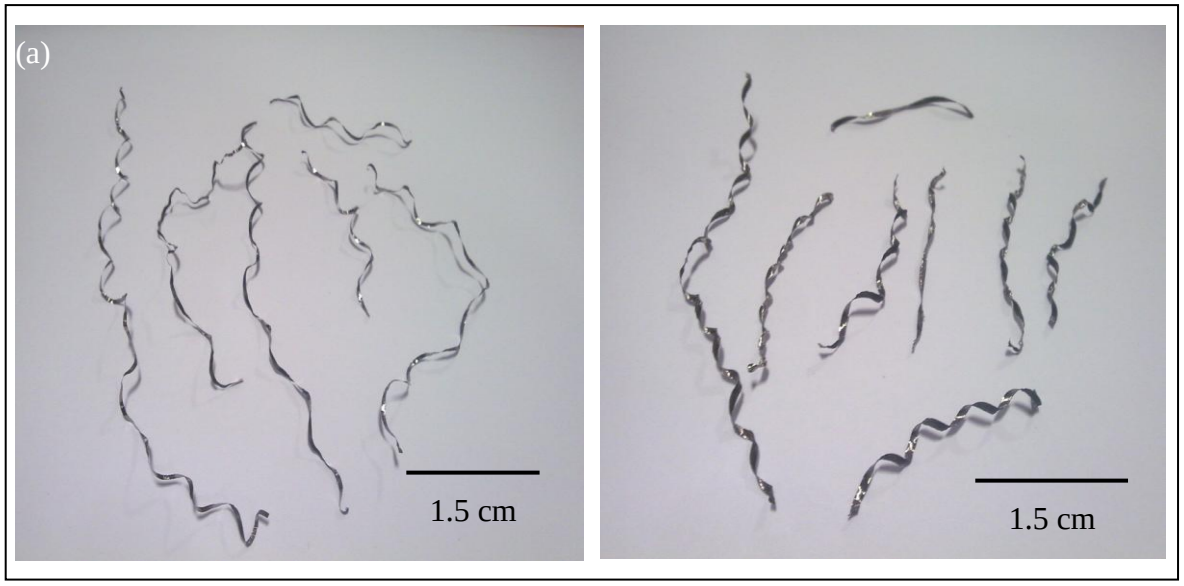

Figure 4.88. Characteristics of (a) initial and (b) final chips formed using TiAlSiN coated carbide tooth (cutting speed: 40 m/min, feed: 10 µm, width of cut: 1 mm).

4.5.2 Performance of AlTiN coated carbide teeth

The SEM images of the new, un-used AlTiN coated carbide tooth is shown in Figure 4.89. The coating appears to be smooth and continuous over the whole of the tooth and the coated honed edge (approximately 135 µm) can be easily observed on the tooth. The same machining parameters (feed, speed and width of cut) which were used previously to evaluate the performance of TiAlSiN coated bandsaw teeth were used to assess the performance of AlTiN coated carbide bandsaw teeth. For the machining tests carried out to evaluate the performance of AlTiN coated carbide teeth, the width of cut was set to 1 mm, which is less than the average width of the carbide tooth (average width of the carbide tooth is 1.6 mm approximately).

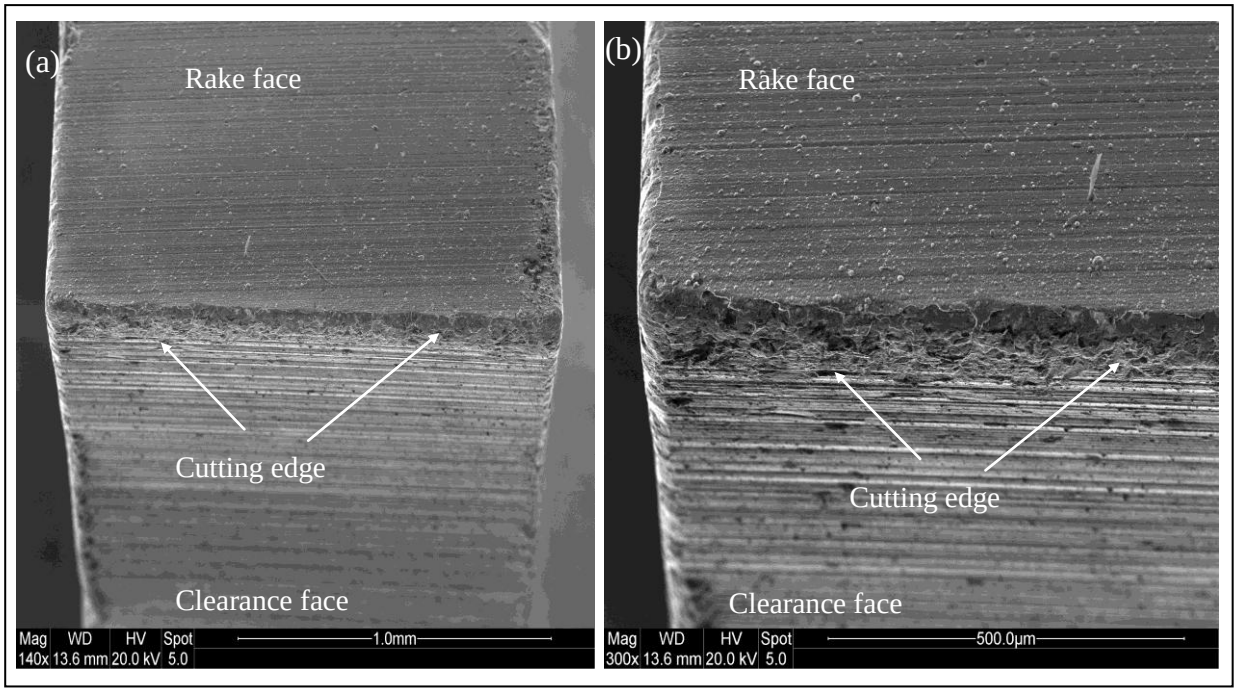

Figure 4.89. Un-used AlTiN coated carbide bandsaw tooth (a) and (b) magnified view of the corner of cutting edge.

The variation in forces for the AlTiN coated carbide bandsaw tooth used at a feed of 20 µm and a cutting speed of 40 m/min is shown in Figure 4.90. It appears from Figure 4.90 that the forces increase steadily throughout the cutting session, indicating that uniform wear is taking place throughout the trial. However, the increase in the thrust force is higher compared to the other forces. This is due to the higher wear taking place on the flank face, since the thrust force originates from the flank face. The variation in Esp for the AlTiN

coated carbide bandsaw tooth used at 20 µm feed and at the cutting speed of 40 m/min is displayed in Figure 4.91. From Figure 4.91 it can be observed that the Esp follows the same trend as that of the cutting force and therefore representing uniform wear taking place on the cutting edge. Since Esp is more sensitive to the area of the cutting edge that is performing the shearing, therefore the variation observed in the Esp indicates that the physical geometry of the tooth is changing at several points. However, this modification of the cutting edge by wear is not sufficient to cause abrupt changes in the Esp curve.

The Esp starts from approximately 3.2 GJ/m^3 and quickly rises to 4 GJ/m^3. This is due to the initial wear that took place on the cutting edge soon after the machining operation started. After this increase the value of Esp continues to rise and reached 6 GJ/m^3 at the end of the test, suggesting that the tooth geometry has changed, due to chipping and therefore a higher value of Esp compared to the initial value.

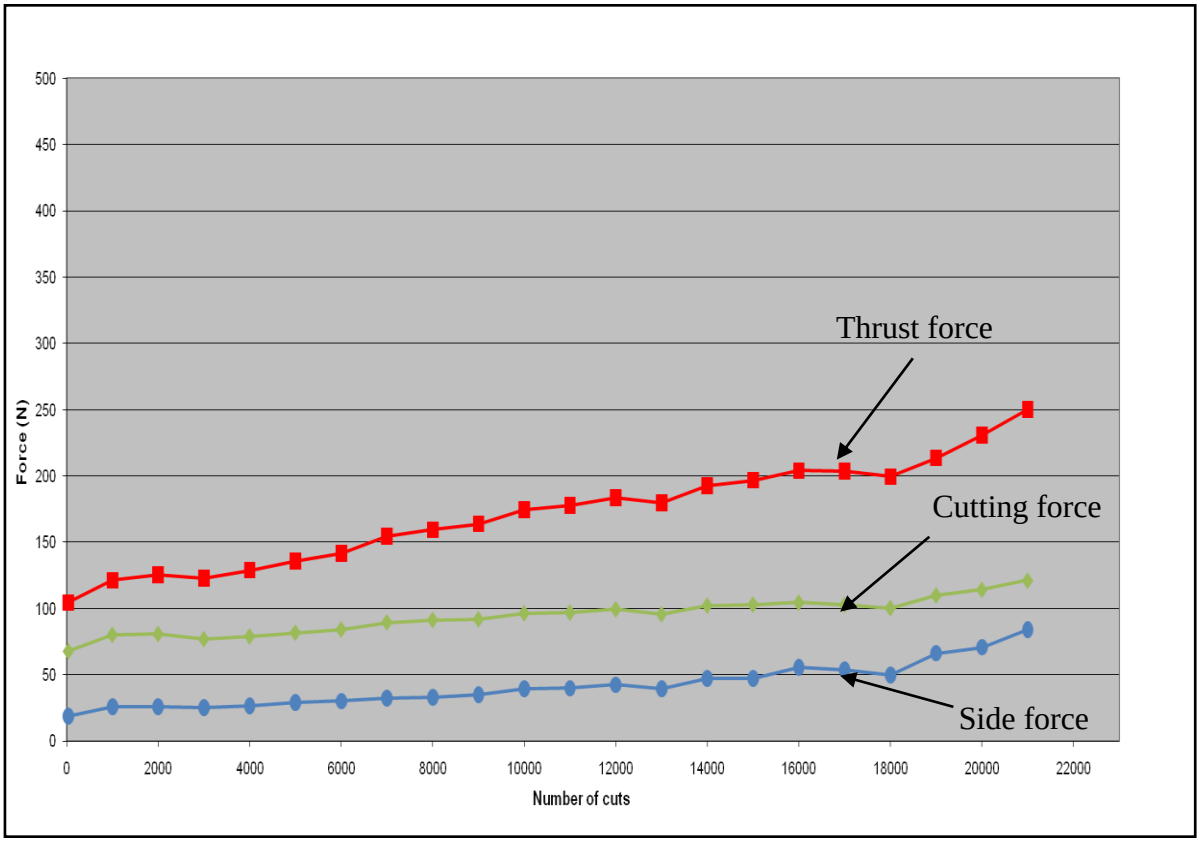

Figure 4.90. Variation of forces for AlTiN coated bandsaw tooth (cutting speed: 40 m/min, feed: 20 µm, width of cut: 1 mm, length of one cut: 0.6 m).

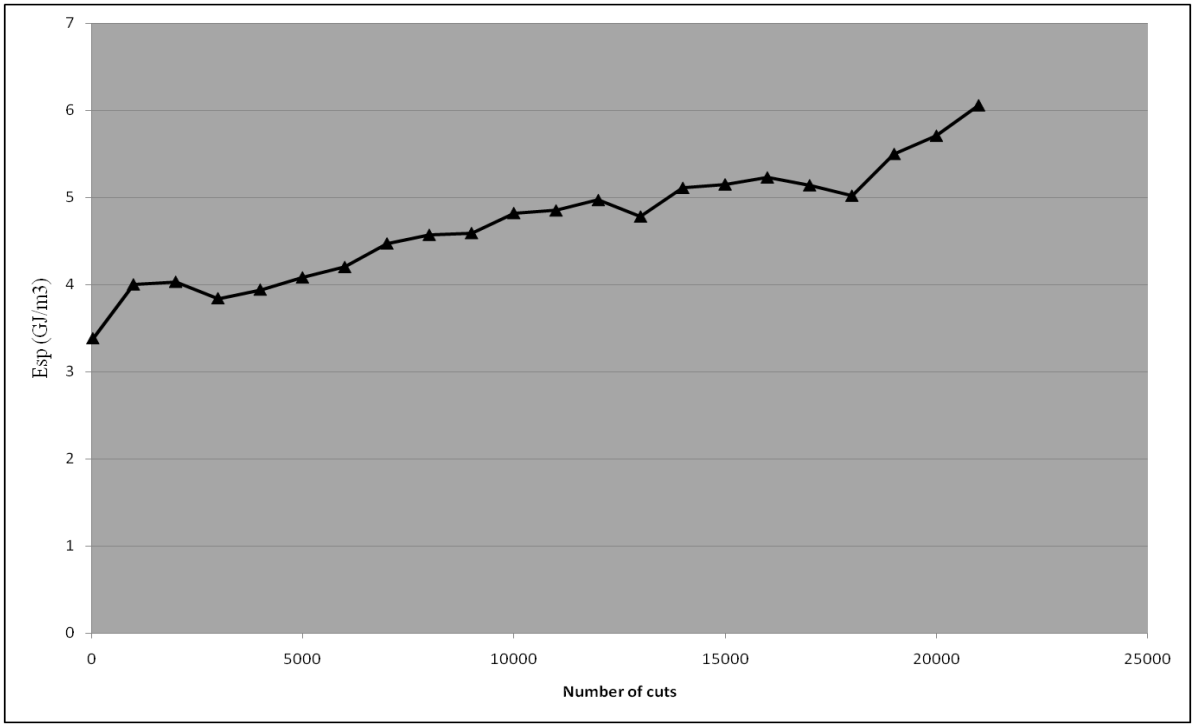

Figure 4.91. Variation in Esp for AlTiN coated bandsaw tooth (cutting speed: 40 m/min, feed: 20 µm, width of cut: 1 mm, length of one cut: 0.6 m).

The condition of the worn AlTiN coated carbide bandsaw tooth is provided in Figure 4.92, which shows the entire worn tooth, whereas Figure 4.92 (b) displays the magnified image of the corner of the tooth. The SEM images reveal the same trend as observed in the case of TiAlSiN coated carbide tooth of chipping at the rake face as well as at the flank surface. Chipping at the rake face can be observed on the side of the tooth which is engaging with the workpiece material. The magnified image of the corner of the AlTiN coated tooth shows chipping of the flank face more clearly. The side view of the tooth is given in Figure 4.92 (c) and shows the condition of the tooth from a different angle. Chipping at the corner can be easily observed and the un-even surface at the flank face is visible.

The same images taken in BSE mode are provided in Figure 4.93. These images show the condition of the worn tooth more clearly. The exposed shining carbide surface can be observed as in all the images and it reveals that the coating has been removed from the area exposed to the cutting operation. Adhering material is apparent on the rake face of the coated tooth, predominantly at the chipped area of the flank face, suggesting that the workpiece material has a tendency to adhere to the tungsten carbide substrate. The side view of the worn tooth is displayed in Figure 4.93 (c) and it can be observed that

workpiece material is also adhering to the side of the carbide tooth. It should be noted that the side of the tooth is rubbing against the workpiece material while the cutting edge is performing the machining. Therefore, the side of the tooth will be exposed to high temperatures generated due to friction between the side of the tooth and the workpiece material. It appears from Figure 4.93 (c), that the side of the tooth has been slightly modified due to chipping and this chipped area is filled with the adhering workpiece material.

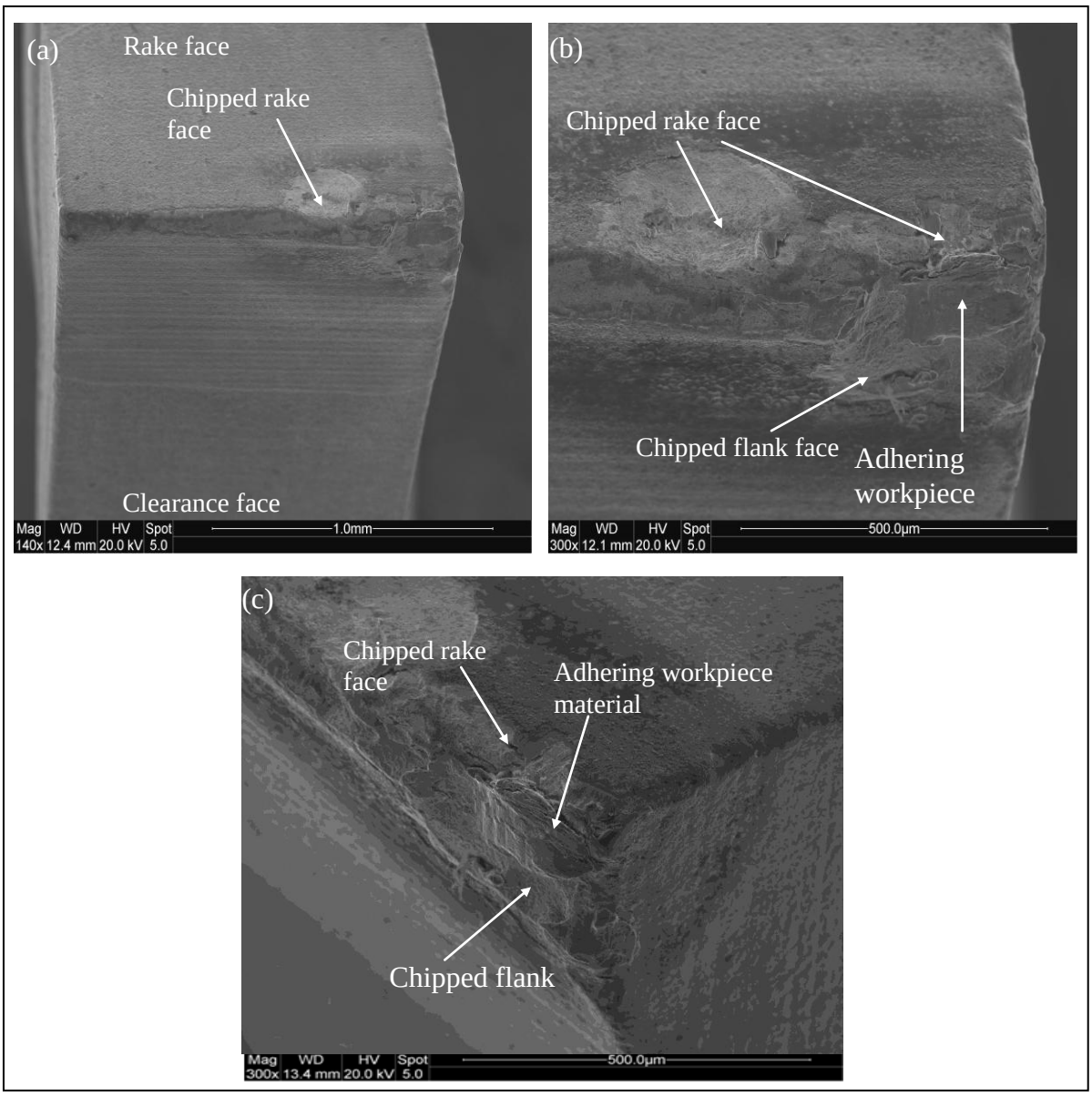

Figure 4.92. SEM images of (a) AlTiN coated carbide tooth at the end of its life, (b) magnified view of the corner of the cutting edge and (c) side view of the worn tooth (cutting speed: 40 m/min, feed: 20 µm, width of cut: 1 mm, length of one cut: 0.6 m)

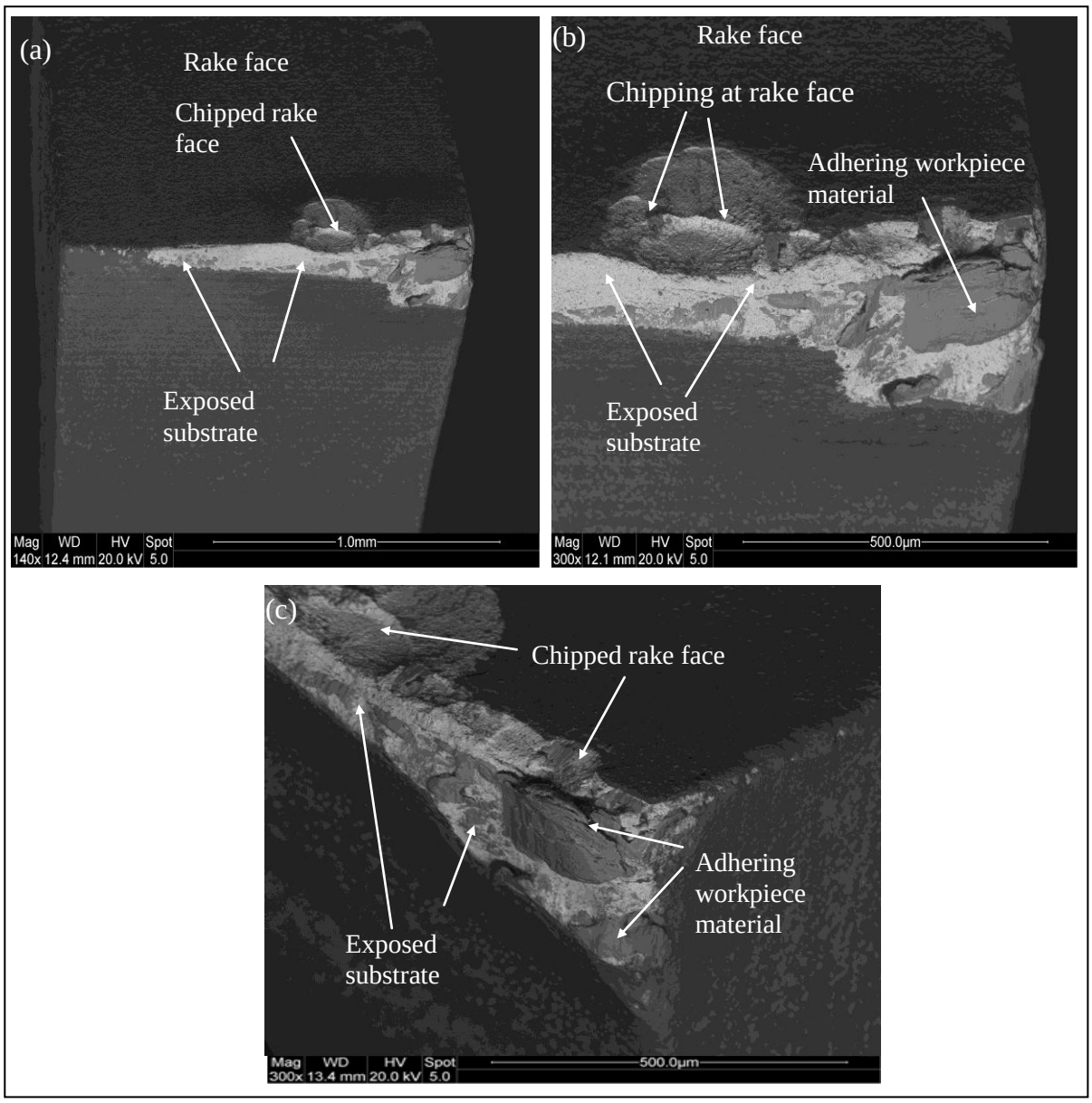

Figure 4.93. SEM micrographs of (a) AlTiN coated carbide tooth at the end of its life in BSE mode, (b) magnified view of the corner of the cutting edge and (c) side view of the worn tooth (cutting speed: 40 m/min, feed: 20 µm, width of cut: 1 mm)

EDS analyses were carried out on the adhering workpiece material at ten different points. The elemental composition was found to be similar to that of Ti-17 alloy. Moreover, carbon and cobalt were also found in the analyses, suggesting the diffusion of these elements into the adhering workpiece from the carbide bandsaw tooth. Representative SEM micrographs and corresponding spectra appear in Figure 4.94.

The initial and final chips formed while machining Ti-17 alloys using AlTiN coated carbide tooth at a cutting speed of 40 m/min and a feed of 20 µm are given in Figure 4.95. It can be seen that the initial chips are longer compared to the features of the chips formed at the end, which show a characteristic twist in them since they are formed from a tooth with changed physical geometry.

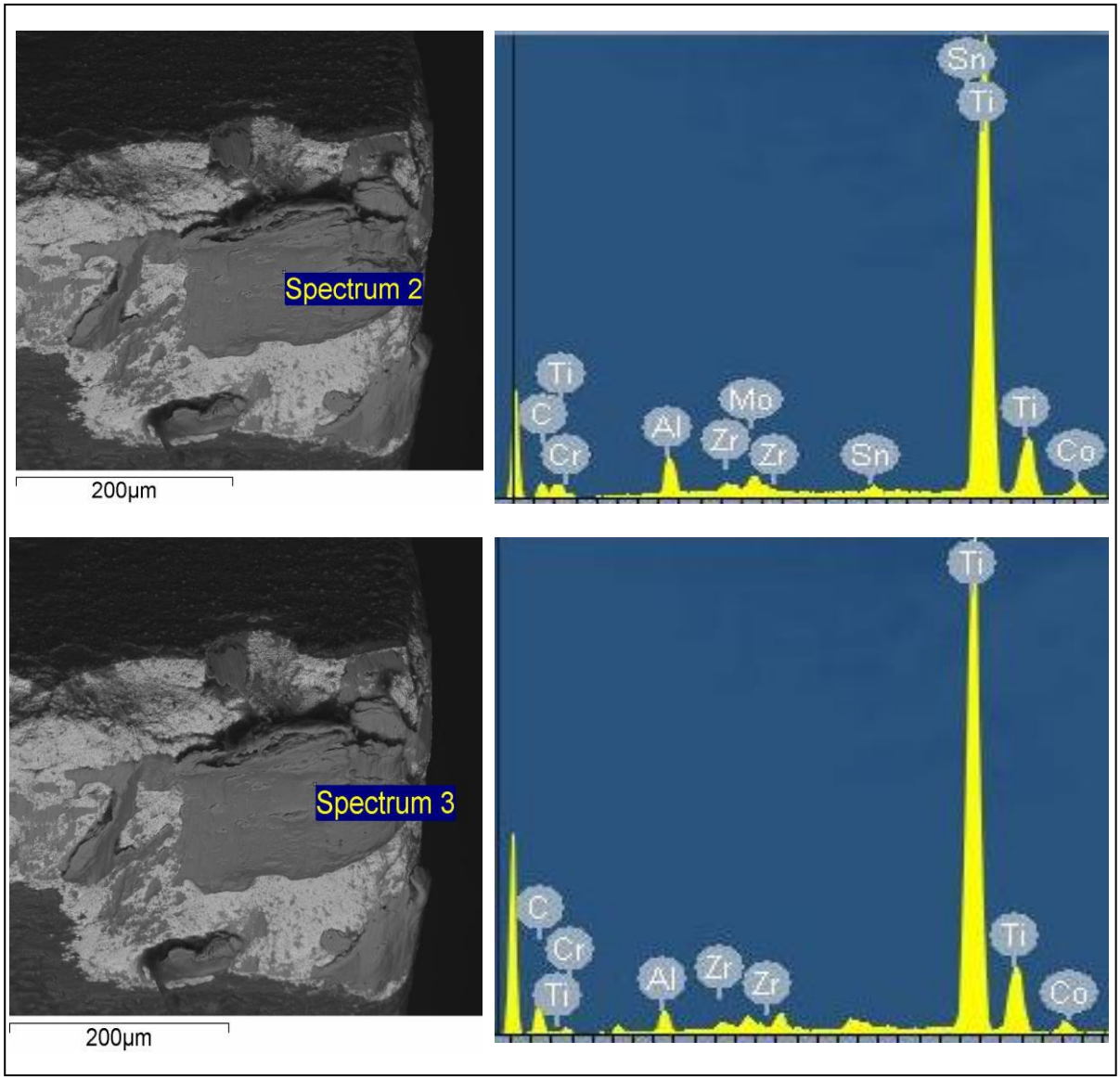

Figure 4.94. Two different analysed points on the AlTiN coated worn flank face and their corresponding EDS spectra (2 and 3) for two different points on the adhering material (cutting speed: 40 m/min, feed: 20 µm, width of cut: 1 mm).

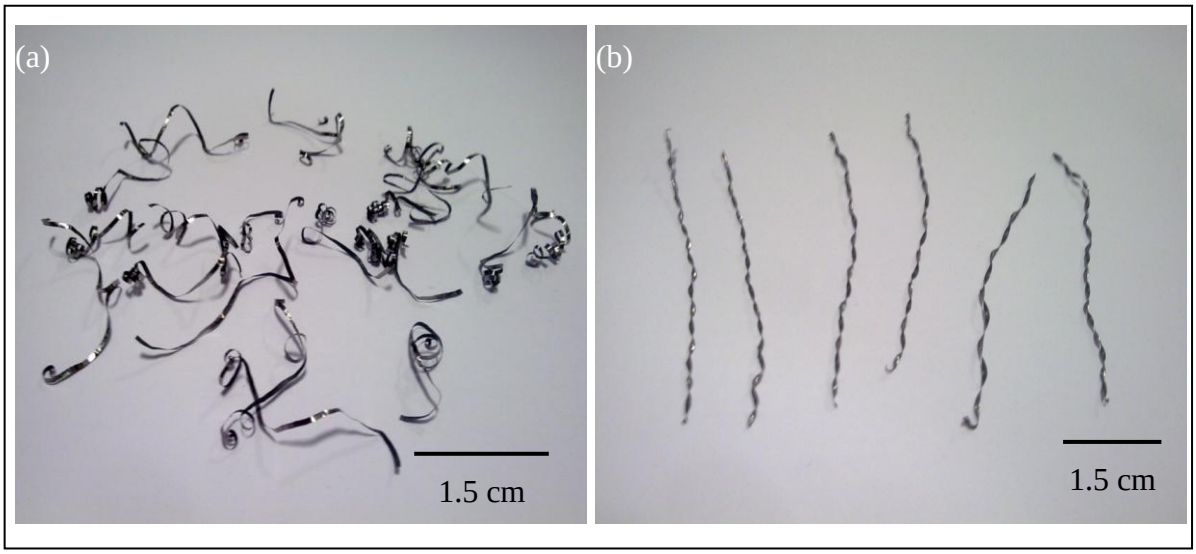

Figure 4.95. Characteristics of (a) initial and (b) final chips formed using AlTiN coated carbide tooth (cutting speed: 40 m/min, feed: 20 µm, width of cut: 1 mm)

In order to observe the effect of decreasing the feed on the performance of AlTiN coated bandsaw tooth, the feed was reduced to 15 µm. The variation of forces for the AlTiN coated carbide tooth used at a feed of 15 µm and at a cutting speed of 40 m/min is offered in Figure 4.96. It appears from Figure 4.96 that the carbide tooth was wearing in a uniform manner until it performed 14000 cuts. After performing 14000 cuts, the degradation of the tooth in terms of wear, accelerated therefore leading to the generation of high forces.

The variation in Esp for the AlTiN coated carbide tooth is shown in Figure 4.97. It appears from Figure 4.88 that the Esp varies in the same way as the cutting force and it starts from approximately 5 GJ/m^3 and rises steadily to 22 GJ/m^3 towards the end of the test, suggesting inefficient cutting towards the end of the machining trial due to the worn condition of the tooth.

The SEM images of the worn AlTiN coated carbide tooth used at a cutting speed of 40 m/min and at a feed of 15 µm appear in Figure 4.98. It appears from the SEM images that a large portion of the corner of the cutting edge was removed from the tooth. Extensive chipping of the rake as well as flank surface can be observed from the magnified view of the corner of the carbide tooth – see Figure 4.98 (b). The side view is shown in Figure 4.98 (c) and it is clear from this image that not only the corner of the tooth has chipped but also the geometry of the cutting edge has been modified due to chipping and therefore the resultant high forces, probably at the end of the test The same images in BSE mode are provided in Figure 4.99 – they clearly reveal a large quantity of the workpiece material adhering to the chipped surface of the flank face. It appears from Figure 4.99 (c), which

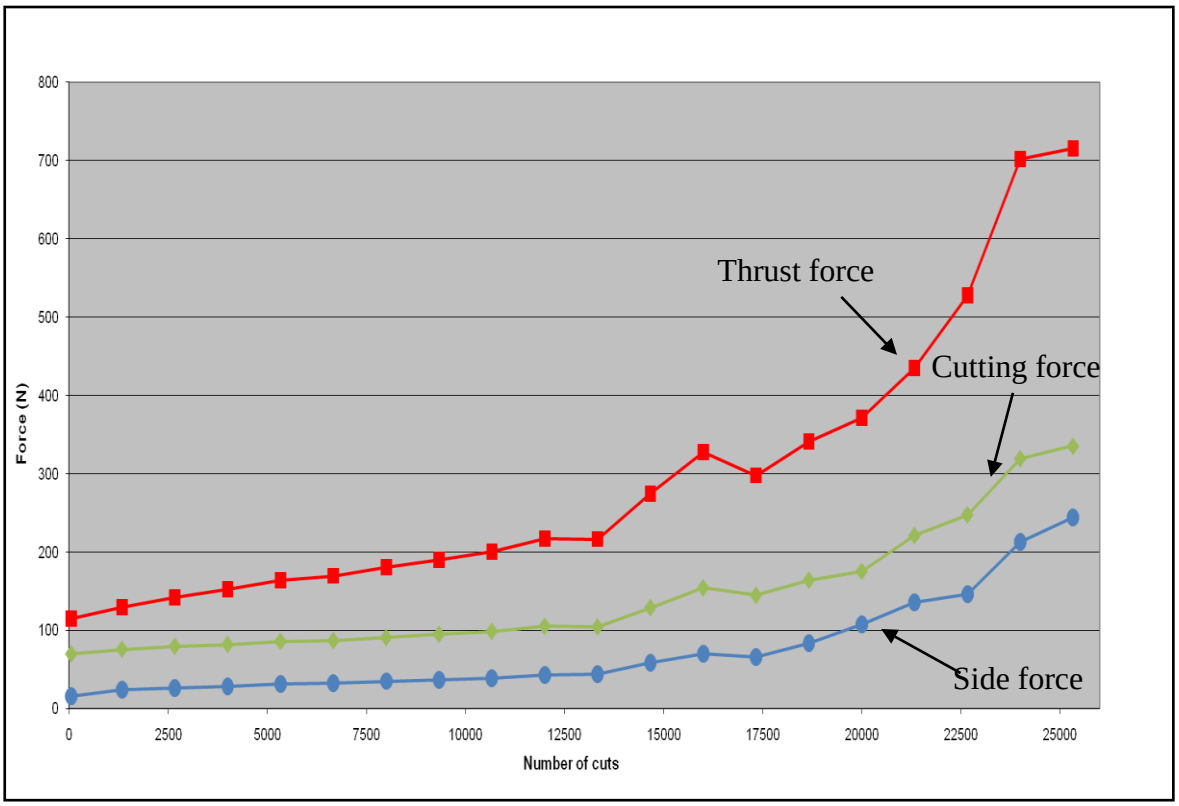

Figure 4.96. Variation of forces for AlTiN coated bandsaw tooth (cutting speed: 40 m/min, feed: 15 µm, width of cut: 1 mm, length of one cut: 0.6 m).

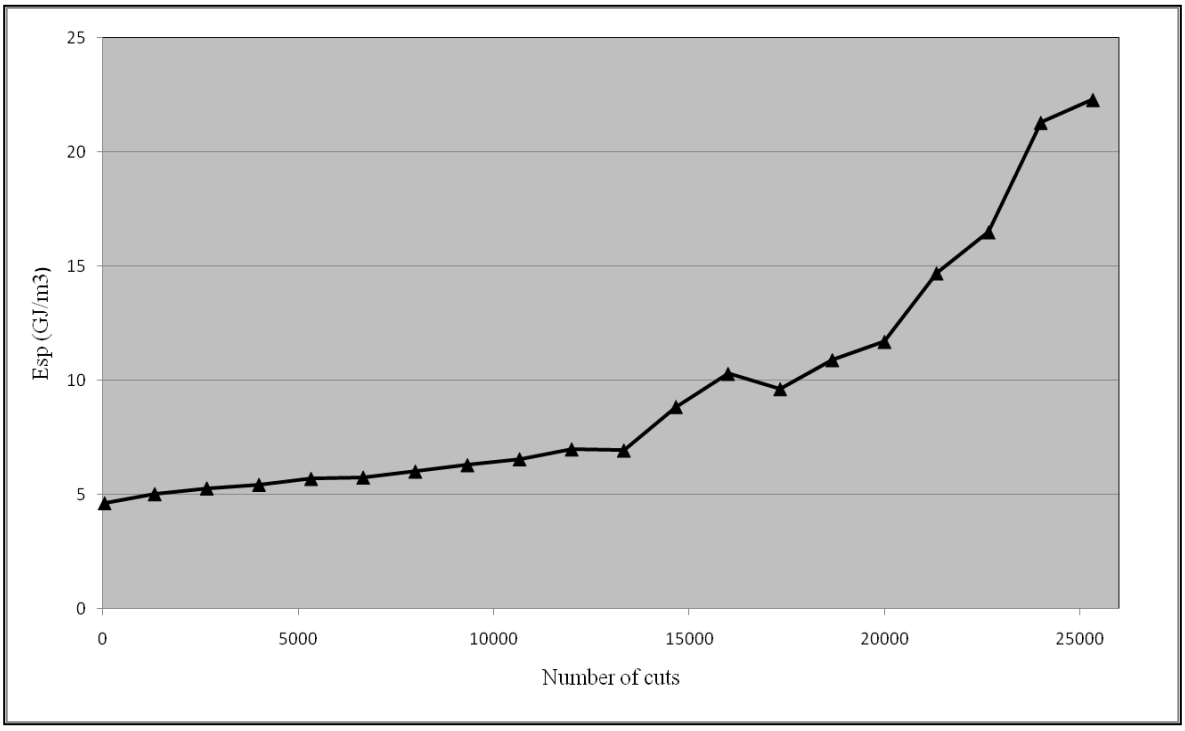

Figure 4.97. Variation in Esp for AlTiN coated bandsaw tooth (cutting speed: 40 m/min, feed: 15 µm, width of cut: 1 mm, length of one cut: 0.6 m).

shows the edge of the cutting surface, that the corner has degraded in terms of chipping at both the rake and flank face. Workpiece material seems to be adhering to the side of the coated carbide tooth as well, due to its rubbing with the workpiece material during the cutting action. Moreover, the exposed substrate material can be observed in Figure 4.98 (c) and it appears that the substrate has chipped-off taking the coatings along with it.

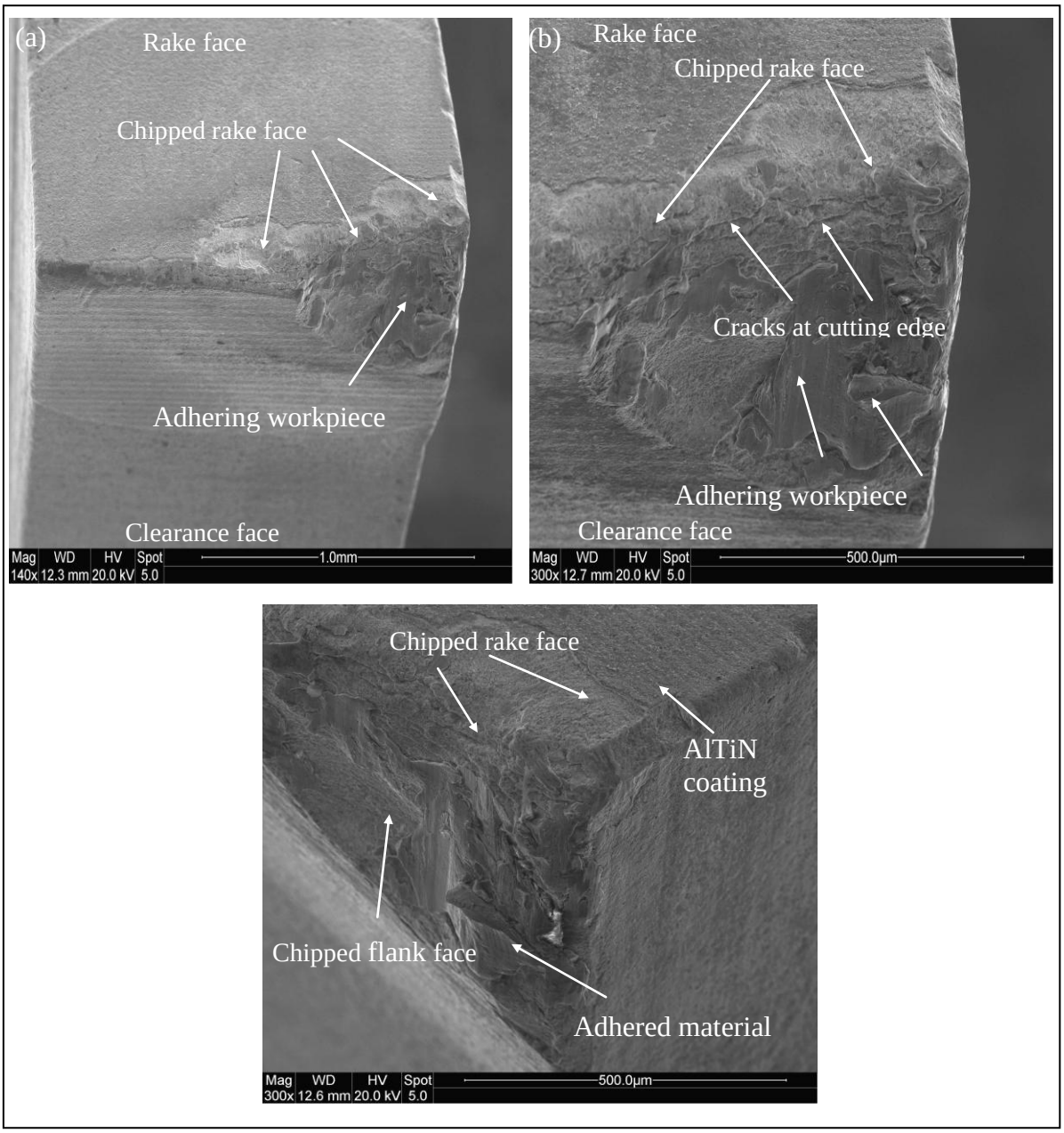

Figure 4.98. SEM images of (a) AlTiN coated carbide tooth at the end of its life, (b) magnified view of the corner of the cutting edge and (c) side view of the worn tooth (cutting speed: 40 m/min, feed: 15 µm, width of cut: 1 mm, length of one: cut 0.6 m)

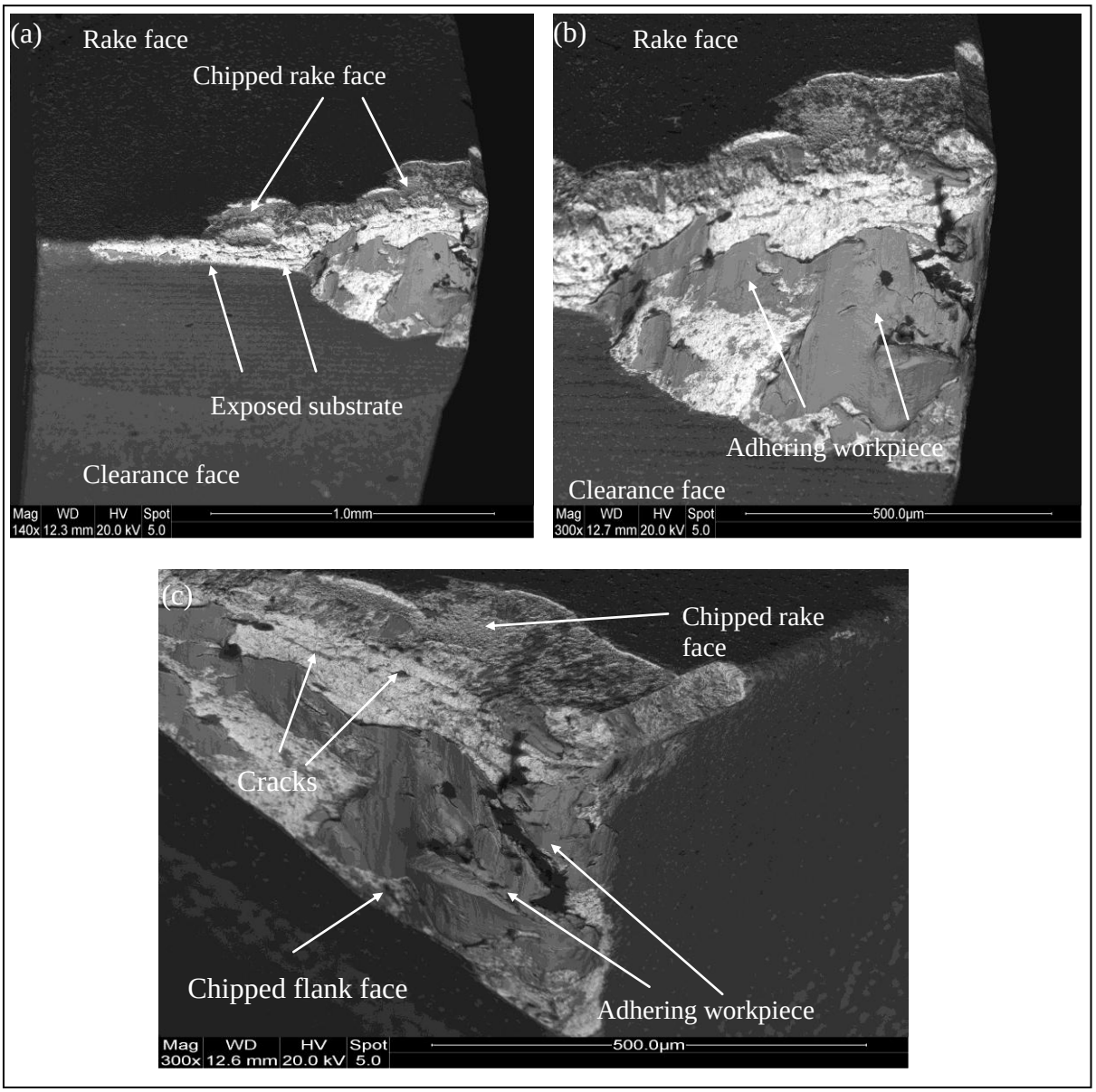

Figure 4.99. SEM micrograph of (a) AlTiN coated carbide tooth at the end of its life taken in BSE mode, (b) magnified view of the corner of the cutting edge and (c) side view of the worn tooth (cutting speed: 40 m/min, feed: 15 µm, width of cut: 1 mm, length of one cut: 0.6 m)

The initial and the final chips for the test carried out using AlTiN coated carbide bandsaw tooth when bandsawing Ti-17 alloy at a cutting speed of 40 m/min and at a feed of 15 µm are contrasted in Figure 4.100. The chips formed during the initial cutting seem to be more flexible and bright in terms of their appearance compared to the chips that were formed in the last part of machining, which appear to be darker in appearance and less flexible.

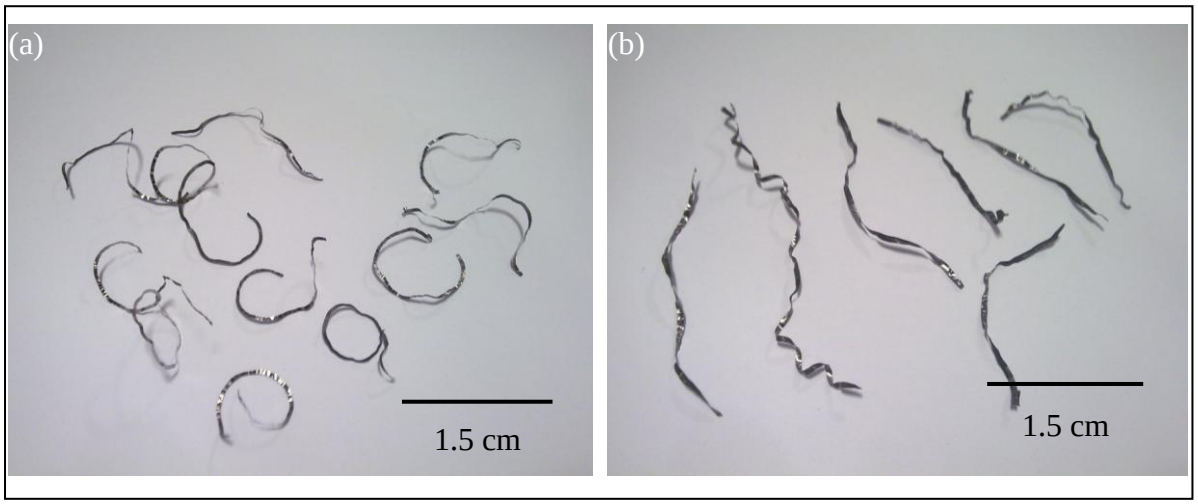

Figure 4.100. Characteristics of (a) initial and (b) final chips formed using AlTiN coated carbide tooth (cutting speed: 40 m/min, feed: 20 µm, width of cut: 1 mm)

The feed was further reduced to a low value of 10 µm in order to observe the effect of feed on the performance of the AlTiN coated carbide bandsaw tooth. The surface cutting speed was maintained at 40 m/min as it was for the previous tests for coated carbide teeth. The variation of forces against the number of cuts for the AlTiN coated carbide tooth used at a cutting speed of 40 m/min and at a feed of 10 µm is shown in Figure 4.101. It is apparent from these force graphs that all the forces increase steadily with the number of cuts performed, suggesting that the cutting edge is wearing in a uniform way and no major change (such as chipping) in the physical geometry of the carbide tooth is taking place during the machining test. The thrust force is increasing at a higher rate compared to the other forces, which can be due to the flank face deteriorating at a faster rate compared to the rake face. This is not the end of the life of the carbide tooth, however, the wear modes and mechanisms can be observed on the worn tooth. The variation of Esp for the AlTiN coated carbide tooth used at a cutting speed of 40 m/min and at a feed of 10 µm is shown in Figure 4.102.

From Figure4.102 it can be observed that the values of Esp increase steadily during the cutting session, which indicates that the cutting edge is wearing in a uniform manner. The Esp values start from approximately 5 GJ/m^3, and quickly rise to 6.2 GJ/m^3 after performing 2500 cuts and reach 9 GJ/m^3 at the end of machining trial. The initial increase in Esp is due to the initial wear which took place during the initial cutting operation. However, after performing 2500 cuts, there is a steady increase in Esp, indicating uniform progressive wear of the cutting edge. From these results it may be concluded that the tooth

has not degraded much in terms of wear. This is due the machining conditions (feed and speed) being less severe compared to the conditions used previously.

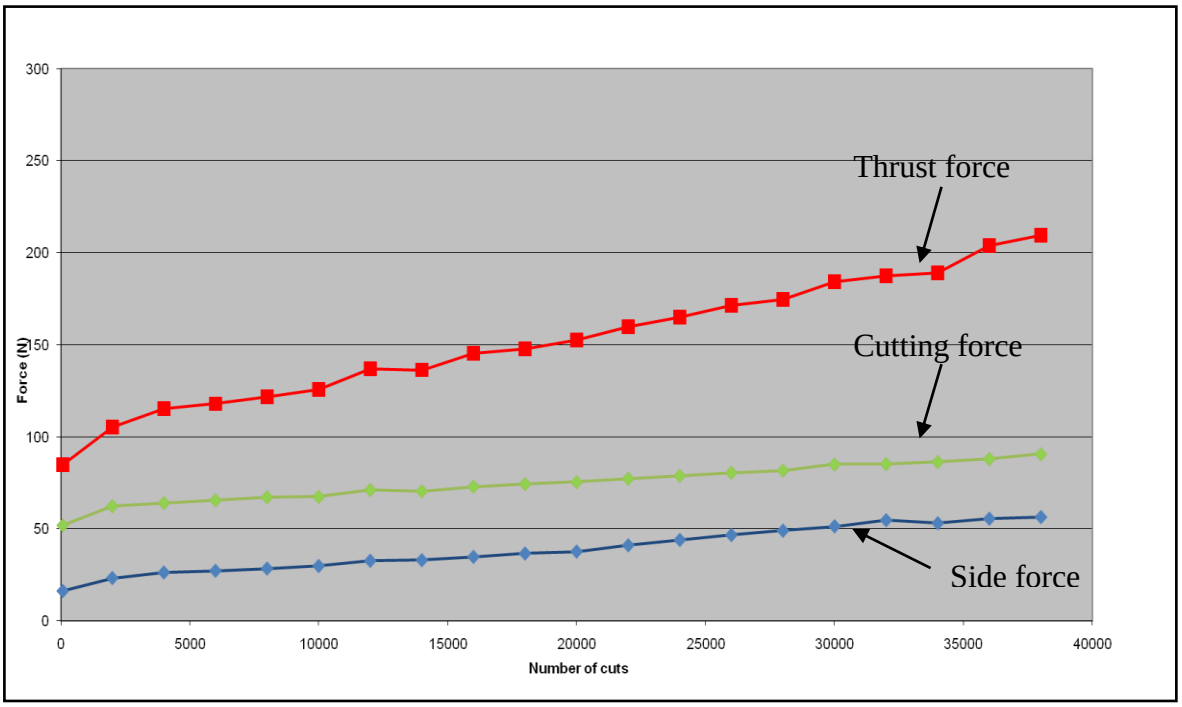

Figure 4.101. Variation of forces for AlTiN coated bandsaw tooth (cutting speed: 40 m/min, feed: 15 µm, width of cut: 1 mm, length of one cut: 0.6 m).

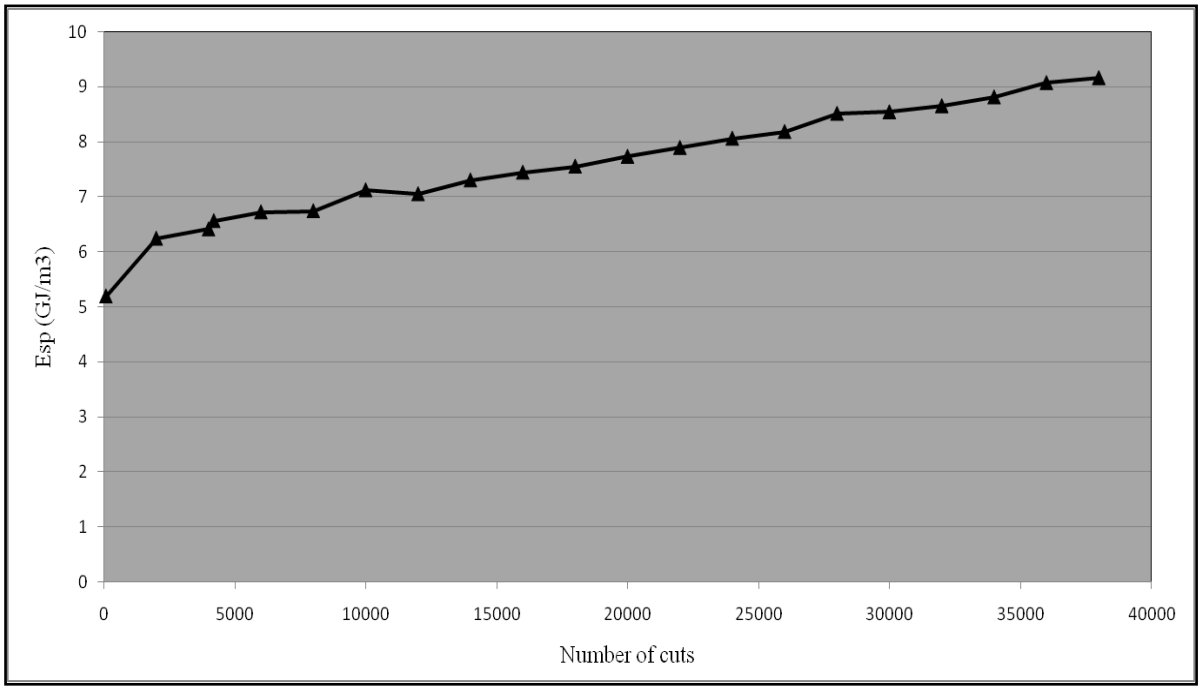

Figure 4.102. Variation in Esp for AlTiN coated bandsaw tooth (cutting speed: 40 m/min, feed: 10 µm, width of cut: 1 mm, length of one cut: 0.6 m).

The condition of the AlTiN coated bandsaw tooth at the end of the machining test is shown in Figure 103. It appears from Figure 4.103 that the rake face has chipped from the side of the tooth which, being weaker than the rest of carbide tooth, is engaging with the workpiece material. This probably happened during the first stages of machining and hence the sudden increase in force levels during the initial machining. The same SEM images taken in BSE mode are provided in Figure 4.104, which clearly shows the exposed tungsten carbide substrate on the cutting edge as well as some adhering material on the worn flank face of the carbide tooth. The worn corner of the tooth is visible in Figure 4.104 (b) and it appears that workpiece material is also adhering onto the side of the carbide tooth. Figure 4.105 shows the magnified SEM images of the chipping at the rake face and the adhering workpiece material on the side of the AlTiN coated carbide tooth. It is clear from these images that the tooth geometry has been modified due to chipping of the cutting edge at the corner.

4.6.0 Wear modes and mechanisms for coated teeth

In all cases for the coated teeth, it was found that the tool life was controlled by flank and corner wear. The severity of the corner wear increased with the increase in feeds. The maximum wear appeared at the corner of the cutting edge that was engaged with the workpiece and gradually decreased across the width of the cutting edge. As stated previously, the corners of the teeth are not as strong as the rest of the carbide tooth and hence can degrade quickly. However, this could be due to the engagement of the cutting edge at an angle with the workpiece as a consequence of the set geometry of the bandsaw tooth. Chipping on the rake and flank face were observed on all the coated bandsaw teeth tested. Cyclic mechanical and thermal loading on the bandsaw tooth due to the periodic engagement and disengagement of the tooth with the workpiece during machining are responsible. Chipping of the cutting edge was identified as the principal wear mode for the coated bandsaw carbide teeth. Adhesion of workpiece was found on all the worn coated bandsaw teeth. However, the quantity of the workpiece material adhering to the worn flank face was less compared to the quantity found on un-coated teeth, from which it can be concluded that the forces experienced by the coated teeth are less as compared to the forces experienced by un-coated teeth and therefore less adhesive wear. The coated teeth may have experienced plastic deformation during the machining operation, which may have contributed to the formation of cracks on the cutting edge. Figure 4.106 shows the chipping on the rake and flank faces, along with adhering workpiece material. EDX

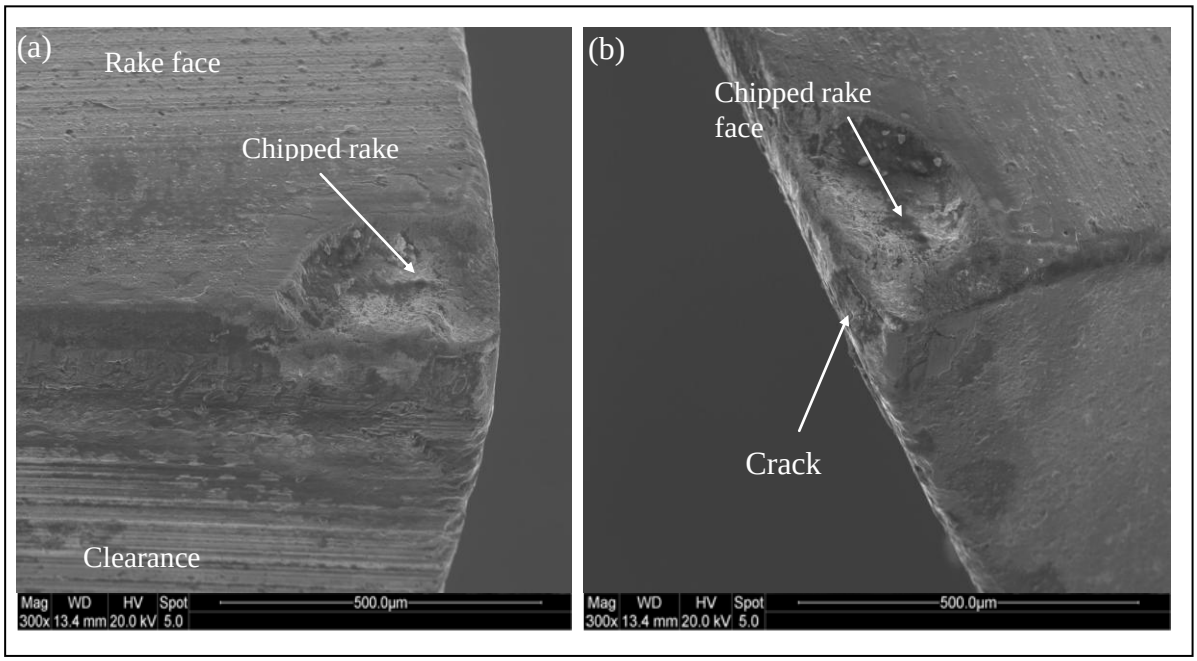

Figure 4.103. SEM micrographs of AlTiN coated carbide tooth (a) magnified view of the corner of the cutting edge and (b) side view of the worn tooth (cutting speed: 40 m/min, feed: 10 µm, width of cut: 1 mm).

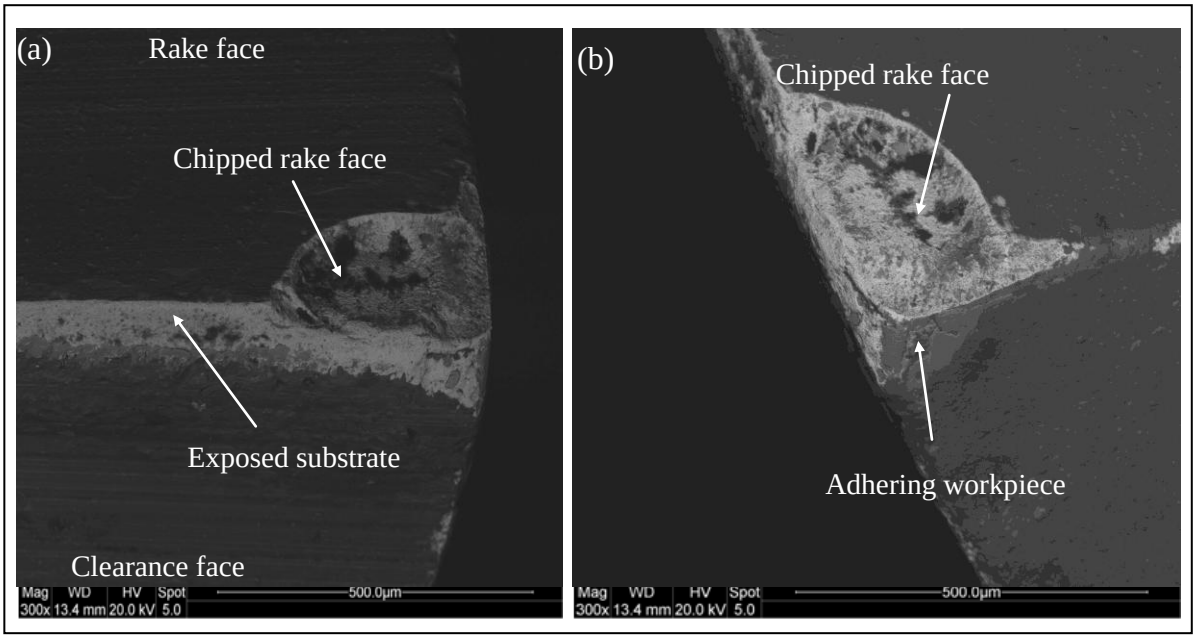

Figure 4.104. SEM images of AlTiN coated carbide tooth in BSE mode (a) magnified view of the corner of the cutting edge and (b) side view of the worn tooth (cutting speed: 40 m/min, feed: 10 µm, width of cut: 1 mm).

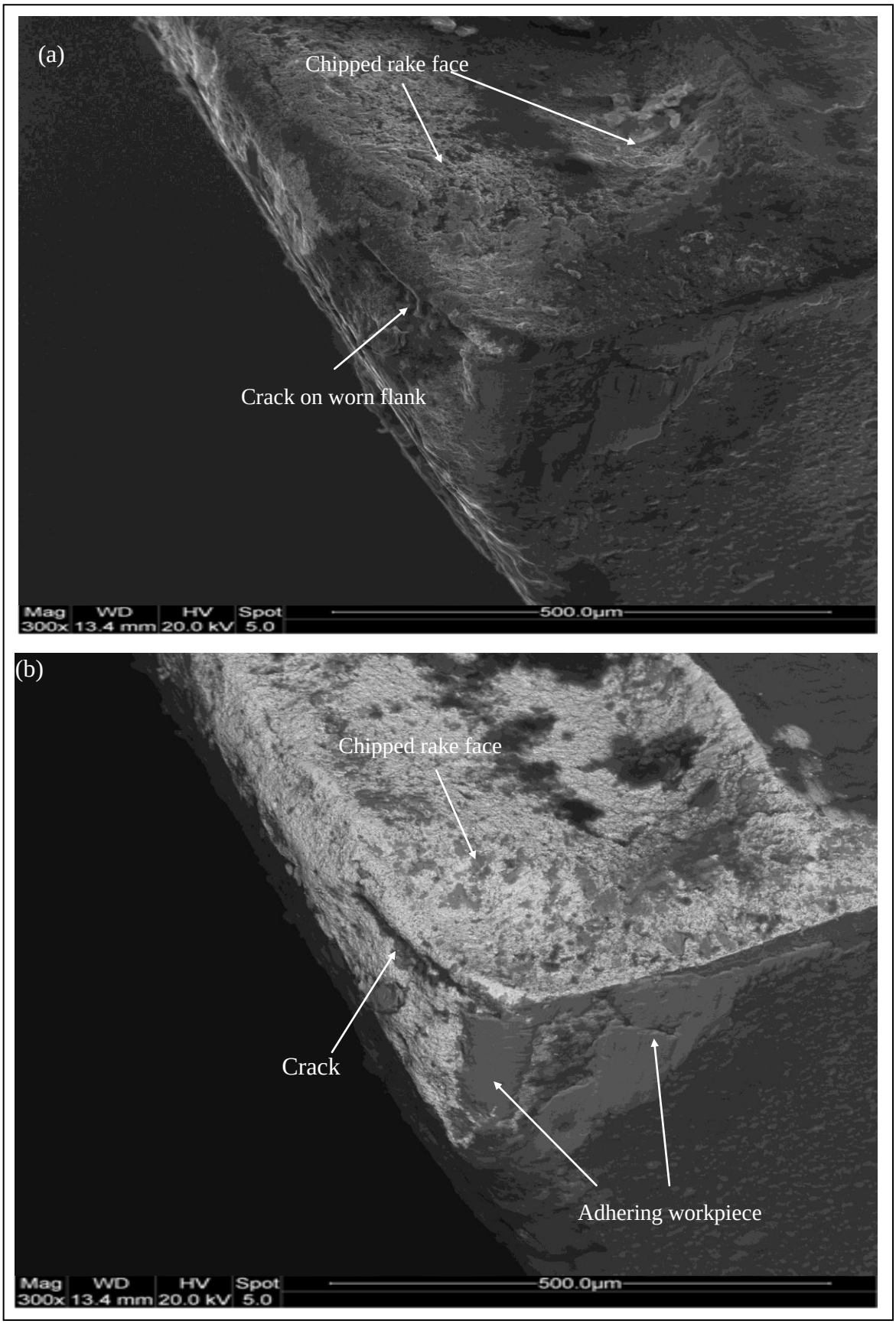

Figure 4.105. Magnified image of (a) the corner of AlTiN coated tooth and (b) BSE mode (cutting speed: 40 m/min, feed: 10 µm, width of cut: 1 mm).

analyses were carried out on the workpiece material adhering on the flank face on at least ten different points. The EDX analyses confirmed that the adhering material has the same elemental composition as that of the workpiece material and also revealed the presence of carbon and cobalt. Therefore, it confirms diffusion taking place between the substrate and the adhering material. Although, the main function of coatings is to arrest diffusion, however, once the coatings are removed, which they inevitably are, the diffusion process is operative. A new layer of workpiece material begins to replace the previously adhering material, after the later has been removed from the cutting edge. This adhering workpiece layer, after being removed from the cutting edge, also plucked the hard particles from the tool causing a gradual increase in the flank wear. Therefore, adhesion at the cutting edge was identified as another wear mechanism for the coated bandsaw teeth.

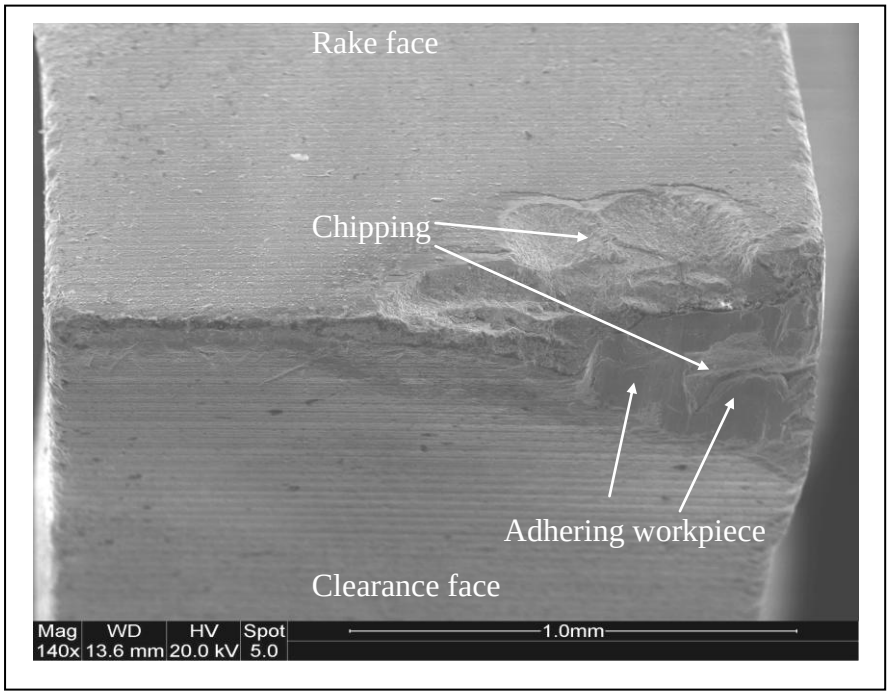

Figure 4.106. TiAlSiN worn tooth, showing chipped cutting edge along with the adhering workpiece on the worn flank face (cutting speed: 40 m/min, feed: 10 µm, width of cut: 1 mm).

However, from the presence of carbon and cobalt in the EDS analyses, diffusion can be identified as the wear mechanism for the coated bandsaw teeth during the steady wear of the coated teeth, while machining Ti-17 alloy. Attrition wear (removal of grains of tool material by the adherent chip or by the workpiece) was observed on the cutting edge of

coated carbide tools for all cutting conditions. The uneven worn surface suggested that fragments of tool material were "plucked" away by the adherent workpiece – as evident in Figure 4.107. Loss of particles due to attrition wear was also observed on the rake face of the worn coated teeth. It should also be mentioned with confidence that the attrition wear mechanism intensifies with the passage of time, resulting in serious damage to the tool edges. The wear modes and mechanisms for the coated teeth are summarized in Table 4.11.

Table 4.11. Summary of wear modes and mechanisms for the coated teeth.

	Initial wear stage	**Steady state wear**	**Tertiary stage wear**
Wear modes	Chipping at cutting edge	Flank formation, corner wear	Accelerated corner and flank wear, chipping
Wear mechanisms	Overloading at the cutting edge, leading to coating delamination	Mild adhesive wear, crack formation at edge, diffusion and attrition wear	Severe adhesive wear

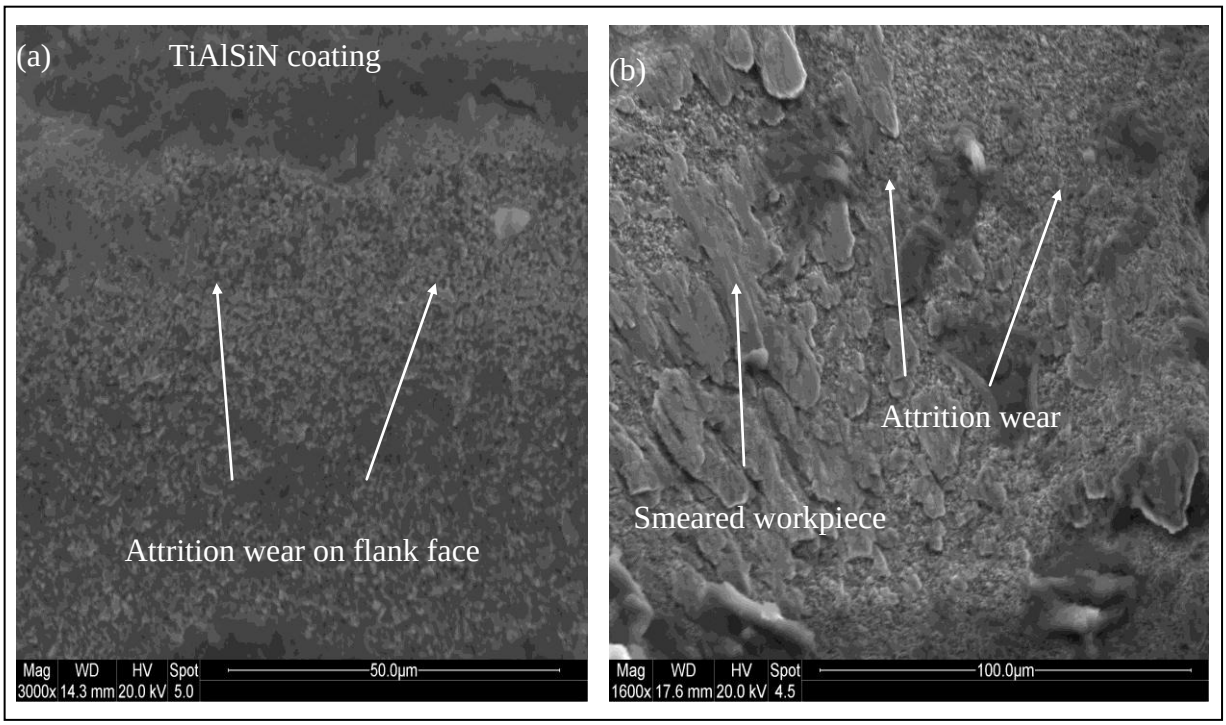

Figure 107. Worn surface of the coated teeth, showing attrition wear (a) cutting speed: 40 m/min, feed: 10 µm, width of cut: 1 mm (b) cutting speed: 40 m/min, feed: 15 µm, width of cut: 1 mm.

4.6.1 Summary of the performance of the coated teeth

As mentioned previously, two different coatings were used to evaluate the performance of the honed carbide bandsaw teeth. It was considered important to summarize the results for the performance of the coated teeth. Flank wear, chipping at the rake face as well as the flank face were observed for coated teeth *ie* AlTiN and TiAlSiN coated teeth. More degradation of the flank face was observed for both coated teeth compared to the rake face, although a considerable part of the rake face was found to be chipped. Non-uniform wear at the flank face was found to dominate on worn teeth for both types of coatings. Un-even wear on the tool face was observed suggesting attrition wear and diffusion wear taking place. The corner of the coated teeth seemed to experience more degradation in terms of wear as compared to the rest of the tooth. This is attributed to the corner being slightly weaker compared to the rest of the carbide tooth and can also be due to the set angle of the carbide teeth. Adhering workpiece material was identified on all the worn coated teeth, although the quantity of the adhered material appears to be less for the coated teeth compared to the un-coated teeth. Less adhering workpiece materials on the worn coated teeth is due to less friction between the coated teeth and the workpiece and hence lower temperatures at the interface compared to the un-coated teeth. Another factor that leads to adhering of workpiece material is the general tendency of titanium alloys to "stick" to almost all the cutting tools due to their high chemical reactivity. The workpiece material seems to be adhering well on the worn surface of the tool demonstrating a strong bond since there is no evidence of a gap between the tool and the adhered material. As in the case of un-coated carbide teeth, more adhering material was found on the worn flank face compared to the rake face. This suggests that the adhered material on the rake face has been removed by the flowing chip, which may have led to chipping of the tool material. The adhered workpiece material could lead to chipping as it will be hit and compressed by the tool upon its re-entry into the workpiece.

Examination of the coated carbide teeth, after they had performed 10000 cuts, for both coatings revealed that the coatings were removed from the substrate. Evidence of coating delamination is apparent in Figure 4.108 which shows the exposed substrate at various magnifications. After the coating has been removed, tool wear continued mainly at the flank face. The worn coatings exposed the substrate to chemical and attrition wear processes. It can be assumed with a high degree of confidence that coating delamination is the initial wear mechanism for AlTiN and TiAlSiN coated carbide teeth.

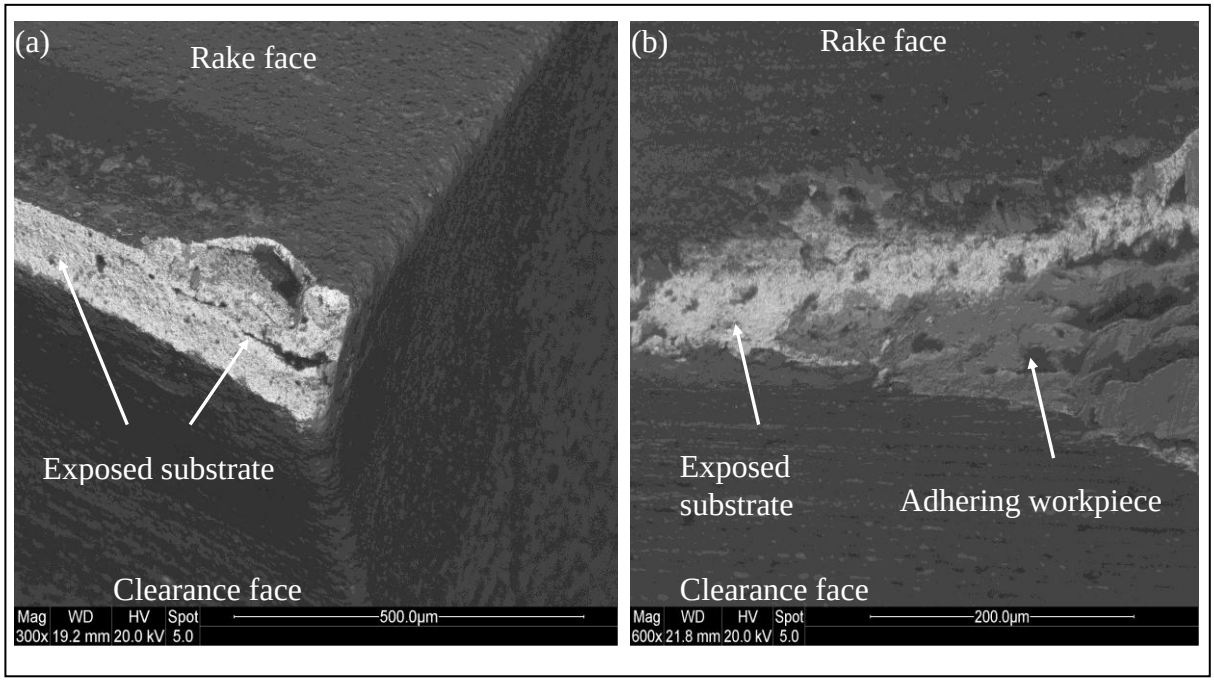

Figure 4.108. SEM images of (a) the AlTiN coated carbide tooth and (b) magnified image showing the exposed carbide substrate (cutting speed: 40 m/min, feed: 15 µm, width of cut: 1 mm).

Thermal cracks were observed at the cutting edges of worn coated teeth – see Figure 4.109. It can be seen clearly that micro-chipping took place at the cutting edge of the tools where the cracks propagated. After the delamination of the coatings, the erosion of carbide particles by attrition became much easier due to the diffusion of cobalt from the matrix.

No signs of abrasive wear or "self abrasion" could be observed on the coated worn carbide teeth. This is probably due to the fact that the workpiece material does not contain hard particles (such as carbides) which lead to abrasive wear on the cutting edge.

The performance of the TiAlSiN coated carbide teeth at three different feeds of 10, 15 and 20 µm is displayed in Figure 110 which shows the comparison of cutting forces for all three feeds but at a constant cutting speed of 40 m/min. It can be seen that the cutting forces for all feeds start from approximately the same magnitude of 60 N. However, the cutting force corresponding to high feed of 20 µm, increases considerably, suggesting that the tooth geometry is being modified in terms of wear, due to aggressive machining conditions. However, the forces corresponding to low feeds of 10 and 15 µm remain steady during the test, suggesting easier cutting condition and gradual wear of the cutting

edge. Similar trends in terms of cutting forces were observed for the teeth coated with AlTiN coatings – see Figure 4.111.

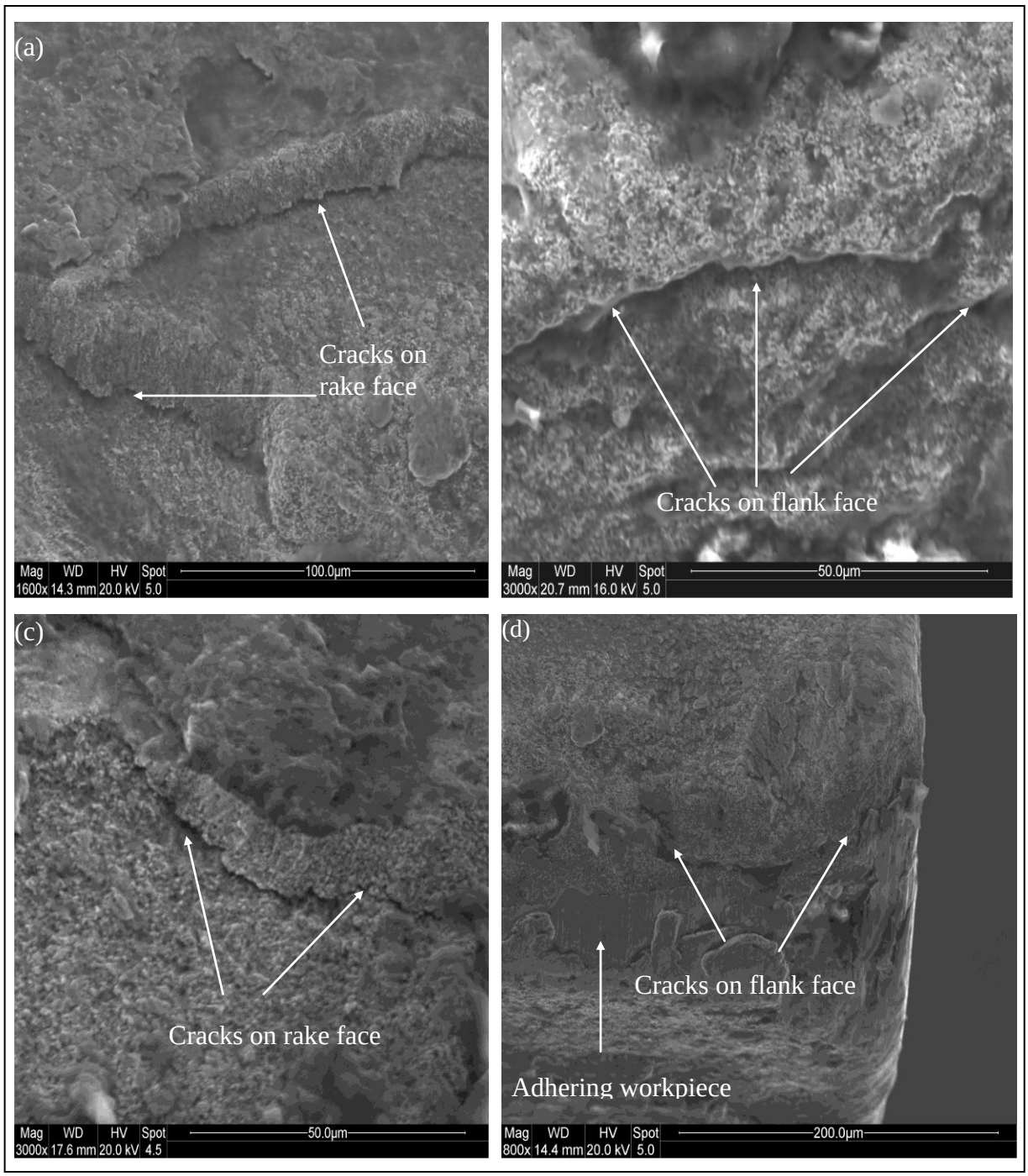

Figure 4.109. Cracks on the worn coated carbide cutting edge (a) and (b) AlTiN coated and (c) and (d) TiAlSiN coated (cutting speed: 40 m/min, feed: 15 µm, width of cut: 1 mm).

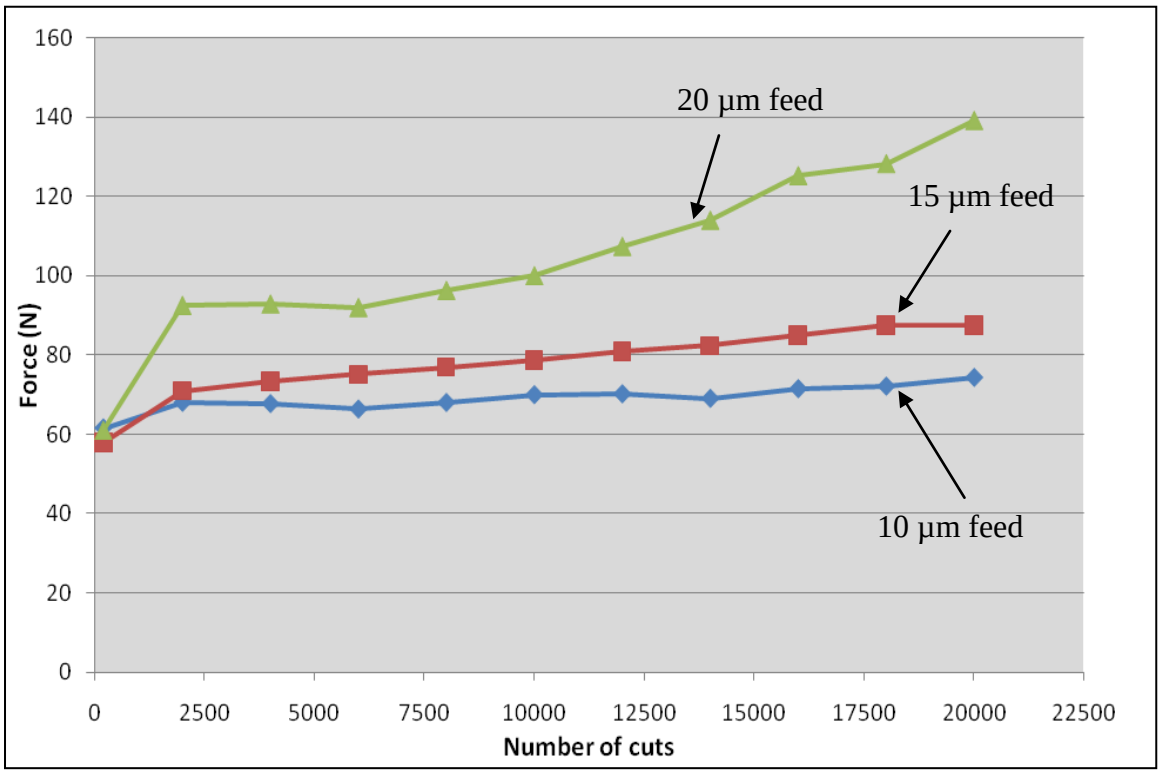

Figure 4.110. Comparison of cutting forces for TiAlSiN coated teeth at different feeds (cutting speed: 40 m/min, width of cut: 1 mm, feed: variable, length of one cut: 0.6 m).

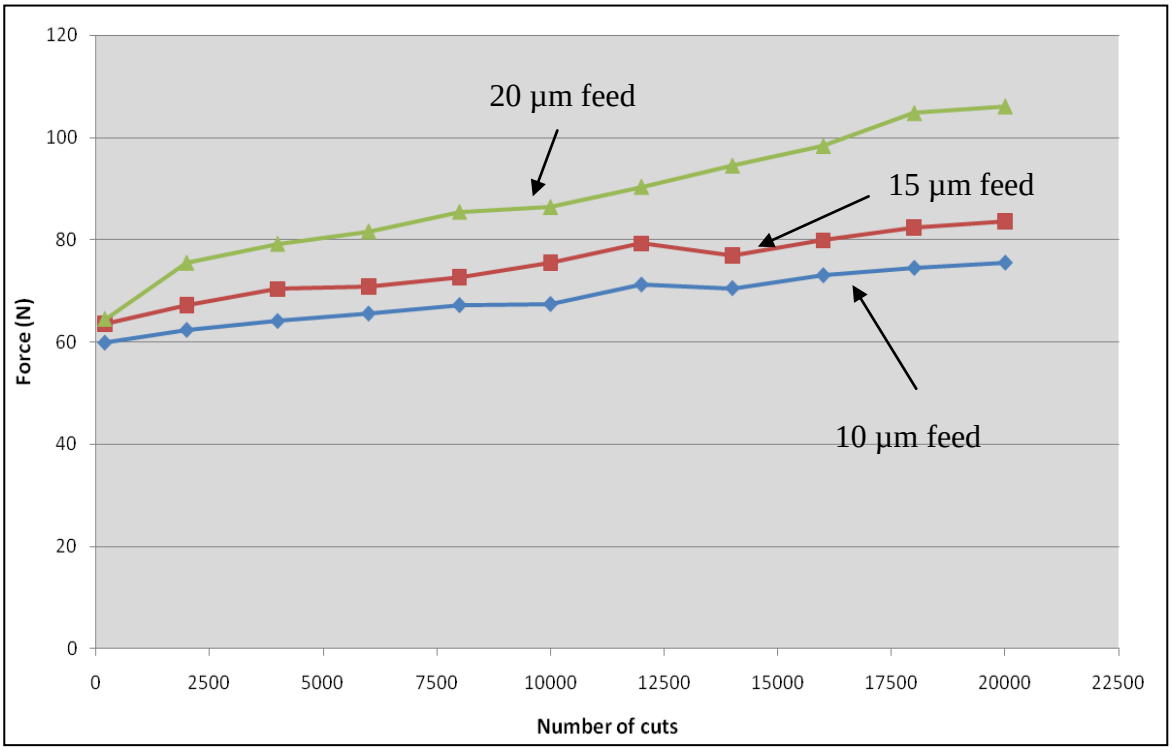

Figure 4.111. Comparison of cutting forces for AlTiN coated teeth at different feeds (cutting speed: 40 m/min, width of cut: 1 mm, feed: variable, length of one cut: 0.6 m).

4.7.0 Comparison of the performance of un-coated and coated teeth

After evaluating the performance of the un-coated and coated bandsaw teeth at various machining parameters, it was considered important to compare the response of un-coated and coated bandsaw teeth. Two different parameters are used to compare their machining performance. These parameters are:

- Forces (cutting force)
- Specific cutting energy

Although both parameters can be used for comparing the performance, Esp has the advantage that it also takes into account the area of the tooth which is actually performing the machining operation.

Unused un-coated and coated teeth were employed for these experiments, in order to avoid any contribution of worn cutting edge which is always present on the used teeth. All these teeth (un-coated and coated [TiAlSiN and AlTiN]) had similar physical characteristics such as rake angle, clearance angle and edge radius). Ten cuts were made at different feeds, ranging from 10 to 50 µm, *i.e.* within the bandsawing range. The forces were measured and the Esp was calculated and plotted against the depth of cut (or feed).

Figure 4.112 shows the comparison of cutting forces experienced by the un-coated, and TiAlSiN and AlTiN coated teeth while machining Ti-17 alloy at a cutting speed of 30 m/min and at variable feed between 10 to 50 µm. It is clear from Figure 4.112 that the cutting forces are less for the TiAlSiN and AlTiN coated tooth compared to the un-coated tooth. This gives further evidence that the coated teeth experiences less force while machining Ti-17 alloy compared to the un-coated teeth, due to less friction between the tool and the workpiece material. However, it must be noted that once the coating is removed from the carbide bandsaw teeth, as they inevitably are, the force experienced by the coated teeth will become higher. Furthermore, it is also important to consider the case if major change alters the physical geometry of the coated teeth (such as chipping), the forces will become higher. In fact, the forces can become higher for the coated teeth than the un-coated teeth if chipping takes place on the coated teeth and the un-coated cutting edge remains intact. Figure 4.113 represents the variation of the Esp with the depth of cut for the un-coated, TiAlSiN and AlTiN coated carbide teeth. It is evident from Figure 4.113 that coated teeth perform the machining operation more efficiently compared to the un-coated teeth since it requires less energy to machine the Ti-17 workpiece material using coated teeth. It appears that AlTiN coated tooth performs slightly better at a low feed of 10

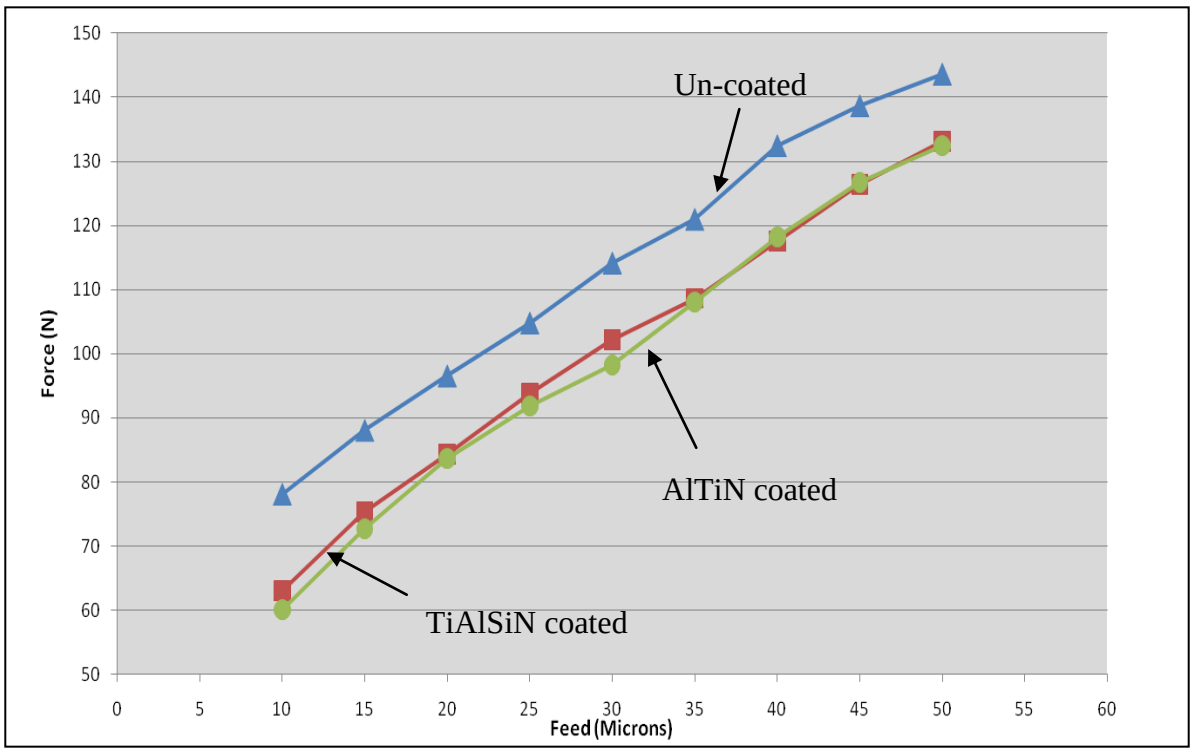

Figure 4.112. Variation of cutting forces for un-coated, and TiAlSiN and AlTiN coated teeth (cutting speed: 30 m/min, feed: variable, width of cut: 1 mm).

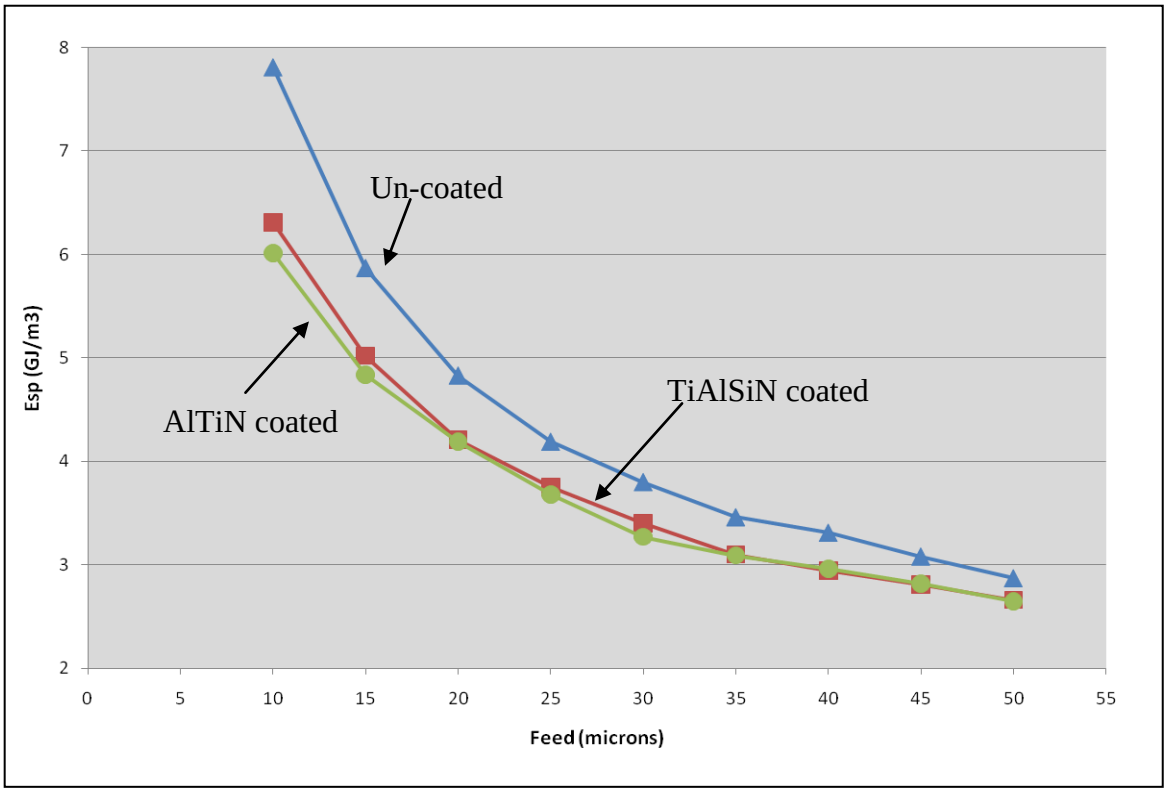

Figure 4.113. Comparison of Esp values *vs.* the feed for un-coated, and TiAlSiN and AlTiN coated teeth (cutting speed: 30 m/min, width of cut: 1 mm, feed: variable).

µm. This can be attributed to the low friction between the Ti-17 workpiece and AlTiN coated carbide bandsaw teeth, since low friction leads to low force and hence a low value of Esp. However, the difference between both the coatings, in terms of Esp, even at low feed is insignificant.

From Figures 4.112 and 4.113 it is also evident that at high depths of cut (or feeds), the difference in Esp of the coated and un-coated teeth becomes less. Therefore, it may be concluded that at higher feeds, although the machining operation becomes more efficient (as indicated by low values of Esp), the difference in performance between the coated and un-coated teeth will not be significant. This conclusion is based on the basis that the difference between Esp values for both coated and un-coated teeth becomes less at higher feed values.

It was considered important to compare the cutting force for the un-coated and coated teeth for a number of specified cuts after which it can be assumed that the coating has been removed from the cutting edge.

Figure 4.114 compares cutting forces for the un-coated, and TiAlSiN and AlTiN coated teeth at a feed of 20 µm and at a speed of 40 m/min. It is clear from Figure 4.11 that the cutting forces are low for the coated teeth compared to the un-coated teeth. It can be observed that the cutting forces increase sharply for the un-coated tooth after it had performed 7000 cuts, whereas the force level remains the same for the coated teeth, with a general increasing trend. Moreover, it appears that the forces experienced by the coated teeth are very similar in magnitude, irrespective of the type of the coatings (AlTiN or TiAlSiN).

The variation of cutting forces for the un-coated and coated carbide teeth at a feed of 10 µm and at a cutting speed of 40 m/min is given in Figure 4.115. It can be seen from Figure 4.115 that the cutting force is less for the coated teeth compared to the coated teeth and the forces show a general increasing trend. Moreover, the cutting forces are very similar for the coated teeth, irrespective of the type of the coating (TiAlSiN or AlTiN). The smooth increase in the force levels indicates mild machining conditions. The comparison of Esp for the un-coated and coated carbide teeth for the cutting test carried out at a feed of 10 µm and at a cutting speed of 40 m/min is shown in Figure 4.116.

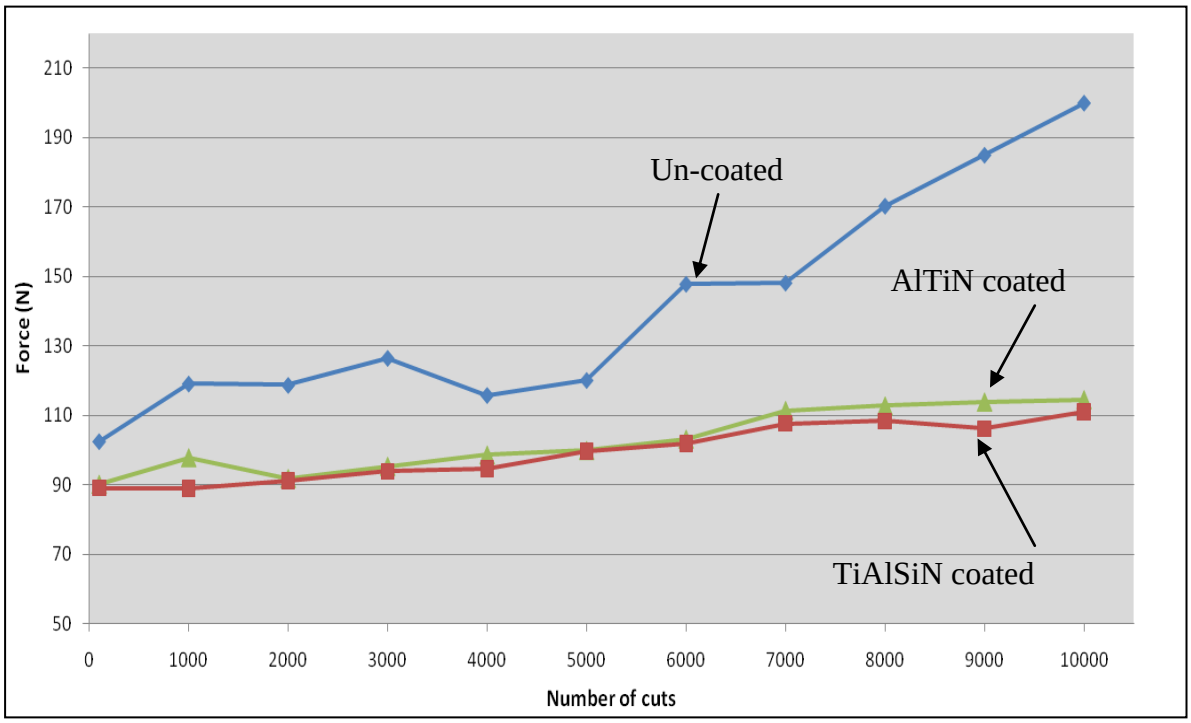

Figure 4.114. Variation in cutting forces for the un-coated and coated carbide teeth used at feed of 20 µm and at cutting speed of 40 m/min (width of cut: 1mm).

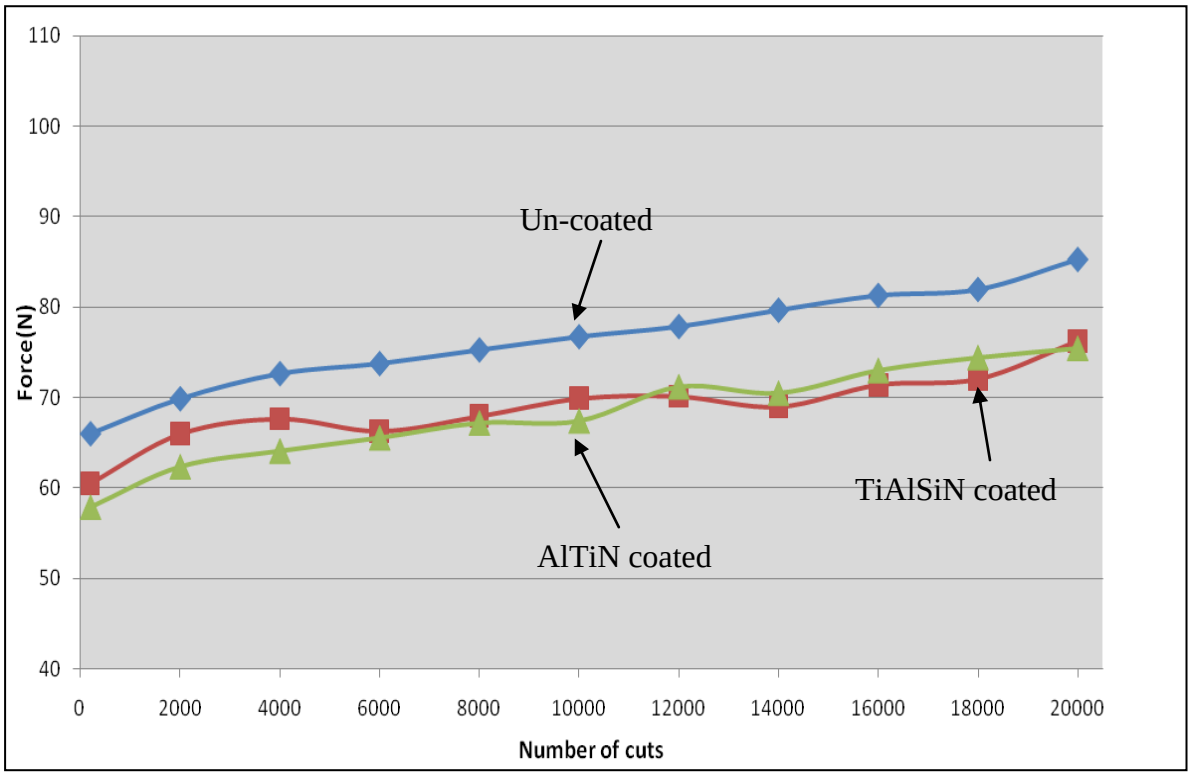

Figure 4.115. Variation in cutting forces for the un-coated and coated carbide teeth used at feed of 10 µm and at cutting speed of 40 m/min (width of cut: 1mm).

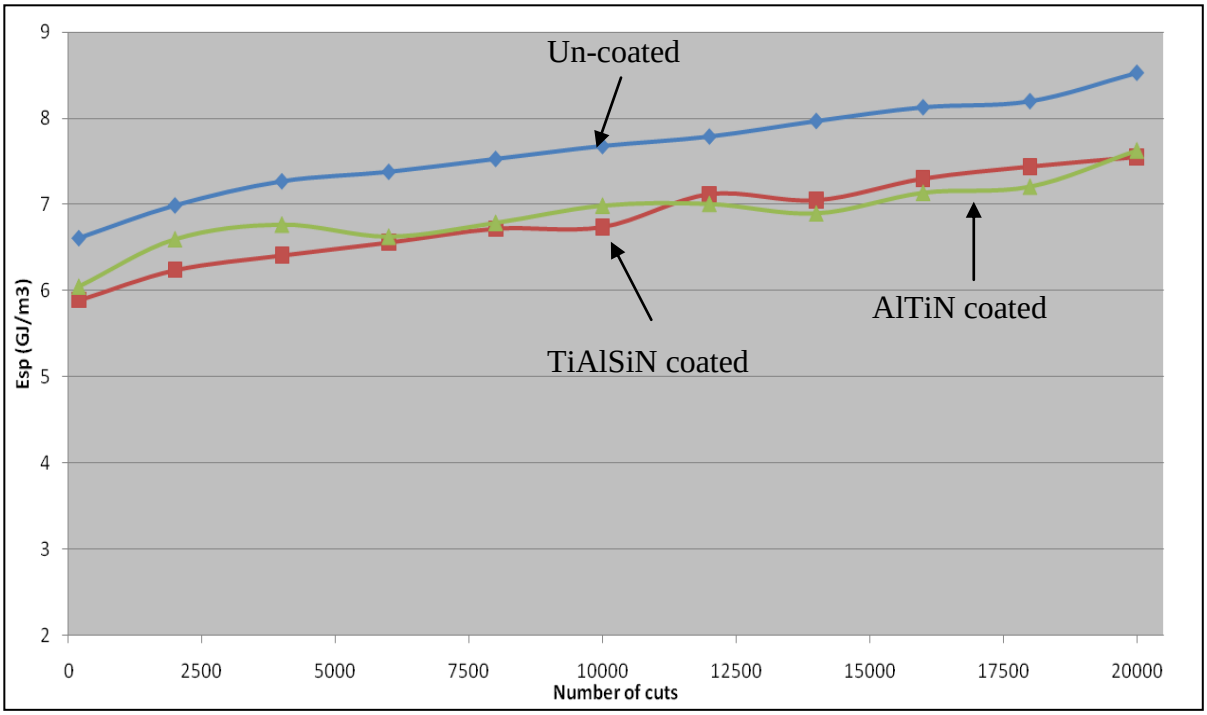

Figure 4.116. Comparison of Esp for un-coated and coated teeth with the number of cuts at the feed of 10 µm and cutting speed of 40 m/min (width of cut: 1mm)

The Esp values for the un-coated carbide tooth start from 6.5 GJ/m^3 and increase steadily to 8.5 GJ/m^3 after the tooth has performed 20,000 cuts, whereas the Esp values for the coated teeth start at approximately 6 GJ/m^3 and increase steadily to 7.5 GJ/m^3 at 20, 000 cuts. The steady increase in Esp indicates that the teeth are wearing gradually and that no significant change in the teeth geometry has taken place during the machining operation. The low value of Esp for the coated teeth also indicates that it is more efficient to machine Ti-17 alloy using coated teeth (AlTiN or TiAlSiN) in contrast to un-coated teeth.

4.7.1 Chip characteristics

There can be a difference in the characteristics and geometry of the chips produced at the beginning of the carbide teeth life and at the end. The chip ratio (un-deformed chip thickness to the deformed chip thickness) can change as the cutting edge geometry changes. In order to investigate this, chips were collected periodically and some optical images have been presented in the previous sections. The compressed chip thickness was measured using a micrometer gauge, at three different points on the chip. An average value was calculated using 5 chips. The same procedure was repeated using the chips

obtained whilst machining using coated teeth. A comparison of the chip ratios between the un-coated and coated teeth would elaborate the efficiency of the cutting process.

Figure 4.117 shows the comparison of the chip ratios between the un-coated, and TiAlSiN and AlTiN coated teeth under similar machining conditions of 20 µm feed and at a cutting speed of 40 m/min. It appears from Figure 4.117 that both types of coatings exhibit similar performance and with an increase in the number of cuts taken the chip ratio decreases, hence the cutting process becomes less efficient. However, due to the coatings, the cutting efficiency is higher compared to the efficiency of the un-coated tooth. However, at the end of the test, the ratios from the coated teeth are very similar to the chip ratio from the un-coated tooth. This is probably due to the coatings being removed as well as to the modification on the teeth geometry.

The same trend is observed at higher feeds of 15 and 20 µm as shown in Figure 4.118 and Figure 4.119. It appears from Figures 4.117 to 4.119 that at the end of the test, due to the removal of the coatings and to the modification in the teeth geometry the efficiency of the cutting process decreases. Furthermore, Figures 4.117 to 4.119 also reveal that both coatings show almost the same level of efficiency, thereby confirming the previous results.

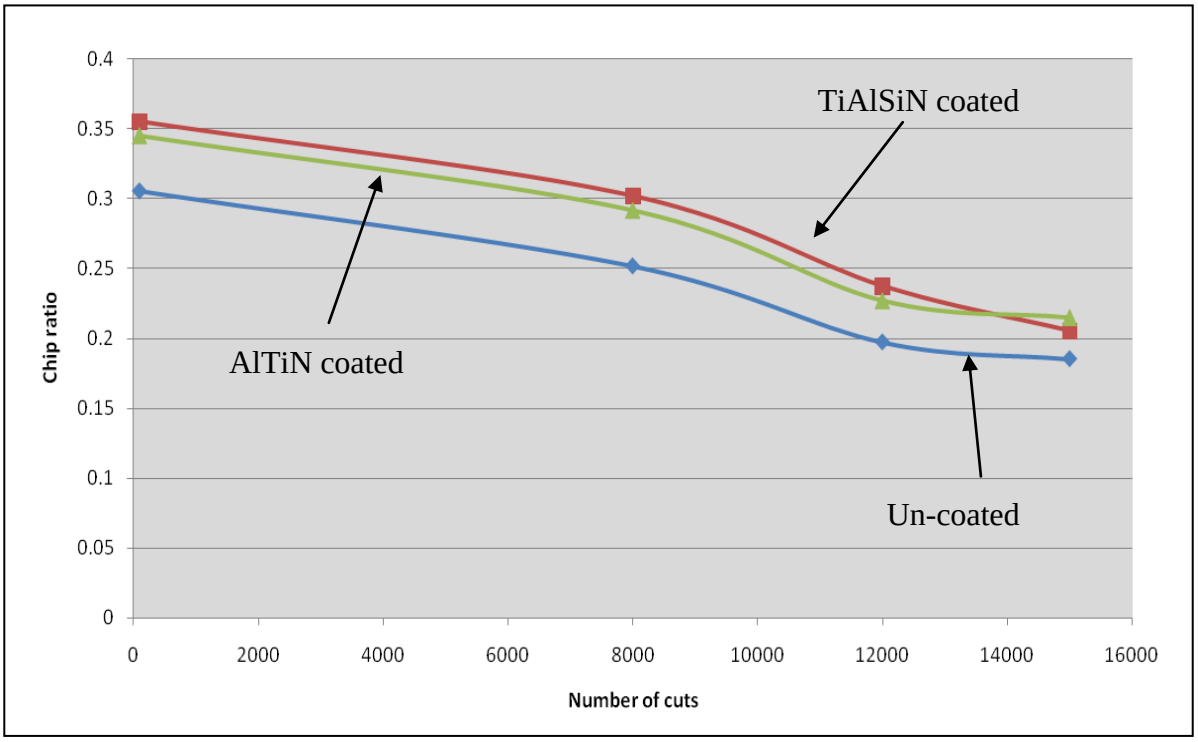

Figure 4.117. Comparison of the chip ratios for the un-coated and coated teeth (feed 20 µm, cutting speed: 40 m/min, width of cut: 1 mm, length of one cut: 0.6 m).

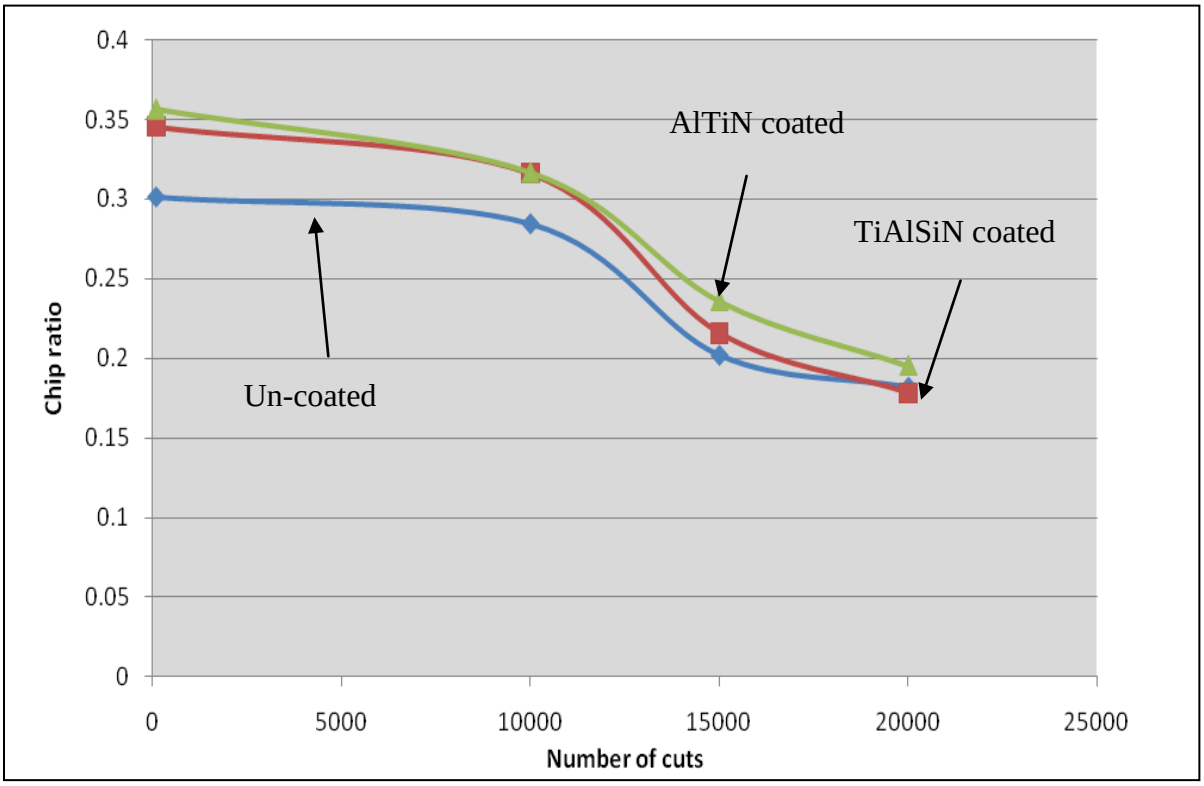

Figure 4.118. Comparison of the chip ratios for the un-coated and coated teeth (feed: 15 µm, cutting speed: 40 m/min, width of cut: 1 mm, length of one cut: 0.6 m).

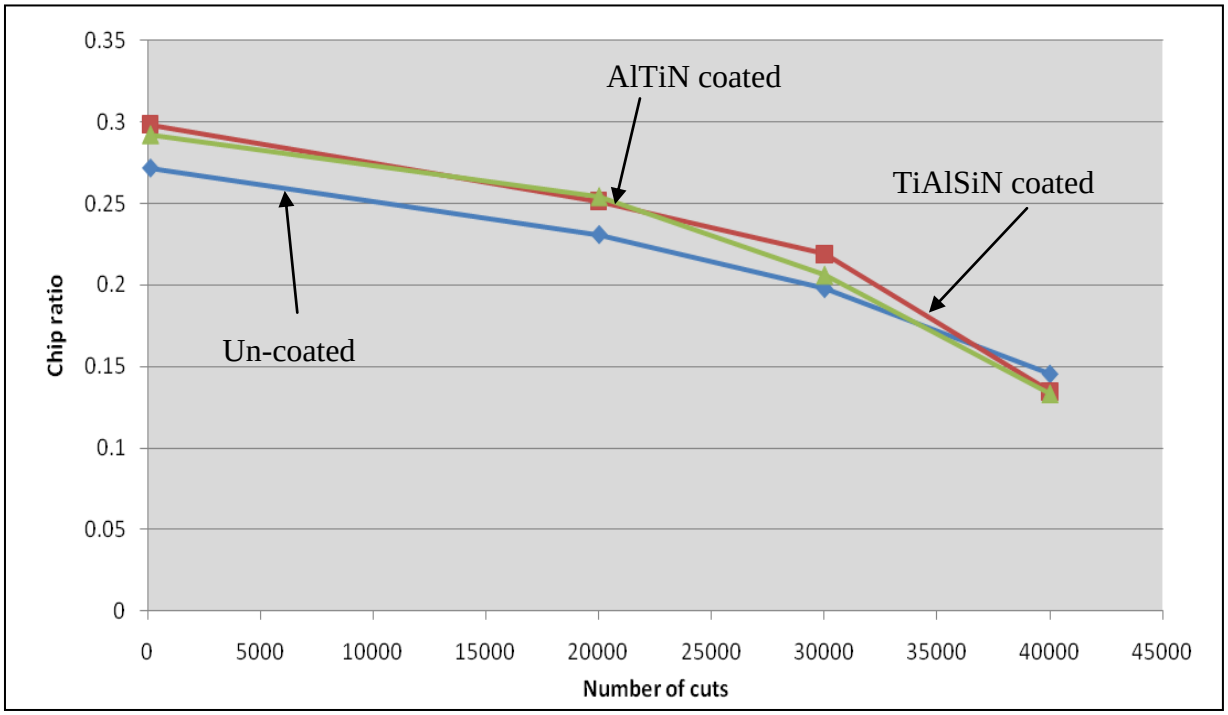

Figure 4.119. Comparison of the chip ratios for the un-coated and coated teeth (feed: 10 µm, cutting speed: 40 m/min, width of cut: 1 mm, length of one cut: 0.6 m).

4.8 Cutting tests using Mild steel

In all the machining tests carried out on the titanium workpiece using tungsten carbide bandsaw teeth, the thrust force was always found to be higher than the cutting force. This was irrespective of whether the teeth were un-coated or coated. This is a unique phenomenon, since in general the cutting force is usually higher than the thrust force, as is the case in machining steels and other conventional materials/alloys such as aluminium and copper alloys. Fang *et al* carried out turning of Ti-6Al-4V using rounded cutting edges and found out that at low feeds the cutting force is less than the thrust force [56]. They further explained this phenomenon using slip line modelling and attributed this to the magnified effect of the tool edge radius as well as to the properties of titanium alloys [57]. Hughes states that machining of titanium alloys leads to high thrust forces as well as workpiece deflection owing to the low modulus of elasticity of these alloys [188]. It was considered important to further investigate this phenomenon by using different workpiece materials, such as mild steel and bandsaw teeth with different edge geometry, *ie* sharp and honed.

Figure 4.120 depicts the results of the cutting test performed using a nominally sharp tooth with mild steel as the workpiece material at various feeds within the bandsawing range. The result, as expected, is a higher cutting force than the thrust force and the variation in forces with an increase in feed is linear.

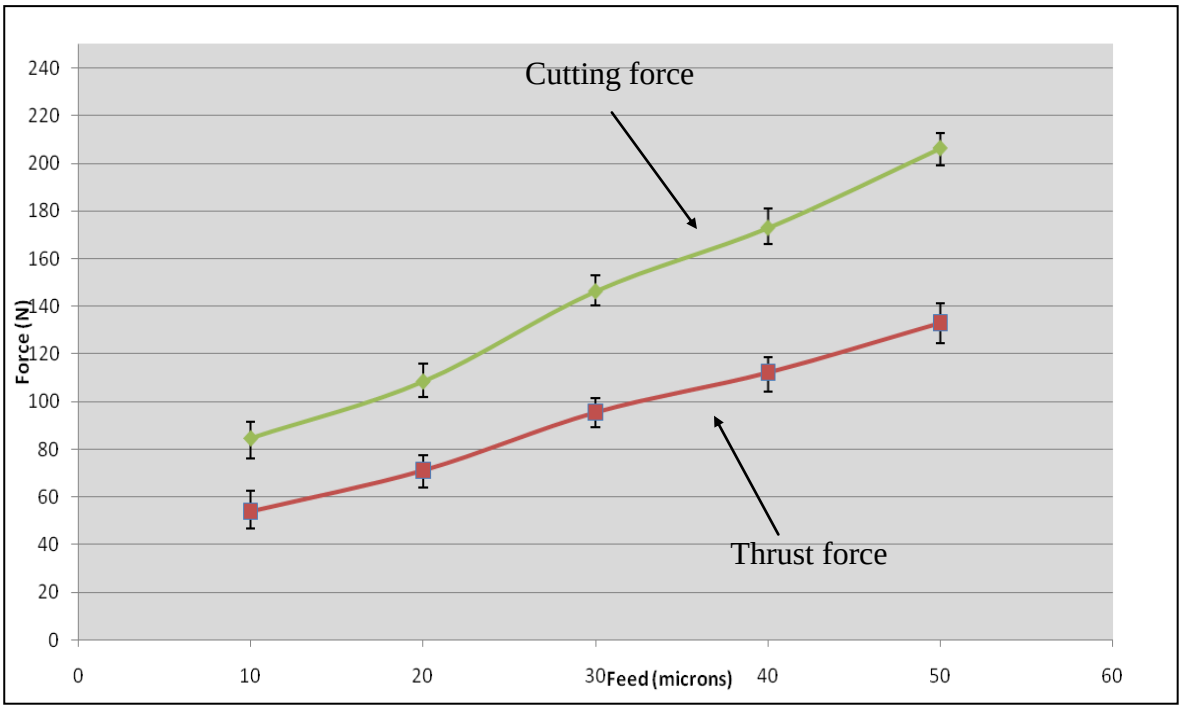

Figure 4.120. Force variation for nominally sharp tooth with mild steel as the workpiece material (width of cut: 1 mm, cutting speed: 30 m/min, feed: variable).

The results for machining mild steel, using a standard honed carbide tooth (honing length of 135 µm) are available in Figure 4.121. It can be observed that the cutting force is higher than the thrust force, as expected. The tests were repeated twice and similar results were obtained. Therefore it was concluded that the phenomenon of cutting force being lower than the thrust force is due to the unique nature of titanium as a workpiece material and the tooth geometry. Hence, it was decided to use carbide teeth with different edge geometries (nominally sharp and standard honed) and perform similar tests using Ti-17 alloy as the workpiece material.

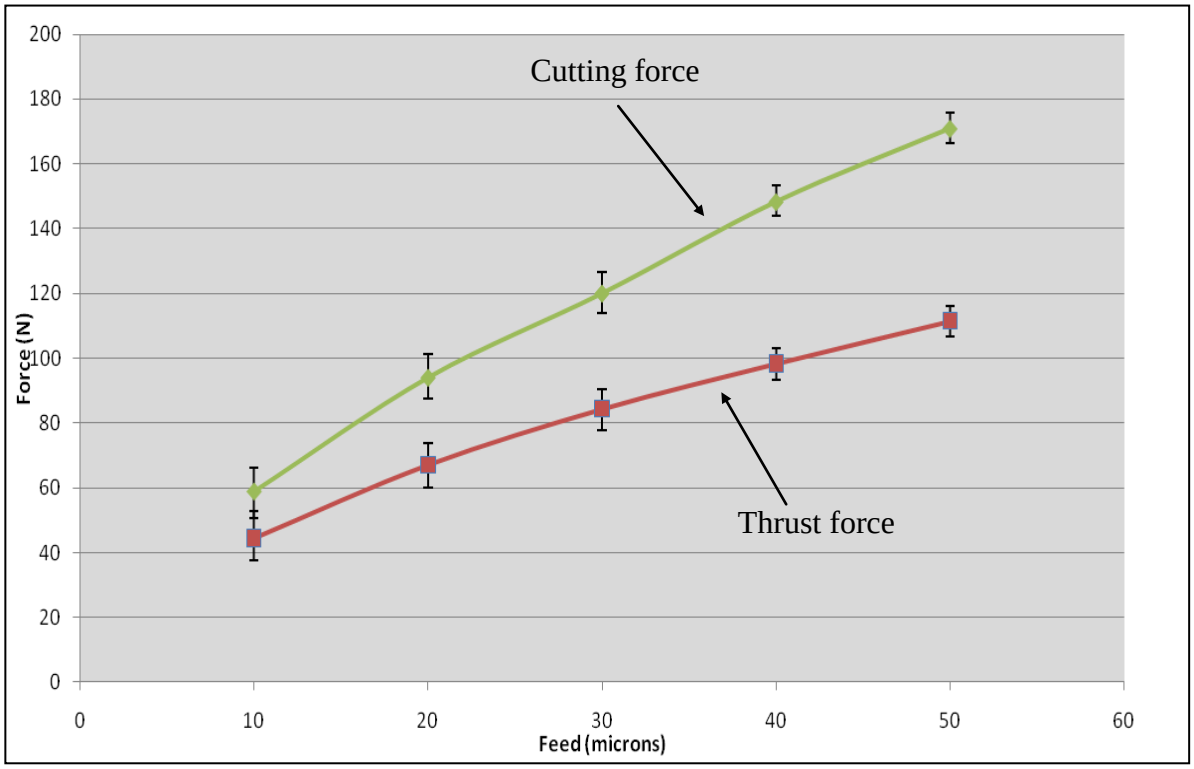

Figure 4.121. Force variation for standard honed tooth with mild steel as the workpiece material (width of cut: 1 mm, cutting speed: 30 m/min, feed: variable)

4.9 Cutting tests using Ti-17 alloy

Interesting results were obtained when Ti-17 alloy was machined using a nominally sharp tooth. Both cutting and thrust forces show a linear trend. The cutting force is lower than the thrust force, and after a 'cross-over' becomes higher than the thrust force – see Figure 4.122.

The results for machining titanium alloy using a standard honed carbide tooth (honing length of 135 µm) are given in Figure 4.123. The thrust force is always higher than the cutting force at all test feeds (*i.e.* within the 10 to 50 µm range). However, the cutting

force shows an increasing trend with an increase in feed; whereas the thrust force shows a decreasing (slight) trend throughout the feed range.

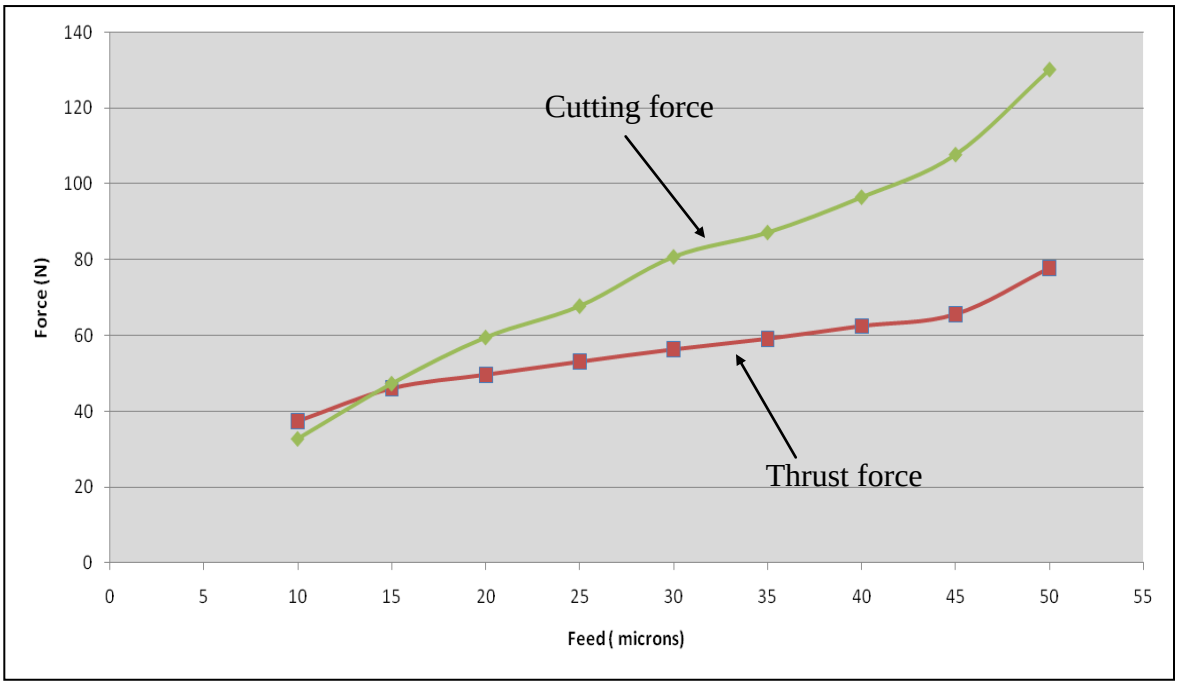

Figure 4.122. Variation in cutting and thrust force for nominally sharp tooth (workpiece: Ti-17, width of cut: 1mm, feed: variable, cutting speed: 30 m/min).

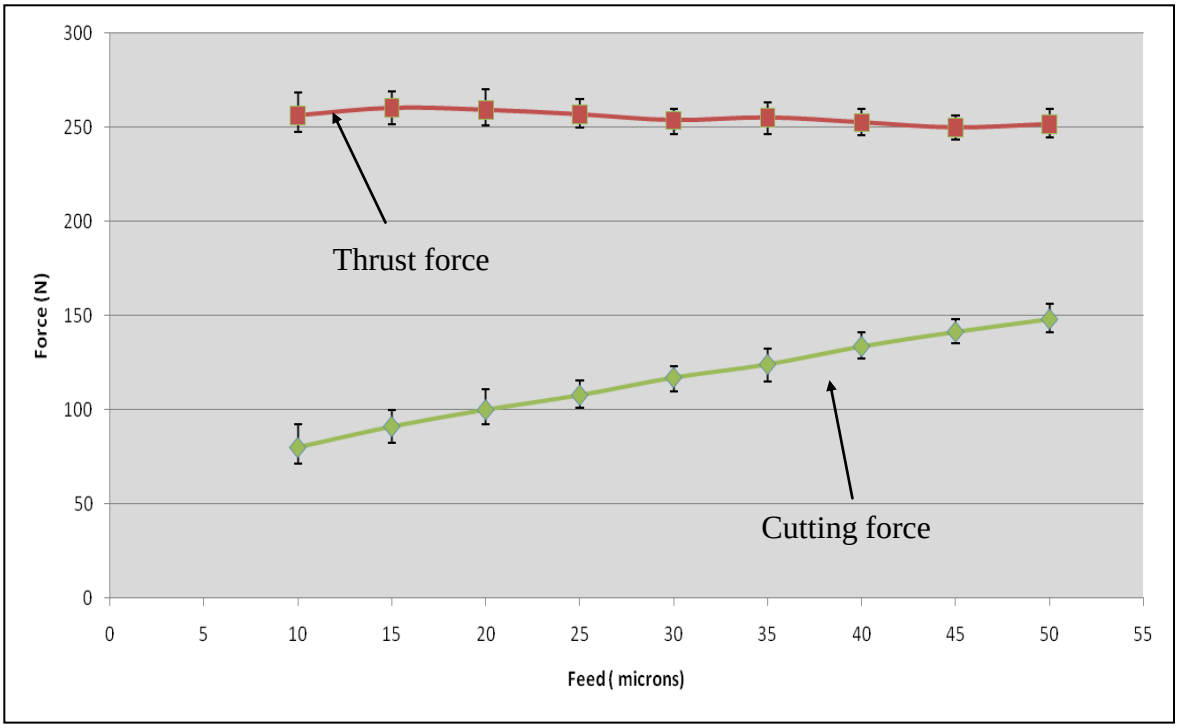

Figure 4.123. Variation in cutting and thrust force for standard honed carbide tooth (workpiece: Ti-17, width of cut: 1mm, feed: variable, cutting speed: 30 m/min)

4.10 Cutting tests using two different workpiece materials in sequence

In order to investigate the effect of the intrinsic properties of the two different workpieces, *i.e.* mild steel and Ti-17 alloy a series of tests was carried out using both workpiece materials simultaneously. Both workpieces were mounted on the chuck of the lathe and a standard honed carbide tooth, with a honing length of 135 µm was used to machine both workpieces. Interesting results were obtained as can be seen from Figure 4.124 which records cuts made by the carbide tooth on mild steel and Ti-17 alloy. It appears that when the tooth is performing the cut on the mild steel, the thrust force is lower than the cutting force, while the thrust force is higher than the cutting force when the tooth machines the Ti-17 alloy.

It appears from Figure 4.124 that the cutting forces are similar while machining both workpieces. However, the thrust force changes in magnitude. Therefore, it can be concluded that the higher magnitude of the thrust force whilst machining Ti-17 alloy is due to the workpiece properties.

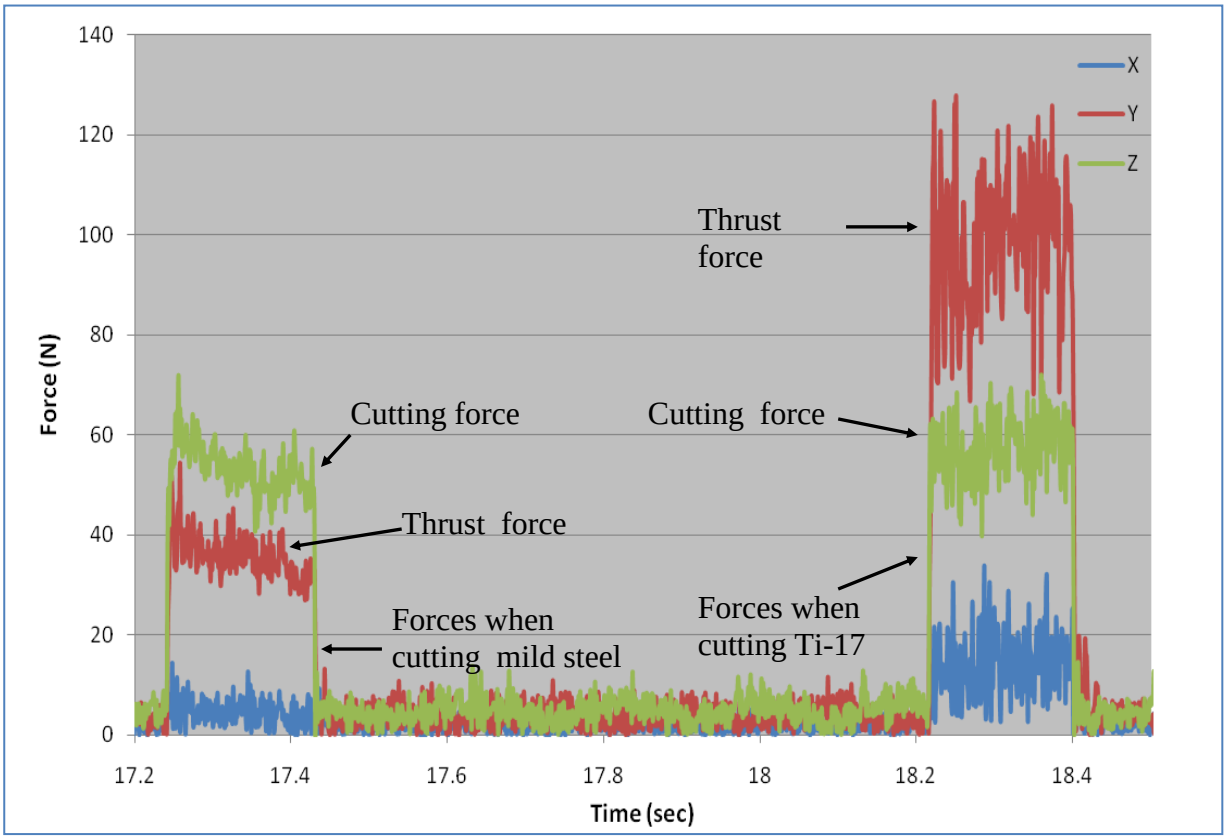

Figure 4. 124. Force graphs while machining mild steel and Ti-17 in a sequence (cutting speed: 30 m/min, feed: 15 µm, width of cut: 1mm).

4.11 Cutting tests using different honing lengths

In order to further investigate this phenomenon, a series of experiments was carried out using carbide bandsaw teeth with different levels of honing. Several different bandsaw teeth were honed to different lengths. The honing length was measured across the whole of the width of the tooth using the SEM and the final stated honing length is the average of at least 10 measurements across the width of the carbide tooth. An example of the measurement of the honing length is given in Figure 4.125.

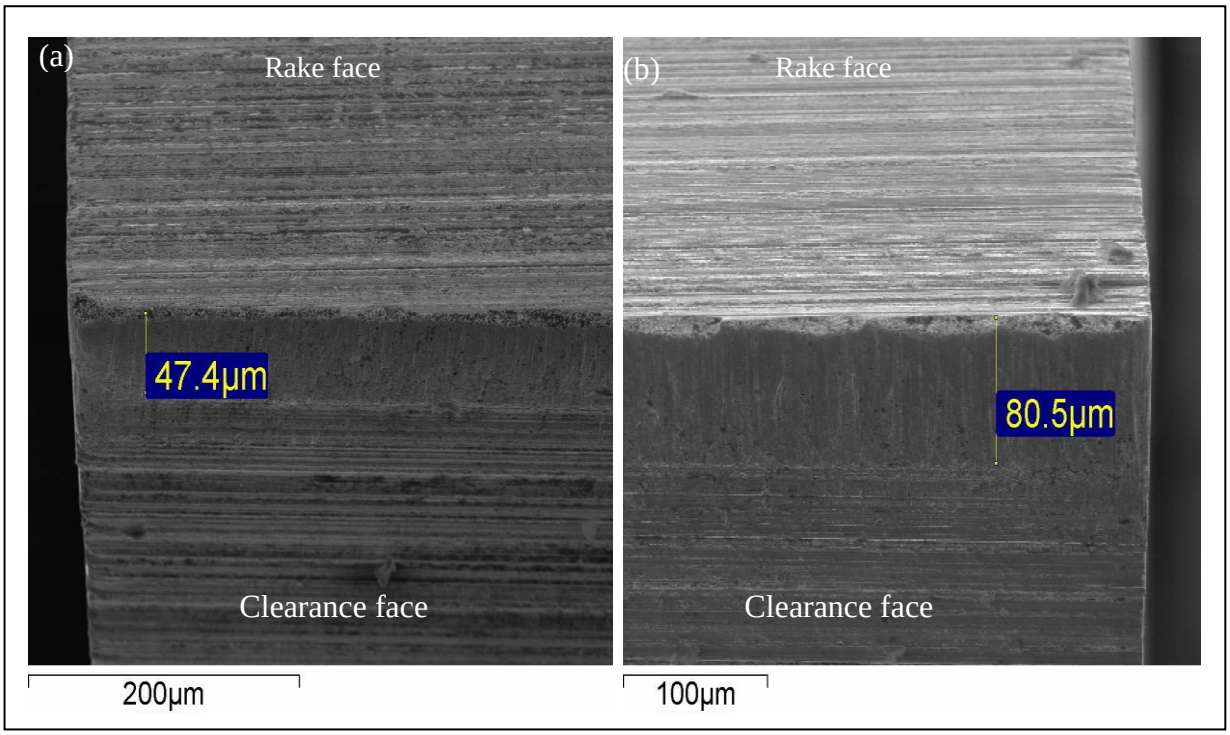

Figure 4.125. Measurement of the honing edge for two different carbide teeth, with different honing length on flank face.

In order to observe the effect of honing length on the cutting/thrust forces, it was decided to use carbide teeth with honing length less than the standard honing of 135 µm. Therefore, cutting tests were performed using two different carbide teeth with honing lengths of 52 and 72 µm respectively. Figure 4.126 displays the results of machining Ti-17 alloy using a carbide tooth with a honing length of 52 µm.

The result of machining Ti-17 using a carbide tooth with a honing length of 52 µm is very similar to the result obtained whilst machining Ti-17 alloy with a nominally sharp tooth, except that the "cross-over" point between the cutting and thrust force has moved to a higher magnitude in both force as well as feed values. The cutting force shows an

increasing, linear trend; whereas the thrust force shows a (slight) decreasing trend with an increase in feed.

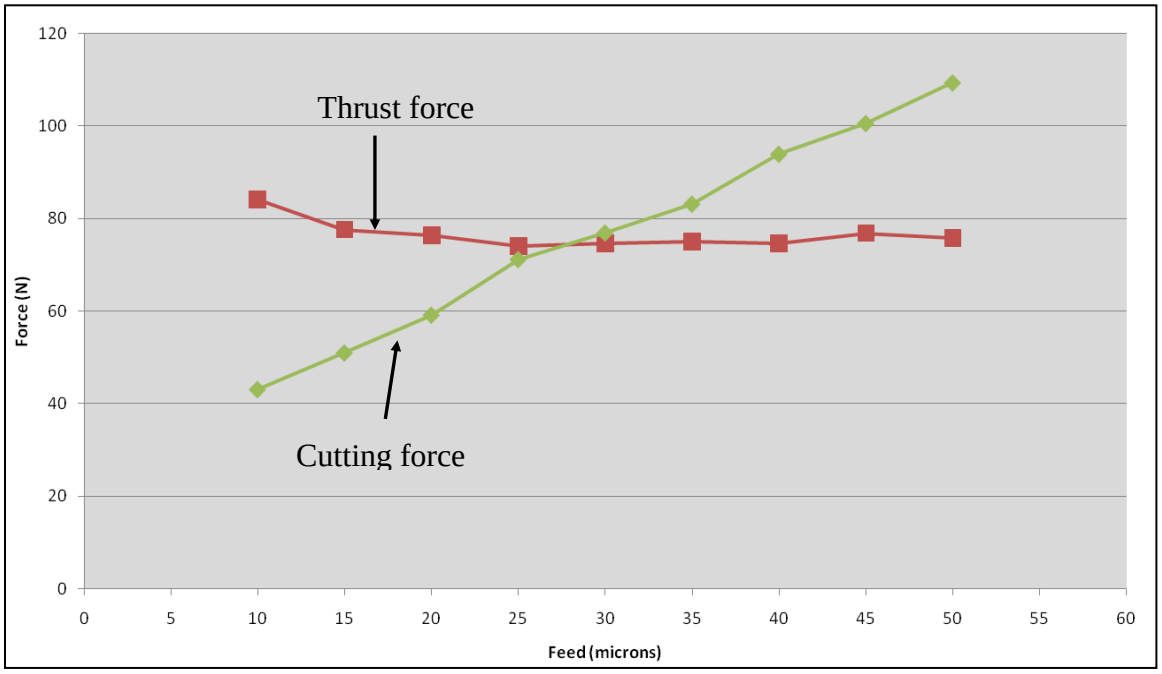

Figure 4.126. Cutting and thrust forces for carbide tooth with a honing length of 52 µm (cutting speed: 30 m/min, feed: variable, width of cut: 1 mm).

Figure 4.127 shows the results of machining Ti-17 alloy using a carbide tooth with a honing length of 72 µm. The trend observed in Figure 4.127 is very similar to the one observed in Figure 4.126, *i.e.* the cutting force increases linearly with an increase in feed, whereas the thrust force exhibits a slightly decreasing trend with an increase in feed. However, the difference is in the cross-over point between the forces. The cross-over point between the forces has moved to higher values of feed and force, with an increase in honing length. Figure4.128 is a comparison of the results and demonstrates the effect of honing on the thrust and cutting forces.

It was considered important to perform cutting tests on a carbide tooth with a honing length greater than the standard honing length of 135 µm. Therefore a cutting test was performed using a carbide tooth with a honing length of 202 µm. Figure 4.129 displays the results of machining Ti-17 alloy using a carbide bandsaw tooth with a honing length of 202 µm. From Figure 4.129, it can be seen that the thrust force is always higher than the cutting force and that the cutting force exhibits an increasing trend, whereas the magnitude of the thrust force decreases as the feed increases.

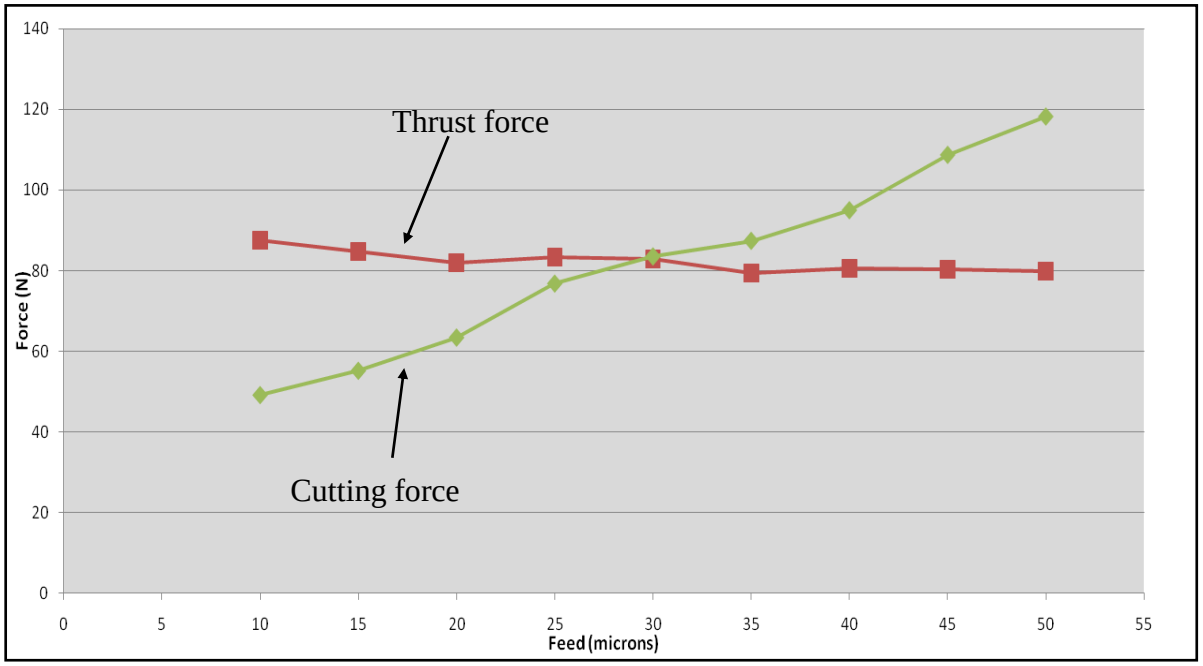

Figure 4.127. Variation of forces for carbide tooth with honing length of 72 µm (cutting speed: 30 m/min, feed: variable, width of cut: 1 mm).

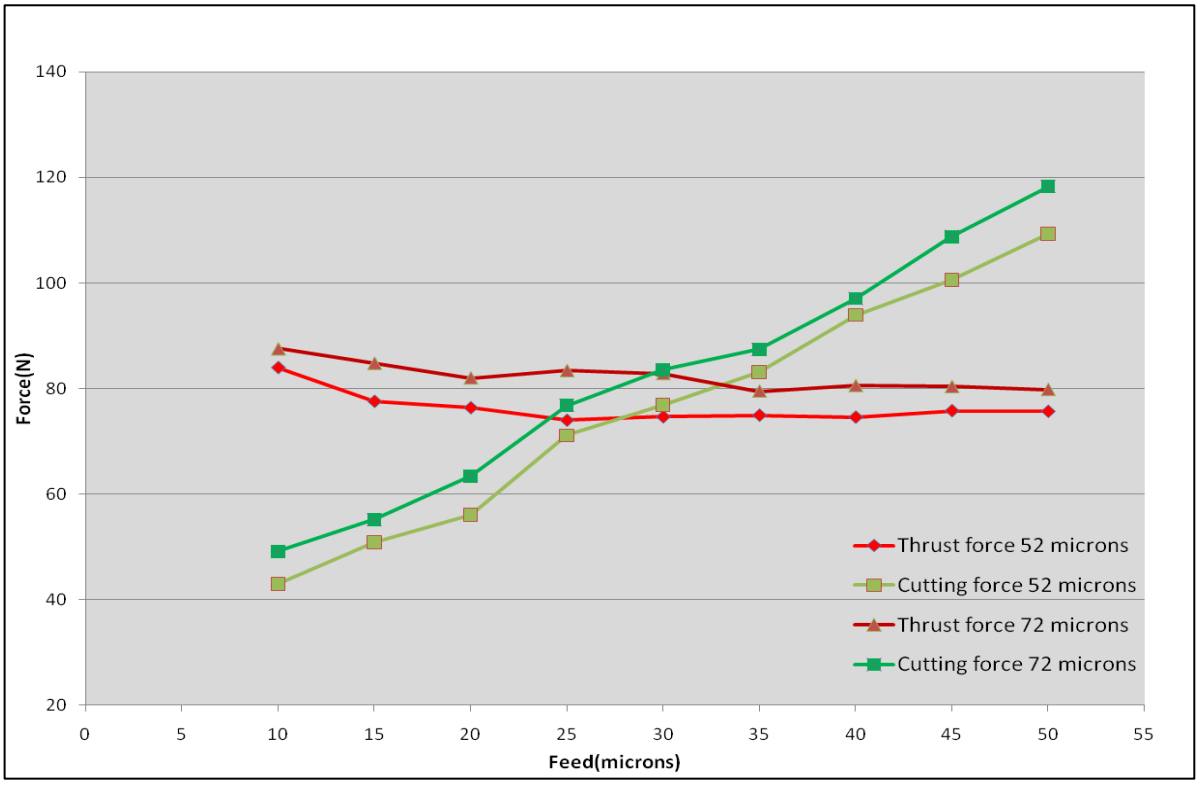

Figure 4.128. Comparison of forces, for the carbide teeth with different honing lengths.

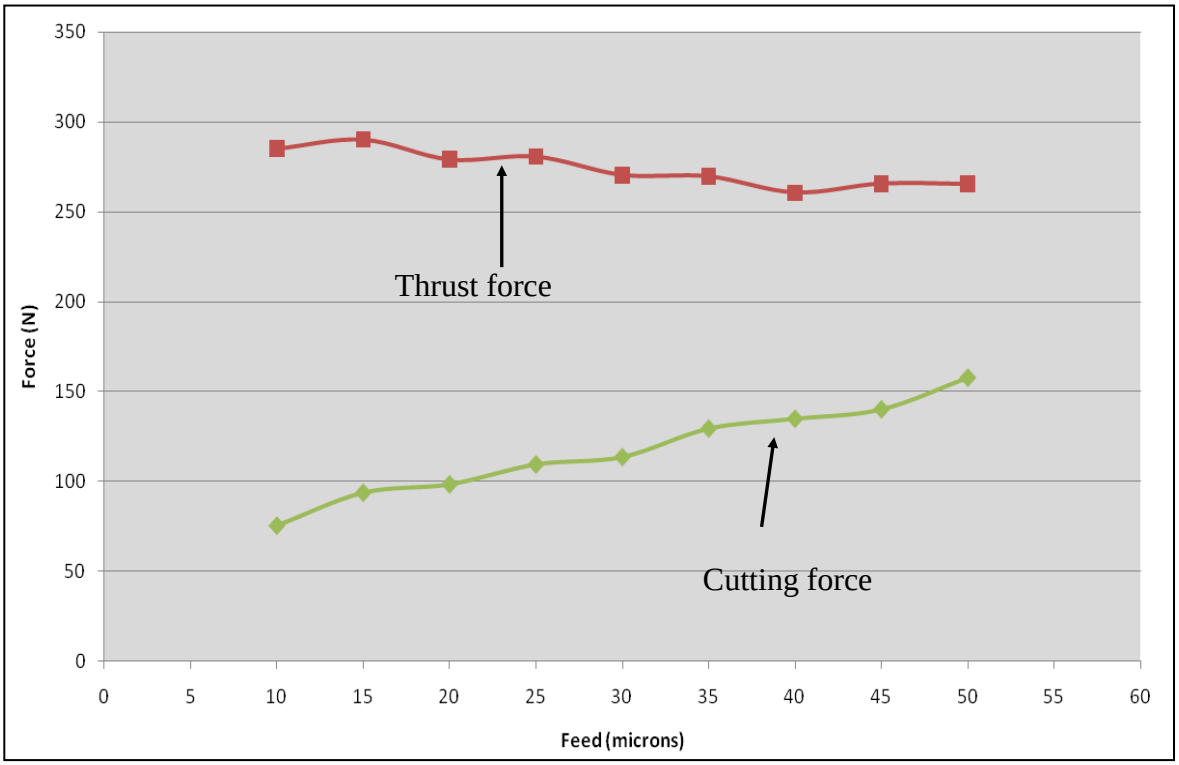

Figure 4.129. Variation of forces for the carbide tooth with honing length of 202 µm (cutting speed: 30 m/min, feed: variable, width of cut: 1 mm)

The comparison of forces obtained from teeth with standard honing length of 135 µm and from the tooth with a honing length of 202 µm offered interesting results– see Figure 4.130 which that the cutting force is not affected significantly by the increase in honing length, whereas higher is the honing on the flank face of the tooth, the higher is the thrust force.

The effect of changing the honing lengths on the flank face on the cutting and thrust forces at the feed of 15 µm is shown in Figure 4.131. From Figure 4.131 it can be seen that the increase in honing length has a large impact on the thrust force, whereas its effect on the cutting force is relatively minor. It further elaborates that the standard honed length chosen by the bandsaw manufacturers is the optimum compromise between the cutting and thrust force, as increasing the honing length beyond 135 µm, results in thrust force becoming very high and therefore this will adversely affect the performance of the carbide teeth in terms of wear.

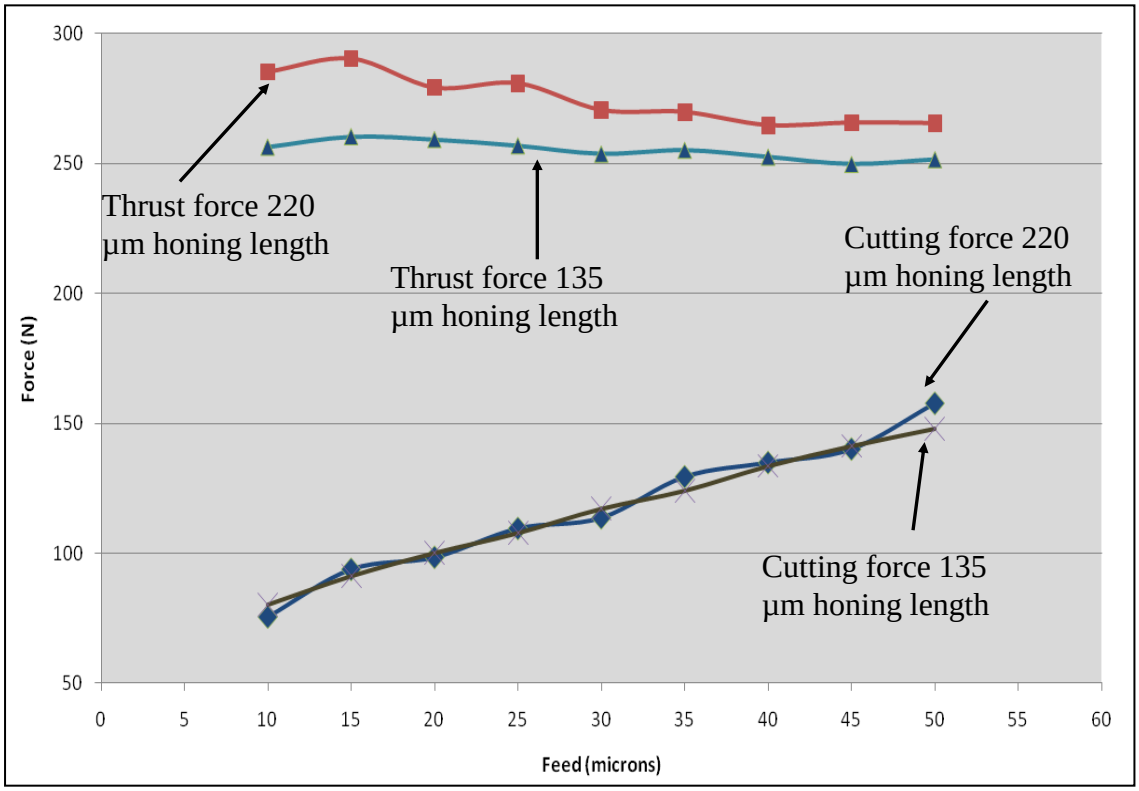

Figure 4.130. Comparison of forces obtained from a tooth with a honing length of 202 µm, with the forces for standard honing length of 135 µm.

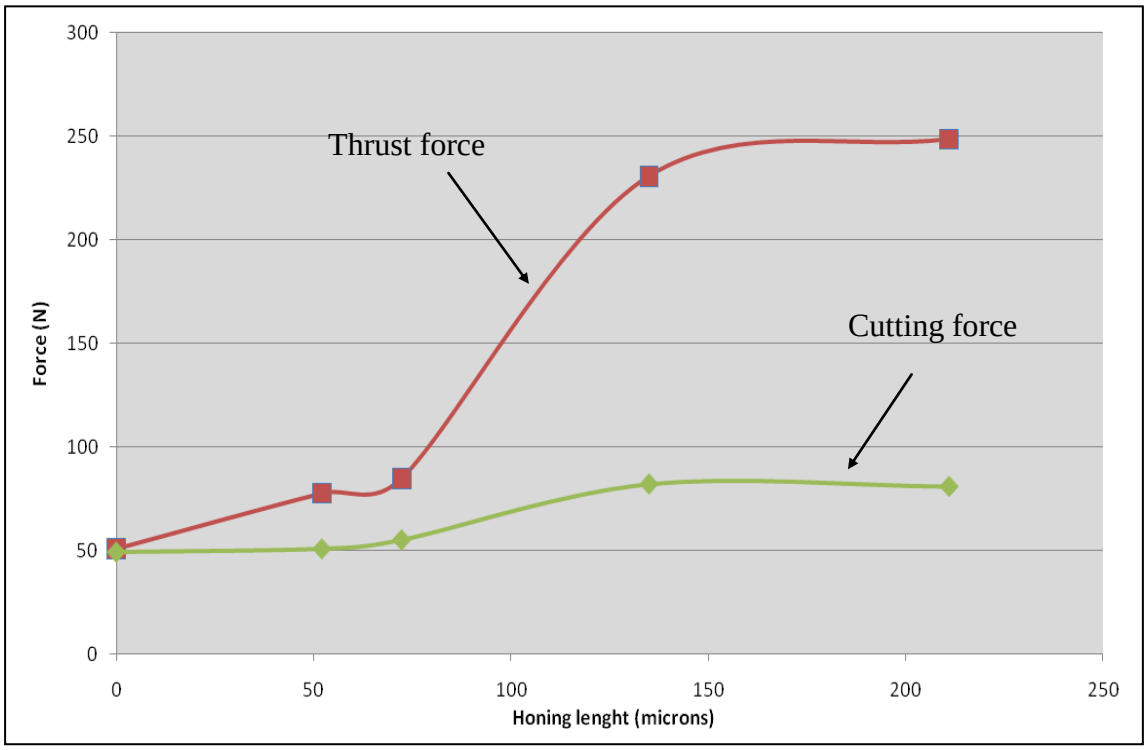

Figure 4.131. Variation in cutting and thrust forces with increase in the honing lengths (cutting speed: 30 m/min, width of cut: 1mm, feed: 15 µm).

4.12 Conclusions

The following conclusions can be drawn from the machining tests carried out on two different workpiece materials, namely mild steel and Ti-17 alloy, using teeth with different edge geometries.

1. The cutting force is always higher than the thrust force whilst machining steel, irrespective of the geometry (honed or sharp) of the tooth.
2. The thrust force is always higher than the cutting force for all the standard honed teeth, whilst machining Ti-17 alloy.
3. Whilst machining Ti-17 using sharp teeth, the cutting force is lower than the thrust force at low depths of cut, but becomes higher than the thrust force at higher feeds, thereby showing a "cross-over" point between forces. This phenomenon, however, is not observed when machining steels. Therefore it could be concluded that this is due to the workpiece material properties.
4. The longer is the honing length, the higher is the thrust force. However, honing has little or no impact on the cutting force. This confirms the fact that thrust force arises from the clearance face.
5. The standard honed teeth always show a thrust force higher than the cutting force. However, the thrust force remains almost constant even at higher feeds. The cutting forces increases linearly.
6. The thrust force will always be higher than the cutting force for machining parameters that have been identified from the work carried out on machining of titanium *i.e.* feed range of 10-20 µm. There are two possible reasons: (i) large flank size (honing) and (ii) difficult-to-cut workpiece material, indicating that the tooth has difficulty in penetrating the workpiece material.

CHAPTER 5: STRESS ANALYSIS DURING CUTTING

5.0 Introduction and background

Several researchers have successfully attempted to model the stress state of the bandsaw teeth using FEA software. However, in general the literature available in the public domain related to stress analysis on bandsaw teeth is far less than what is available for other machining operations such as tuning and milling. In the present work, finite element analyses were carried out to obtain stresses developed on the tool when it interacts with the workpiece material and quantify them. A brief overview of the previous work carried out by researchers is given below.

Andersson used a three dimensional model to investigate the saw teeth and concluded that maximum principal stresses decrease with an increase in the edge radii of the saw teeth. Moreover, the stresses calculated by Anderson were higher than the rupture strength of the tool material due to the relatively sharp geometry of the saw teeth. This essentially suggests that the tip of the saw teeth chips almost as soon as it comes in contact with the workpiece [156].

Sarwar *et al* [157] modelled three teeth in a row with a sharp edge geometry using a two dimensional model and their results reach a very high value of von Mises' equivalent stress, σ_{max} = 113 000 MPa. Chandrasekaran *et al* [189] studied different types of chipping of saw teeth during power hack-sawing, which included FEA of a saw tooth during the forward and return stroke. They concluded that there are large stress variations during different stages of sawing and that the large stresses in the contact region are predominantly compressive.

This chapter will focus on the stress patterns generated on carbide teeth with different geometries in terms of various honing lengths. The forces were obtained from actual cutting tests using the single tooth methodology. A simple, static model was made using Solidworks, without considering the friction between the tool and the workpiece. The stress patterns obtained by using teeth with different edge geometries will be elaborated. Moreover, the effect on the coatings on the changes in stress patterns will also be discussed.

5.1 Details of the Solidworks model

A 3D model was created according to the dimensions of the original carbide bandsaw tooth using Solidworks. The tooth was given the same mechanical properties as that of tungsten carbide. The width of the tooth was made as 1.6 mm. A square shaped workpiece was made and the two were mated with the carbide tooth, so that the carbide tooth and the Ti-17 workpiece were in contact with one another for a length of 1 mm. The workpiece material was given the same mechanical properties as those of Ti-17 alloy. The side view of the model is shown in Figure 5.1.

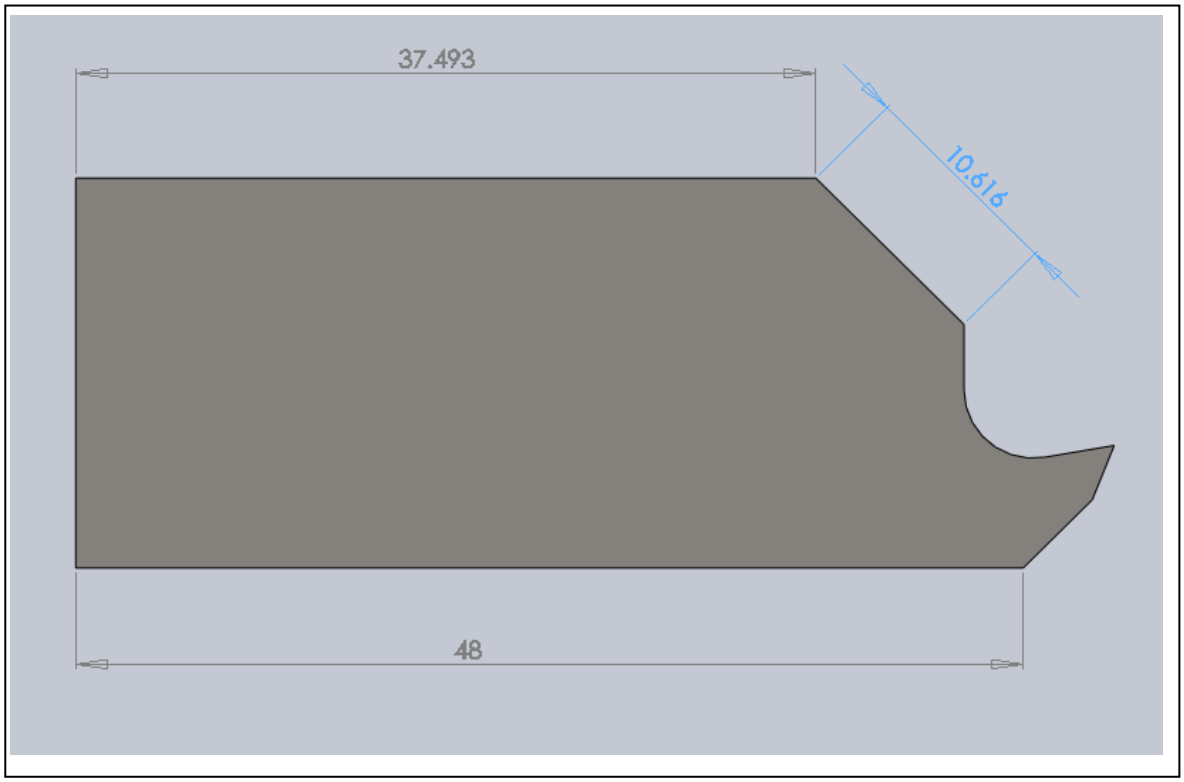

Figure 5.1. Front view of the carbide bandsaw tooth model (all dimensions are in mm)

Figure 5.2 illustrates the carbide teeth model with an edge radius, whereas Figure 5.3 provides an example of the tooth model with a honed tooth and having an edge radius of 12 μm. The tooth model was constrained, whereas the cutting and thrust forces were applied on the workpiece as shown in Figure 5.4, which also displays the rake and clearance angles of the carbide tooth model.

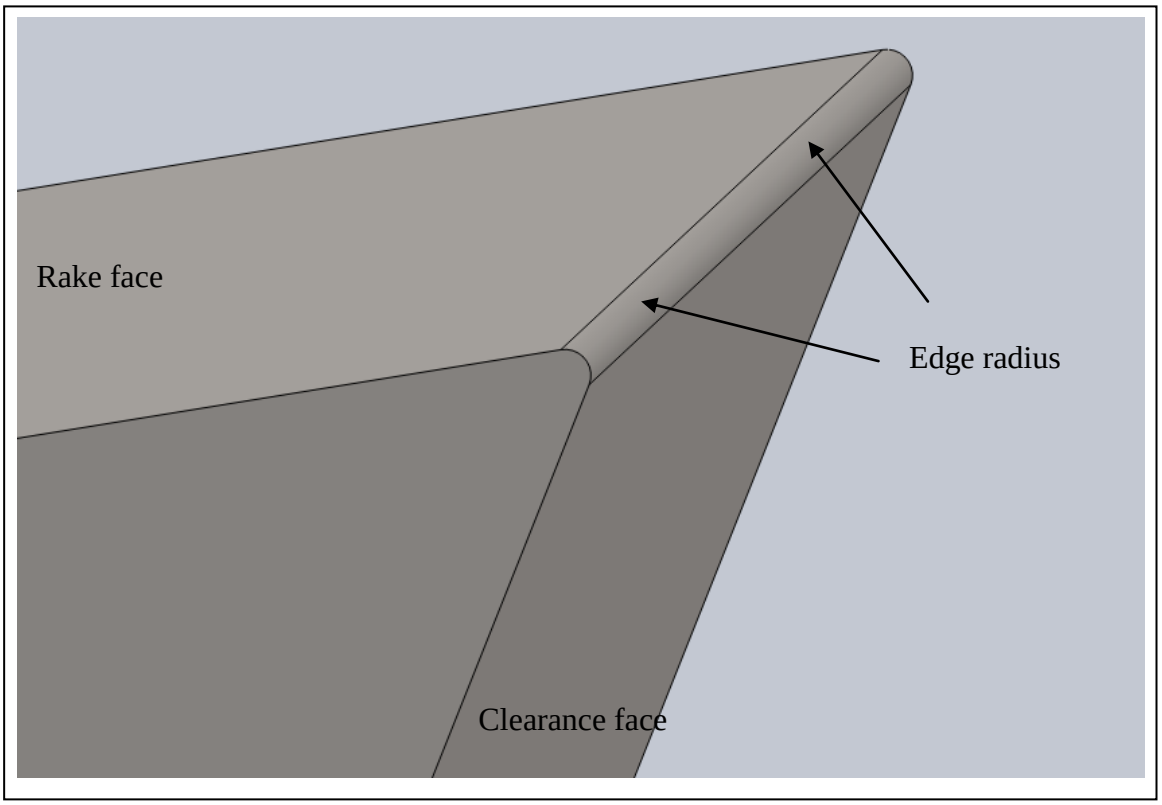

Figure 5.2. An example of carbide tooth model with edge radius.

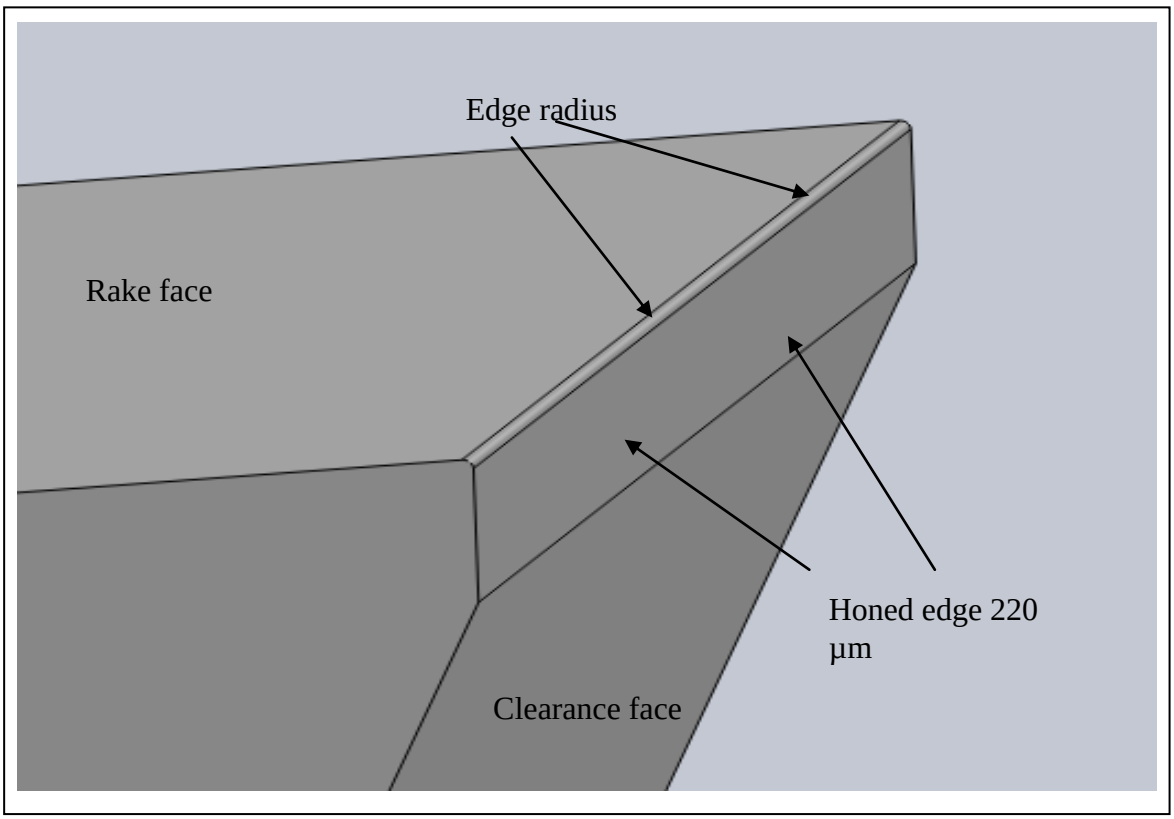

Figure 5.3. An example of honed carbide tooth model with an edge radius.

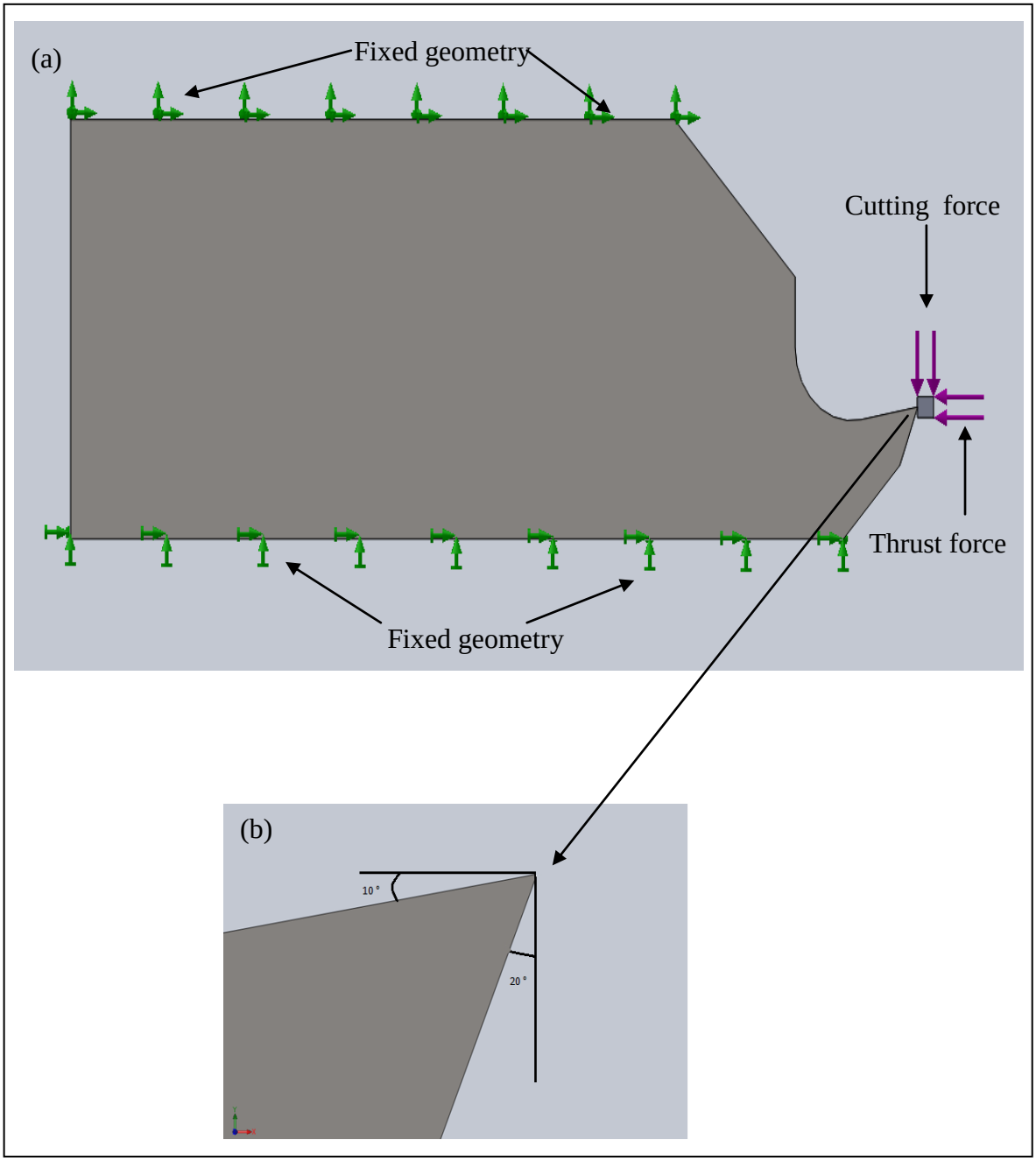

Figure 5.4. Side view of the carbide tooth model showing (a) application of forces as well as the restrictions applied on the tooth model and (b) side view of the carbide tooth model indicating the rake and clearance angles.

5.2 Mesh sensitivity

There are several checks and balances that can be used to assess the quality of the mesh in order to find the optimum mesh size. Some of them are:

- maximum stress
- degree of freedom
- total nodes
- total elements
- maximum aspect ratio.

In the present study, results were assessed against the variation of the degree of freedom so as to note the convergence and select an appropriate mesh size. The mesh sizes used in order to determine the sensitivity of the mesh are given in Table 5.1.

Table 5.1. Mesh sizes used for mesh sensitivity analysis

Mesh size (mm)	0.3	0.225	0.15	0.1225	0.09	0.075	0.07	0.065	0.06	0.055

The degree of freedom for each study was plotted against the different mesh sizes and the results are presented in Figure 5.5. It appears from this Figure 5.5 that with the decrease in mesh size, there is an increase in the number of degree of freedom and the values tends to converge to a limit.

From Figure 5.6, it can be seen that the increase in the degree of freedom leads to converging of the maximum stress values. Since the degree of freedom is related to the mesh size used, it was therefore decided to use a mesh size of 0.07 mm.

Figure 5.7 is an example of the model which has a mesh size of 0.07 mm – applied to both the workpiece and the tooth model.

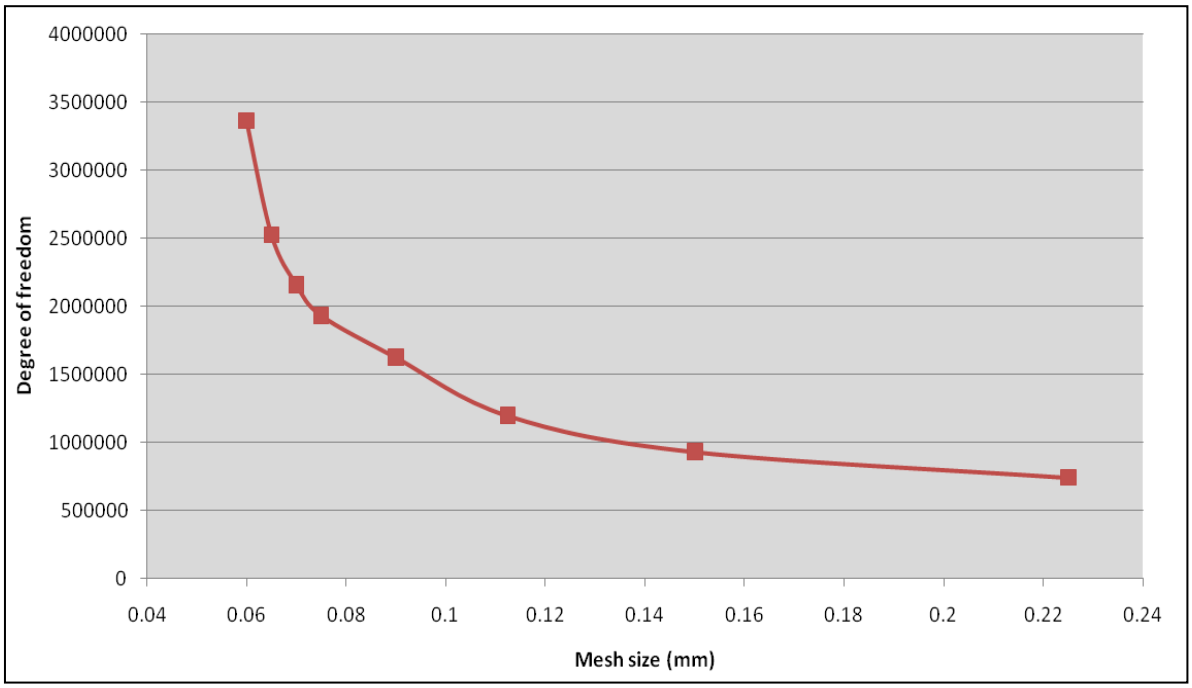

Figure 5.5. Mesh size against the degree of freedom.

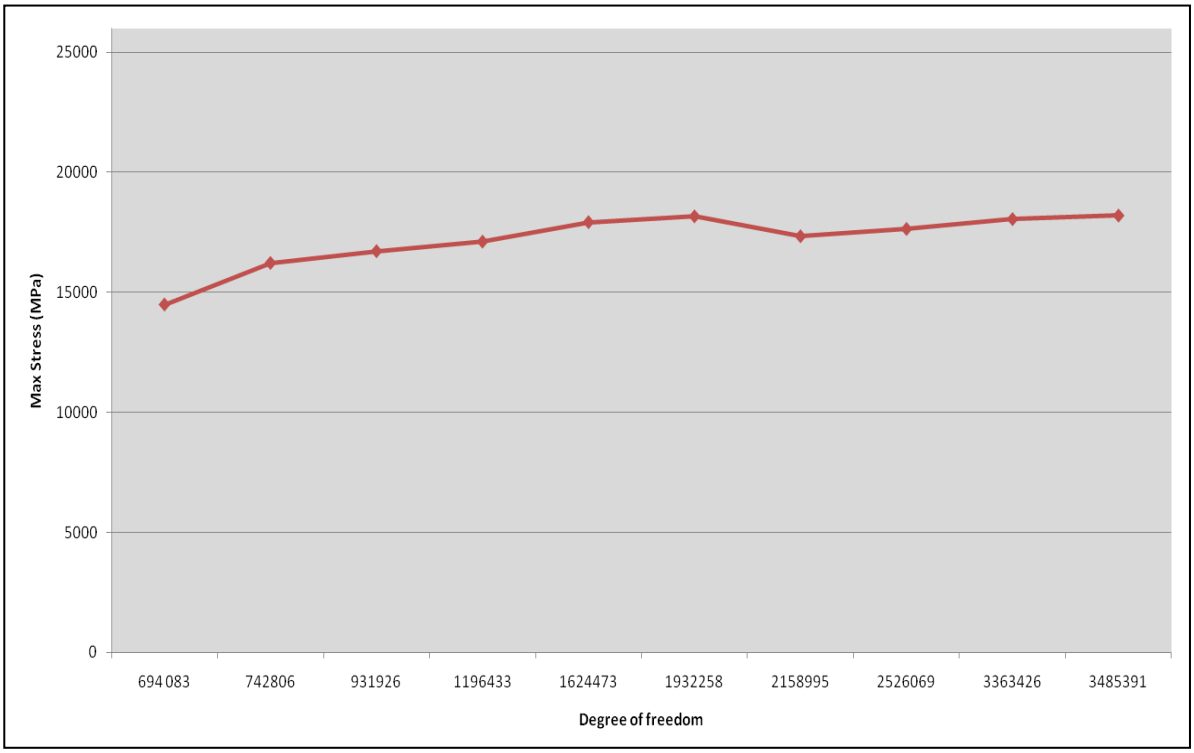

Figure 5.6. Variation in maximum stress with the degree of freedom.

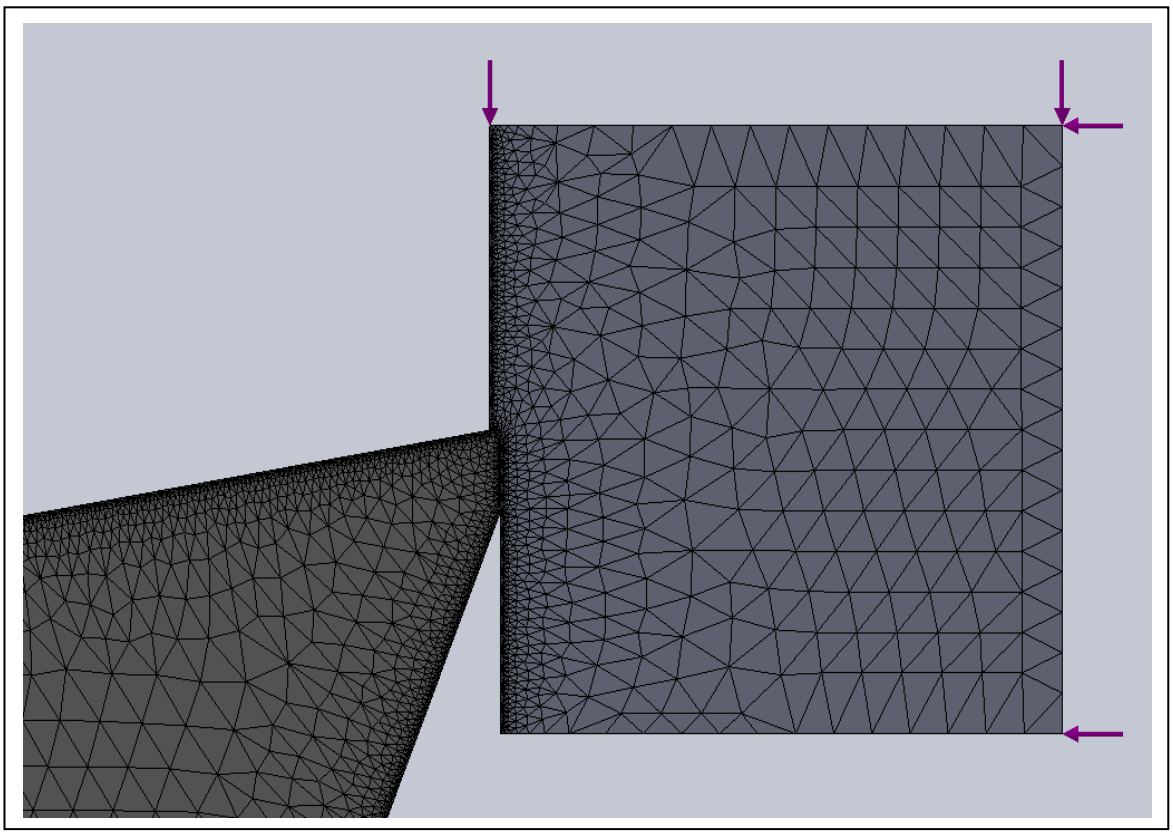

Figure 5.7. An example of the mesh created on the tooth and the workpiece, and the distributed loads being applied on the workpiece (mesh size = 0.07mm).

5.3 Finite element modelling using different honing lengths

The important variable in the geometry of the carbide teeth is the honing lengths on their flank face. The standard honing length on the carbide teeth is approximately 135 μm. For the purpose of this investigation, several models were created with different honing lengths on their flank face (an example is shown in Figure 5.3). Two feeds of 10 μm and 15 μm were chosen for this investigation as these are the most common feeds for bandsawing Ti-17 alloy. The edge radius selected for these analyses is 12 μm since this is a typical edge radius on the manufactured carbide bandsaw teeth. The forces recorded at the feed of 10 μm for the carbide teeth from the single tooth methodology are listed in Table 5.2, whereas Table 5.3 shows the force values at the feed of 15 μm.

Table 5.2. Cutting and thrust forces for carbide teeth at a feed of 10 μm

Honing length (μm)	Cutting force (N)	Thrust force (N)
0 (nominally sharp)	36.4	43.8
50	43.01	84.01
135 (standard honed)	78	241
220	78.2	238

Table 5.3. Cutting and thrust forces for carbide teeth at 15 μm feed

Honing length (μm)	Cutting force (N)	Thrust force (N)
0 (nominally sharp)	49.8	50.4
50	50.9	77.6
135 (standard honed)	88	244
220	80.8	248.6

The results of these analyses for the feed of 10 μm are provided in Figure 5.8. From Figure 5, it appears that with the increase in honing lengths on the flank face, the stress pattern shifts from the edge of the rake face onto the edge of the flank face. For example, Figure 5.8 a, shows the stress pattern for the nominally sharp tooth (no honing length), whereas Figure 5.8 d depicts the stress pattern for the carbide tooth with a honing length of 220 μm. From the force levels arising from actual experiments using the single tooth test methodology, the forces experienced by the teeth with a honing length of 220 μm are higher, and the stress pattern generated shows that the stresses (compressive) are concentrated on the edge of the flank face. This effect is more visible when comparing the stress patterns generated on teeth which have honed flanks, *e.g.* Figure 5.8 c and Figure 5.8 d. A similar trend in stress patterns is observed for the feed of 15 μm – see Figure 5.9.

5.4 Finite element modelling for coated teeth

The forces measured using the coated teeth were less than those for the un-coated teeth. It was, therefore, considered important to analyse and observe the stress patterns generated for the coated teeth. The measured forces for the un-coated and coated teeth at two

different feeds of 10 and 15 μm, using a standard honed tooth (honing length of 135 μm and edge radius of 12 μm) are shown in Table 5.4 and Table 5.5.

Table 5.4. Forces for the un-coated and coated teeth at 10 μm feed

Feed (μm)	**Un-coated**		**Coated**	
	Cutting force (N)	Thrust force (N)	Cutting force (N)	Thrust force (N)
10	78	241	60	141

Table 5.5. Forces for the un-coated and coated teeth at 15 μm feed

Feed (μm)	**Un-coated**		**Coated**	
	Cutting force (N)	Thrust force (N)	Cutting force (N)	Thrust force (N)
15	88	244	75.3	156.6

The comparison of the maximum stress for the un-coated and coated teeth at the feed of 10 μm is given in Figure 5.10 where it can be observed that the maximum stress for the un-coated tooth (13443.4 MPa) is greater than that for the coated tooth (11056.2 MPa). A similar trend is apparent when the feed is increased to 15 μm as shown in Figure 5.11. The maximum stress observed in the case of the un-coated tooth (17325.7 MPa) is greater than that for the coated tooth (15407.2 MPa).

5.5 Discussions and conclusions

A simple, static FE model was created, which included the tooth and the workpiece materials. The model was developed in such a way that the tooth remained static, whilst the (cutting and thrust) forces were applied to the workpiece material. It was observed that the honing length has a significant effect on the stress patterns. The increase in honing length on the flank of the carbide tooth leads to the maximum stress (which is compressive) shifting towards the edge of the flank face, whilst simultaneously reducing the maximum stress from the edge of the rake face. Stresses do also exist on the rake face; however, their magnitude is reduced considerably with increase in honing lengths. This is in conformity with experimentally obtained results, where SEM images have proven that the carbide teeth do chip at the rake face, however, more degradation (chipping) is observed on the honed flank face. A comparison of the FEA results and a SEM image is provided in Figure 5.12, which shows the stress pattern on the tooth at a feed of 10 μm. The stress pattern is given in Figure 5.12 a, whilst Figure 5.12 b shows the SEM image. From Figure 5.12 a, it can be observed that the stresses are mainly concentrated on the edge of the rake face, whereas the stress level is greater at the edge of the flank face

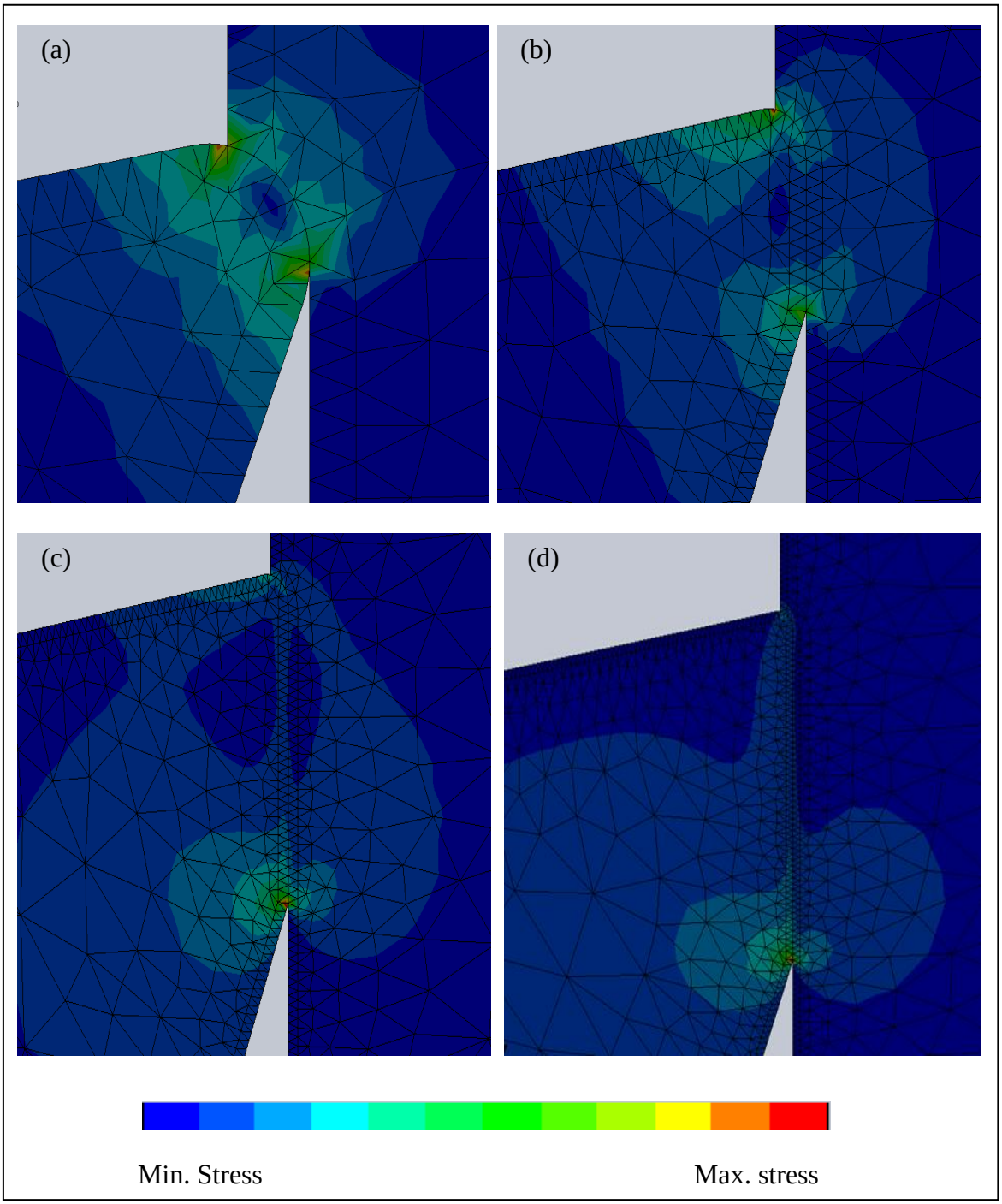

Figure 5.8. Stress patterns for the carbide teeth at a feed of 10 μm with different honing lengths, (a) nominally sharp, (b) 52 μm, (c) 135 μm and (d) 220 μm.

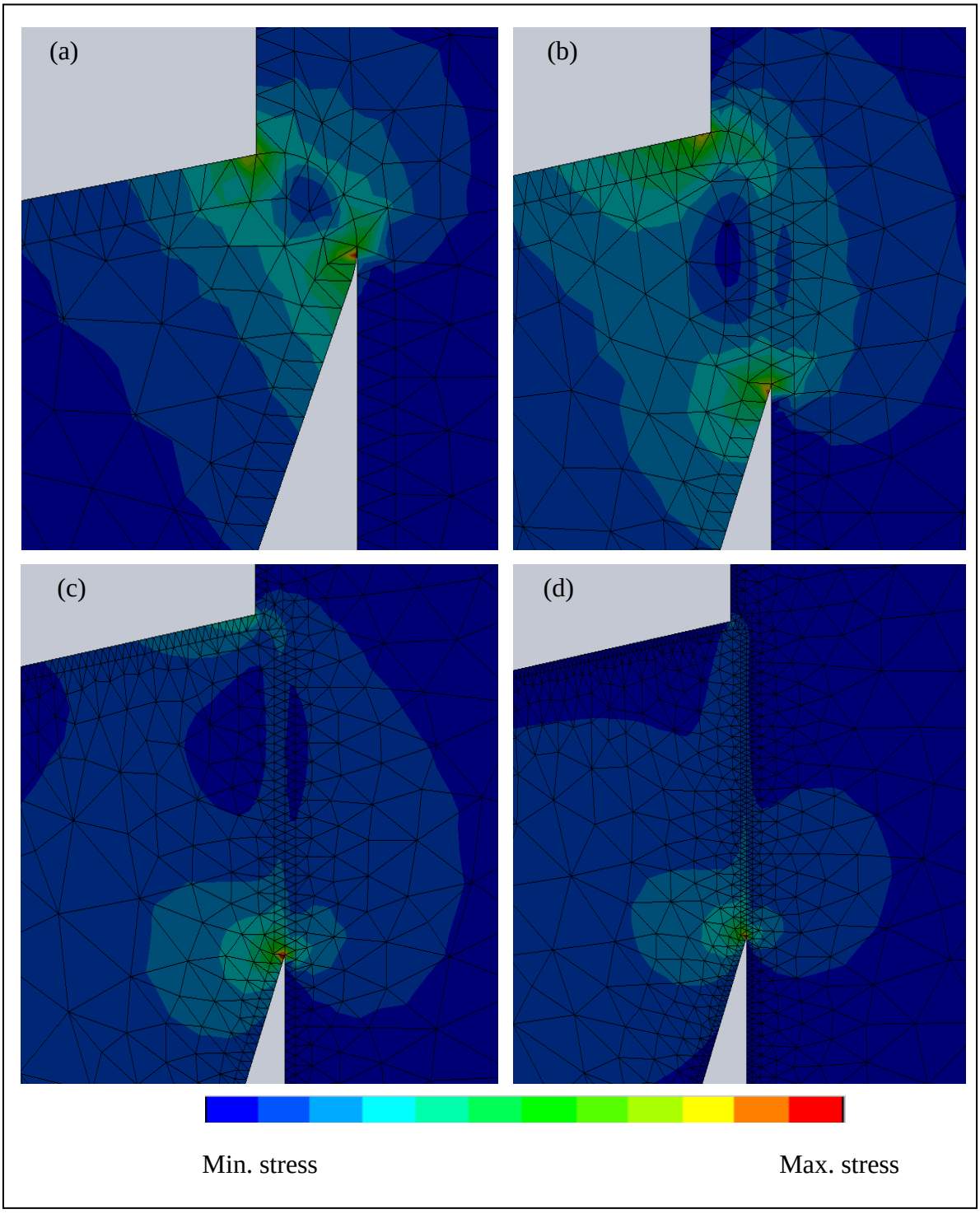

Figure 5.9. Stress patterns for the carbide teeth at a feed of 15 μm with different honing lengths, (a) nominally sharp, (b) 52 μm, (c) 135 μm and (d) 220 μm.

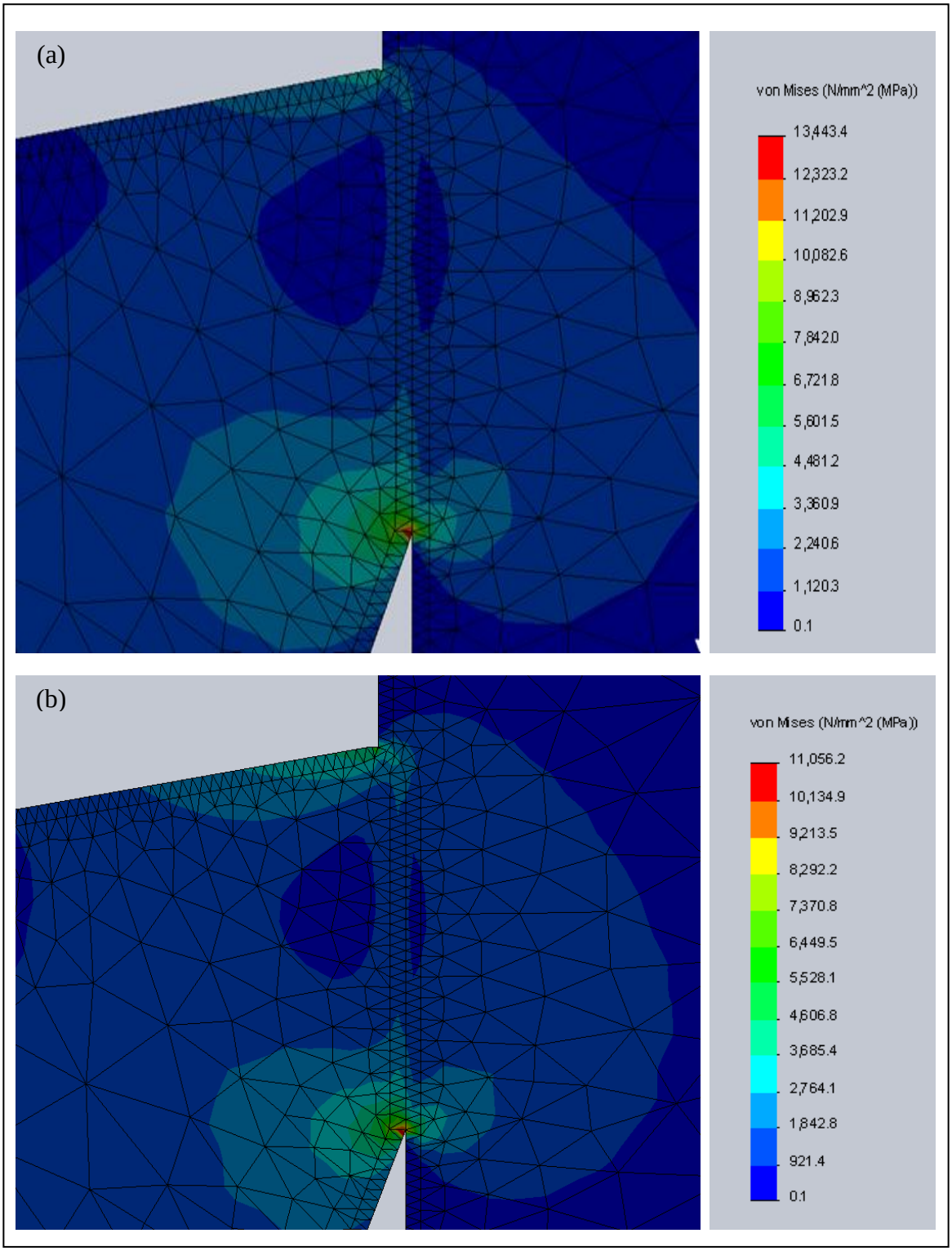

Figure 5.10. Stress patterns and maximum stress for (a) un-coated and (b) coated, at 10 μm feed

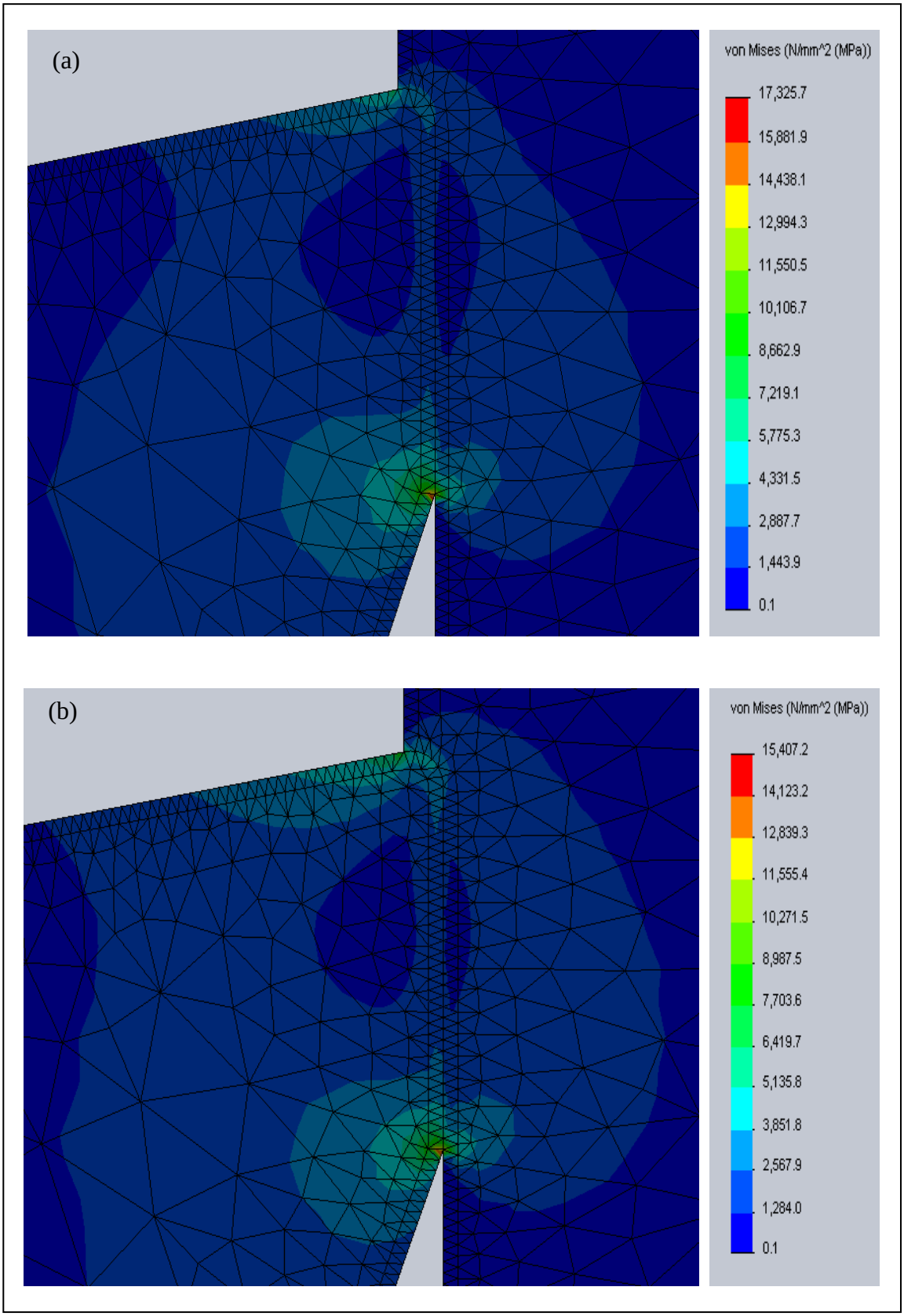

Figure 5.11. Stress patterns and maximum stresses for (a) un-coated and (b) coated, at 15 μm feed.

compared to the stresses at the rake face. Comparing the SEM image and FE model, it can be seen that the FE analysis highlights/identifies the area of the tooth which degrades in terms of wear/chips, due to high levels of stress. Furthermore, the incorporation of the coatings on the carbide teeth leads to a reduction in (cutting and thrust) forces. These forces were used in the same model where it was apparent that maximum stress experienced by the tooth is reduced, due to the incorporation of coatings.

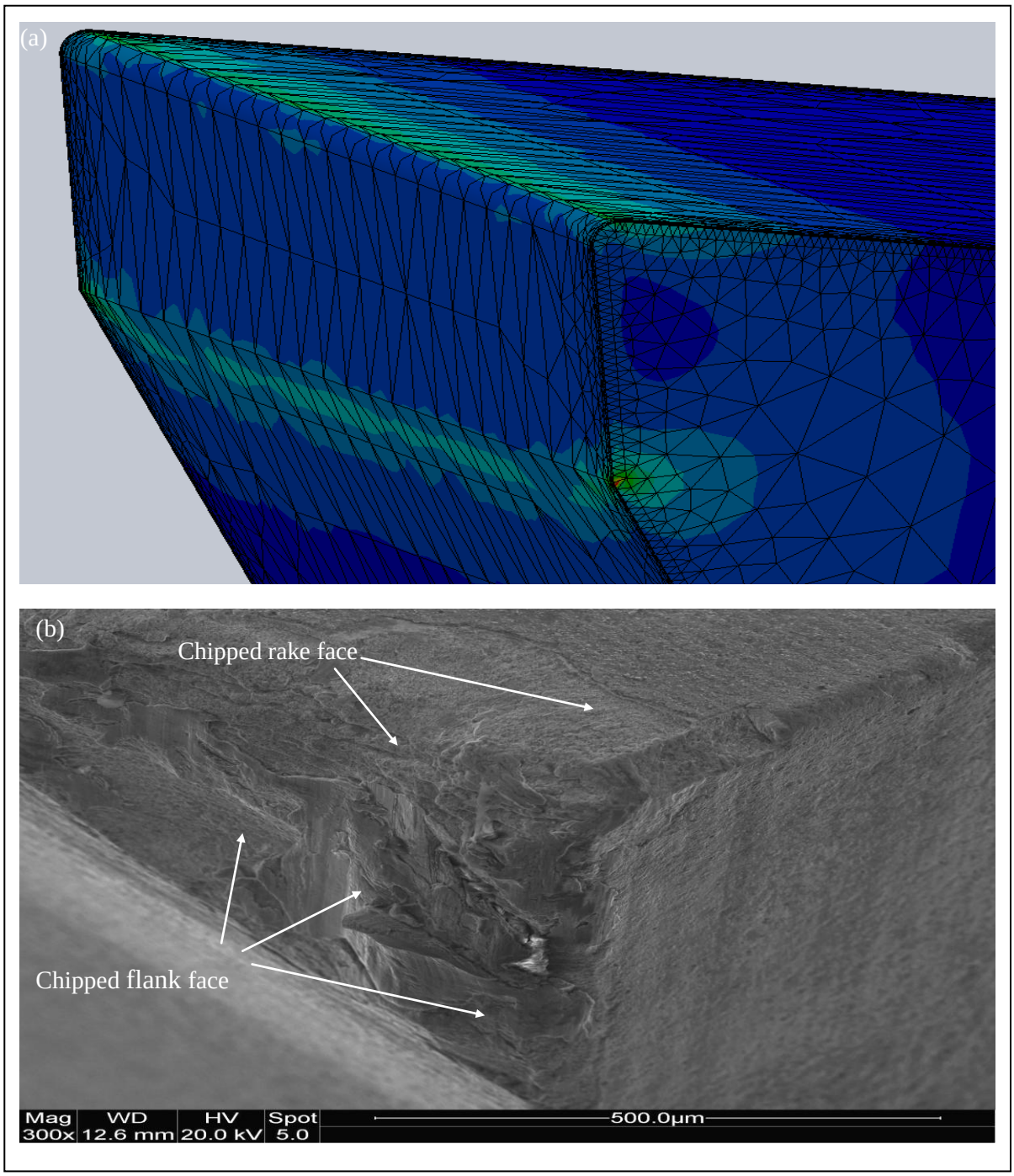

Figure 5.12. (a) Stress pattern for 10 µm feed and (b) micrograph of worn tooth used at 10 µm feed.

CHAPTER 6: CONCLUSIONS AND FUTURE WORK

6.1 Conclusions

The extensive programme of testing has led to new findings in the area of bandsawing of titanium alloys, using the un-coated and coated carbide tipped bandsaw teeth. As a consequence of these findings, there is now a better understanding and knowledge of the performance of un-coated and coated bandsaw teeth while bandsawing Ti-17 alloy.

The main conclusions from the single tooth tests carried out using un-coated and coated carbide tipped bandsaw teeth while machining Ti-17 alloy are:

1. **Machining conditions:** The following conclusions were drawn for the bandsawing parameters from the series of machining tests carried out :

- Flank wear, deformation at the corner and chipping at the rake face were identified as the wear modes which controlled the life of the un-coated and coated carbide bandsaw teeth. In the selected range of feeds (10 µm, 15 µm, 20 µm and 25 µm), flank wear and corner wear were much higher at higher feed rates (15 µm, 20 µm, 25 µm) and therefore higher feed rates reduce rapidly the life of the carbide bandsaw teeth. From the range of chosen feeds, it was found that the carbide teeth performed the highest number of cuts at a low feed of 10 µm and less degradation in the tooth geometry was observed as compared to the degradation at higher feeds. Therefore it was concluded that this is the suitable feed for bandsawing Ti-17 alloy. Higher cutting speeds reduce the life of carbide tipped bandsaw teeth during machining Ti-17 alloy and it was found that the carbide tooth produced the highest number of cuts at cutting speed of 40 m/min, with minor degradation in tooth geometry. Therefore it was concluded that 40 m/min is the suitable cutting speed within the selected range (40, 60, 80 m/min). However, a well-defined built-up edge was absent on the worn un-coated and coated carbide bandsaw teeth.
- The chips formed during the machining of Ti-17 alloy were uniform in size and shape, except the ones formed at the end of the tooth life. The wear mechanisms in un-coated and coated carbide bandsaw teeth, while machining Ti-17 alloy, are adhesion and attrition at the cutting edge.

2. **Wear of carbide teeth:** The following conclusions were drawn for the wear and degradation of carbide teeth while bandsawing Ti-17 alloy when observed under the SEM:
    - All the un-coated and coated worn teeth showed adhesion of workpiece material (Ti-17) on the worn flank surface. This is due to the high chemical affinity of titanium alloys to "weld" to the tool materials and due to the poor thermal conductivity of these alloys, which leads to generation of high temperatures at the took-workpiece interface.
    - Diffusion wear mechanism was identified by the presence of carbon and cobalt in the adhered workpiece on the worn cutting edge when analysed by EDX.
    - No evidence of abrasive wear was found on un-coated and coated bandsaw teeth, while machining Ti-17 alloy.
    - Specific cutting energy was found to be a useful parameter to correlate the various stages of wear and edge conditions to the performance of un-coated and coated carbide teeth at various machining parameters of the bandsawing range.

3. **Effect of honing on the mechanics of cutting:** The following conclusions were drawn when machining Ti-17 alloy, using carbide teeth with a honed edge:
    - The thrust force was always found to be higher than the cutting force while machining Ti-17 alloy using honed carbide teeth, irrespective of coatings on the cutting edge. This was attributed to the inherent properties of Ti-17 alloy as well as to the honed flank face.
    - The cutting and thrust forces were found to be strongly dependent on the degree of honing on the flank face of the coated carbide teeth. For a nominally sharp tooth, the thrust force was higher than the cutting force at low feeds. However, at higher feeds, the cutting force became higher than the thrust force. For standard honed teeth (honing length of 135 μm), the cutting force was always less than the thrust force, within the bandsawing feed range (10 μm to 50 μm).

4. **Finite element analyses:** From the basic, static and simple finite element analyses carried out using the forces obtained from machining tests, following conclusion was made:

- The quantitative comparison between the stresses experienced by the coated and un-coated teeth showed that the stresses were reduced considerably with the application of coatings on the carbide bandsaw teeth.

All the above mentioned conclusions should hold true for bandsawing of Ti-17 alloy using honed carbide tooth geometry.

6.2 Future work

Although the programme of cutting tests carried out using un-coated and coated carbide bandsaw has been extensive, there are some areas which can be probed further. Some of them are listed below:

a. Use of multi-layered coatings on carbide tipped bandsaw teeth to machine titanium alloys.
b. It would be very interesting to perform cutting tests using carbide teeth under dry conditions and analyse adhering workpiece material. This method would eliminate any role of carbon which may have derived from the lubricant.
c. Machining of other difficult-to-cut alloys, such as martensitic steels, hardened stainless steels, using carbide tipped un-coated and coated teeth.
d. Further investigation of the effect of honing on the forces, by machining other high performance nickel and titanium alloys using carbide teeth with different honing lengths.
e. It would be very interesting to carry out machining of titanium alloys using complete bandsaw loop with honed teeth geometry.
f. Although this project dealt with the application of two coatings (AlTiN and TiAlSiN) on carbide tipped bandsaw teeth, it would be interesting to deposit these coating on other metal cutting tools, such as broaches and observe their wear/degradation while machining difficult to cut alloys.

APPENDIX A: CALIBRATION OF THE SINGLE TOOTH TEST RIG

A1. Introduction

Calibration is the process of establishing the relationship between a measuring device and the units of measurement. This is done by comparing a device or the output of an instrument to a known standard. For example the length of a stick can be calibrated by comparing it to a standard that has a known length. Once the relationship of the stick's length to the standard is known the stick is calibrated and can be used to measure the length of other things.

For many operations the quality of the calibration needs to be known and is quantified by an uncertainty estimate for the calibration. This is so important for the scientific community and manufacturing operations that it has been proposed that an evaluation of the measurement uncertainty was added as part of the calibration process. Calibration can be called for:

- with a new instrument,
- when a specified time period is elapsed,
- when a specified usage (operating hours) has elapsed,
- when an instrument has had a shock or vibration which potentially may have put it out of calibration, and
- whenever observations appear questionable.

In non-specialized use, calibration is often regarded as including the process of adjusting the output or indication on a measurement instrument to agree with the value of the applied standard, within a specified accuracy.

A2. Background

The requirement to calibrate the STT rig in Northumbria University arose when the author was performing the single tooth test using an uncoated tungsten carbide single tooth against a titanium workpiece. It was observed that the thrust force was greater than the cutting forces. An example of these forces is recorded in the LabVIEW interface in Figure A.1, and it is clear that the system is out of calibration.

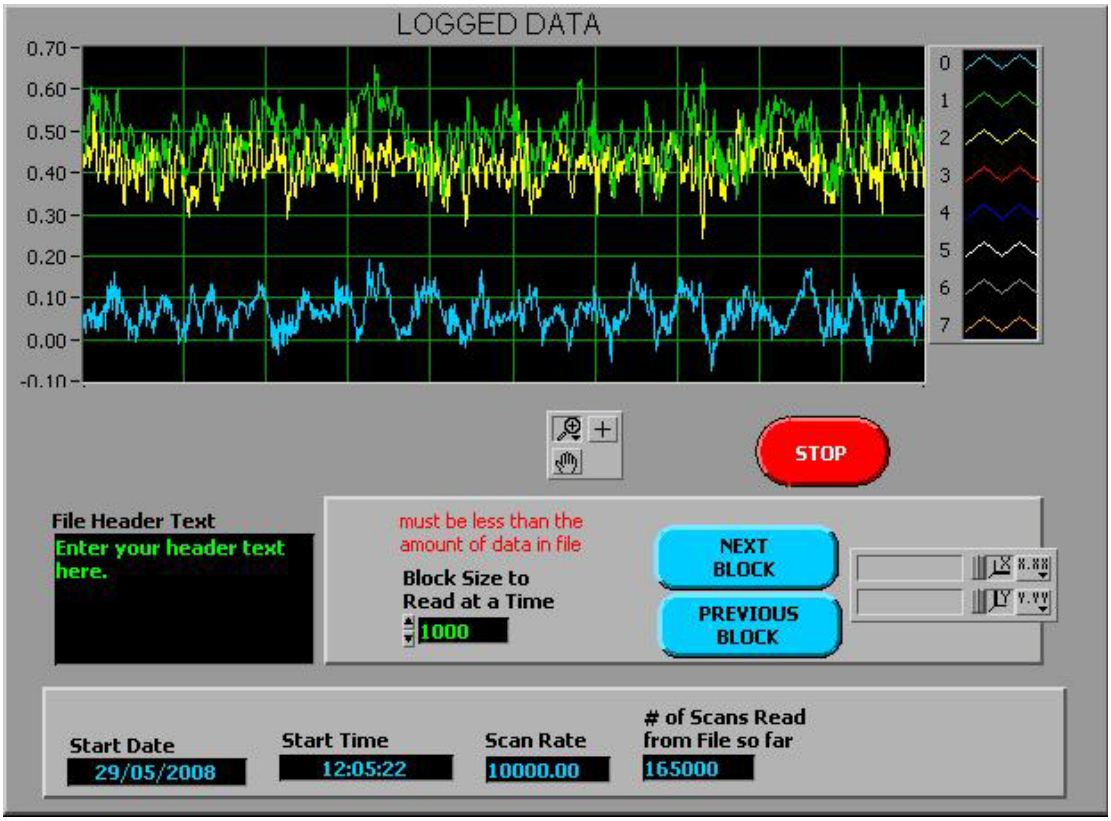

Figure A.1. Cutting forces for machining titanium alloy. The setup is in non-calibrated state [blue = cutting force, yellow = thrust force and green = side force]

A3. Equipment used in calibration of the test rig

In order to calibrate the test rig, the following pieces of equipment were utilized.

- Tektronix TDS 210 double channel oscilloscope,
- Salter spring balance with a capacity of 250 N,
- dead weights, 1 kgf each (total of 13 kgf),
- turn buckle, attached to two strings on both sides, and
- Wykeham-Farrance proving ring, maximum capacity 300 lbs.

Although the existing setup has an oscilloscope fixed (Gould scope), in order to ensure that it is calibrated, and that we are achieving the correct output from the charge amplifier, another oscilloscope was installed in parallel to the Gould scope. All these components are shown on the following pages.

A4. Calibration methodology

In order to calibrate the setup, the following two methodologies were used:

- spring balance and
- proving ring.

Since the proving ring is too big to fit in the setup, it was therefore utilized only in calibrating the cutting forces. The spring balance was used to calibrate all three forces.

Figure A.2. Salter spring balance with a capacity of 200 N.

Figure A.3. Dead loads used to calibrate the spring balance.

Figure A.4. Tektronix TDS 210 double channel oscilloscope.

Figure A5. A turn buckle used to calibrate the STT setup.

A5. Calibration using spring balance

In order to calibrate the setup, it was necessary to check whether the spring balance gave accurate values if a dead load was applied. For this purpose, dead weights up to 13 kgf (approx. 130 N), were added to the spring balance, and a graph of applied load against the readings obtained on the spring balance were plotted. These readings were noted from the outcome shown on the oscilloscopes and were recorded on the computer and are displayed in Figure A6. It can be observed from the graph that the spring balance shows a linear behaviour (going through the origin) for the applied load, and therefore the spring balance is calibrated properly.

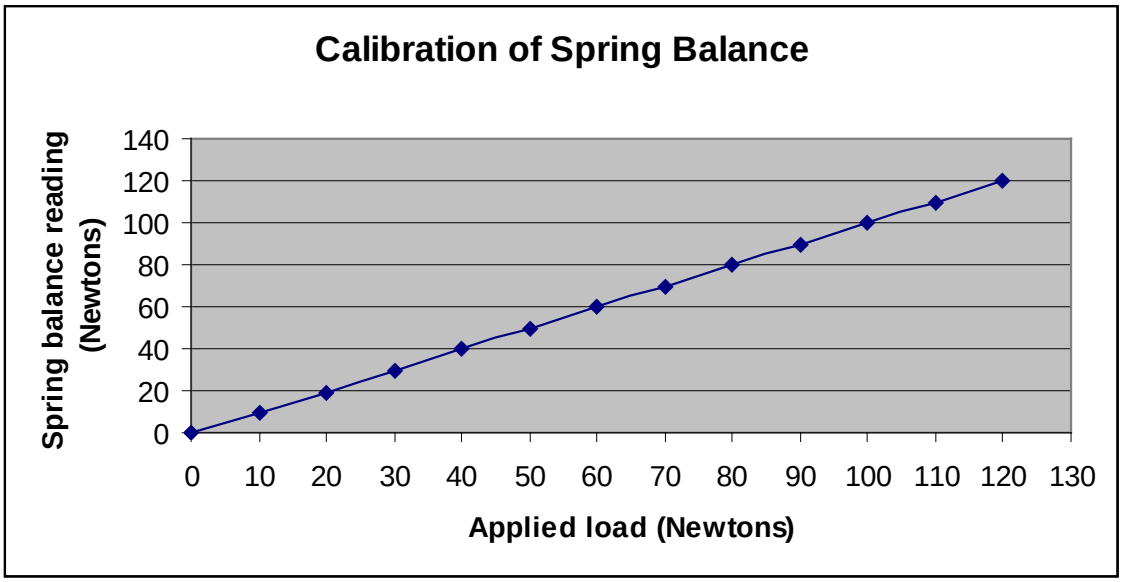

Figure A.6. Applied load against extension graph for the Salter spring balance.

After the calibration of the spring balance, this was used to apply forces in the three directions, and the outcome was observed on the two oscilloscopes and was recorded on the personal computer, which is equipped with LabVIEW 6.02 software.

The three principal cutting forces are shown in Figure A7 and therefore in order to calibrate the dynamometer and the charge amplifier, it was required to apply the known forces in these principal directions.

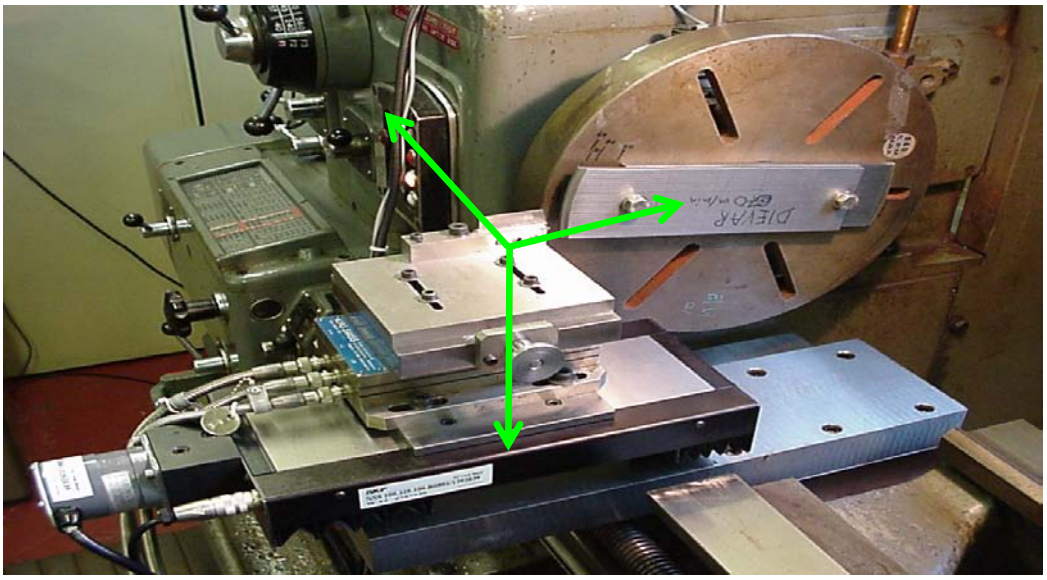

Figure A.7. Principal directions of system. X = feed, Y = lateral, Z = vertical force components. X, feed (thrust) force F_P: Y side (lateral) force F_S, Z cutting force F_V.

A6. Calibration for the cutting force (Fv)

In order to calibrate the cutting force (F_v), it was required that known loads are applied in the downward direction, and to ensure that the force is applied vertically, and that no torque is applied. In order to do this, the string was placed on the cutting edge of the single tooth that was fixed on the platform. This is shown in Figures A8 to A9.

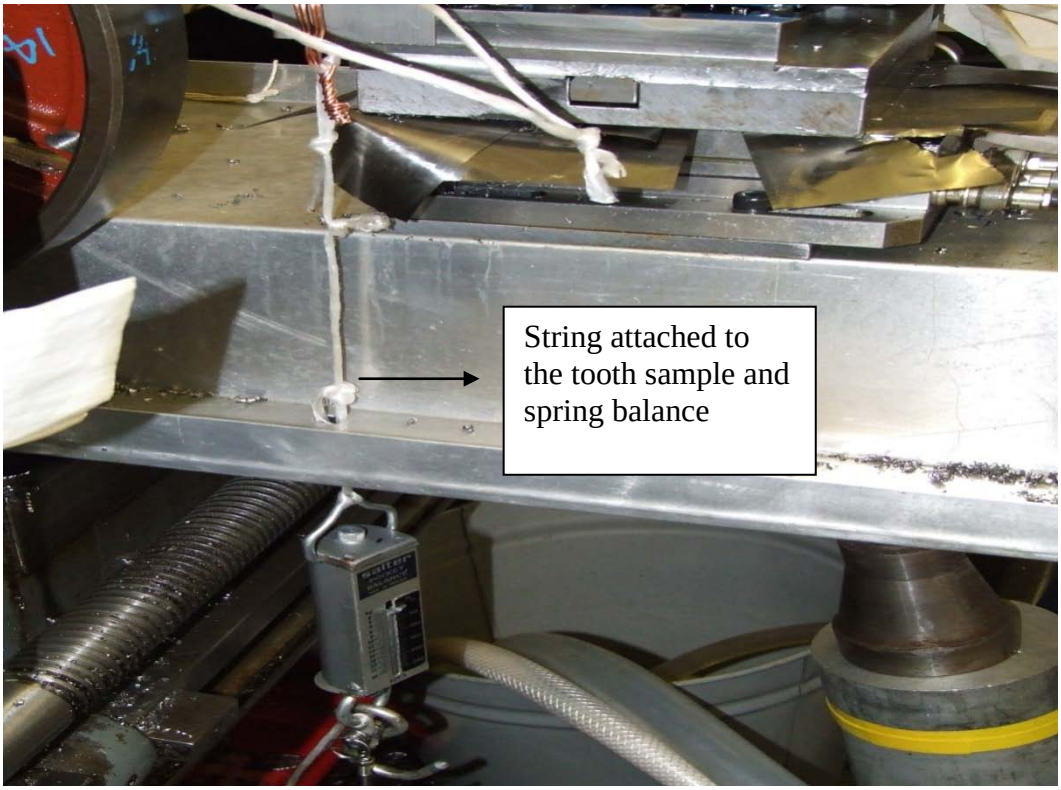

Figure A.8. Test rig used to apply forces in Z direction (F_v)

A7. Calibration for the thrust force (Fp)

In order to apply the known weight/force in the X-direction, it was important that the applied force does not take any contribution from the torque. This proved to be difficult, since due to the applied load, the downward component of force could not be neglected. Therefore, a turn buckle was attached to strings on both sides. One of the sides was attached to the single tooth, and the other side was attached to the spring balance, which was connected to a rigid body. The turn buckle was set in tension and was unwound until the required load/force was achieved on the spring balance. This was also done in the reverse manner, in which the turn buckle was moved clockwise, so that it provided tension to the spring balance. This method is shown in the following photographs.

Figure A.9. Test rig used to apply forces in Z direction (Fv), showing the spring balance attached to the lathe bed.

Figure A.10. Setup used to apply load in X-direction (feed)

.

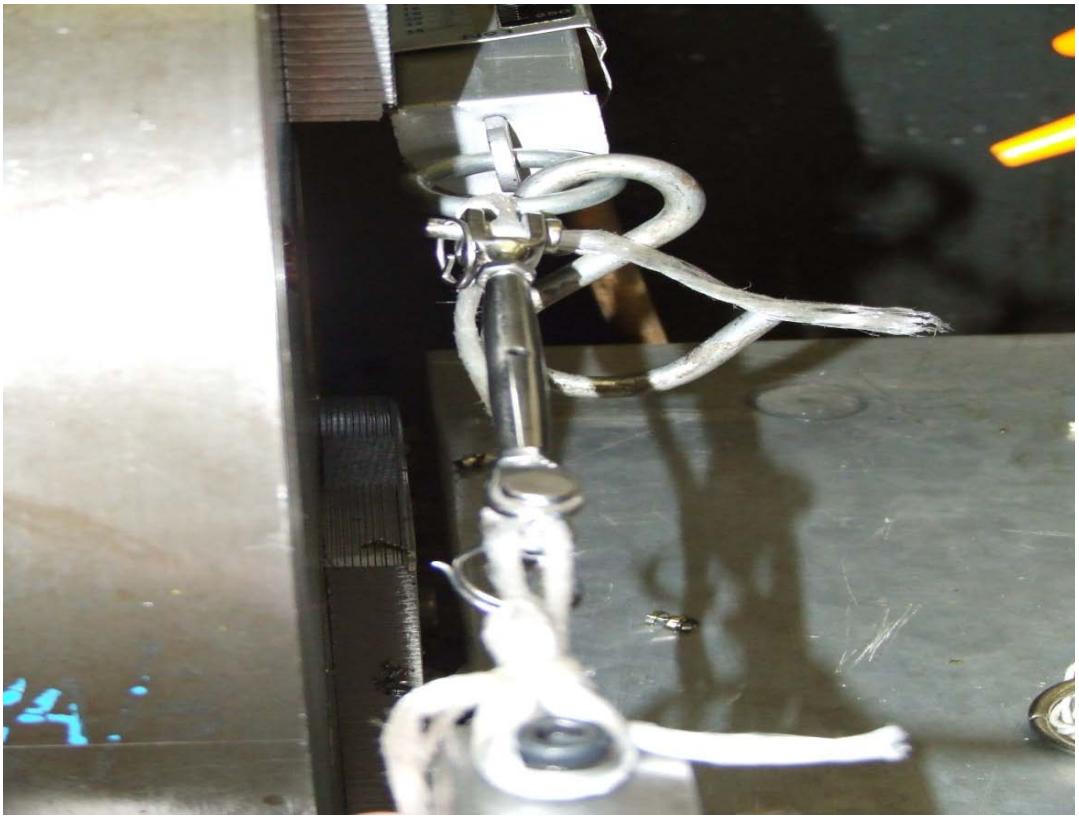

Figure A.11. Front view of the setup for calibrating thrust forces.

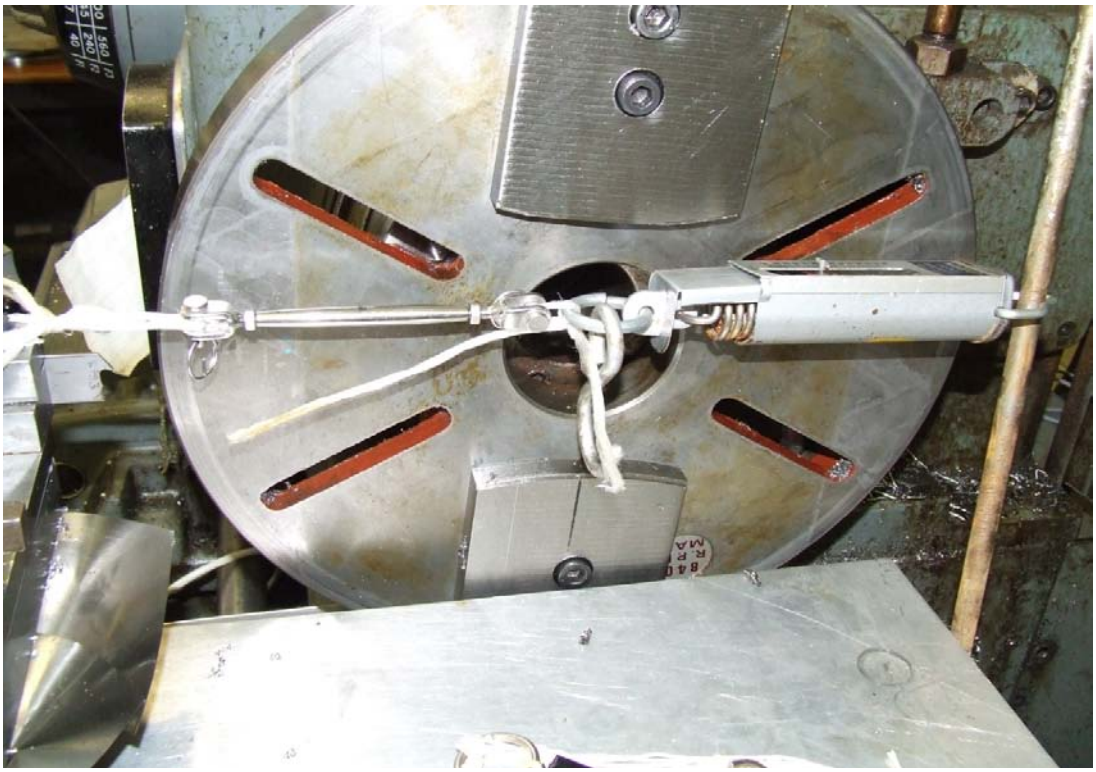

Figure A.12. Side view of the setup used to calibrate the thrust forces.

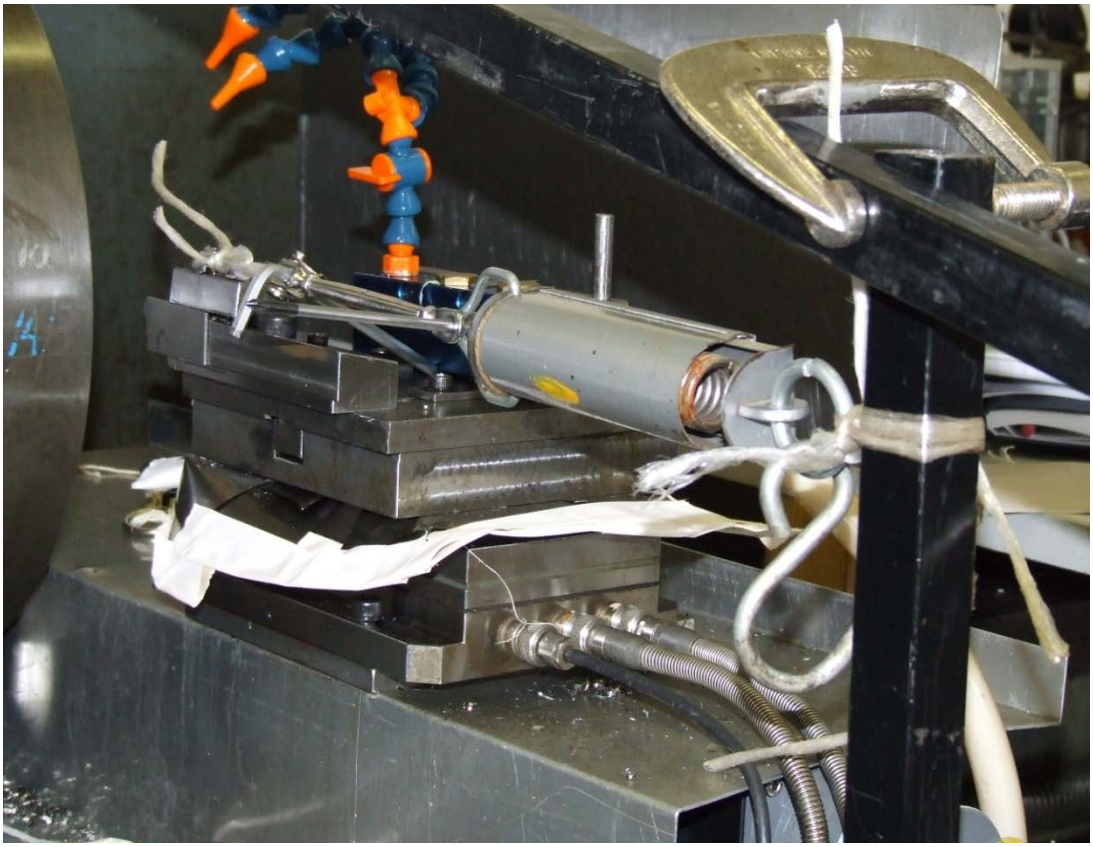

Figure A.13. Another side view of the setup used to calibrate thrust forces

A8. Calibration using a proving ring

The calibration was carried out using the spring balance and cross-checked using a Wykeham-Farrance proving ring with a maximum capacity 300 lbs. The proving ring has a large diameter, and therefore could only fit in the setup to calibrate the thrust force. In order to place the proving ring, an angled iron piece was fitted onto the chuck of the lathe using M8 bolts, as shown in the Figures A14 and A15.

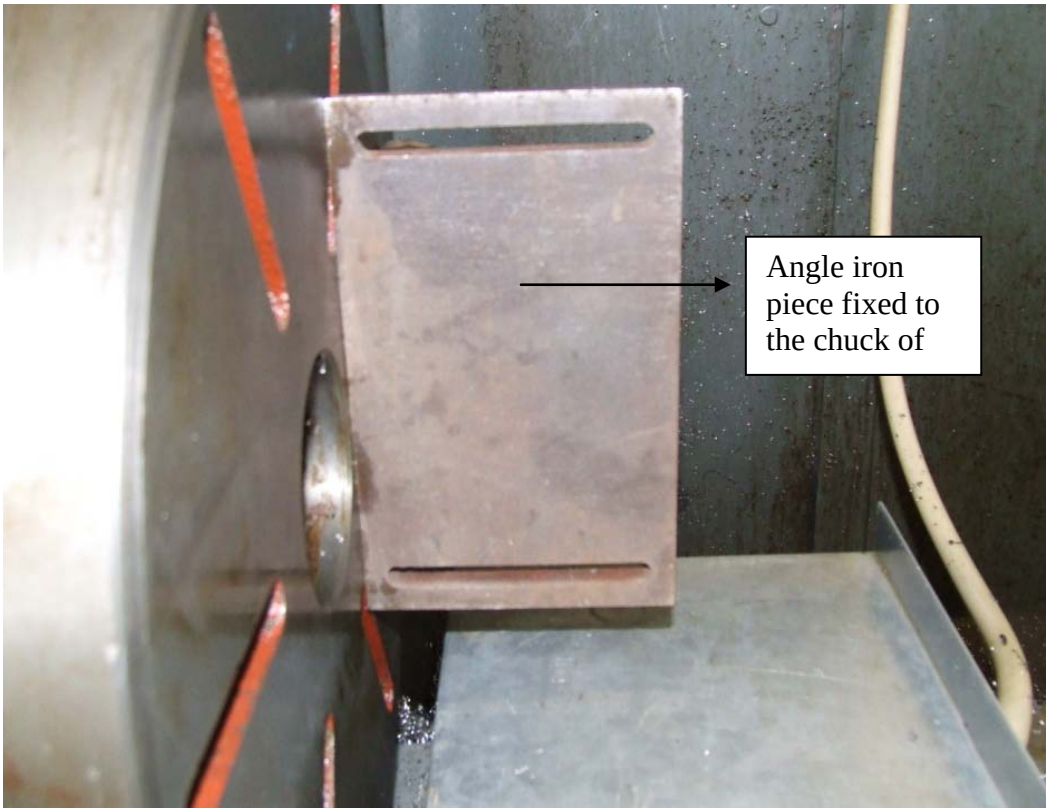

Figure A.14. Angle iron fixed onto the lathe chuck

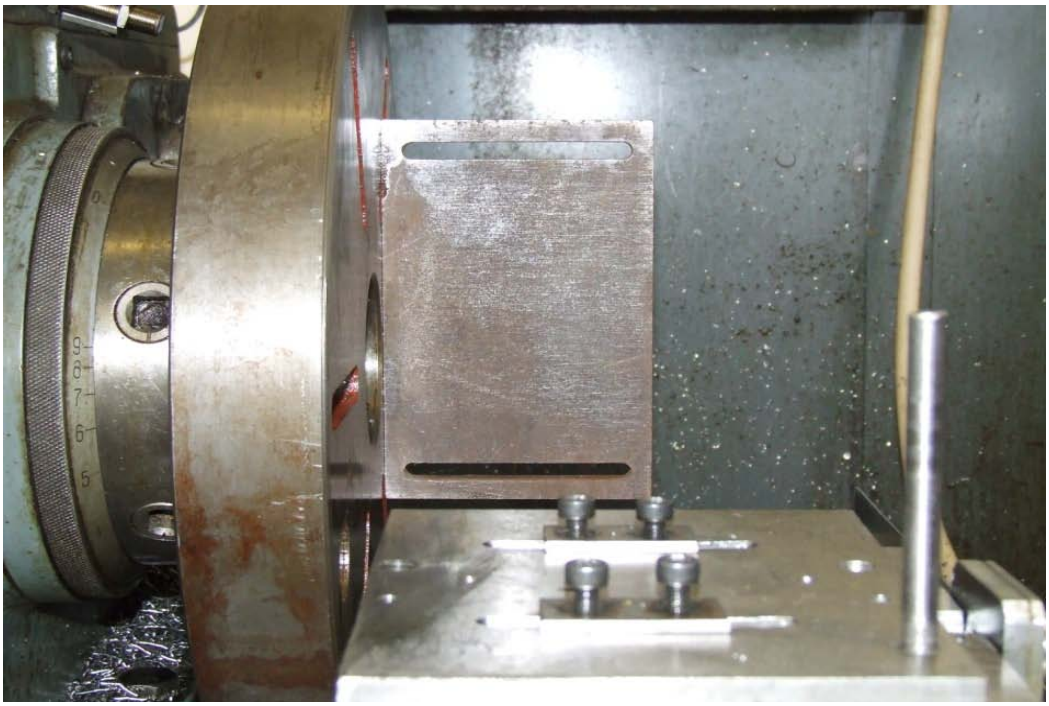

Figure A.15. Another view of the angle iron fixed to the lathe's chuck.

The proving ring was fixed between the dynamometer and the angle iron piece, and incremental force was applied by the computer. The setup is displayed in Figure A16.

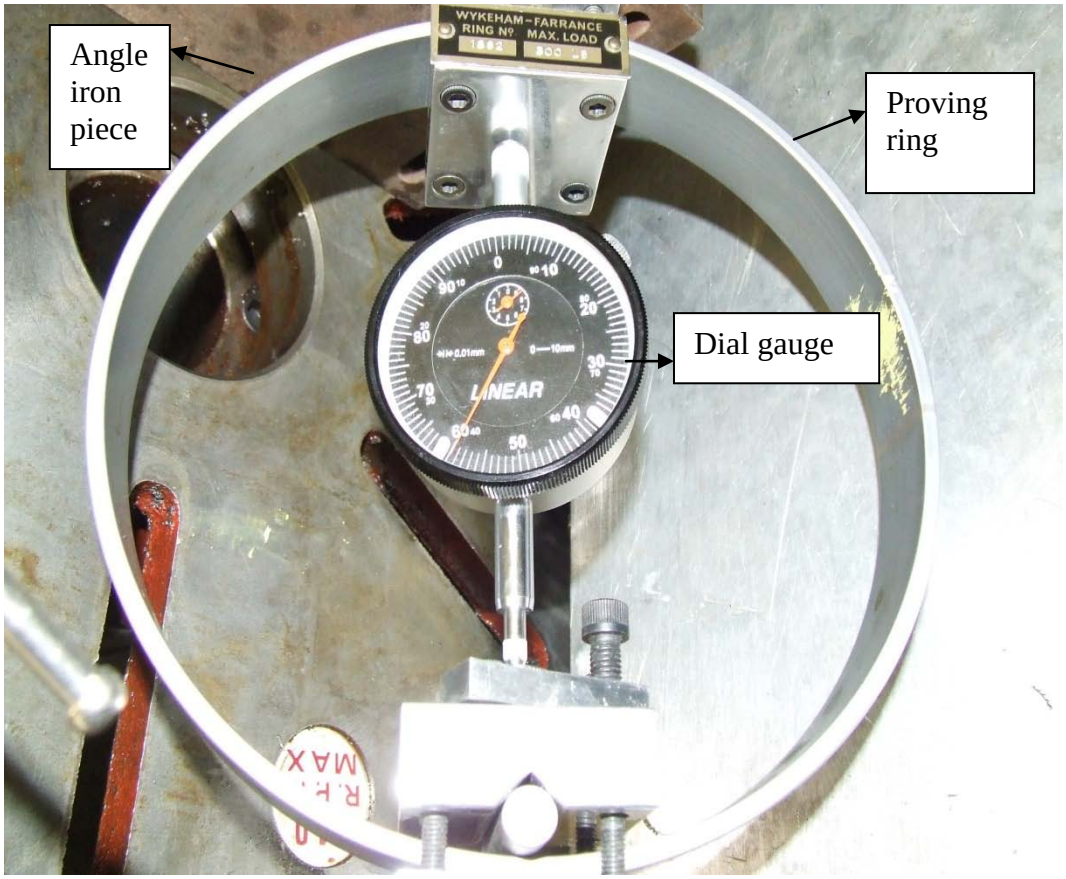

Figure A.16. The proving ring setup used to calibrate the thrust (feed) force

A9. Results

The outputs from the charge amplifier were monitored on three different pieces of equipment – two oscilloscopes and the LabVIEW software. Although in the LabVIEW we could not see the results as the forces were being applied or altered, nevertheless, the changes were recorded and analysed later. The following sensitivity conditions were used for the charge amplifier:

Fz: -3.5 pC/N

Fx: -7.5 pC/N

Fy:-7.5 pC/N

An appropriate time-base and volts/division had to be selected for the oscilloscopes – typical values were 500ms to 1 second and 0.5 volts per division.

For the charge amplifier, the conditions were altered from 1 volt equals 100 N to 1 volt equals 50N. An important point was to stabilize the charge amplifier by switching it ON at least 1 hour before taking the measurements: and it had to be "reset" after each set of readings was taken. The results are shown in Figures A17 to A19.

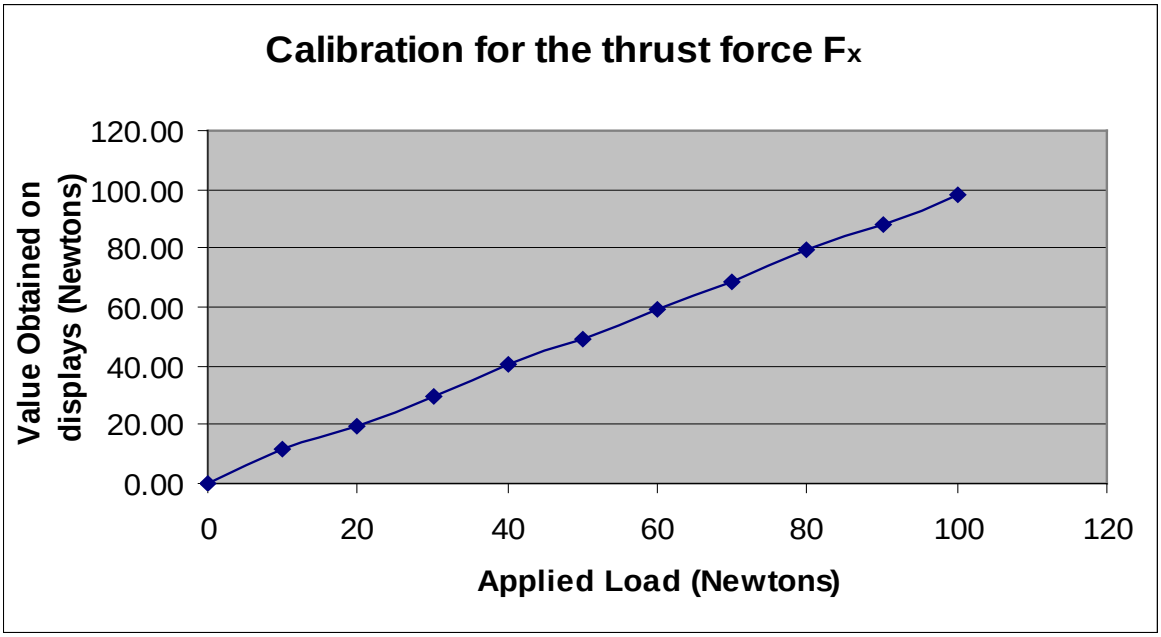

Figure A.17. Calibration curve for the thrust force component (F_x)

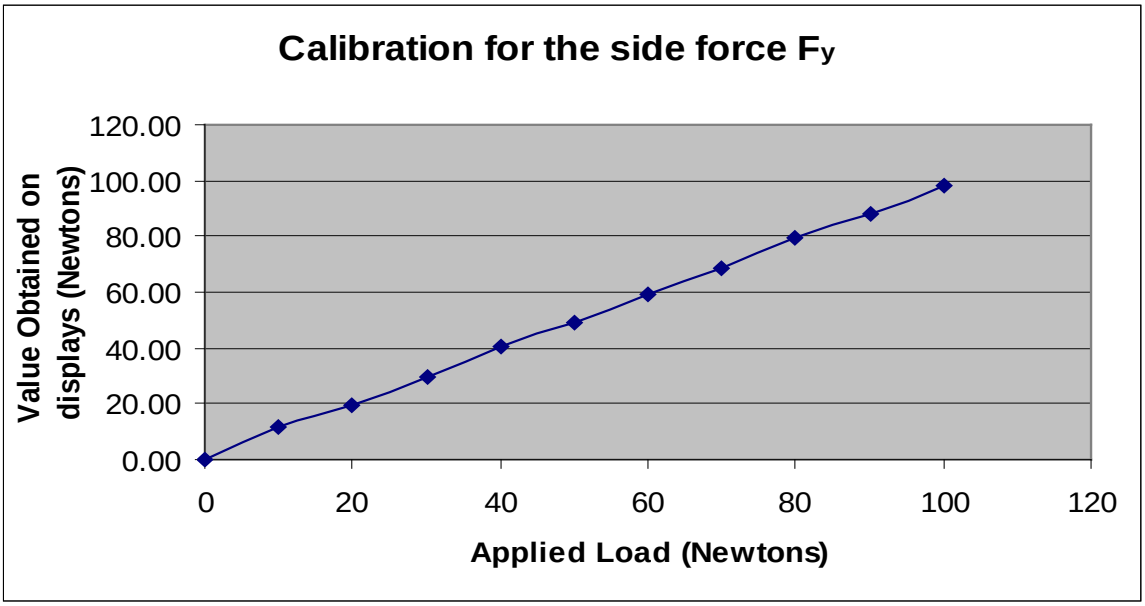

Figure A.18. Calibration curve for the side force component (F_y)

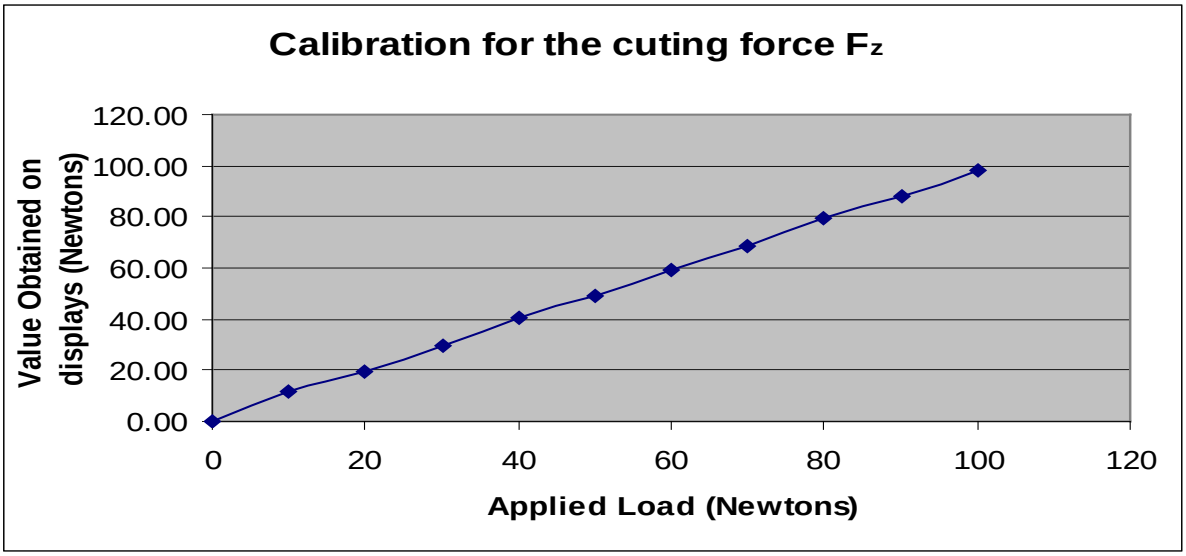

Figure A.19. Calibration curve for the cutting force component (F_z)